PHYSICAL, CHEMICAL AND BIOLOGICAL CHARACTERIZATIONS OF URETHANE DIMETHACRYLATE BIOMATERIAL COMPOSITE

by
Nahed M. Mohsen

A dissertation submitted in partial fulfillment
of the requirements for the degree of
Doctor of Philosophy
(Bioengineering)
in The University of Michigan
1995

Doctoral Committee:

Professor Emeritus Robert G. Craig, Co-Chairperson
Professor Frank E. Filisko, Co-Chairperson
Professor Carl T. Hanks
Assistant Professor David C. Martin
Professor Richard E. Robertson

To Huda and Mohsen with *love*

ACKNOWLEDGEMENTS

First and foremost, and at a loss of words, I would like to thank the Creator, the Maker, and the divine Scientist who gave me the power and well to be where I am at now, contributing, though an infinitesimal contribution, to the great "toy" of science. Thank you GOD.

I would like to express my thanks and appreciations to my co-advisor, Professor Robert G. Craig, for his invaluable advice, encouragement, patience and support (financial and otherwise) throughout the course of this research. I would like to thank my co-advisor Professor Frank E. Filisko and my committee members for reviewing my dissertation and for helping me each in his own way; Professor Frank E. Filisko for his generosity in providing laboratory facilities and equipment; Professor Richard E. Robertson for his stimulating theoretical and practical lectures on polymers and composites throughout his invaluable courses; Professor Carl T. Hanks for his advise and patience in teaching me cell culture techniques and his unlimited generosity for using his laboratory, equipment and materials and also for his interesting suggestions and discussions; Professor David C. Martin for serving on the committee.

I would like to express my deepest gratitudes and appreciations to every member of my family for their endurance, assistance, and endless love; My parents, Mohsen and Huda who taught me how to walk, how to hold the pencil, provided all the comfort that I needed when I was a child, and continued their unlimited giving when I grew older by supporting me every step of the way, encouraged me, put their trust

in me and gave me the thrust and power to excel as well as to venture in a wide spectrum of disciplines; My father Mohsen, for his "few" words that always left great marks, his encouragements for me to be in the "first" place have paid off and always will, his unlimited ambitions have given me the utmost strength to pursue my goals, and for his unlimited support that made it possible to achieve these goals; My mother Huda, for her endless love, care and unlimited prayers that have enlightened my way. Her teachings and invaluable advises have inspired me in every step of the way, and her true friendship has made it possible for me to overcome many obstacles and always will. Their contributions cannot be measured and their marks will be felt generations to come.

I would also like to thank my *dearest* brother Ali, for sharing every "new" experience together and for supporting me in every step of the way, his unlimited wisdom and interesting discussions have inspired me and his sincerity and forever love will always be cherished; My *dearest* sister Salwa, for her great love and respect, for sharing the beginning of this long journey with love, assistance and infinite support, her nice and honest qualities are the rarest, for which I will always be in debt; My dear brother Mohammed, for his unlimited patience, trust and endless respect which have given me the strength to excel in achieving my goals, and for which I will always acknowledge; My dear sister Rawdah, for sharing the last days of this hard work, her encouragement, assistance, and forever love will always be appreciated; My dear sister Mona, for her ever-evolving wisdom and knowledge that added a new dimension to my life, her infinite support, love and respect will always be felt; My dear and *youngest* brother Abdul-Rahman (Boudi), for his honesty, faith, and sensitivity that influenced my thinking, and for his "sweet" talks that enriched my sole; My cousin Obey, for his prayers and deep faith in my goals and potentials; My nephew

Mohammed (Nin'noo) and my niece Dana for all of the bright things they hold in their future as well as their smiles and contemporary endless cries.

I would like to give my special thanks and gratitudes to my *dearest* friend, Dr. Khaled Shahwan for his cooperative help, infinite support and advice. Our intellectual and technical discussions were extremely interesting and will always be cherished. Without his assistance, especially in the automation of the sorting and manipulation processes of the massive amounts of numerical (experimental) data, much of this work would not have been completed in due time.

Finally, I would like to acknowledge the financial support received through the Center Grant from USPHS grant P50 DE 09296 from the National Institute for Dental Research, Bethesda, MD, 20892. The partial support from the Bioengineering program at The University of Michigan, Ann Arbor, is also gratefully acknowledged.

TABLE OF CONTENTS

LIST OF FIGURES

LIST OF TABLES

CHAPTER I

INTRODUCTION AND LITERATURE REVIEW

1.1 Introduction

Medical and pharmaceutical applications of synthetic polymers have contributed significantly to the quality and advancement of implants and medical devices. These applications range from catheters to vascular grafts, from orthopaedic implants to dental anterior filling materials and from transdermal drug delivery systems to medicated patches. In general, their vast acceptance in biomaterial applications was increased because of their compliance with soft tissue, cardiovascular tissue, or as a result of their being partially non-irritating to the skin for transdermal applications. In addition, such biomaterials exhibit mechanical adaptability to their designated function where their tensile strength, modulus, strain, and temperature-related properties meet the required application.

Of the vast variety of biomaterials, synthetic polymer-based composites are used in wide applications, such as orthopaedics and dental restorations. These composites consist of inorganic fillers entrapped in a three-dimensional highly cross-linked organic polymer matrix. The filler and the polymer are chemically attached by a coupling agent such as organofunctional silane. The combination of the two phases

gives better material properties for these particular applications than the individual phase. In these polymer-based composites, the properties of the organic matrix and the stability of the organic-inorganic interface strongly influence the behavior of the composite material.

The synthetic polymer-based composites enjoy outstanding versatility in their range of length of monomer molecules, functionality, and polymerization reactions. A particular class of these synthetic polymers consists of an organic matrix composed of large difunctional monomers molecules which undergo polymerization with themselves by a free radical mechanism to form a highly cross-linked, three-dimensional network.

The polymerization of the polymer composites by the free radical mechanism occurs by opening a reactive carbon double bond which results in a linkage to another molecule to form the polymer. Such opening of the bonds is due to an initiation reaction involving activation of an agent which breaks down and forms a free radical. These agents are chemical or light initiators.

Despite the advances made in composite resins in the last 30 years, three problems with light-cured composites, which have been addressed by many researchers, remain under investigation, namely: curing of the matrix with time (chemical aging), polymer-filler interaction, and the stability of the coupling agent phase that binds the organic matrix with the inorganic matrix, especially in severe biological environments.

Curing with time (chemical aging) in light-cured composites is a result of many factors. One of these factors is incomplete conversion of the difunctional vinyl monomers during the formation of the highly cross-linked network as a result of polymerization. The incomplete conversion leads to the presence of (a) residual un-

reacted double bonds in the form of pendant vinyl groups, (b) unreacted monomers or (c) unreacted oligomers [6]. Another factor is the high viscosity and rigidity of the organic matrix, especially the dental organic matrix. The high viscosity causes slow diffusion of free radicals during polymerization, which causes a decrease in the polymerization rate and increases the probability of a termination reaction. This consideration leads to a high content of unreacted methacrylate groups [105].

Chemicals in the biological environment, especially in the oral cavity, and incompatibility of organofunctional silanes with the resin or filler during polymerization are some of the major contributing factors in the failure of the organic-inorganic bond. Chemicals such as water could easily hydrolyze the siloxane bonds, the bonds which bind the organofunctional silane with the inorganic surface, once water reaches the interface [96]. Incompatibility of the siloxane bond or its slow rate of reaction as compared to curing rate of the resin may lead to inadequate bonding to the resin.

Thus, the presence of unreacted double bonds, continual curing, post-curing of the resin and the hydrolytic degradation of the biomedical composites may lead to major clinical problems. For instance, in dental restorations, where the dental material is in a highly reactive environment, the unsaturated vinyl causes slow degradation, leading to disruption of restorative marginal integrity and indirect exposure of the dental pulp to exogenous influences. In addition, it leads to poor esthetics, color instability, poor durability and loss of anatomic form. The presence of the unreacted monomers and oligomers leads to plasticization effects (lowering of the glass temperature), which causes changes in the physical as well as the mechanical properties of the dental restoration. The presence of unreacted pendant groups, especially on the polymerized surface of the implant, makes the polymeric matrix more susceptible to oxidative degradation reactions [6, 105]. Further, post-curing will cause the restora-

tion to change its structure and physical properties. The hydrolytic degradation and leaching of compounds from the composite can cause wear, and bulk fracture.

Therefore, the significance of this research is that it will add to the fundamental understanding of the curing and post-curing mechanisms of a dental composite system. Since most of the trends in new material development have been empirical than scientific in nature, the understanding of these mechanisms should help to improve the criteria for the development of these materials. Also, a connection between the curing chemistry and structural properties should help in predicting and developing a consistent material with long term stability in the biological and oral environment. In addition, exploring the use of an old method such as dielectric spectroscopy, although it has not been used extensively in the field, should promote future research in monitoring sensitive processes using this nondestructive tool.

Therefore, the goals of this research were:

1. To examine the continual curing of a polymer of a difunctional vinyl monomer and to examine the effect of presence of an inorganic phase on this continual curing process using microcalorimetry. The work pertaining to this goal will be presented in Chapter II.

2. To investigate the polymer-filler interaction in order to determine how a non-compatible inorganic phase modifies the molecular behavior of the polymer-based composite as compared to the pure polymer using dielectric measurements, and to determine how a modification of this inorganic phase by silanation affects these molecular behaviors. The work pertaining to this goal will be presented in Chapter III.

3. To determine the effect of moisture on the polymer and polymer-filler interface

with and without a coupling agent using dielectric measurements. The work pertaining to this goal will be presented in Chapter IV.

4. To examine the effects of different curing- and post-curing times on the cytotoxicity of unreacted vinyl groups in the polymer-based composite in *in vitro* cell culture before and after leaching and polishing the composites, and to identify the major components that might be responsible for cells reactions. The work pertaining to this goal will be presented in Chapter V.

1.2 Literature Review

Dental composite resins were developed in 1957 by R. L. Bowen and are now extensively used in dental and some medical applications. They are now generally used for orthopaedic implants and restorative dentistry as anterior restorations. The composite materials consist of different resin systems, which are now available with different monomers and monomer combinations [8, 25]. They also contain filler particles made from a variety of ceramics, which are available in different particles sizes [25, 96]. In addition, they contain compatible organofunctional silane with a variety of organic groups and a variety of different functionalities on the silicon atom. This variation results in a wide compositional range of biomaterials [65, 66].

1.2.1 Chemical Aging

The use of radiant energy to initiate polymerization by free radical formation was a major development in composite technology. Early methods of initiation used ultraviolet (UV) light, but UV light as an initiator is potentially biologically damaging to both patient and operator, and the development of visible light systems was a significant advancement [17]. The mechanisms of free radical polymerization are

discussed in the literature [12, 36, 70, 114]. In particular, the free radical polymerization mechanism of urethane dimethacrylate (UDMA) resins used in this research is discussed in [25, 26, 27].

Briefly, in the visible light systems, a photoinitiator system based on a diketone and a reducing agent are used to initiate the polymerization. An example of a diketone, which absorbs blue light with wavelengths of 450 to 600 nm, and a reducing agent are camphoroquinone and N,N dimethylaminoethylmethacrylate, respectively. In such system, the radiant energy of blue light with a wavelength of 560 nm excites the diketone and transforms it to a triplet state. The excited diketone then combines with the reducing agent to form an exited state complex called exiplex. This complex breaks down to give reactive free radicals that initiate the polymerization reaction in the monomer system. However, due to the presence of oxygen and of polymerization inhibitors, which prevent premature setting during storage, the free radicals do not commence the polymerization of the system until the inhibitor is consumed by reacting with the free radicals. When most of the inhibitor is consumed, the polymerization of the methacrylate moities starts, leading to the growth of a chain, the end of which is a free radical. At the initial stages of polymerization, a rapid build-up in viscosity and a consequent reduction in molecular mobility result in a drastic reduction of the rate constant for termination. This effect results in an acceleration in the rate of polymerization and an increase in the molecular weight of the newly formed radical chains. At a later stage in the polymerization, the polymer reaches the glassy state and the molecular mobility of the methacrylate moities decreases which results in a drastic decrease of the rate of the reaction. Thus, the growing chain radicals may react with other chain segments, other free radicals, or other species to either terminate the reaction or form a new radical species. Schematics of

the free radical polymerization reactions are presented in Figure 1.1.

The presence of unreacted double bonds causes continual resin curing, and they have been shown to react with time [57]. Experimental evidence of resin curing have been documented in several ways in literature. For instance, self-curing up to 50 days after initiation was attributed to the existence of free radicals in methyl methacrylate resins [88]. Sample hardness with time was also been followed for half a year and increases of hardness were noted in areas of lower hardness, which were attributed to either chemical and/or physical changes [69]. In another study, sample hardness was noted to increase, until it reached a plateau in 24 hours [58]. In addition, hardness was observed for one month and a slow continual increase was also noted in another study, which was attributed to an increase in cross-linking of the composite resin [108]. Further, numerous investigators have shown that polymerization does not proceed to 100 percent conversion, and unreacted double bonds were as high as 74% in commercial resins [89, 105]. The incomplete conversion of different systems was related to the formulation of the composite resins [86]. The effect of post-curing of composite resins has been also reported by many other investigators [45, 54, 108].

1.2.2 Organic-Inorganic Interface

Curing of the resin may also be affected by the incorporation of inorganic fillers and by the introduction of organofunctional silane coupling agents. The incorporation of the filler may lead to insufficient polymerization, while the silane coupling agents, which are used to chemically bridge the filler and the resin, may improve polymerization by increasing the wetout phenomena of the filler by the resin. The silane bond should be permanent and reliable, especially in a severe biological environment.

Free Radical Polymerization Mechanism

Photo-initiation:

$$I \xrightarrow{h\nu} I^*$$

$$I^* + D \longrightarrow R.$$

where, I is a photo-initiator, I^* is an activated species, D is a photo-reducer, and R. is a free radical.

Inhibition:

$$R. + X \longrightarrow RX.$$

where X is an inhibitor.

Propagation:

$$R. + M \longrightarrow RM.$$

$$RM. + M \longrightarrow RM_2.$$

$$RM_n. + M \longrightarrow RM_{n+1}.$$

where M is a methacrylate moiety.

Termination:

a) Disproportionation

$$RM_n. + RM_m. \longrightarrow RM_n \text{ (saturated)} + RM_m \text{ (unsaturated)}$$

b) Annihilation

$$RM_n. + R'M_m. \longrightarrow RM_n M_m R'$$

c) Transfer

$$RM_n. + MH \longrightarrow RMH + M.$$

Figure 1.1: Free radical polymerization mechanism reactions.

The incorporation of the inorganic phase in the light-cured composite may also lead to insufficient polymerization and modify the effect of post-curing in the polymer matrix. For example, the quantity and type of filler was noted to affect the degree of conversion of the composite [86]. Also, transparent filler, which is used usually in light-cured composites, was observed to scatter the light at the organic-inorganic interface. This light scattering reduces the depth of transmission [26], increasingly severely as the surface area and volume fraction of the filler increase. In addition, filler incorporation has been shown to restrict the polymer molecular motion by absorption of the polymer onto its surface, as reflected by Differential Scanning Calorimetry (DSC) measurement of the glass temperature [38]. Although there are discrepancies in the literature regarding the effect on the glass transition temperature (T_g) by incorporation of fillers into polymers [75], many researchers reported significant changes in the T_g of the polymer by addition of filler [38, 47].

Silane coupling agents are dual-function molecules that consist of a non-hydrolyzable organofunctional group (R) at one end and a hydrolyzable group (X) at the other end. The two groups bind predominantly chemically, to both resin and filler [30, 76, 80]. The R group enables the organofunctional silane to bind to the organic resins and polymers, while the X group, which may typically be an alkoxy, acyloxy, amine or chlorine group, enables the silane to bind to the filler. Thus, the silane molecule is capable of reacting with both organic and inorganic substances and function as a coupling agent to join the two. At the silane-organic interface, the R group of the silane binds covalently to the reactive species in the polymer matrix. Thus, proper selection of the silane type to be employed becomes a matter of matching the silane functionality to that of the organic phase. At the silane-inorganic interface, however, the silane typically binds to the inorganic surface with high degree of ionic character.

That is, when the silane hydrolyzes to silanol it condenses with the silanol and oxide functional sites on the filler surface, linking the molecules to each other and to the filler surface by siloxane bonds. In addition, the silane may hydrolyze and condense to oligomeric siloxanols that are soluble initially, but ultimately condense to rigid cross-linked structures. If the siloxanols are soluble enough, they may be compatible with the liquid matrix and form a copolymer during resin curing. Alternatively, the siloxanol layer may also form an interpenetrating polymer network, as a result of both the resin and siloxanol curing separately. Finally, between the two interfaces, the silane forms a film which is thicker than a monolayer, which appears to be a polysiloxane network along with small polysiloxane molecules. The silane seems to form granules of high density polymer, which are separated by narrow boundary regions [96]. Schematics of organofunctional silane mechanism at the organic-inorganic interface are presented in Figure 1.2.

Although adhesion is the central function of the coupling agent, there are many factors involving the silane modifications of the interface that change the properties of the composite. The first factor is the reduction of the absorption of the amine by the filler and the reduction of the filler inhibitory action on the curing of the resin [77]. The second factor is the protection of the filler surface from fracture, and strengthening the boundary layer of the resin, so failure will not occur at the interface [80]. The third factor is the modification of the rheology of the polymer mix by changing wet-out, dispersion of filler particles, and viscosity [79].

In the biological environment, exogenous chemicals such as water may contribute to the failure of the composite clinically [92, 93, 94, 95]. Water hydrolyzes the siloxane bonds as it reaches the interface, which has been attributed to a decrease in the activation energy to initiate hydrolysis of the Si-O. This does not occur in a dry

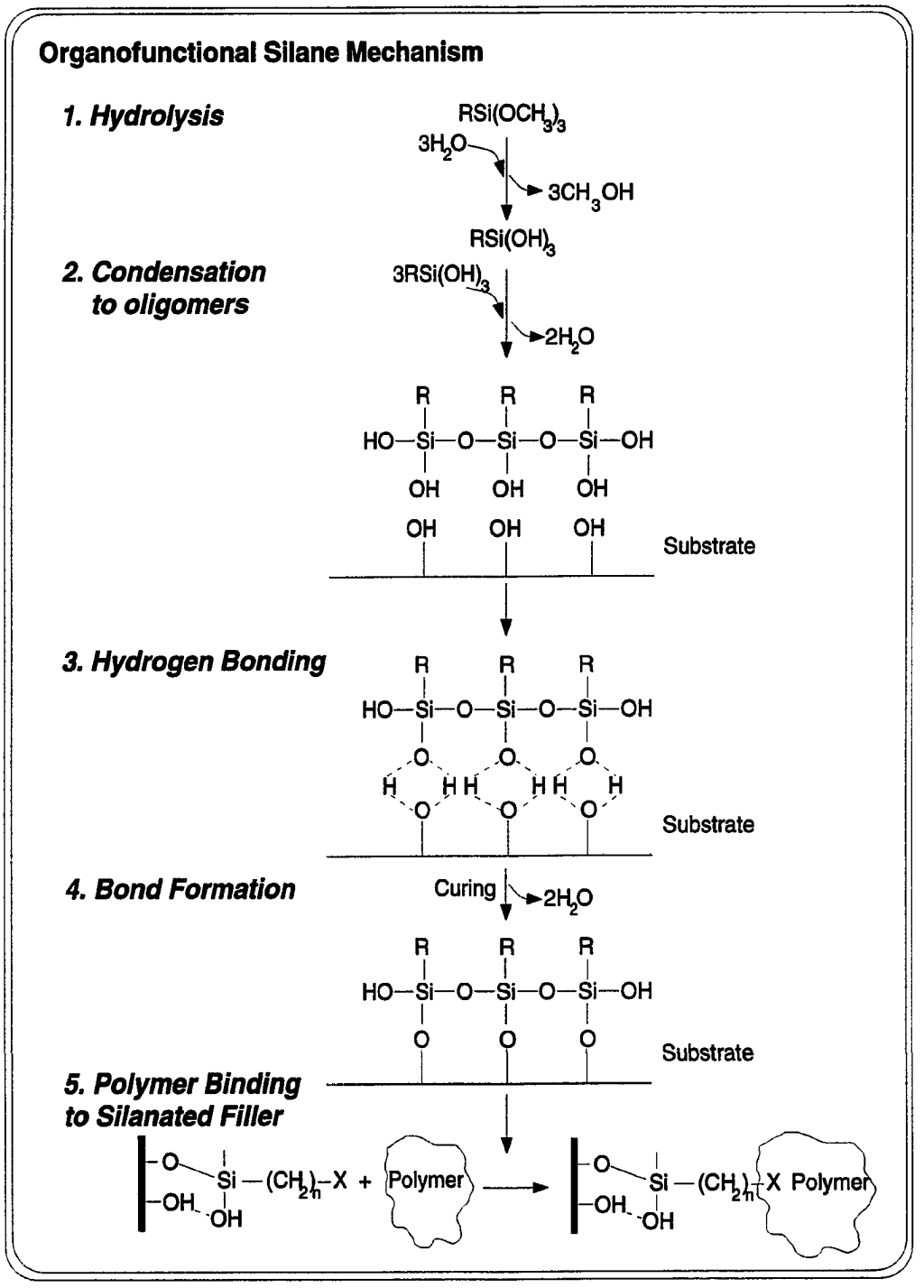

Figure 1.2: Silanation mechanism of organofunctional silane at an organic-inorganic interface.

environment [96]. Hydrolytic degradation, may cause the breaking of the chemical bonds in resin [10, 37], but it may also cause a softening through the plasticizing action of water [80]. In addition, water may attack the filler surface and cause leaching of composite elements in the presence of silane film [92, 93, 94, 95].

1.2.3 Biocompatibility from Insufficient Polymerization

A great concern has developed about the biocompatibility of incompletely polymerized composite resin with oral and other body tissues. Composite resins have been shown to cause cytotoxic effects using *in-vitro* cell culture tests, which resulted from residual uncured monomers or oligomers [83]. The extraction of the unreacted components decreased the cytotoxic effects by about 90 % . Also, composites (Silar) were shown to elute 50 % of its leachable species within three hours of soaking in water, while 75 % of its leachable molecules were shown to be eluted into a mixture of water and ethanol [35]. Most of the composite's leachable components were eluted within a 24-hour period in either solvent. Further, eleven components of restorative resins were tested for their cytotoxic effects on DNA synthesis, total protein content, protein synthesis of a cell system and the concentration at which these effects caused irreversible inhibition of these metabolic parameters [44]. The cytotoxicity by these components were reported as the concentrations that inhibited either 10 % (LD_{10}) and 50 % (LD_{50}) of the metabolic processes, and the range of concentrations where cell metabolism was inhibited. Ethoxylated Bis-phenol A dimethacrylate was the most toxic molecule of the group, where the LD_{50} was between 1 and 10 $\mu mol/L$, while the LD_{50} concentration for the resin used in this research, UDMA, was between 10 and 100 $\mu mol/L$.

1.2.4 Evaluating the Degree of Polymerization

The following section discusses the methods used in previous investigations to evaluate the degree of polymerization. Further, the method used in this research as well as its applicability and previous attempts will also be discussed in this section.

Evaluation methods to examine the degree of polymerization include either measurement of the amount of unreacted double bonds directly, or indirectly by measuring a physical property related to the degree of polymerization. One of the earliest direct methods used was transmission infrared (IR) spectroscopy, which was used by Ruyter and coworkers to determine the extent of polymerization in dental sealant [86, 87]. The IR technique, however, is inadequate for the determination of the degree of the polymerization in composite resins, because the inorganic filler interferes with the carbon double bond absorbance region. Therefore, Multiple Internal Reflection (MIR) infrared spectroscopy has been used as an improved method to determine the amount of unreacted double bonds in light-cured and chemically-cured composites [88]. This technique has been also used at the interface of conventional and microfilled composites. It has shown a residual saturation of carbon double bonds from 24 to 74 % [105]. Fourier Transformation Infrared (FT-IR) spectroscopy is another method used to determine the remaining double bonds [22]. In addition, Differential Scanning Calorimetry (DSC) has been also used to determine the degree of conversion of thermally activated as well as chemically activated polymerizations [6].

One of the indirect methods was to correlate the monomer conversion with surface hardness. For example, surface hardness was used by Johnson and coworkers to evaluate the effects of post-irradiation polymerization rate and the initial polymerization on the final polymerization of the light-cured composites [58]. It was also

used to determine the effect of filler size and level on the depth of cure [59]. In addition, this technique has been used by many researchers to evaluate and determine the degree of vinyl polymerization [21, 45, 84, 108], while others have used other physical properties to evaluate curing, such as viscosity and contact angle measurements [105].

Microcalorimetry offers a convenient, sensitive, direct and accurate method of measuring the rate of enthalpy changes of the reaction under isothermal conditions as a function of time at the annealing temperature of the sample. For example, solution microcalorimetry was used to measure the changes in excess enthalpy isothermally, which was demonstrated to be highly sensitive without the complication of the dynamic factors that may occur in DSC [67]. However, the operational procedure is complex and time consuming, and a typical run takes 2 to 3 hours of set-up, 1 to 3 hours of equilibration and 2 to 3 hours of measurement. A Tian-Calvet Microcalorimeter has also been used to measure the rate of excess enthalpy changes in pressure-densified polystyrene [112].

In the current research, microcalorimetry was used to examine the extent of the reaction due to curing by means of the Tian-Calvet apparatus. This apparatus was conceived in 1920-1932 by A. Tian and was developed since 1932 by E. Calvet [112]. In this technique the rate of heat production (rate of enthalpy change) by the process under investigation was measured at each instant of time. Such a technique offers a direct and continuous measurements of the heat of reaction without knowing the heat capacity of the material. In addition, it is used for rapid reactions as well as long duration measurements. However, one problem with this technique is the requirement of a long time to reach instrumental equilibration.

1.2.5 Evaluating the Organic-Inorganic Interface

Many techniques are available to evaluate the interface in composites, such as x-ray photoelectron spectroscopy, contact angle and electroosmosis measurements. To evaluate the interface in this research, the dielectric methods was used to measure polymer transitions and relaxations in highly filled polymers, where a significant portion of the total polymer molecules are adjacent to solid interface. Although the theories of dielectrics and dielectric dispersions are discussed and reviewed thoroughly in the literature [20, 47, 71, 91], a brief discussion will be presented, followed by reviews of some of the previous work relevant to this research.

Dielectric relaxation is the exponential decay with time of the polarization in a dielectric when an applied electric field is removed. It involves orientation of dipoles that exist in the material which depends on the structure of the molecules and the molecular rearrangement of the dielectric in response to an alternating electric field (AC). When an AC is applied to a polymer placed between two parallel plates, the material reacts to the field by storing charges and becoming polarized. Such polarization is a function of electronic, atomic and orientational components. At low frequency AC all of these components can react, while at extremely high frequencies none can react. Gross overall dipolar motion or chain segment motion in polymers occurs at relatively low frequencies (10^{-4} to 10^{5} Hz) [91]. If the applied AC frequency is above these values, dipolar motion can no longer follow the field.

Since the dielectric measurements can be applied over fourteen decades of frequency, one single method cannot be used to measure the entire range, so there are different methods for measuring the frequency responses in particular frequency regions. However, this discussion will concentrate on the frequency bridge method because most of the dielectric work on polymers and the work in this research has

been performed in this frequency region. This method is divided into two parts, the lumped and distributed circuit. The lumped circuit method covers frequencies from about 10^{-4} to 10^{8} Hz, while the distributed method works in the frequency range of 10^{8} to 10^{10} Hz [110]. The former method is based on the measurement of equivalent capacitance and resistance at a given frequency, whereas the later is designed to measure the attenuation factor α and the phase factor β at a given frequency [110].

As stated above, since the dielectric measurements on polymers is confined to the frequency range of 10^{-4} to 10^{6} Hz [91, 110], the lumped circuit method is used. In this technique, a polymer sample is placed between two parallel electrodes and regarded as being electrically equivalent to a capacitor, C, in parallel with a resistance R, at a given frequency. As in Figure 1.3(a), the capacitance of a vacuum-filled parallel plate capacitance is given by

$$C_o = \frac{A\epsilon_o}{d} \tag{1.1}$$

where A is the plate area, d is the plate separation, and ϵ_o is the absolute permittivity of free space. In the polymer filled capacitor (Figure 1.3(b)), the capacitor is given by

$$C = \epsilon C_o \tag{1.2}$$

where C and C_o are the capacitances measured with sample 'in' and sample 'out' of the charged capacitor plates, respectively, and ϵ is the relative dielectric permittivity, which is also known as the dielectric constant.

For an ideal capacitance in the frequency domain, applying a steady state AC electric voltage in the form of $V(\omega) = V_o \exp(i\omega t)$ would show that the charging

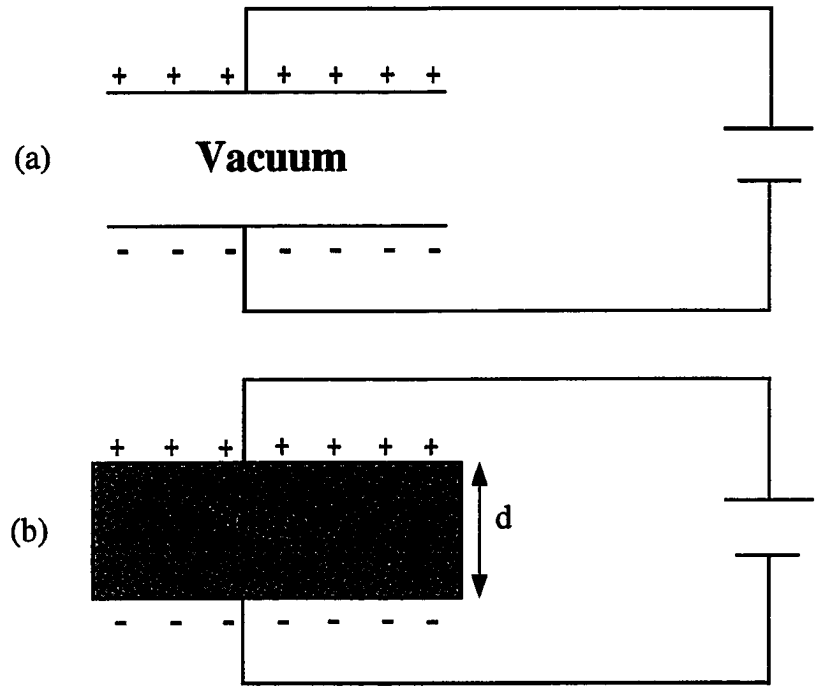

Figure 1.3: Simple capacitor apparatus (a) without and (b) with dielectric material.

current $I(\omega)$ is 90° out of phase with the applied voltage, where $I(\omega)$ is given by

$$I(\omega) = i\omega\epsilon^* C_o V(\omega) \tag{1.3}$$

Such behavior is not achieved by real dielectric materials due to the dielectric relaxation and DC conductivity. This leads to a time dependence of the permittivity measured in the time domain and becomes a complex quantity in the frequency domain. The time domain dependence is given by

$$\epsilon(t) = \frac{C(t)}{C_o} \tag{1.4}$$

and the frequency domain dependence is given by

$$\epsilon^*(\omega) = \epsilon'(\omega) - i\epsilon''(\omega) \tag{1.5}$$

The complex quantity is composed of an out-of-phase capacitor current (storage current) $I_C(\omega)$ and an in-phase resistive current (dissipative current) $I_R(\omega)$. A vectorial diagram of these two $I(\omega)$ components in relation to the voltage $V(\omega)$ are shown in Figure 1.4. The capacitive current component is orthogonal to the applied voltage, while the resistive component is in-phase with the applied voltage. The total current is given by the following

$$I(\omega) = I_R(\omega) + I_C(\omega) \tag{1.6}$$

with its components are described by the following

Lumped Circuit Analysis of Dielectric Filled Capacitor

Applied voltage : $V(\omega) = V_0 \exp(i\,\omega\,t)$

Resulting current : $I(\omega) = i\,\omega\,C_0\varepsilon^*\,V(\omega)$

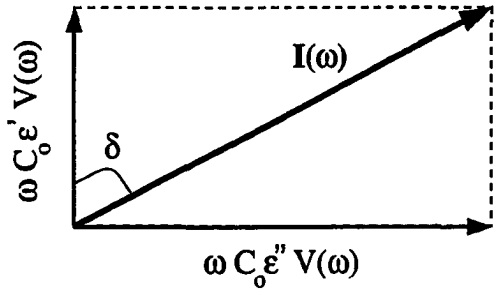

Figure 1.4: Vectorial representation in the complex plane of the current-voltage relationship in sample-filled parallel plate capacitor.

$$I_C(\omega) = i\omega\epsilon' C_o V(\omega); \qquad I_R(\omega) = \omega\epsilon'' C_o V(\omega) \tag{1.7}$$

where ϵ' and ϵ'' are the permittivity and the dielectric loss, respectively.

It follows that the energy measures the alignment of dipoles, and the energy required to align dipoles and move ions is proportional to the dielectric loss factor, which is expressed in terms of $\mathrm{Tan}(\delta)_\epsilon$ given by

$$Tan(\delta)_\epsilon = \frac{\epsilon''}{\epsilon'} = \frac{loss\ current}{capacitor\ current} \tag{1.8}$$

The loss factor is made up of relaxation, space charge conduction processes and DC conductivity of the material and is given by

$$\epsilon''(\omega) = \epsilon''_r(\omega) + \epsilon''_\sigma(\omega) \tag{1.9}$$

where $\epsilon''_r(\omega)$ takes the form of a bell-shaped curve and $\epsilon''_\sigma(\omega)$ shows a rising loss at the lowest frequency, when ϵ'' is plotted against $\log(f)$. The classical development of the relations between ϵ', ϵ'', dipole moment, molecular size, and viscosity of the dielectric were formulated by Debye and are reviewed by some researchers [20, 47, 91].

In multicomponent systems, additives may be divided into two main groups: compatible and incompatible. In the first group, the additives do not form a separate phase in the polymer compound, which results in a homogeneous compound to some degree. Such additives are referred to as compatible additives. The expected dielectric features of these additives are: the glass transition (α peak) shifts position for different polymer-additive systems of different polarity, as in Figure 1.5; and with increasing additive concentration, the oscillator strength ($\epsilon_0 - \epsilon_\infty$) changes, where ϵ_0

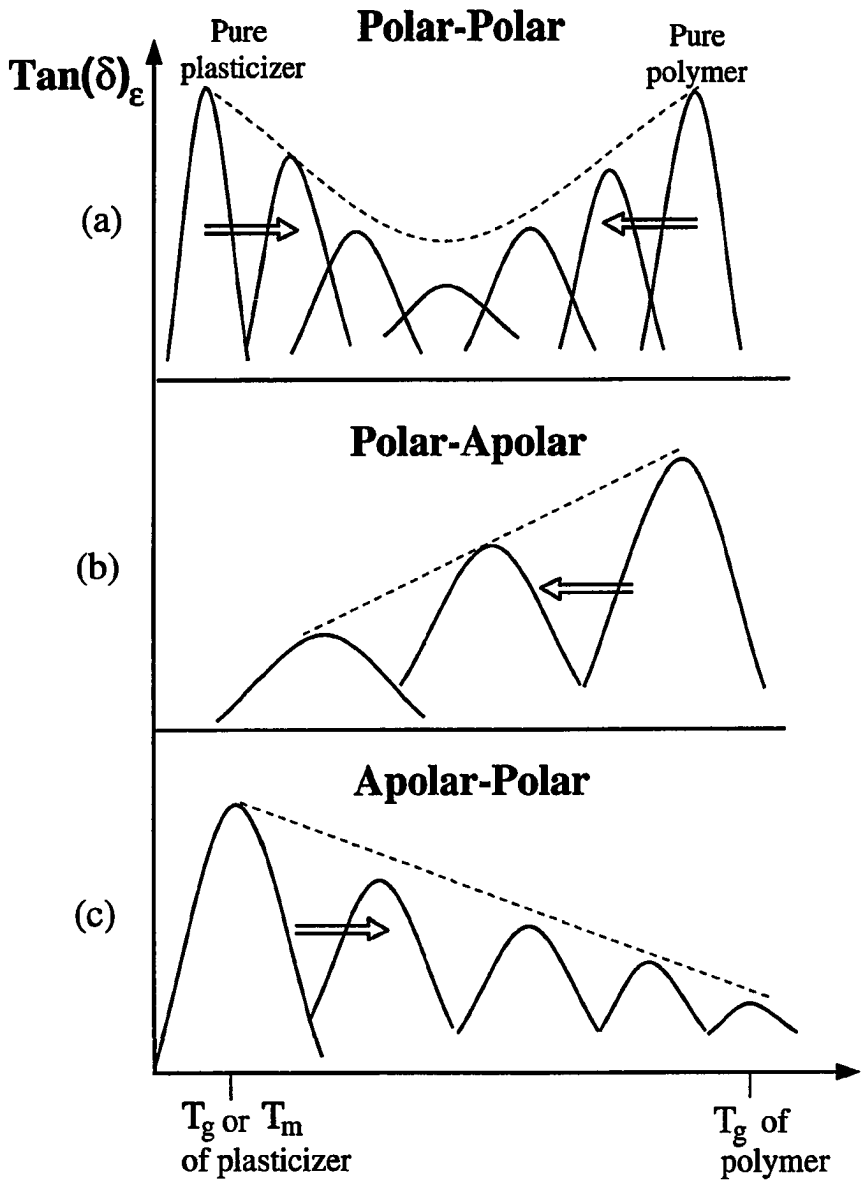

Figure 1.5: Expected shifts of the dielectric α—transitions for polymer-plasticizer systems of different polarity [47].

and ϵ_∞ are the relaxed and unrelaxed permittivities, respectively, and the dielectric band width also changes [47].

In the second group, the additives form a separate phase that results in a heterogeneous system. These additives are referred to as incompatible additives (examples are fillers and dyes). The dielectric behavior of heterogeneous systems has an additional type of polarization, interfacial polarization, which is determined by Maxwell-Wagner-Sillars (MWS) polarization. This polarization arises, for a two phase heterogeneous dielectric, when the product of the dielectric constant of one phase ϵ_1 and the conductivity of the second phase σ_2 is unequal to the product of the dielectric constant of second phase ϵ_2 and the conductivity of the first phase σ_1 [20, 47, 91]. This results in an accumulation of charges at the interface, which occurs as a distinct relaxation peak. Such accumulation of charges requires a flow of current within the phases, which requires seconds or minutes. The observation of MWS, therefore, can normally only occur at very low frequencies and involves high dielectric permittivity (ϵ') and loss (ϵ'') values [47]. However, if one phase such as water occlusion has a high conductivity, the MWS polarization may occur at very high frequencies. Models for MWS have not been completely developed, but they have been addressed in the literature by researchers [20, 39, 47, 106].

Although inorganic phases are considered to form a heterogeneous system with polymers, their expected dielectric features were shown by investigators to resemble those of the homogeneous mixtures. For instance, filled polymers did not form MWS polarization that characterizes the interface, rather their $\alpha-$ and $\beta-$relaxations shifted to higher and lower temperatures, respectively as shown by Lipatov and Fabulyak [62]. Such behavior was attributed by these investigators to restrictions of the motion of the backbone by the solid surface which caused a loosely packed

layer where the side chains can move freely. In addition, in silane-treated bead composites the α-relaxation shifted to a higher temperature, while it shifted to a lower temperature in elastomer-coated filler composites as was shown by Lacabanne *et al.* [56]. The former behavior was attributed to a decrease of chain mobility due to linkages between the silane at the matrix-filler interface, while the later was attributed to plasticization of the matrix by the elastomer. Further, in carbon fiber composites the β-relaxation was shifted to a lower temperature as compared to the non-reinforced matrix which was associated with a lower degree of matrix curing in the presence of the fiber [56].

Few observations of the MWS transitions in experiments have been documented in the literature, and some problems associated with observing them have also been discussed [46, 104]. The loss peaks, due to conductivity and dielectric constant, must be measurable and fall in the appropriate frequency range. In addition, the shape of the conductive occlusions must be well determined for successful analysis, as Aldrich and coworkers [1] report from Sillars. In general, ideal cases of MWS are rare. Occlusion of water in polymer may also give MWS relaxations; however up to the present, most of MWS relaxation due to interfacial polarization has been observed in water-in-oil (W/O) emulsions [39, 40]. However, it has not been observed in oil-in-water (O/W) emulsions [41]. This observation is attributed to the fact that dispersions of dielectric constants and conductivites are too small to be observed in O/W emulsions and are considerable in W/O emulsions [39]. The MWS loss peak has recently been reported to be in the 10^2-10^5 Hz frequency range in a hollow glass based thermoset [1], which indicates MWS might be valuable for monitoring the inorganic-organic interface in the composites.

1.3 Organization of the Dissertation

This dissertation presents some detailed examination of a 'dental-medical' synthetic polymer, urethane dimethacrylate (UDMA). Such examination involves chemical, physical and biological characterization of this polymer. Chapter II examines the rate of enthalpy changes of continual curing of resin (chemical aging) as a function of different curing times using a microcalorimetry method. This chapter also examines the effect of filler incorporation and filler surface modification with organofunctional silane on the continual curing of resin. Chapter III discusses the identification of molecular transitions of UDMA by a dielectric method. It also discusses the effect of polymer-filler interaction by examining the effect of the inorganic filler on the molecular transitions. In addition, this chapter examines the effect of filler surface modification by the organofunctional silane on these interactions. Chapter IV presents the effect of moisture on the polymer and on the polymer-filler interface. Chapter V examines the cytotoxic effects of unreacted vinyl groups in the composite using an *in vitro* cell culture technique. Finally, chapter VI contains summary and conclusions of this research.

CHAPTER II

THE EFFECTS OF DIFFERENT CURING TIMES AND FILLER CONCENTRATION ON CURING AND POST-CURING OF URETHANE DIMETHACRYLATE COMPOSITES: A MICROCALORIMETRIC STUDY

2.1 Introduction

In polymer-based composites, the properties of the organic matrix strongly influence the behavior of the composite material. The long term stability of the matrix, therefore, is an important aspect of composite performance [60] and is highly dependent on the extent of the polymerization during the cure. For instance, inadequate cure and the presence of unreacted chemicals in the composite resin used in a highly reactive biological environment may lead to major clinical problems such as slow degredation, color instability, poor durability and loss of anatomic form. In addition, the presence of the unreacted monomer and oligomer leads to plasticization effects (lowering of the glass temperature), which causes changes in the physical as well as the mechanical properties of the biomaterial.

Curing with time (chemical aging) in light cured composites is caused by a continual conversion of unreacted groups in the difunctional vinyl monomers during polymerization and over long periods of time. This reaction is a highly exothermic

process, and the heat liberated tends to raise the local temperature and accelerates the curing reaction.

The mechanism of free radical polymerization of vinyl monomers can be divided into three stages; an initial stage in which the rate of polymerization decreases; an intermediate stage in which the polymerization increases and is defined as autoacceleration, which is known as the the gel effect; and a final stage in which the monomer is depleted. In the intermediate stage, the mobility of the system and the frequency of collisions decreases rapidly as the gel forms. In addition, since the frequency of the termination reaction is a function of the rate of their meeting other growing chains, the proportion of the termination reaction is decreased, while that of addition reaction is increased. The increase in the addition reaction causes more heat to be liberated and thus the structure rapidly becomes more rigid and the mobility decreases. The heat also increases the activity of the growing chains as well as the free radicals. This results in further densification of the structure and the formation of a glass. Upon further curing with time, diffusion of molecular segments of chains occurs, due to spontaneous evolvement towards equilibrium (physical aging), further increasing crosslinking of chemically unreacted groups. These crosslinks cause further spontaneous relaxations to occur. Thus, the physical aging and the chemical aging are mutually dependent [68].

Many factors may have catalytic effects on curing of the resin such as impurities, unreactive raw materials, catalysts, monomeric species, and additives such as filler. The effect of these agents is specific for each resin system. For examples, mineral fillers were found to have both positive and negative catalytic effect on the resin cure. Both silica and E-glass can reduce the exotherm in an epoxy resin-aromatic amine [77], while silane coupling agents may give higher exotherms and provides

composites with better mechanical properties and chemical resistance [78].

Although determination of the curing process of thermosets, particularly beyond the gel stage is very difficult, numerous methods have been used to investigate this process such as chemical and spectrographic methods. However, these methods have their limits and constraints to measure the extent of the curing process with time, since the continual cure involves a minute evolution or absorption of heat over a long duration. To detect these small changes with time accurately, an instrument with high sensitivity and long-term stability is required. Therefore, a Tian-Calvet microcalorimeter was used in this study to monitor these changes continously since it has been proven to be suitable for this kind of measurement [90, 112].

Therefore, the purpose of this portion of the study was to investigate the isothermal enthalpy changes with time for a dental composite that was cured for different curing times (chemical aging), and to investigate the effects of incorporation of filler on this process.

2.2 Experimental

2.2.1 Materials

Urethane dimethacrylate (UDMA) (Esschem Co., Essington PA) was used as a monomer system. Zirconia-silica (ZS) with a surface area of 1.6 m^2/g and an average diameter of 1.5 μm (3M Dental Products, St.Paul MN) was used as a filler. 3-methacryloxypropyltrimethoxysilane (MAPM) (Huls America, Piscataway NJ, formerly Petrarch Systems, Bristol PA) was used as a coupling agent to silanate the filler. MAPM was selected because it has been shown by Craig and Mohsen [28] to be one of the most effective silanating agents for increasing the dispersion and wetting behavior of the filler particles by the monomer, and has a carbon double bond to

react with the monomer.

2.2.2 Sample Preparation

The filler was silanated by depositing the silanes from aqueous solution of 75 % ethanol (190 % proof) to 25 % silane (weight ratio) as was described by Craig and Mohsen [28]. The amount of silane coupling agent (X) used for the filler treatment was based on the following relationship reported by Arkles [7]:

$$X = \frac{A}{w} f \tag{2.1}$$

where

X = amount of coupling agent in grams needed to obtain minimum uniform coverage,

f = amount of filler (g),

A = surface area of the filler (m^2 /g), and

w = wetting surface of silane (m^2 /g)[1].

Composites were formulated from UDMA, zirconia-silica and MAPM-silanated zirconia-silica, using *dl*-camphoroquinone catalyst and 2-dimethylaminoethylmethacrylate accelerator in concentrations described by Douglas, Craig and Chen [31]. The amount of silane used to treat the filler given by Equation (2.1), was three times the minimum uniform coverage (3X).

The mixed composite paste was placed in Teflon disc shaped molds (6.0 mm diameter x 3.5 mm thick) which were covered with glass to extrude excess material

[1] w numbers are listed for each silane in the Petrarch Systems catalog.

and prevent the formation of surface inhibited layer. The composite paste was made in two layers and each cured by visible light in a TRIAD II oven (Dentsply International,York, PA) for 13, 30, 90, 150 and 300 sec at room temperature. The weight percentages of the unsilanated zirconia-silica in the composite samples were 0, 15, 45 and 75 wt %, while it was 75 wt % for the MAPM-silanated zirconia-silica-filled UDMA samples.

2.2.3 Methods

Microcalorimetry apparatus. The enthalpy changes were measured to monitor the extent of cure in composites over long durations using a Tian-Calvet microcalorimeter. This instrument measures isothermally the heat evolution/absorption by continuously monitoring of heat flow from/to the material. Such instruments have been shown to be suitable for these kinds of measurements. Three Tian-Calvet microcalorimeters (Setaram, Lyon, France) were used in this portion of the study. A vertical cross section and the experimental assembly of the Tian-Calvet microcalorimeter is shown in Figure 2.1. The microcalorimeter itself consists of insulation, a thermostat, an aluminum block and a calorimetric element. The thermal insulation is the outside portion of the instrument, which insulates the system from the surroundings. The thermostat is next to the insulation which consists of concentric aluminum shells surrounded by an electric heating element and a thermoprobe. These aluminum shells distribute uniformly any thermal disturbances coming from the outside environment. In the middle of the aluminum block, two heat-flow detecting chambers are located symmetrically, one chamber for the sample while the other for the reference. Each chamber is surrounded by 496 serially-connected thermocouples that are electrically isolated from the walls of the chambers. The thermocouple banks are connected in

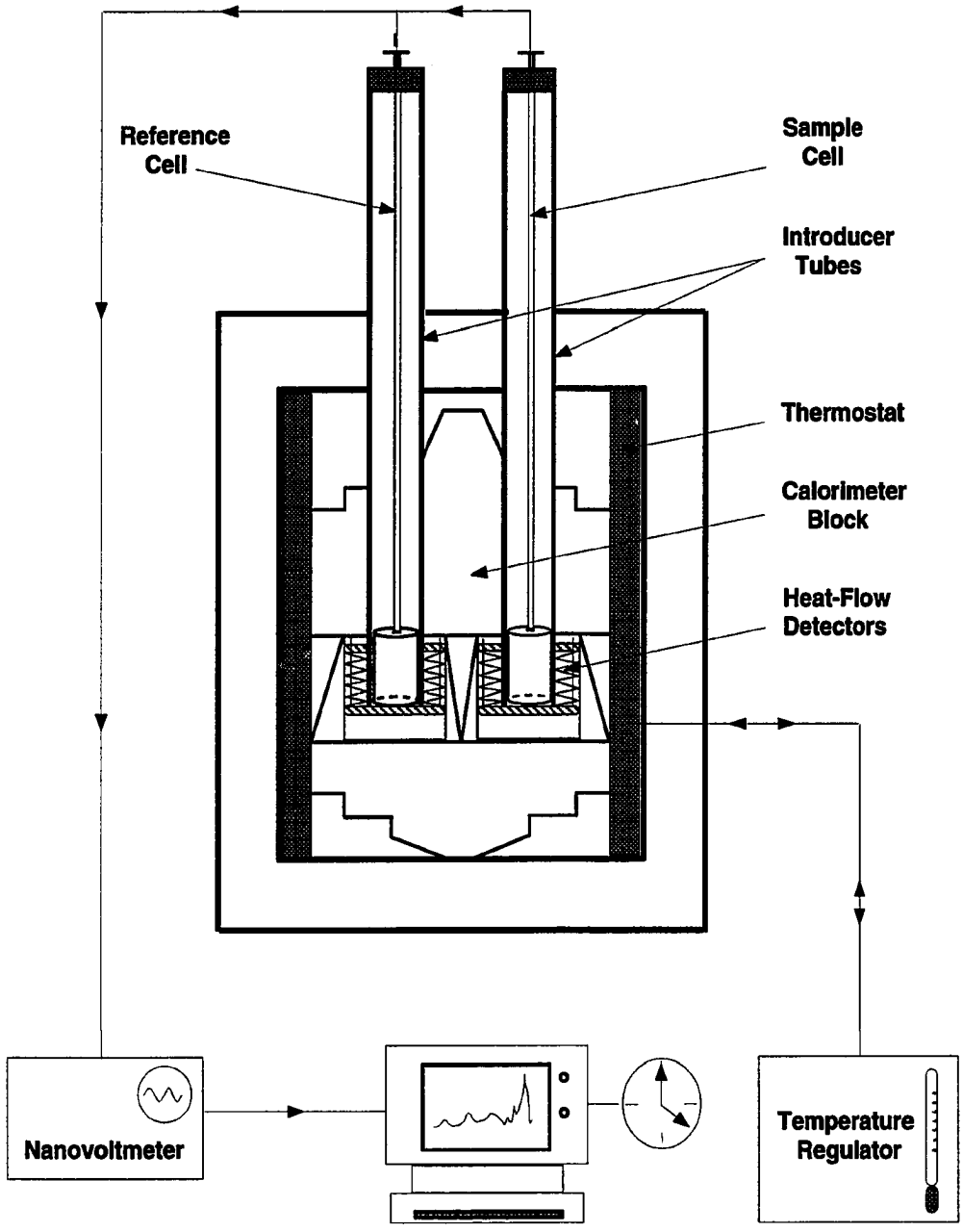

Figure 2.1: Tian-Calvet microcalorimeter cross-section and apparatus assembly.

opposition so that the thermal-voltage measured is the differential between the sample and the reference. The heat generated or absorbed by the sample or the reference is transferred between the block and the chambers by conductance of the thermocouples. Therefore, it is essential to have high conductance of the thermocouples for effective measurements which is accomplished by the existence of a large number of high thermal conductance thermocouples. These thermocouples are also uniformly distributed around the walls of the chambers to minimize any difference in conduction due to sample geometry and/or temperature inhomogeneity in the surrounding portion of the block.

The microcalorimeter is connected to a temperature regulator (PRT 3000 RA, Setaram, Lyon, France) for stabilizing the temperature of the thermostat for any chosen value between ambient to 200 °C with a sensitivity/stability of 10^{-3} °C. The apparatus is also connected to a nanovoltmeter (Model 181, Keithley), which detects the measurement of the calorimetric signal with a resolution of 10 nV. The microcalorimeter is interfaced with an automated data acquisition system based on a Macintosh II computer and LabVIEW (International Instruments) software programs. The entire assembly is placed in an air conditioned closed room to stabilize the ambient temperature to within ± 1 °C.

Enthalpy measurement. Due to a time delay required to reach thermal equilibrium between the sample and the calorimetric block, meaningful data cannot be obtained until some time after insertion of the sample, depending on the instrument temperature. Preliminary experiments were conducted to determine the temperatures and times needed for the resin to polymerize under heat, so the thermal equilibrium constraint could be accounted for. The UDMA resin was placed in glass tubes and kept in an oil path at a constant high temperature. A glass rod was used to stir the resin

constantly with a slow circular motion. The temperature at the time required for the resin to turn from a viscous liquid to an elastomer beyond the microcalorimetry equilibrium time was chosen as an instrument temperature.

Based on the preliminary results, the three microcalorimeters were set at temperatures below the T_g for the entire investigation. One instrument was set at 65.5 °C, another at 57.0 °C, while the third was set at 37.0 °C to resemble the biological (body) temperature. The thermal equilibrium for each instrument was determined by introducing equal amounts of ZS into both sample and reference cells and monitoring the time needed for the thermo-voltage to level off. Thus, the thermal equilibrium for the instruments were 3.3, 2.5 and 0.5 hrs at 65.5, 57.0 and 37.0 °C, respectively.

After reaching the temperature setting, the instruments were allowed to stabilize for at least a week before conducting any experiment. For each measurement, the sample cells, which were cylindrical in shape and made of stainless steel, were cleaned with soap and water and dried thoroughly. 1.5 - 2.5 g of specimen and a similar amount of reference material (ZS) were introduced into the sample and reference cell, respectively. Both cells were loaded into the calorimeter chambers simultaneously, the data acquisition program was invoked immediately and measurements were started instantaneously. The sampling rate varied during the course of measurement with shorter intervals at short times and longer intervals at long times. The measurement was ended when the thermo-voltage levelled off.

The measurements were recorded in the form of thermo-voltage ($\frac{dE}{dt}$) changes with time (t), that were detected by the thermocouples instantly and continuously. The correlation between the measured thermo-voltage and the actual rate of heat generated or absorbed by the samples was carried out by a calibration procedure to determine calibration factors for each instrument. Briefly, two calibration cells, each

with resistance of 1 kΩ that were supplied with the instrument, were simultaneously inserted into the sample and reference chambers. After the instrument equilibration, a known level of current was applied to the sample cell to generate a heat flow between the cell and the calorimetric block. When a steady state of thermo-voltage power was reached, the thermo-voltage readings were also leveled off to reach a constant value. The height of the change of the thermo-voltage that corresponded to the known current was recorded. A series of known current magnitudes were applied, which corresponded to different power generations, and resulted in different thermo-voltage values. Thus, a linear regression was established to determine the correlation between the thermo-voltage and the actual rate of heat generation. The slope of the regression line is the calibration factor k, which is given by

$$k = \frac{RI^2}{E} \tag{2.2}$$

where R is the resistance of the calibration cell, I is the magnitude of the applied current, and E is the height of the thermo-voltage between the two equilibrium states before and after the current application. For the three microcalorimeters used in this study, the values of k were 3.6364×10^{-6}, 3.944×10^{-6}, and 4.055×10^{-6} mcal/sec nV.

The $\frac{dE}{dt}$ versus t curves were converted into variation of enthalpy changes $(\frac{dH}{dt})$ versus t curves by using the calibration factors. In $\frac{dH}{dt}$ versus t curves, the baseline was determined by averaging the last fifty calorimetric points when the measured voltage became constant with time. The enthalpy changes (dH) versus time were determined by integrating $\frac{dH}{dt}$ from the equilibrium time to the beginning of the results. The extent of the reaction or *conversion* as a function of time was determined by integrating the isothermal curves, using the relationship

$$Conversion(\%) = \frac{100}{\Delta H_T} \int_o^t \frac{dH}{dt}\, dt \qquad (2.3)$$

where ΔH_T is total enthalpy change which is calculated from the integral of $\frac{dH}{dt}$ from $t = 0$ (begining of the measurement, i.e., when instrument thermal equilibrium is reached) to $t = \infty$ (end of measurement, i.e, when sample equilibrium is reached). The $\frac{dH}{dt}$ and dH as a function of time were reported per weight of the polymer in the samples.

2.3 Results

2.3.1 Rates of Enthalpy Change

In this study, isothermal enthalpy measurements were made using Tian-Calvet microcalorimeters to follow the reaction rates of UDMA, ZS-filled UDMA and MAPM-silanated ZS-filled UDMA cured for different length of time. These rates were also measured at different annealing temperatures. The rates of enthalpy changes and enthalpy changes are based on the weight of polymer in each specimen.

Curing Time Effects

The finite rate of enthalpy changes ($\frac{dH}{dt}$) for 13 - 300 sec light-cured UDMA polymer annealed at 37.0, 57.0 and 65.5 °C are plotted against annealing time (t) in Figures 2.2 - 2.4, respectively. Similar results were found for light-cured ZS-filled UDMA and MAPM-silanted ZS-filled UDMA cured at the same annealing temperatures. At 57.0 and 65.5 °C, the changes in $\frac{dH}{dt}$ for the 13 sec light-cured UDMA polymer and UDMA-based composite are lower than those for the 300 sec light-cured systems at short and long annealing times. Regardless of the annealing

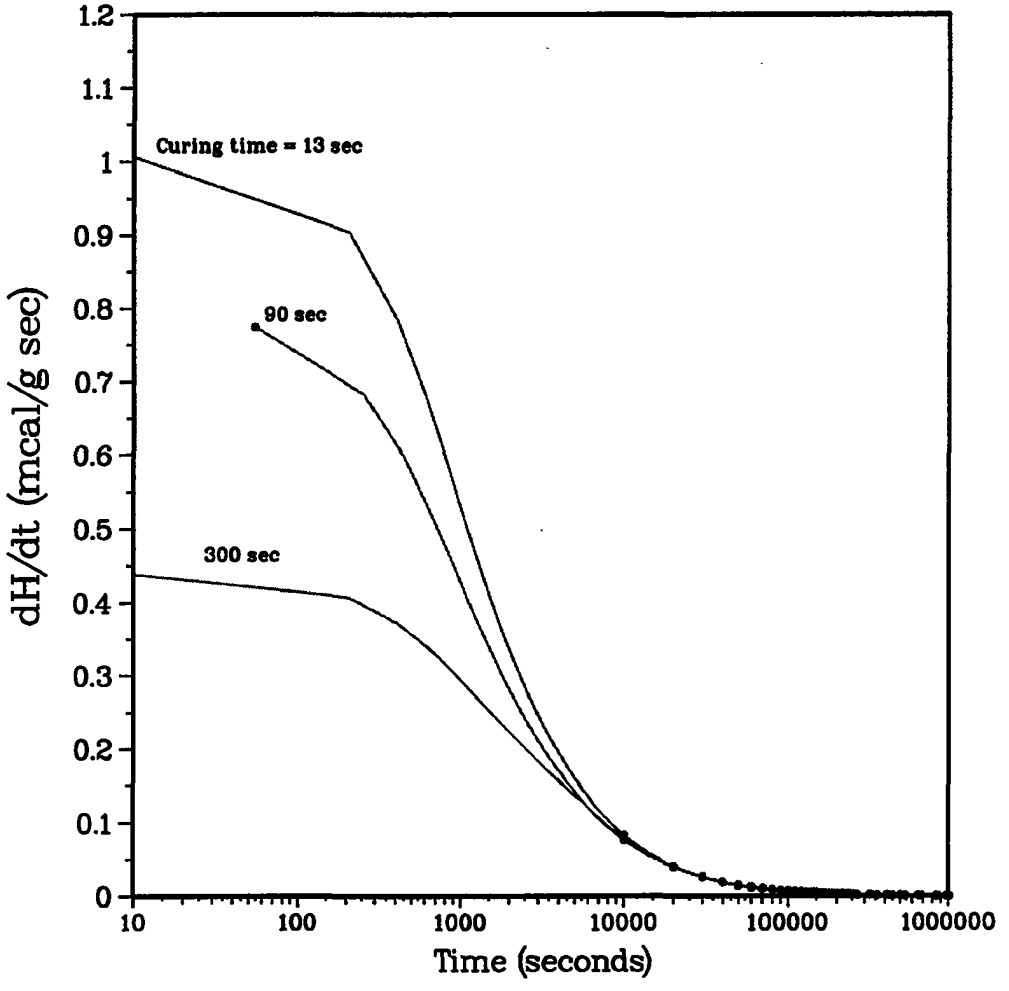

Figure 2.2: The rate of change of enthalpy (mcal/g sec) as a function of time (sec) for UDMA polymer cured for different length of time and annealed at 37.0 °C.

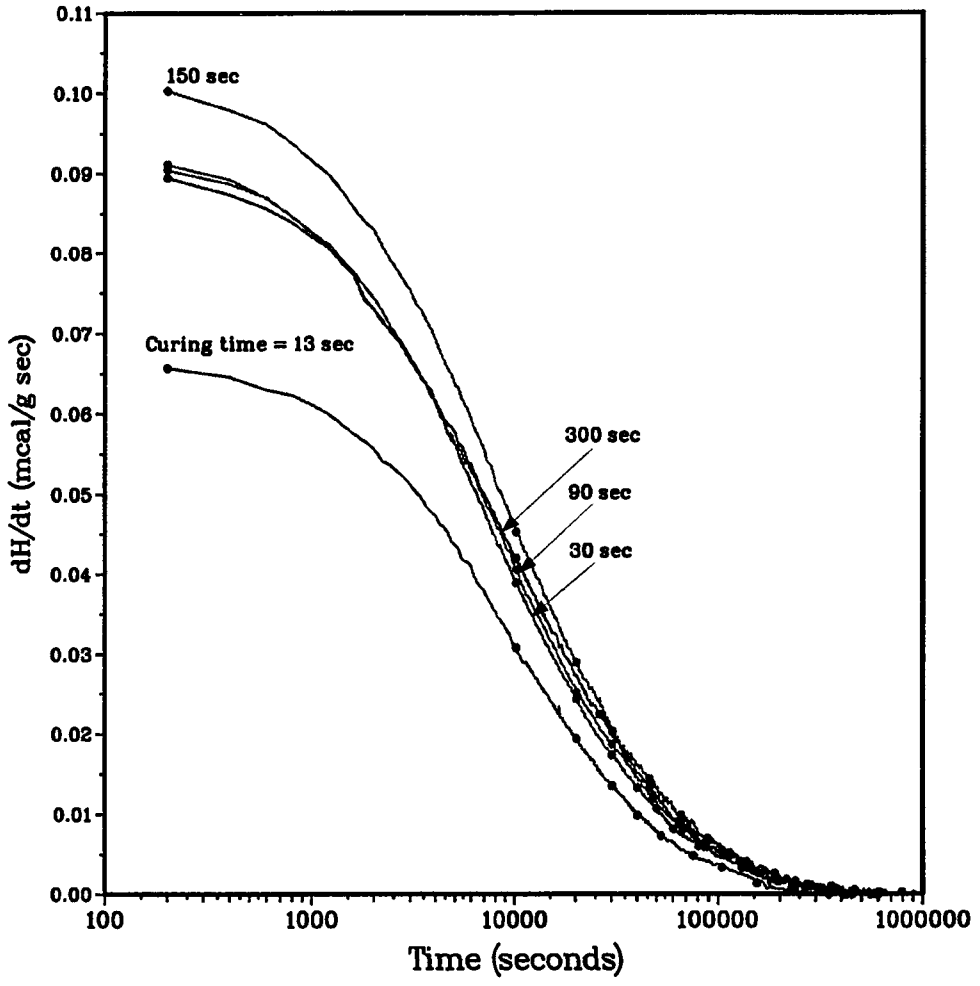

Figure 2.3: The rate of change of enthalpy (mcal/g sec) as a function of time (sec) for UDMA polymer cured for different length of time and annealed at 57.0 °C.

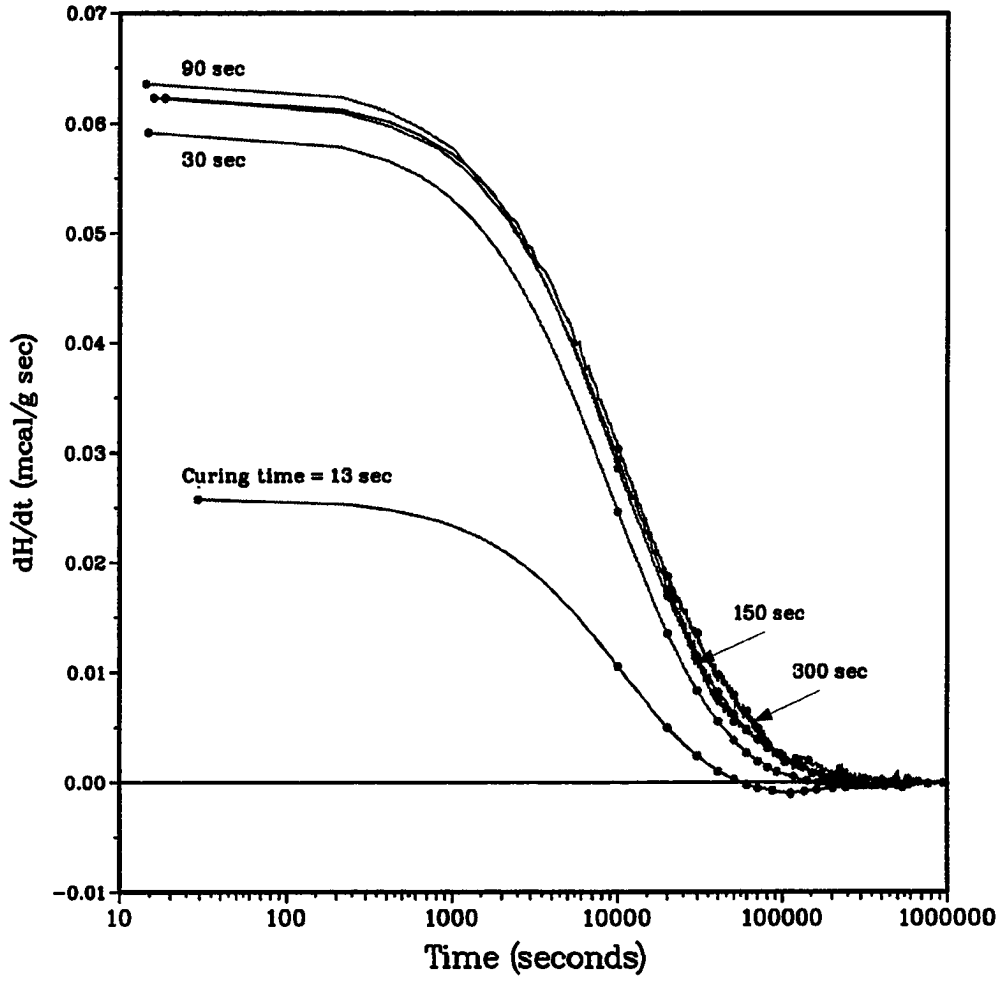

Figure 2.4: The rate of change of enthalpy (mcal/g sec) as a function of time (sec) for UDMA polymer cured for different length of time and annealed at 65.5 °C.

temperatures and the composite systems tested, the samples cured for longer periods with visible light reached apparent equilibrium faster than those cured for shorter times. For example, the UDMA polymer samples that were annealed at 57.0 and 65.5 °C and cured for 13 sec reached equilibrium at 4.5 x 10^5 and 4.0 x 10^5 sec, respectively, while those that were cured for 300 sec reached equilibrium at 4.0 x 10^5 and 2.4 x 10^5 sec at the same annealing temperatures, respectively, However, at 37.0 °C, the change in $\frac{dH}{dt}$ was higher for the composite systems that were cured for 13 sec than those cured for 300 sec. In addition, the equilibrium time was reached at 1.0 x 10^6 sec for UDMA polymer when cured for 13 and 300 sec, while it was reached at 3.5 x 10^5 and 5.5 x 10^5 sec for samples containing 75 wt % filler and cured for 13 and 300 sec, respectively. Further, the equilibrium time was reached at 5.0 x 10^5 and 1.0 x 10^6 sec for samples containing silanated filler when they were cured for 13 and 300 sec, respectively.

Filler Effects

The $\frac{dH}{dt}$ for 0 - 75 wt % ZS-filled UDMA and MAPM-silanated ZS-filled UDMA cured with visible light for 13 and 300 sec and annealed at 57.0 °C are plotted against t in Figures 2.5 and 2.6, respectively. Similar results were obtained for these systems at the different annealing temperatures. These results showed that the change of $\frac{dH}{dt}$ increased with increasing filler concentration in the composites, while the time required to reach apparent equilibrium decreased with higher filler content. For example, at 57.0 °C annealing temperature, the rate of $\frac{dH}{dt}$ increased from 2.2 x 10^{-6} to 3.5 x 10^{-6} for increasing filler incorporation from 0 to 75 wt % when the composite was cured for 13 sec, while the apparent equilibrium time decreased from 4.5 x 10^5 to 1.1 x 10^5 sec, respectively. In addition, the rate of change of $\frac{dH}{dt}$ increased in

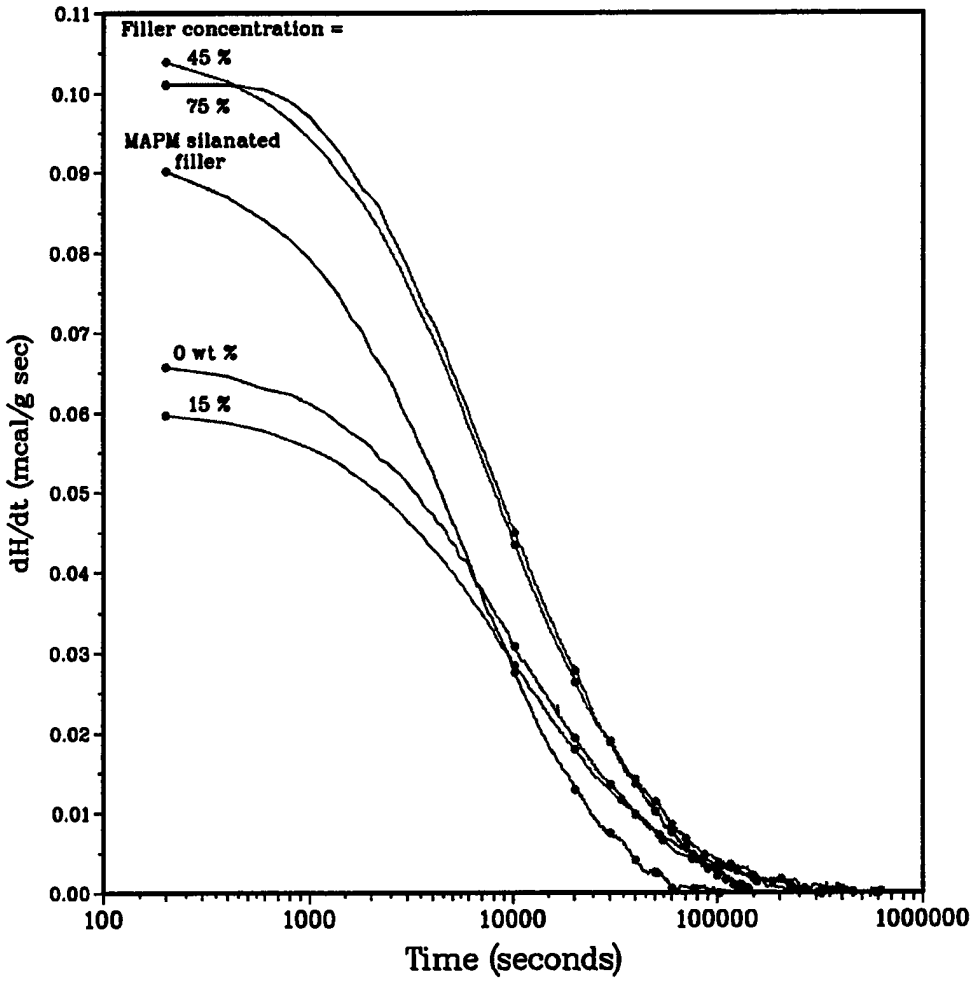

Figure 2.5: The rate of change of enthalpy (mcal/g sec) as a function of time (sec) for UDMA-based composites containing 0 - 75 wt % unsilanated filler and 75 wt % MAPM-silanated filler which were cured for 13 sec and annealed at 57.0 °C.

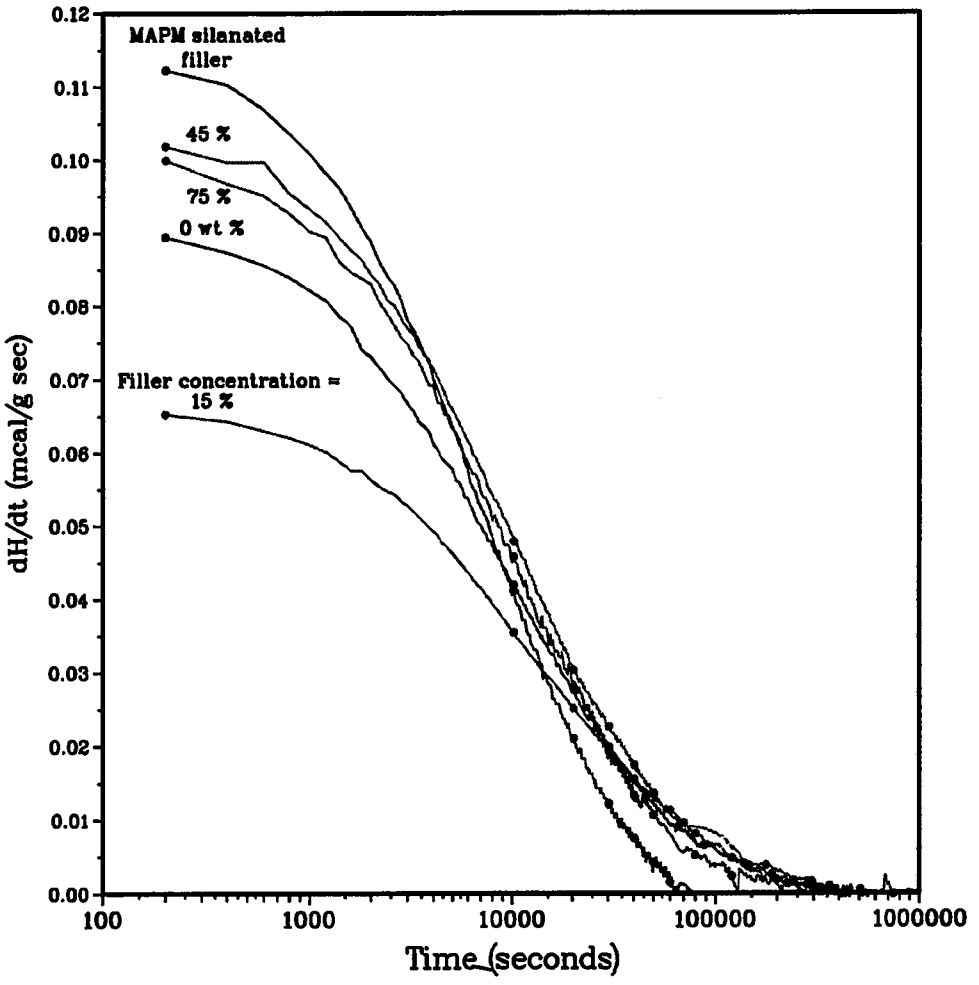

Figure 2.6: The rate of change of enthalpy (mcal/g sec) as a function of time (sec) for UDMA-based composites containing 0 - 75 wt % unsilanated filler and 75 wt % MAPM-silanated filler which were cured for 300 sec and annealed at 57.0 °C.

samples consisting of composites containing silanated filler and the time required to reach equilibrium also decreased in these samples. For instance, the rate of change of $\frac{dH}{dt}$ for samples containing 75 wt % silanated filler was 3.6 x 10^{-6} while it was 2.8 x 10^{-6} for samples containing 75 wt % unsilanated filler when the samples were cured for 300 sec and annealed at 57.0 °C. Further, the time required to reach apparent equilibrium decreased from 2 x 10^5 sec for samples containing 75 wt % unsilanated filler to 8 x 10^4 sec for samples containing 75 wt % MAPM-silanated filler.

Temperature Effects

The $\frac{dH}{dt}$ for 75 wt % ZS-filled UDMA and 75 wt % MAPM-silanated ZS-filled UDMA annealed at 37.0, 57.0 and 65.5 °C and cured for 13 sec are plotted against t in Figures 2.7 and 2.8, respectively. Similar results were obtained for filled and unfilled samples cured for different curing times. These results showed that the initial values of $\frac{dH}{dt}$ and the rate of change of $\frac{dH}{dt}$ were higher at the lower annealing temperatures and lower curing times. Also, the time needed for the 75 wt % ZS-filled UDMA samples to reach apparent equilibrium were 5.5 x 10^5, 2.1 x 10^5 and 1.5 x 10^5 sec at 37.0, 57.0 and 65.5 °C, respectively, when they were light-cured for 300 sec. However, the time required to reach equilibrium for composites containing silanated filler was independent of the annealing temperatures and it took 1.0 x 10^6 sec.

2.3.2 Enthalpy Change and Total Heat of Reaction

The change of enthalpy (dH) isotherms were determined from the integration of the finite changes of rates of enthalpy per gram of polymer with respect to t, from the equilibrium to the beginning of annealing time.

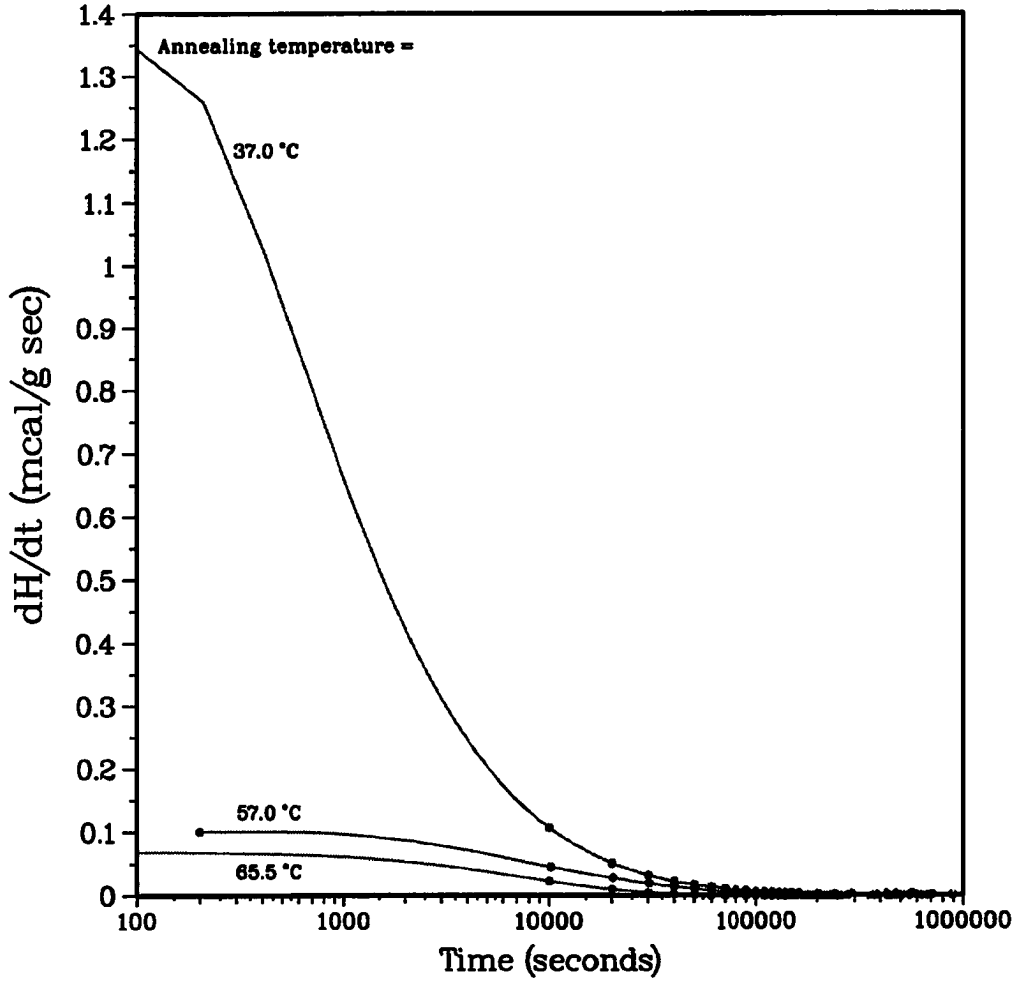

Figure 2.7: The rate of change of enthalpy (mcal/g sec) as a function of time (sec) for 75 wt % ZS-filled UDMA cured for 13 sec and annealed at 37.0, 57.0, and 65.5 °C.

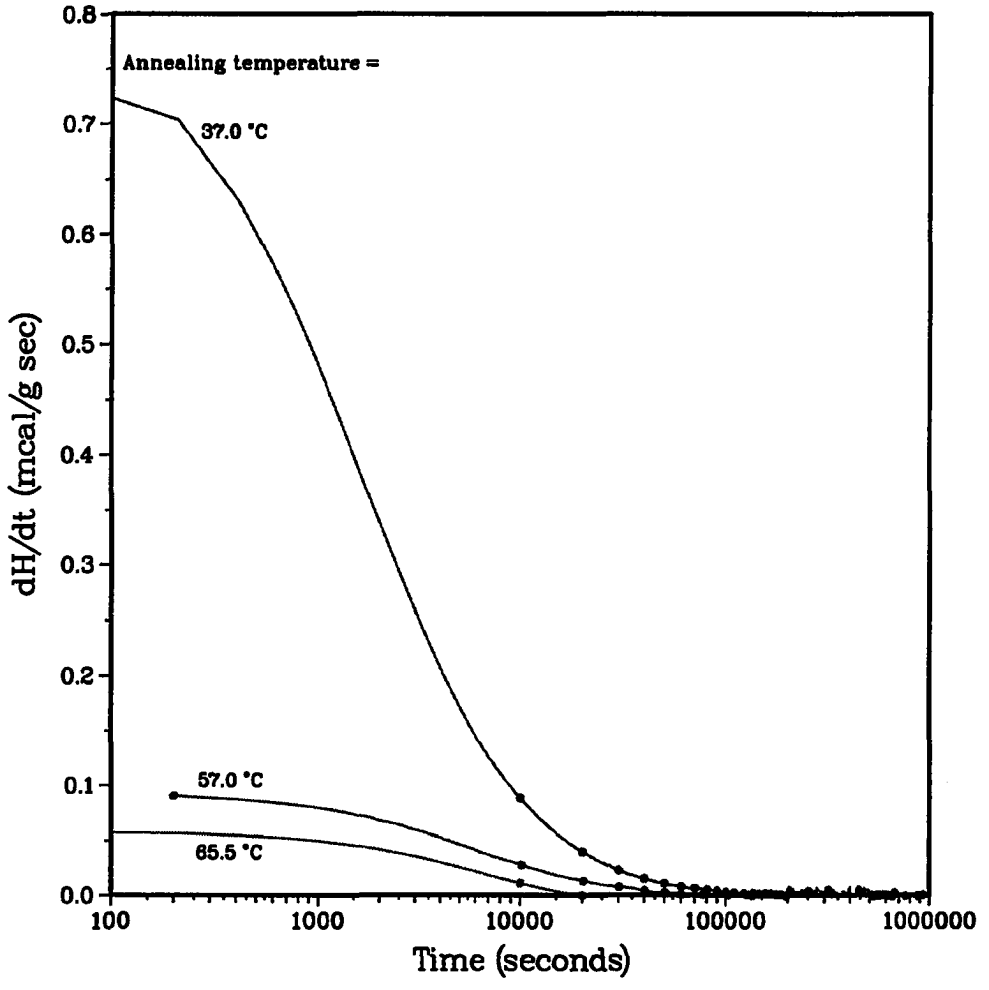

Figure 2.8: The rate of change of enthalpy (mcal/g sec) as a function of time (sec) for 75 wt % MAPM-silanated ZS-filled UDMA cured for 13 sec and annealed at 37.0, 57.0, and 65.5 °C.

Curing Time Effects

The dH for UDMA polymer cured with visible light for 13 - 300 sec and annealed at 37.0, 57.0 and 65.5 °C were calculated and are plotted against t in Figures 2.9 - 2.11, respectively. In addition, the dH for 75 wt % ZS-filled UDMA cured for different times and annealed at the different temperatures are plotted against t in Figures 2.12 - 2.14, respectively, while the dH as a function of t for composites containing silanated filler that were cured for different times and annealed at different temperatures are shown in Figures 2.15 - 2.16, respectively. From these results, it can be seen that samples were continuously giving off heat before reaching equilibrium at low annealing temperatures, which is typical of glassy polymers when annealed at temperatures below their glass temperature (T_g). However, at low curing times (13 and 30 sec) and high annealing temperatures (65.5 °C), the samples absorbed heat at longer annealing times. In addition, the composites that contained silanated filler also showed similar behavior. Further, at these temperatures, samples cured for longer periods of time with visible light had greater enthalpy change than samples cured for shorter periods of time. Also, the initial measurable dH (i.e. dH at t = 3.3, 2.5 and 0.5 hrs for 65.5, 57.0 and 37.0 °C, respectively) increased with increasing curing time of composites.

To further illustrate the curing time effect on the enthalpy changes, dH obtained at 0, 10^4 and 10^5 sec for 0 - 75 wt % ZS-filled UDMA and MAPM-silanated ZS-filled UDMA are plotted against curing time in Figures 2.17 - 2.19 at 37.0, 57.0 and 65.5 °C, respectively. These results showed that dH values increased with increasing curing times and gradually leveled off to constant values at very high curing times when the composites contained unsilanated filler. However, for composites containing silanated filler, the dH values reached a minimum and then increased with increases

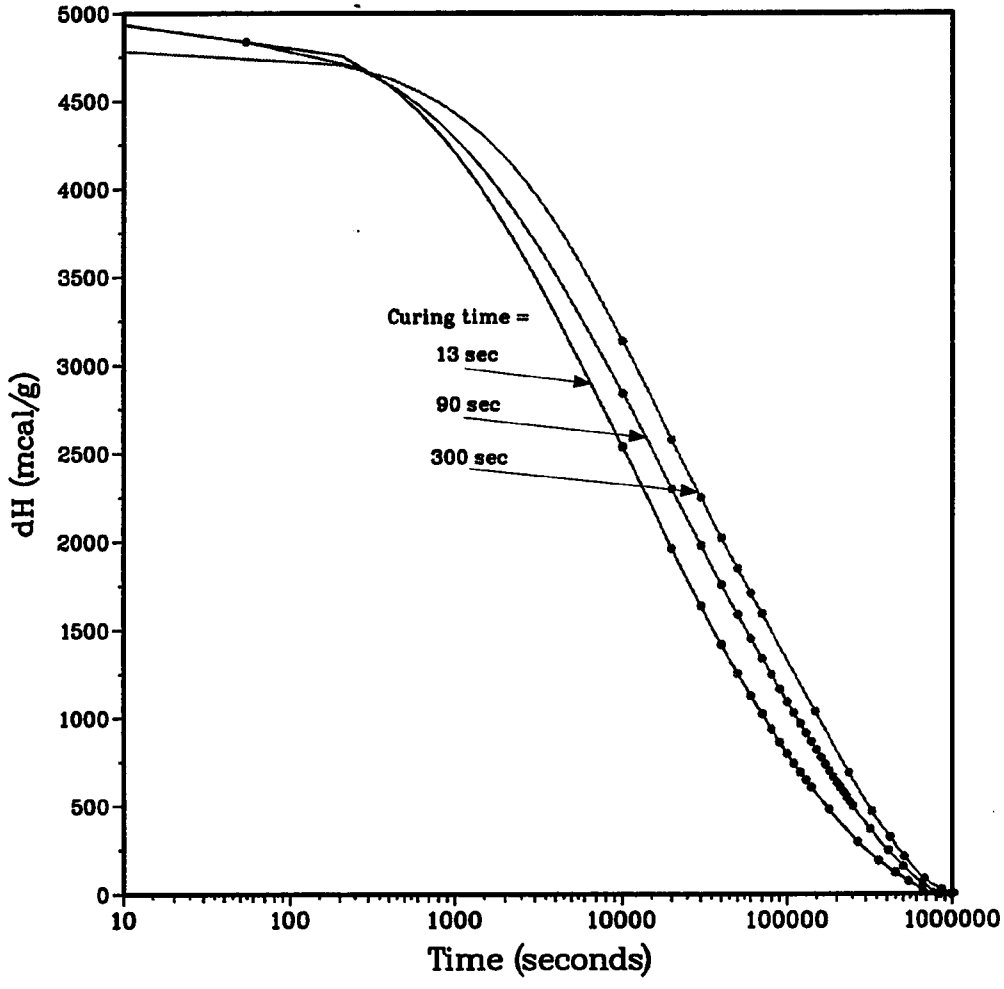

Figure 2.9: The change of enthalpy (mcal/g) as a function of time (sec) for UDMA polymer cured for different length of time and annealed at 37.0 °C.

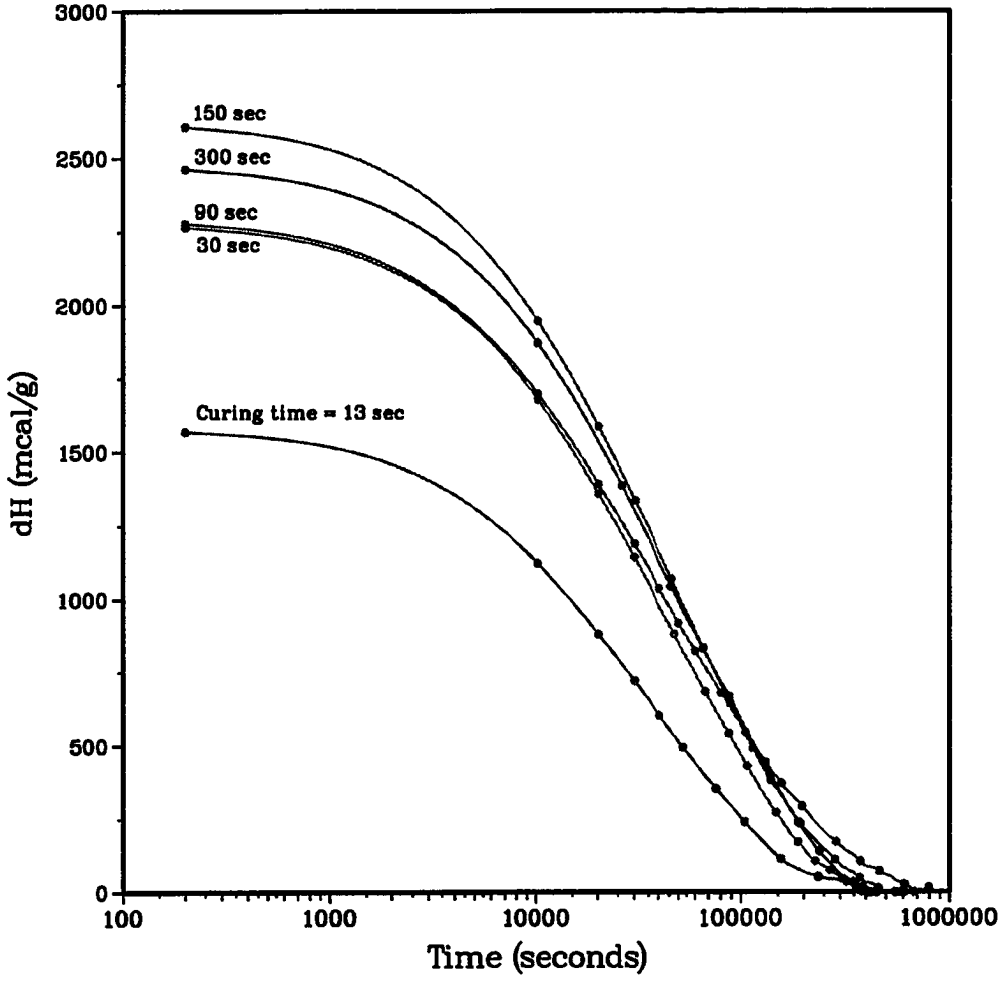

Figure 2.10: The change of enthalpy (mcal/g) as a function of time (sec) for UDMA polymer cured for different length of time and annealed at 57.0 °C.

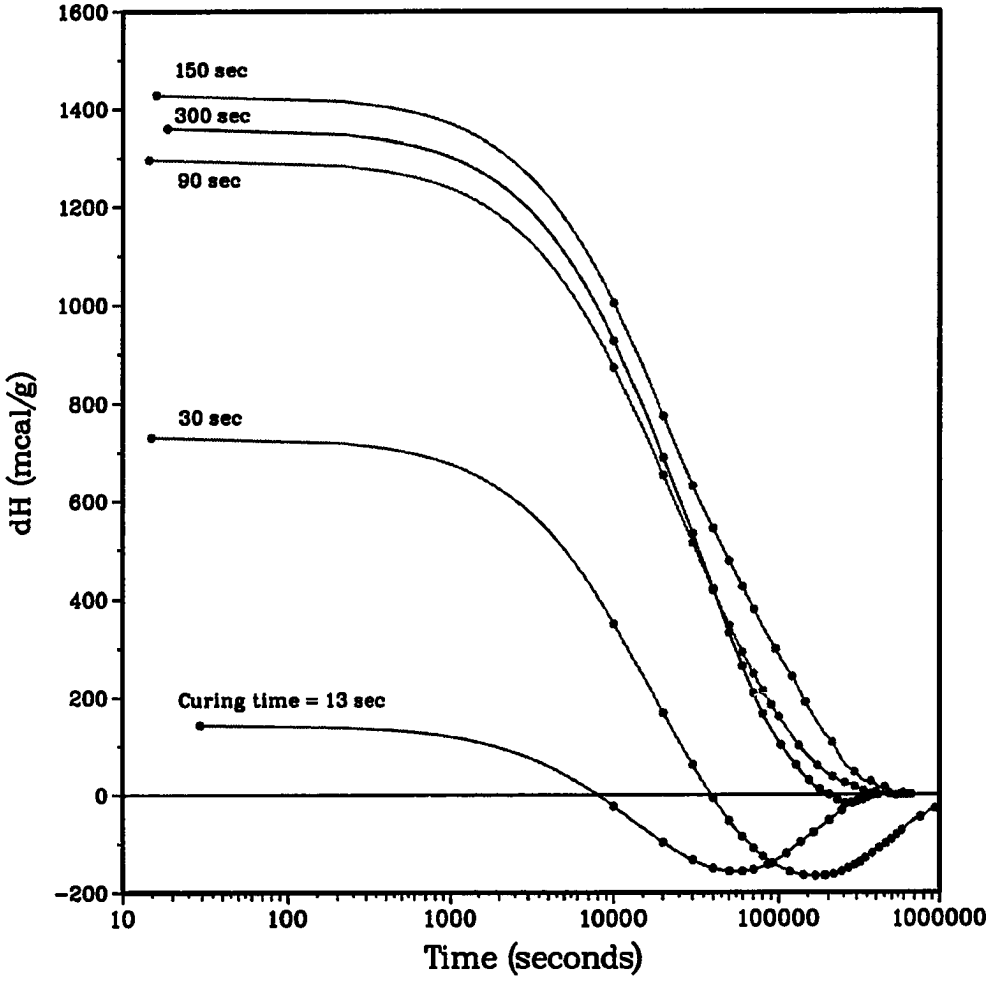

Figure 2.11: The change of enthalpy (mcal/g) as a function of time (sec) for UDMA polymer cured for different length of time and annealed at 65.5 °C.

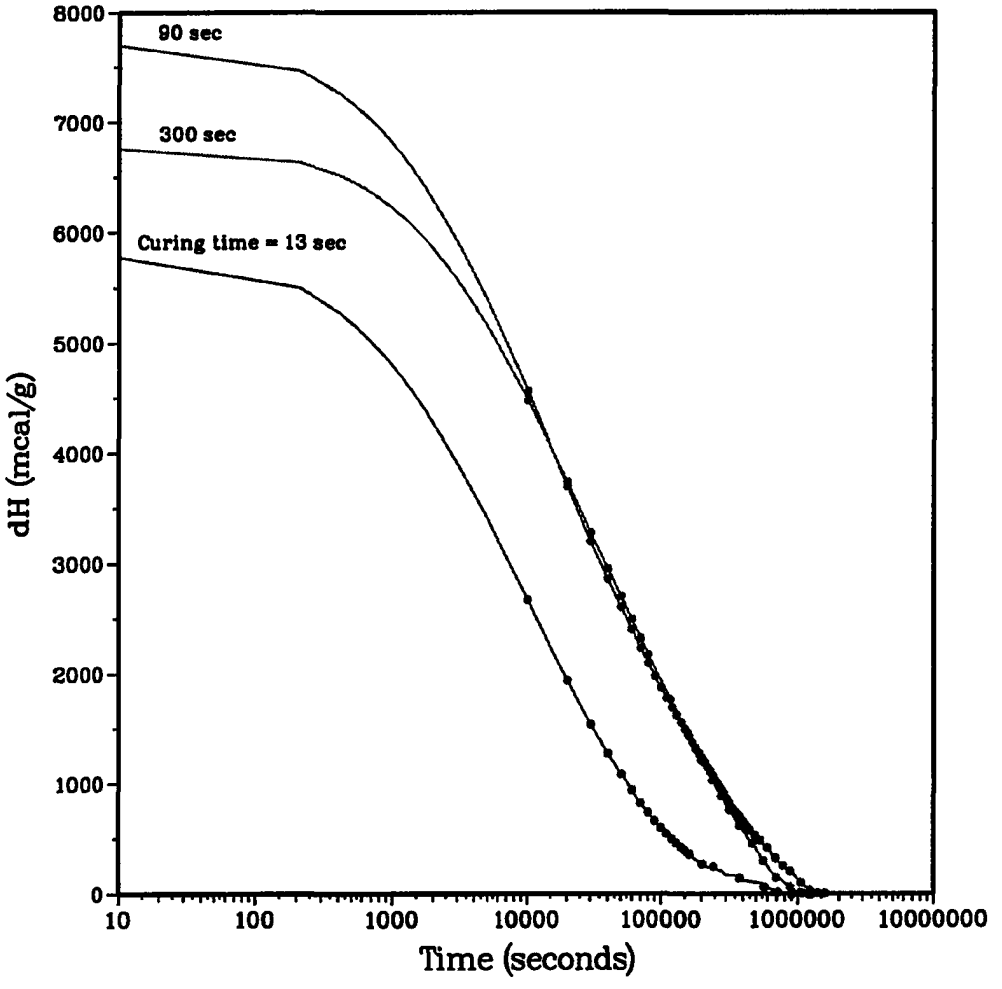

Figure 2.12: The change of enthalpy (mcal/g) as a function of time (sec) for 75 wt % ZS-filled UDMA cured for different length of time and annealed at 37.0 °C.

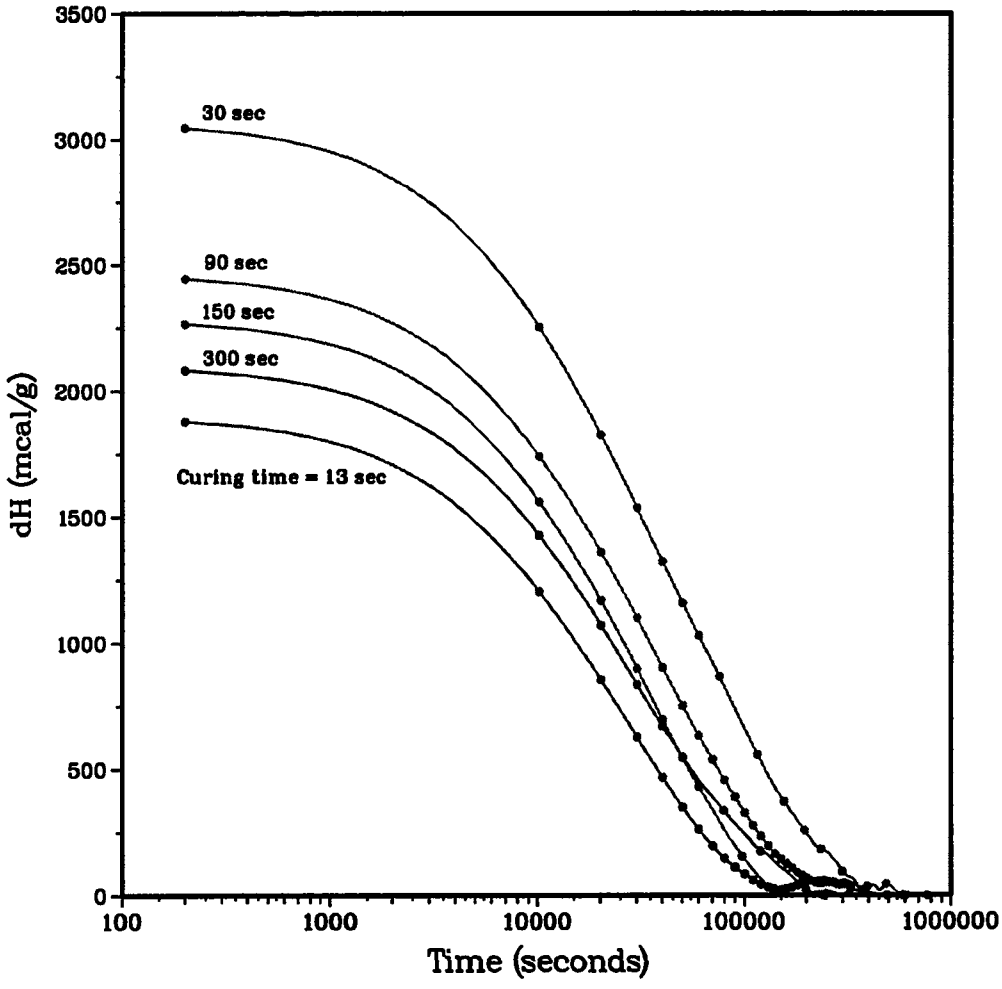

Figure 2.13: The change of enthalpy (mcal/g) as a function of time (sec) for 75 wt % ZS-filled UDMA cured for different length of time and annealed at 57.0 °C.

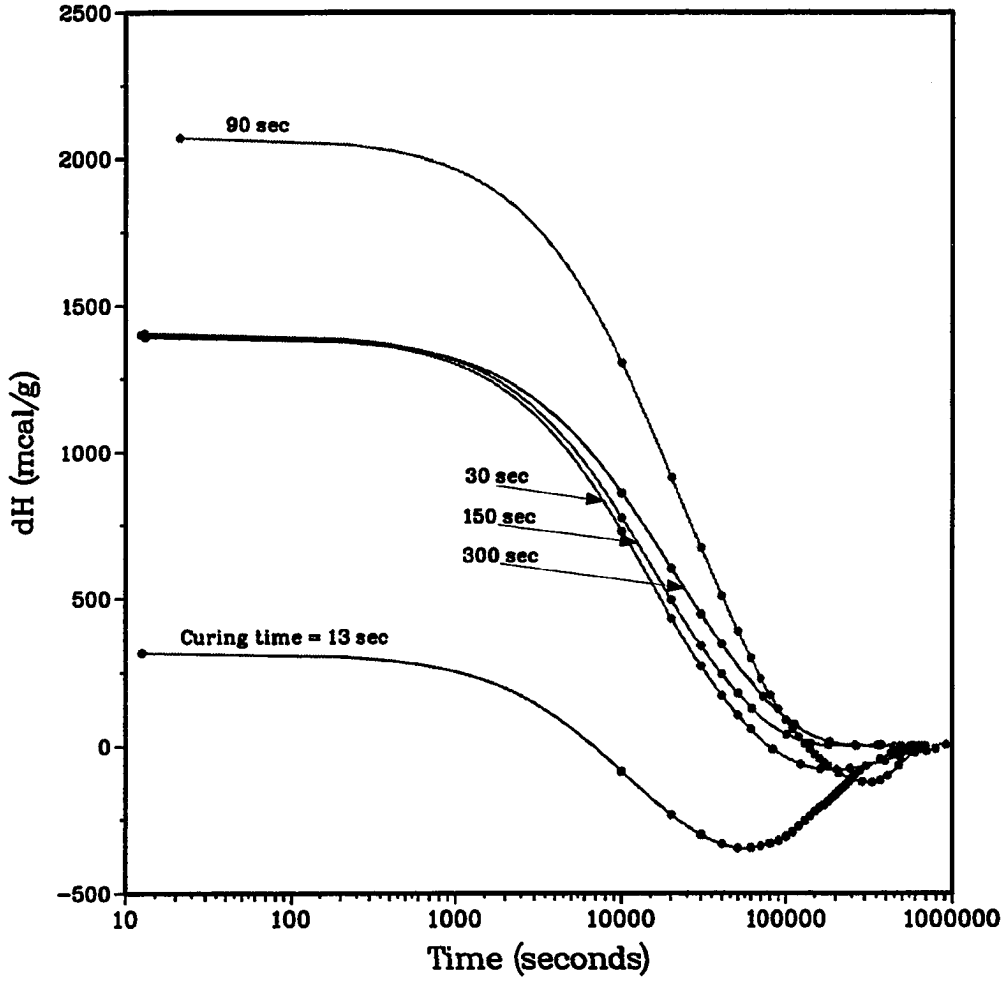

Figure 2.14: The change of enthalpy (mcal/g) as a function of time (sec) for 75 wt % ZS-filled UDMA cured for different length of time and annealed at 65.5 °C.

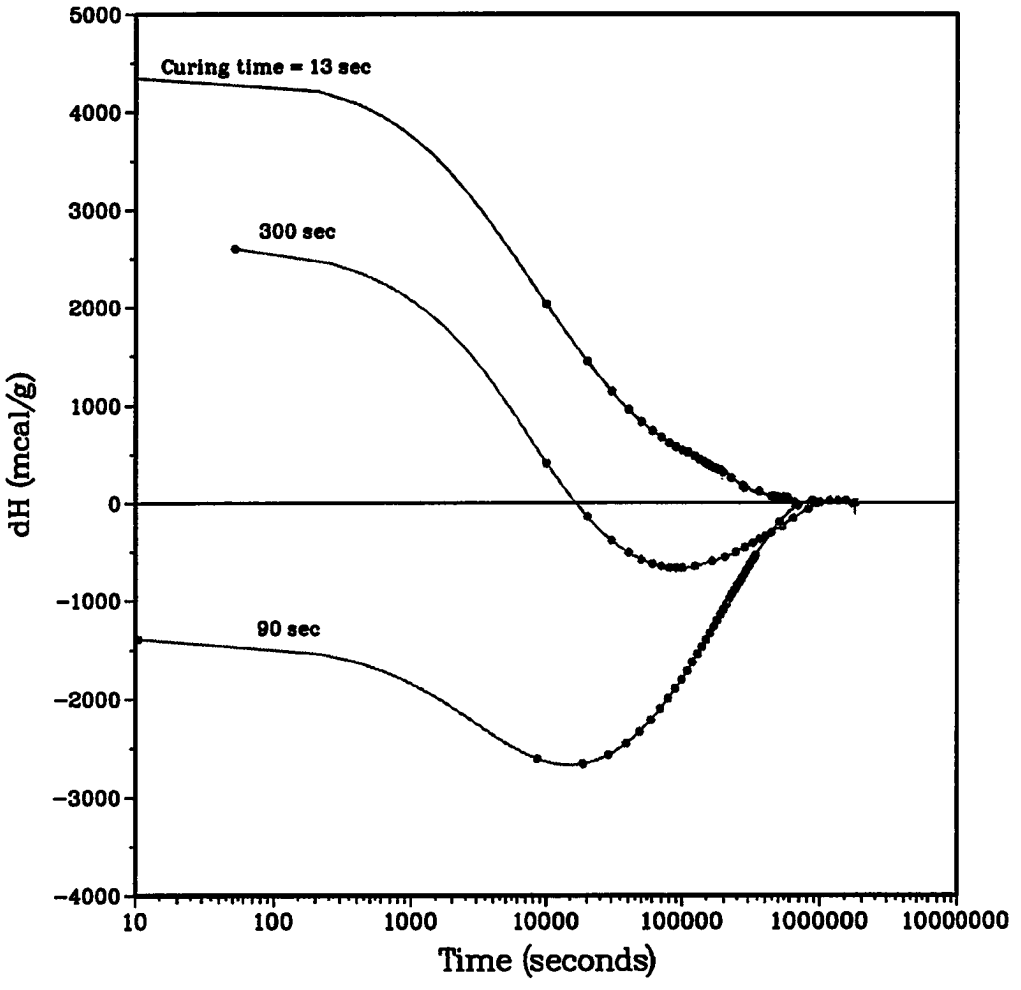

Figure 2.15: The change of enthalpy (mcal/g) as a function of time (sec) for MAPM-silanated ZS-filled UDMA cured for different length of time and annealed at 37.0 °C.

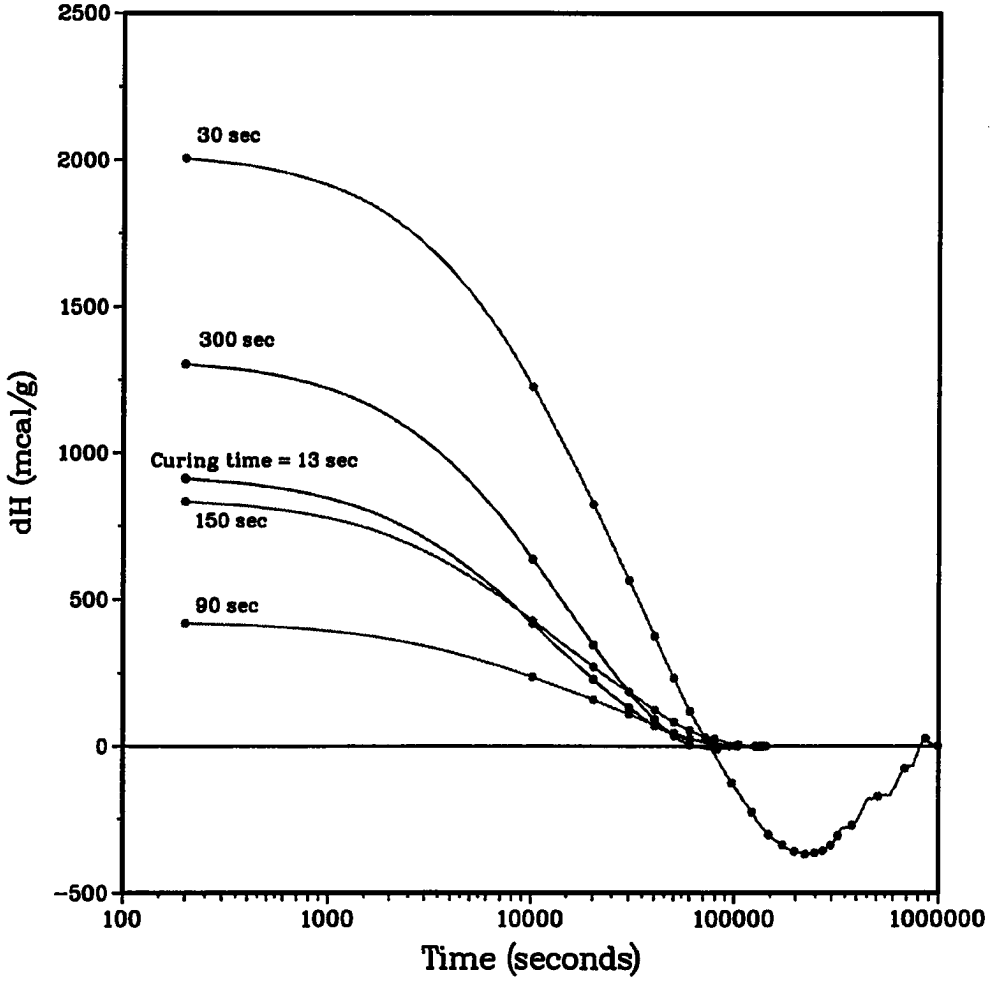

Figure 2.16: The change of enthalpy (mcal/g) as a function of time (sec) for MAPM-silanated ZS-filled UDMA cured for different length of time and annealed at 57.0 °C.

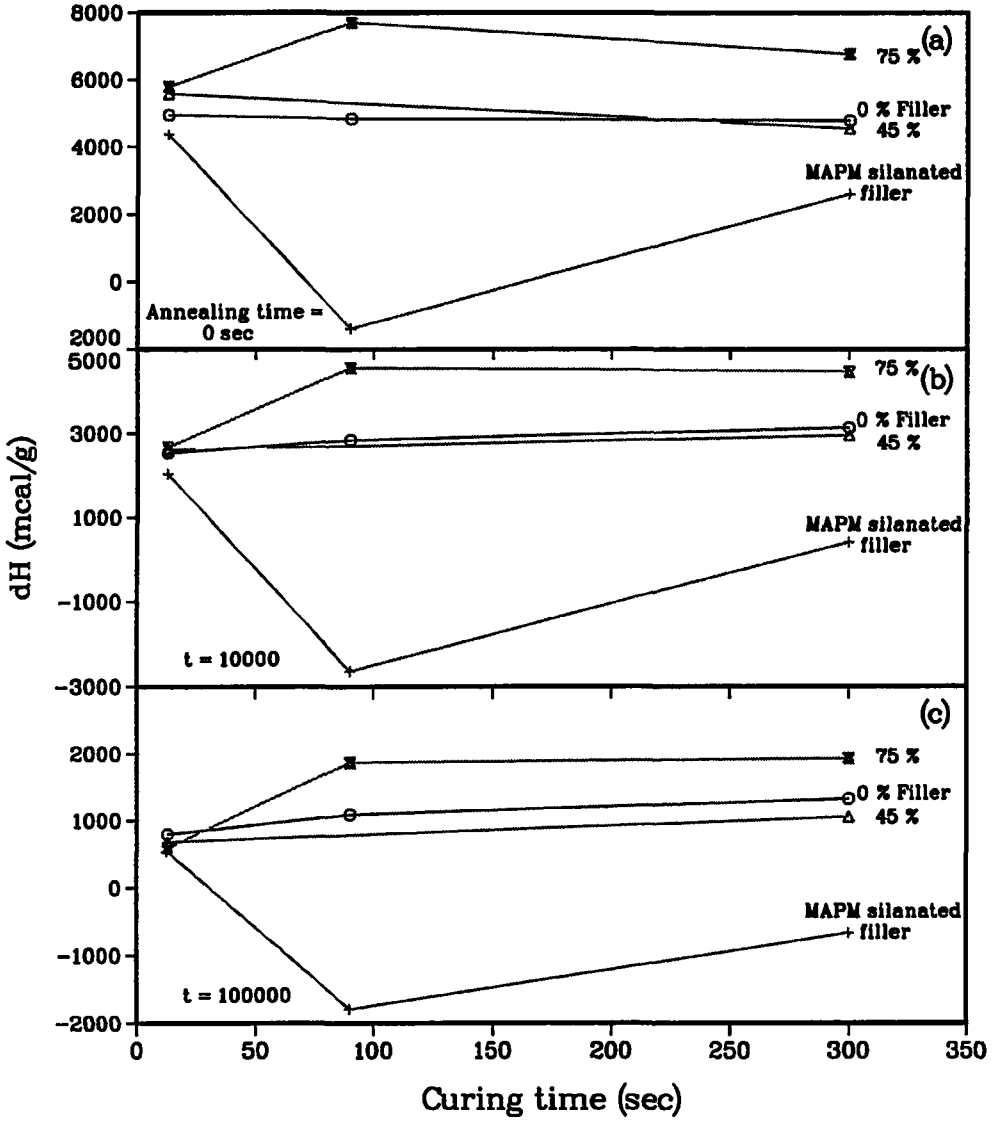

Figure 2.17: The change of enthalpy (mcal/g) as a function of curing time (sec) for 0, 15, 45, 75 wt % ZS-filled UDMA and MAPM-silanated ZS-filled UDMA annealed at 37.0 °C for (a) 0 sec, (b) 10^4 sec, and (c) 10^5 sec.

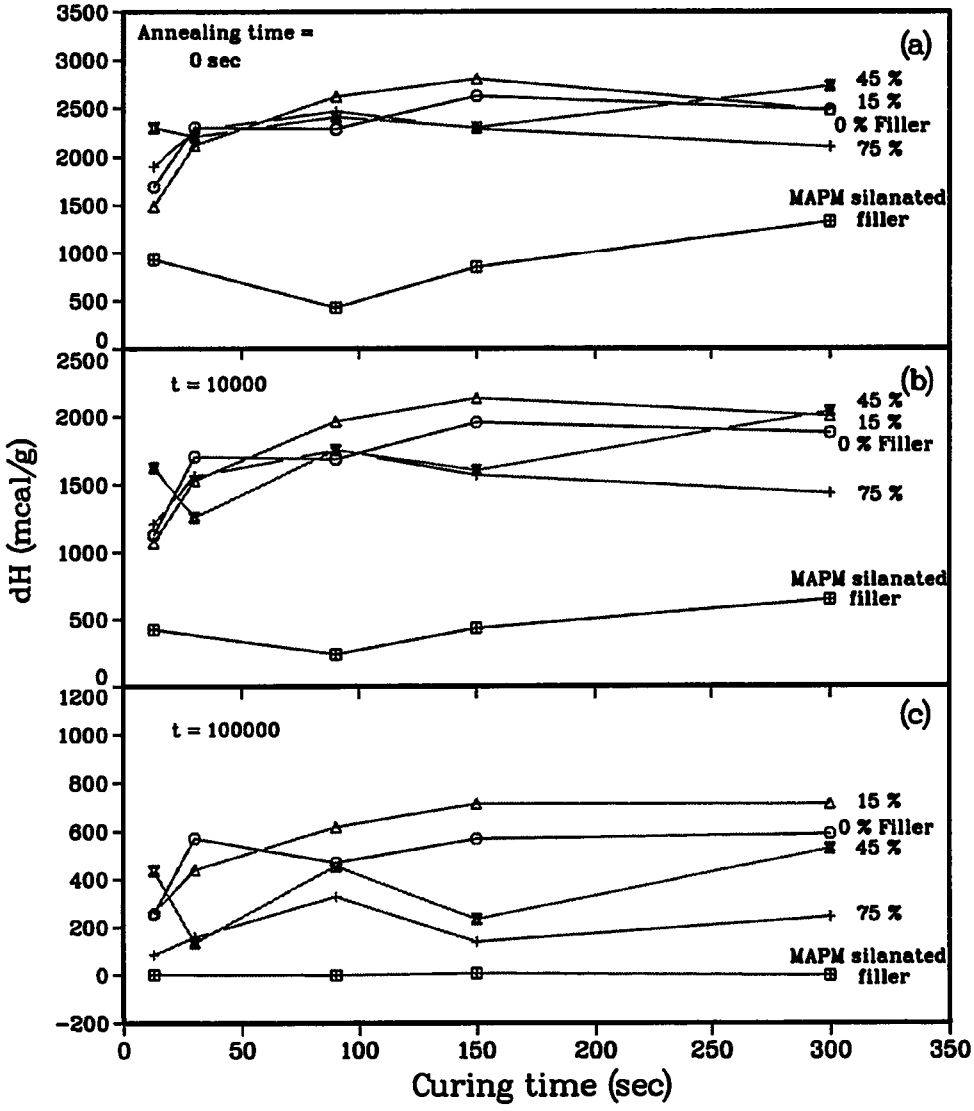

Figure 2.18: The change of enthalpy (mcal/g) as a function of curing time (sec) for 0, 15, 45, 75 wt % ZS-filled UDMA and MAPM-silanated ZS-filled UDMA annealed at 57.0 °C for (a) 0 sec, (b) 10^4 sec, and (c) 10^5 sec.

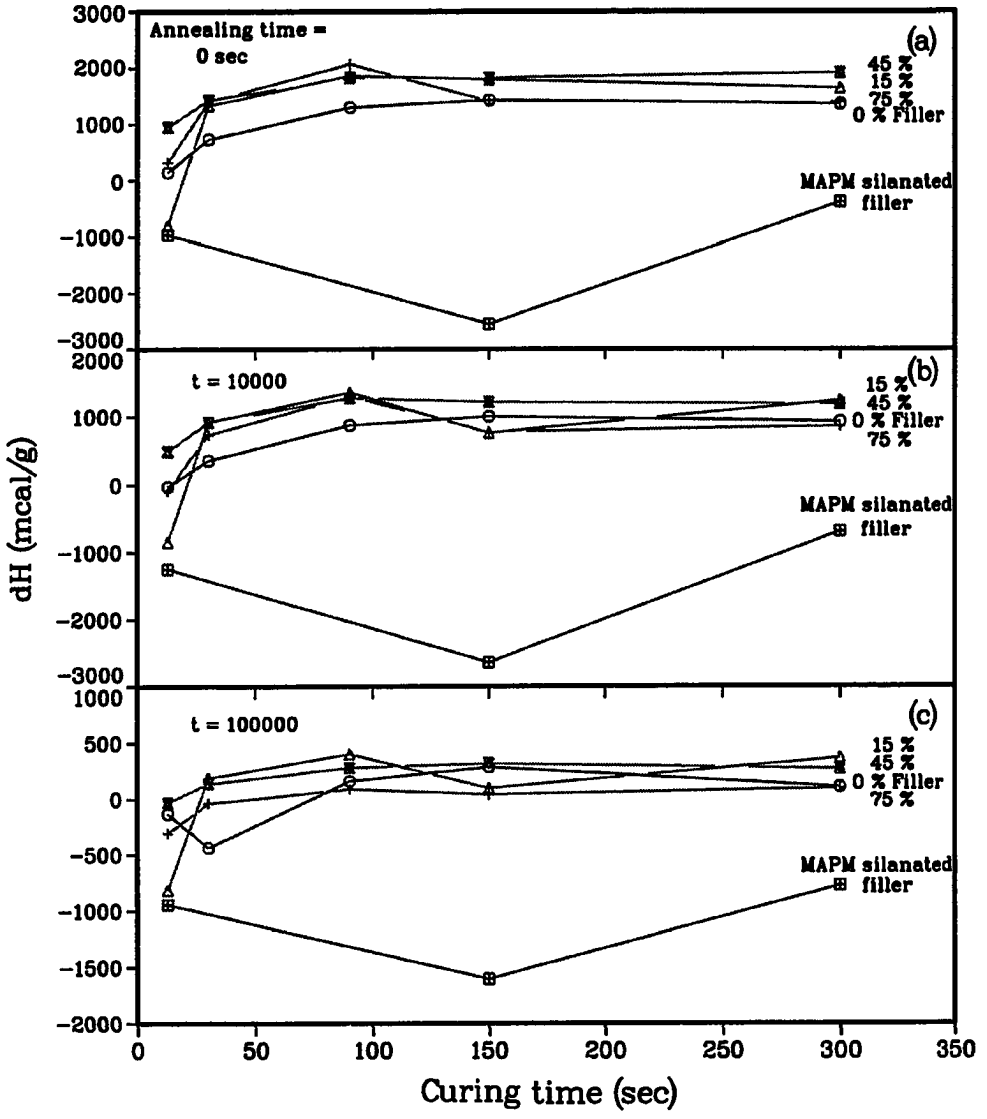

Figure 2.19: The change of enthalpy (mcal/g) as a function of curing time (sec) for 0, 15, 45, 75 wt % ZS-filled UDMA and MAPM-silanated ZS-filled UDMA annealed at 65.5 °C for (a) 0 sec, (b) 10^4 sec, and (c) 10^5 sec.

in curing time.

Filler Effects

To illustrate the effect of filler concentration on the enthalpy changes, dH obtained at 0, 10^4 and 10^5 sec for samples cured with visible light for different times and annealed at 37.0, 57.0 and 65.5 °C are plotted against filler concentration in Figures 2.20 - 2.22, respectively. These figures showed nonlinear dependence of the change of enthalpy with filler concentration. The dH curves showed maxima for samples containing 25 wt % filler at high annealing temperatures, while the dH values increased linearly with the increase of filler concentration at low annealing temperatures.

Temperature Effects

The enthalpy changes as a function of annealing time for UDMA samples that were cured for 300 sec and annealed at temperatures of 37.0, 57.0 and 65.5 °C are shown in Figure 2.23. Similar results were obtained for the other systems. These figures showed that the dH values for the samples annealed at 37.0 °C were always larger than those annealed at 57.0 °C, which were correspondingly larger than those at 65.5 °C. These results are typical of a glassy polymer, where the initial enthalpy change increases with decreasing annealing temperature [100, 102]. Also, within the sensitivity of the measurement, the time required to reach enthalpy equilibrium rapidly increased with decreasing annealing temperature. For example, The UDMA samples annealed at 37.0 °C reached apparent equilibrium at 1.0×10^6 sec, while the samples annealed at 57.0 and 65.5 °C reached equilibrium at about 3.5×10^5 and 1.5×10^5 sec, respectively.

To illustrate further the effect of annealing temperature on the enthalpy changes,

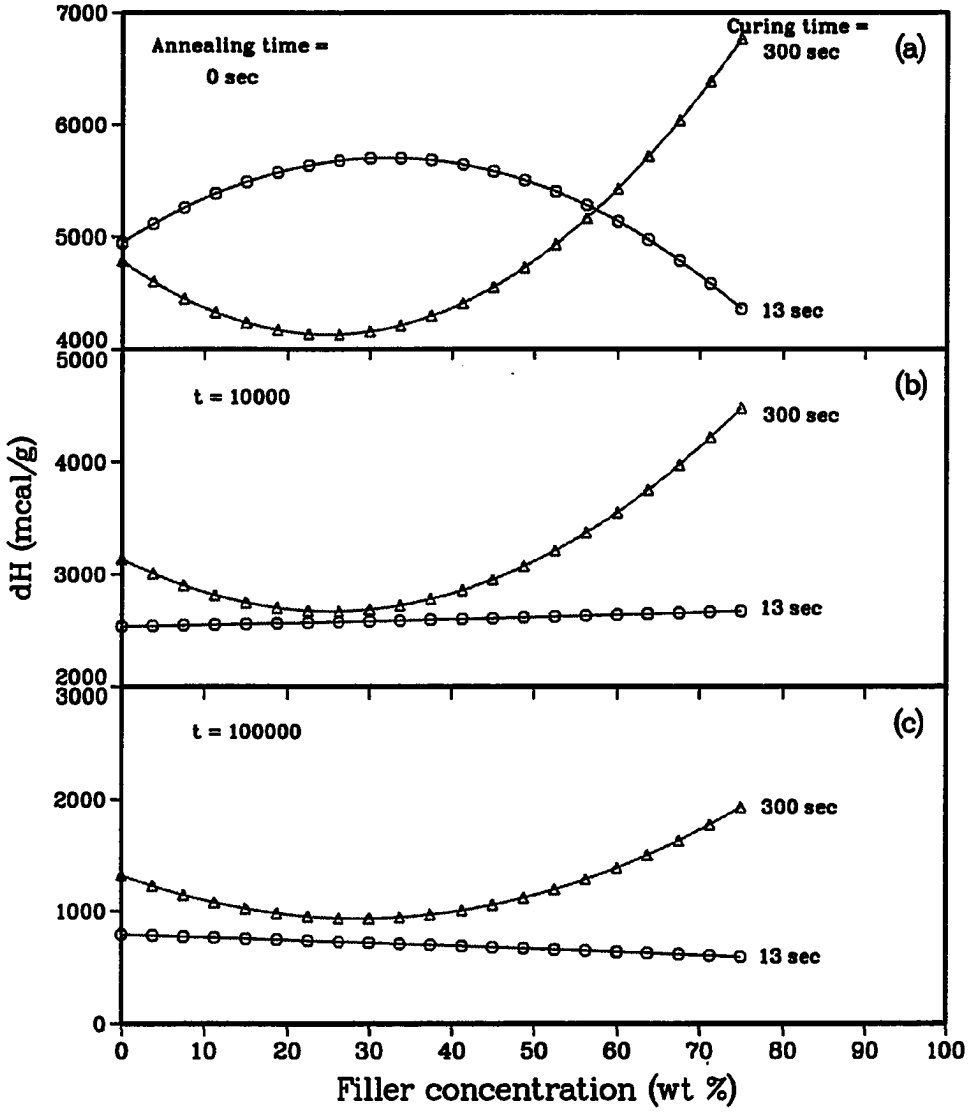

Figure 2.20: The change of enthalpy (mcal/g) as a function of filler concentration (wt %) for 13 - 300 sec cured ZS-filled UDMA annealed at 37.0 °C for (a) 0 sec, (b) 10^4 sec, and (c) 10^5 sec.

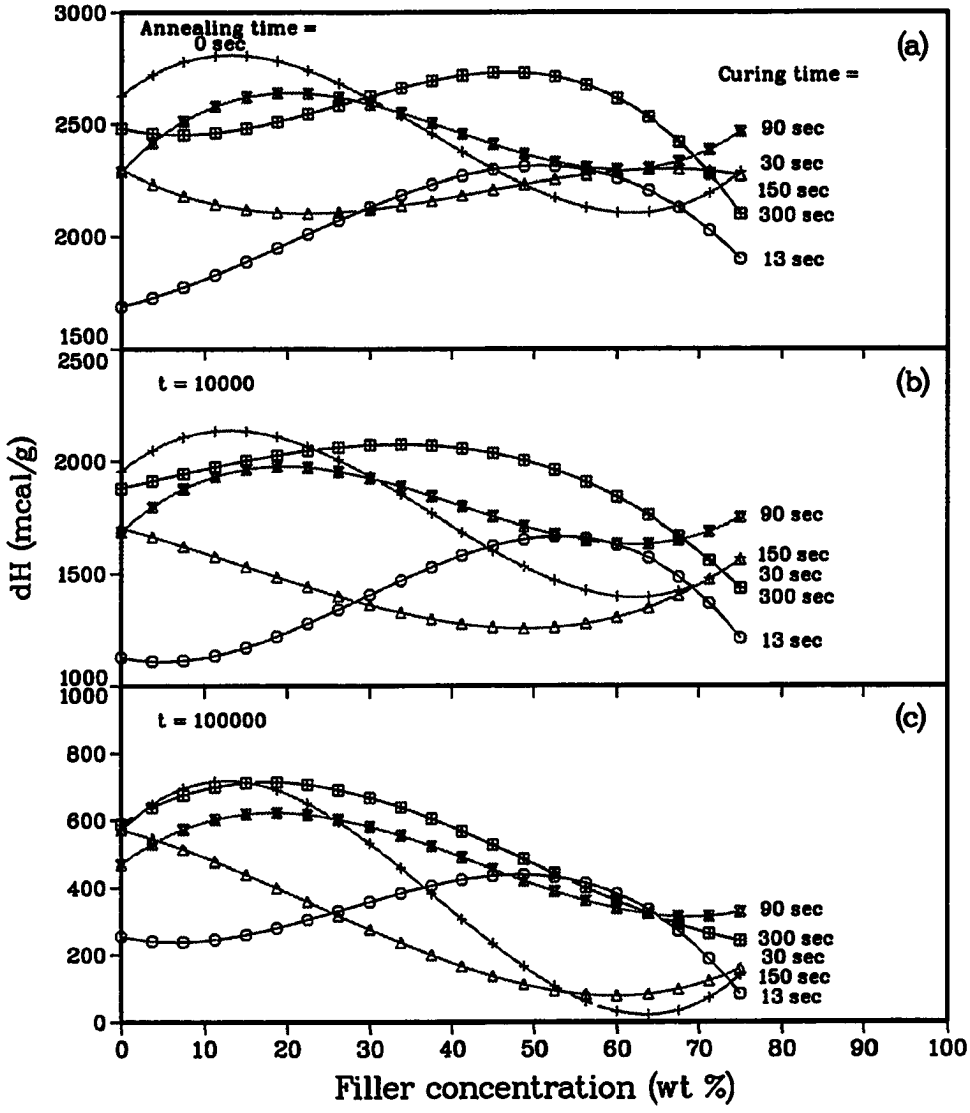

Figure 2.21: The change of enthalpy (mcal/g) as a function of filler concentration (wt %) for 13 - 300 sec cured ZS-filled UDMA annealed at 57.0 °C for (a) 0 sec, (b) 10^4 sec, and (c) 10^5 sec.

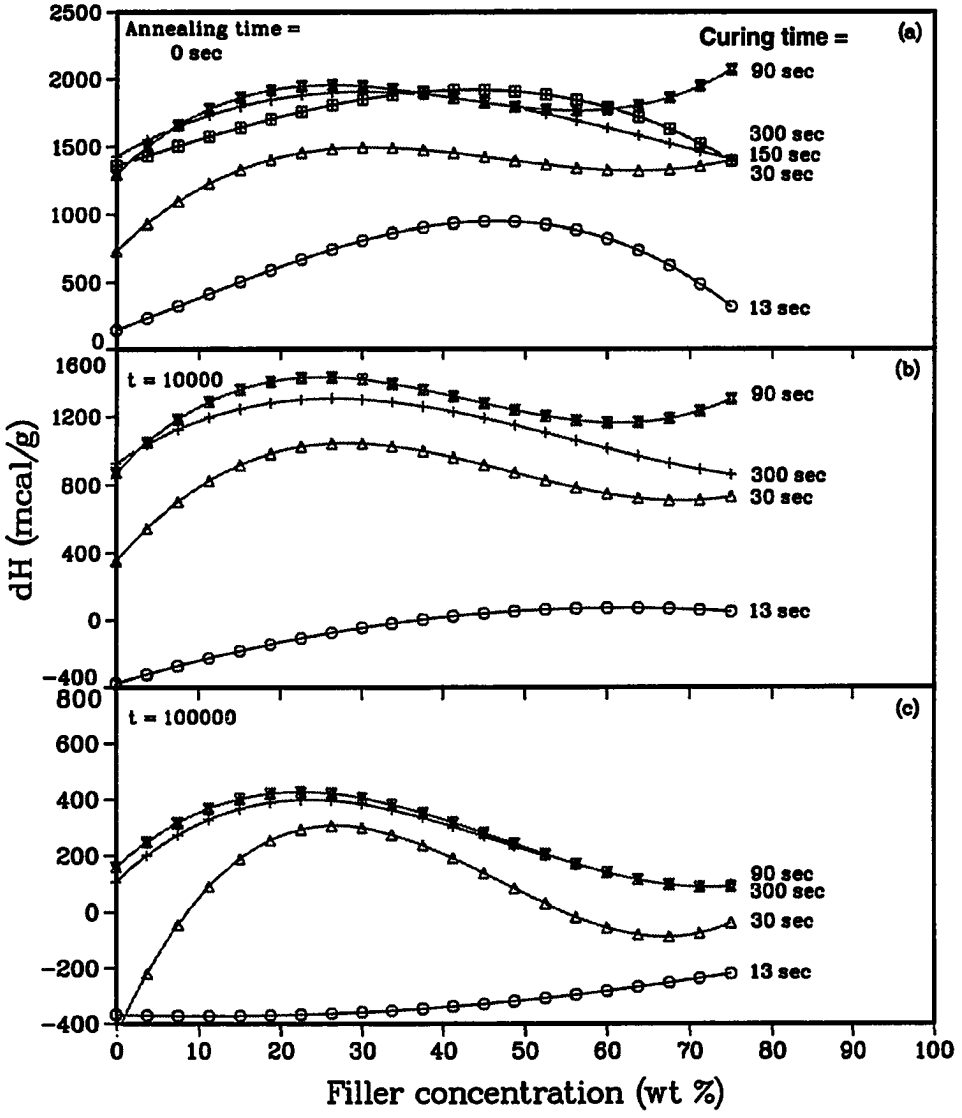

Figure 2.22: The change of enthalpy (mcal/g) as a function of filler concentration (wt %) for 13 - 300 sec cured ZS-filled UDMA annealed at 65.5 °C for (a) 0 sec, (b) 10^4 sec, and (c) 10^5 sec.

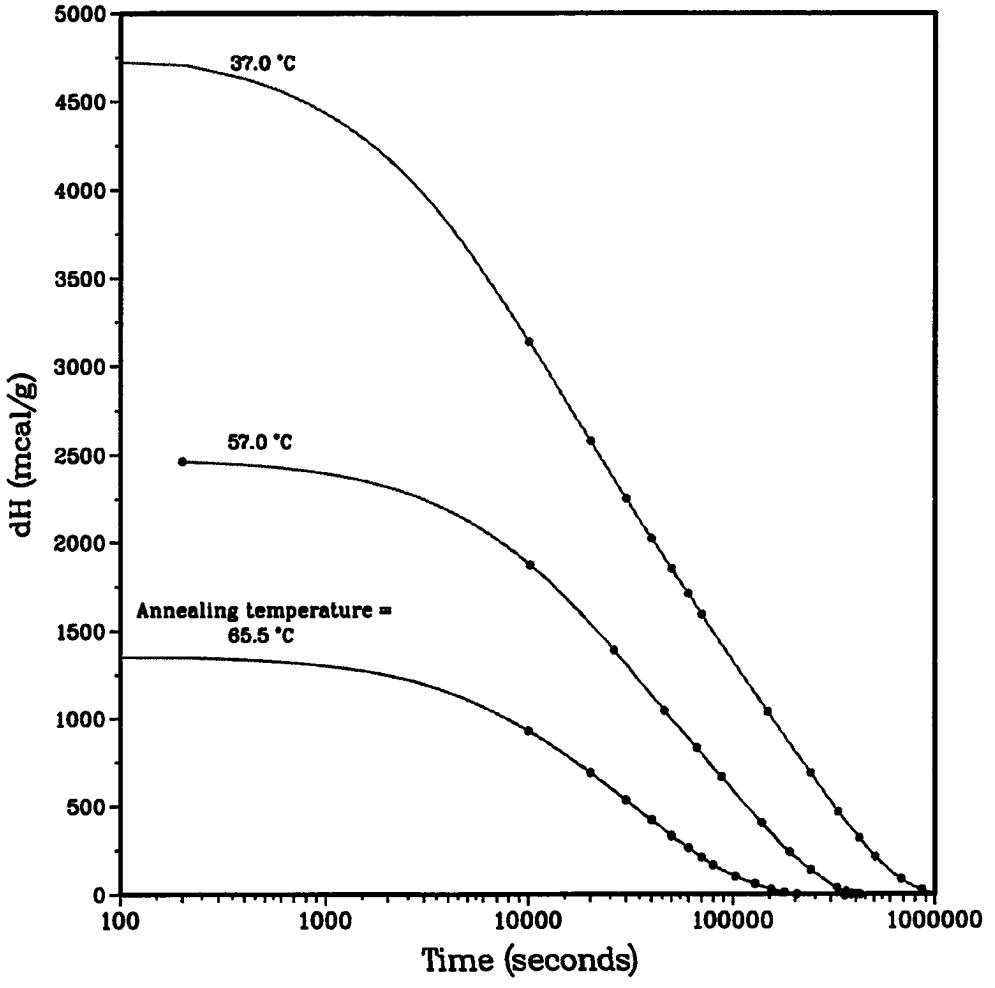

Figure 2.23: The change of enthalpy (mcal/g) as a function of annealing time for UDMA polymer cured for 300 sec and annealed at 37.0, 57.0 and 65.5 °C.

the enthalpy for the different samples cured for 13 and 300 sec, were obtained at 0, 10^4 and 10^5 sec of annealing are plotted against annealing temperatures in Figures 2.24 and 2.25, respectively. These figures also showed the decrease of the enthalpy change with increasing annealing temperature. In addition, the dH values showed a linear dependence with annealing temperature, thus, the specific heat of the different systems were calculated from the slopes of these curves at 0 sec annealing time and the values are presented in Table 2.1. The specific heat values showed significant decreases with the increase of the curing time in UDMA polymer and in the composite containing silanated filler, while the values increased with increasing filler concentration in the composites and reached a constant value regardless of the effect of curing time.

2.3.3 Conversion Rates

Conversion of the reaction was determined for the different testing conditions using the relation given by (2.3) and the results were plotted as a function of normalized time, which is defined by $\frac{t_i}{t_{max}}$, where t_i is the ith annealing time and t_{max} is the apparent equilibrium time.

Curing Time Effects

Relative conversion for UDMA annealed at 57.0 °C are plotted as a function of normalized time in Figure 2.26. Similar results were found for the filled systems. Regardless of the system tested, the conversion with normalized time was higher for samples cured for short exposure times of visible light. For example, in the initial 10 % of the annealing period, the relative conversion of the 13 sec cured UDMA polymer was 75 %, while the relative conversion of the 300 sec cured polymer was 55 %. In addition, in 50 % of the annealing period, the conversions were 97 and 90 %

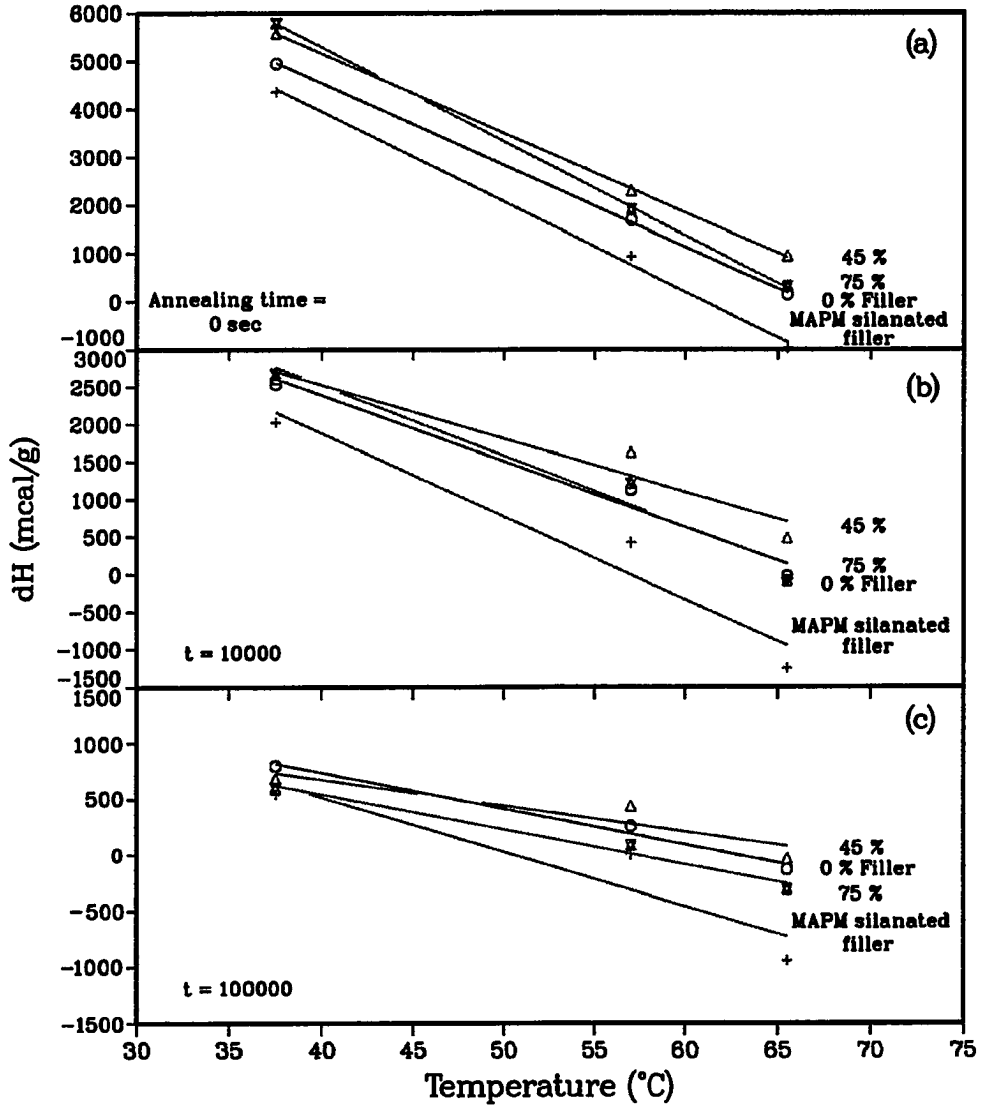

Figure 2.24: The change of enthalpy (mcal/g) as a function of annealing temperatures (°C) for 13 sec cured 0, 45, 75 wt % ZS-filled UDMA and 75 wt % MAPM-silanated ZS-filled UDMA annealed for (a) 0 sec, (b) 10^4 sec, and (c) 10^5 sec.

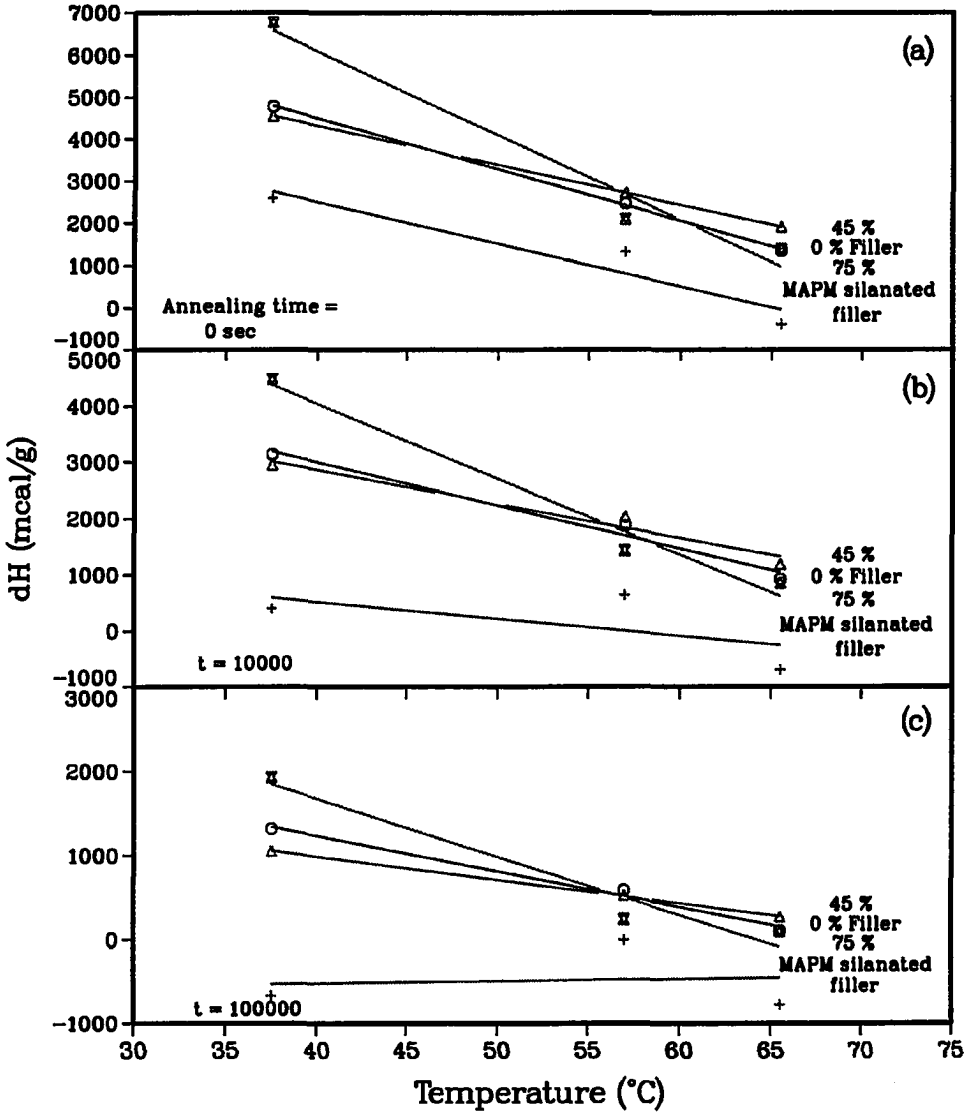

Figure 2.25: The change of enthalpy (mcal/g) as a function of annealing temperatures (°C) for 300 sec cured 0, 45, 75 wt % ZS-filled UDMA and 75 wt % MAPM-silanated ZS-filled UDMA annealed for (a) 0 sec, (b) 10^4 sec, and (c) 10^5 sec.

	Specific Heat (mcal/gm °C)		
Filler	Curing time (sec)		
wt %	13	90	300
0	172	120	108
75 unsilanated	200	200	200
75 MAPM-silanated	192	—	100

Table 2.1: Specific heat (mcal/gm °C) for the different composite systems cured for 13, 90 and 300 sec.

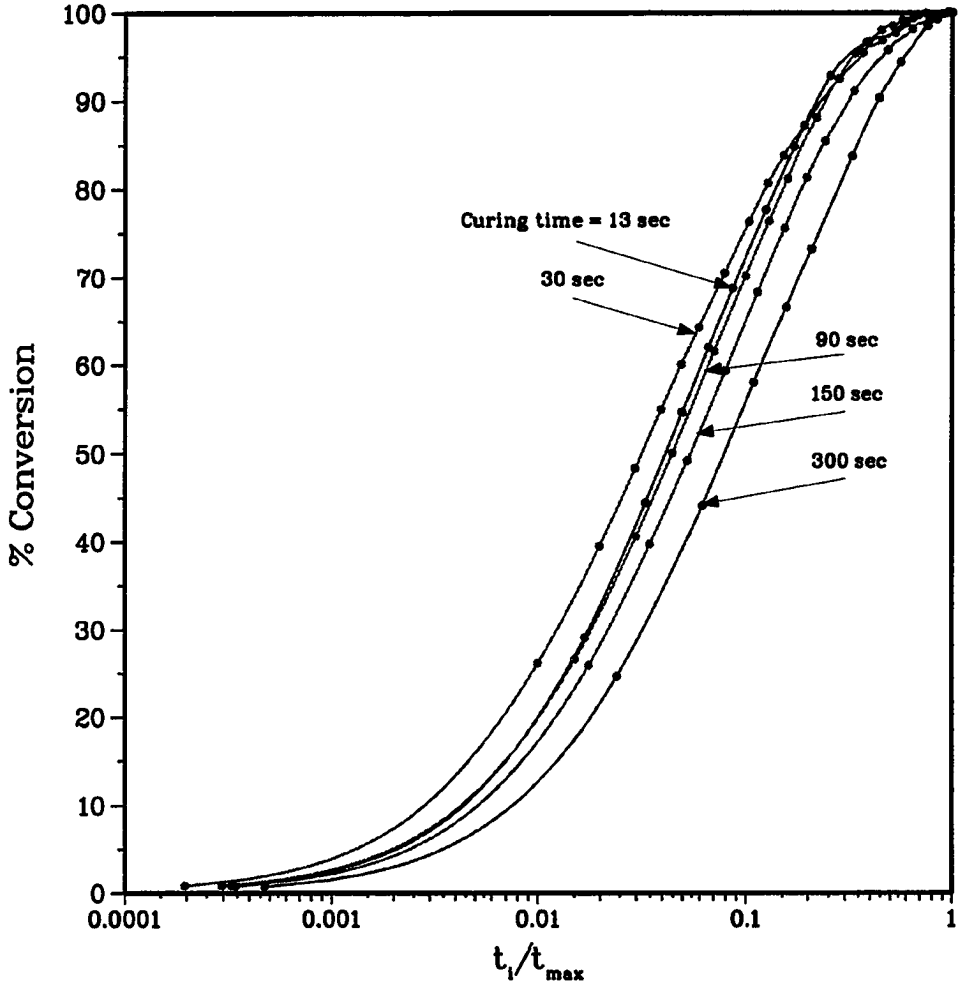

Figure 2.26: % conversion as a function of normalized annealing time for UDMA polymer cured for 13 - 300 sec and annealed at 57.0 °C.

for UDMA polymer cured for 13 and 300 sec, respectively.

Filler Effects

The conversion of 0 - 75 wt % ZS-filled UDMA and MAPM-silanated ZS-filled UDMA annealed at 57.0 °C are plotted as a function of normalized time in Figures 2.27 and 2.28 when they were cured for 13 and 300 sec, respectively. As can be seen from these figures, increasing filler concentration increased the relative conversion from 75 to 85 % for 0 and 75 wt % ZS-filled UDMA, while silanating the filler caused a decrease in the conversion to 66 % when the samples were annealed at the initial 10 % of the time (Figure 2.27).

Temperature Effects

The conversion of 75 wt % ZS-filled UDMA annealed at different temperatures and cured for 13 and 300 sec are plotted as a function of normalized time in Figures 2.29 - 2.30, respectively. imilar results obtained for all of filled and unfilled systems. As expected, the conversion of the composite increased with increasing annealing temperatures. Also, there is interaction between the effects of curing times and the annealing temperatures. That is, at very low curing times and high temperatures, a maximum appeared in the conversion curves, indicating that some complexes between the UDMA resin and other extraneous materials present in the system. These agents are possibly hydrogen-bond doner molecules which may be either moisture or the tertiary amine accelerator.

2.4 Discussion

The crosslinking reaction of thermosets is a highly exothermic process, and heat liberated from such a process also tends to accelerate the curing reaction. To follow

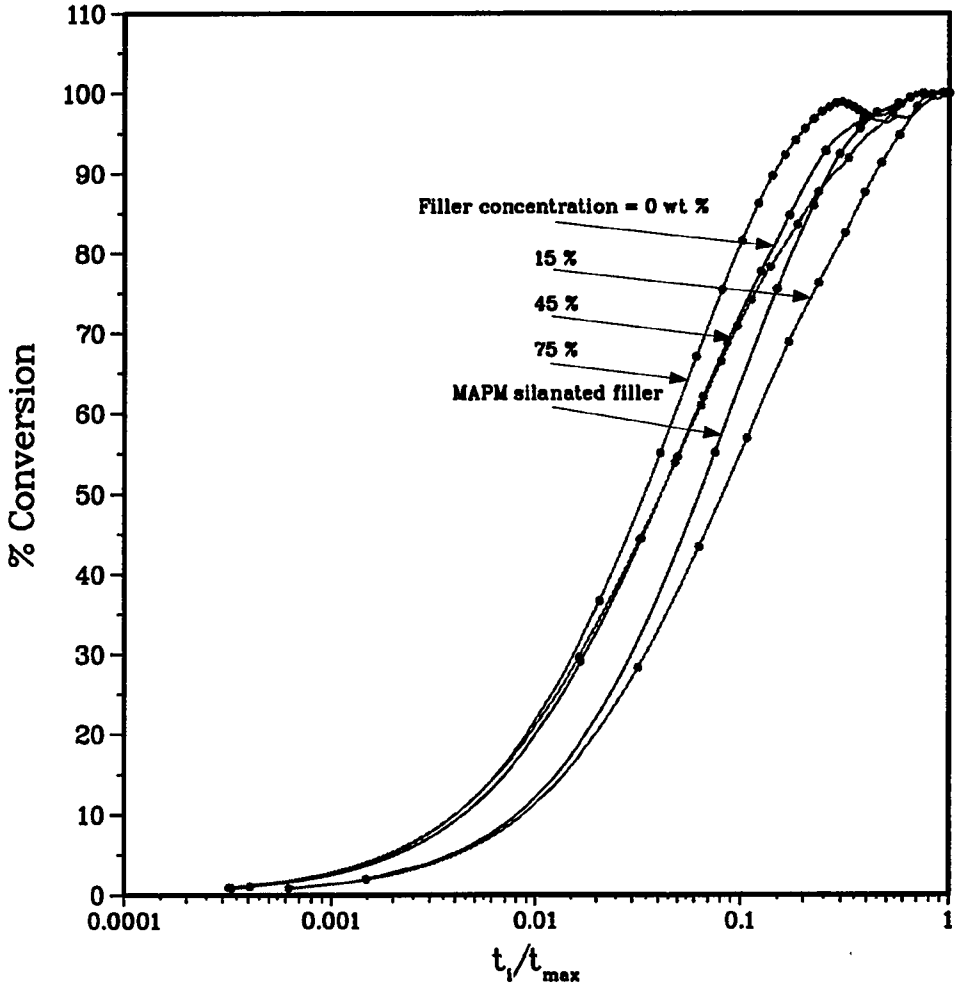

Figure 2.27: % conversion as a function of normalized annealing time for 0 - 75 wt % ZS-filled UDMA and MAPM-silanated ZS-filled UDMA cured for 13 sec and annealed at 57.0 °C.

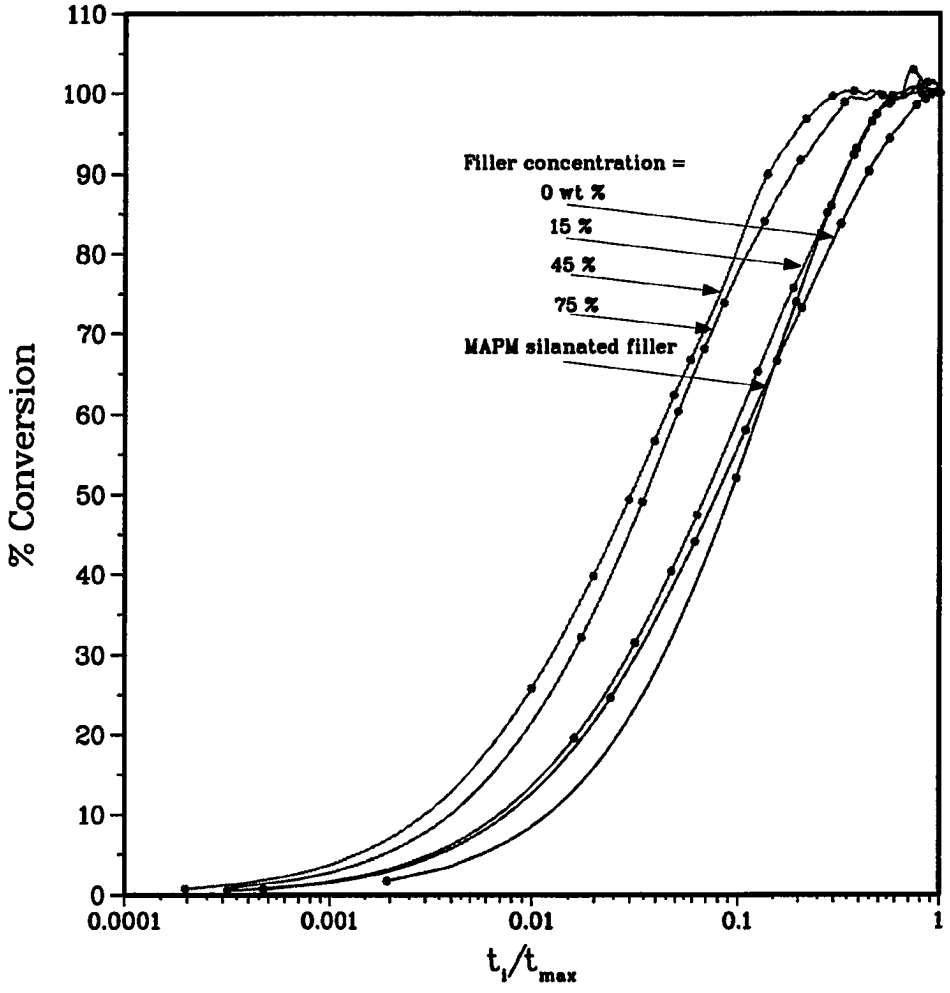

Figure 2.28: % conversion as a function of normalized annealing time for 0 - 75 wt % ZS-filled UDMA and MAPM-silanated ZS-filled UDMA cured for 300 sec and annealed at 57.0 °C.

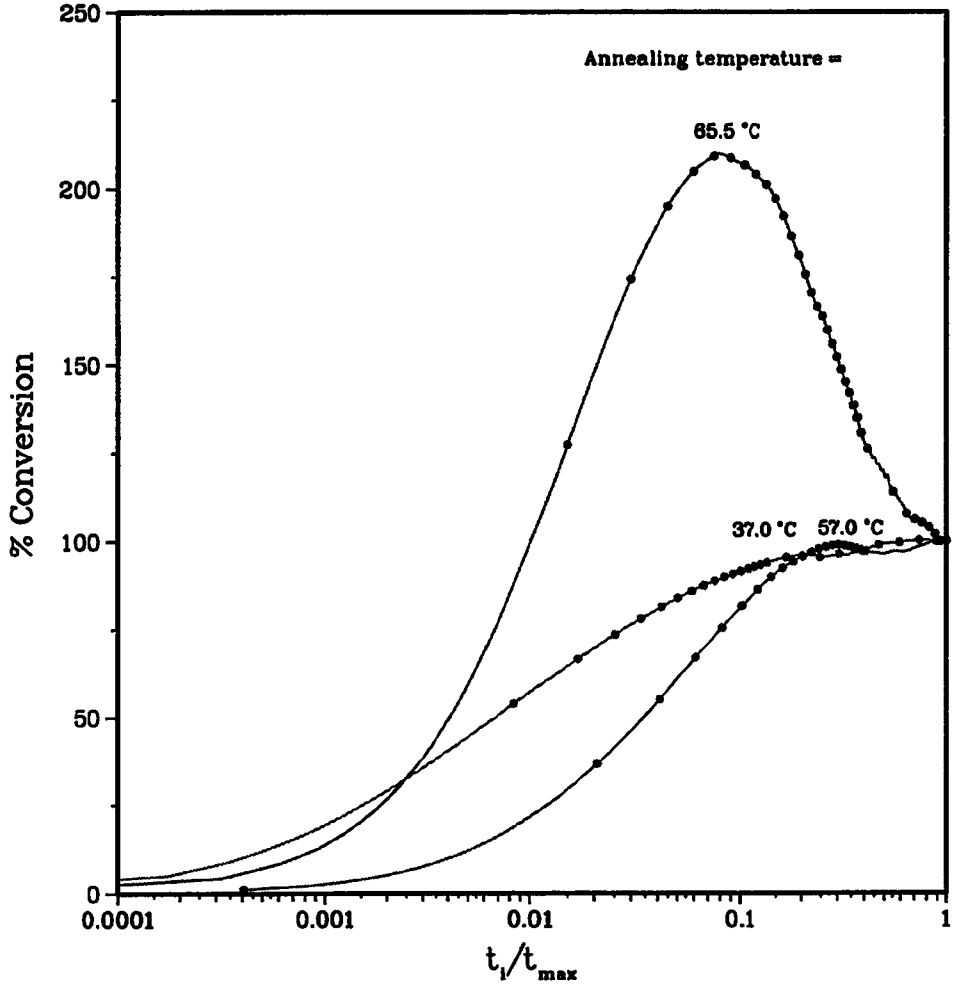

Figure 2.29: % conversion as a function of normalized annealing time for 75 wt % ZS-filled UDMA cured for 13 sec and annealed at 37.0, 57.0 and 65.5 °C.

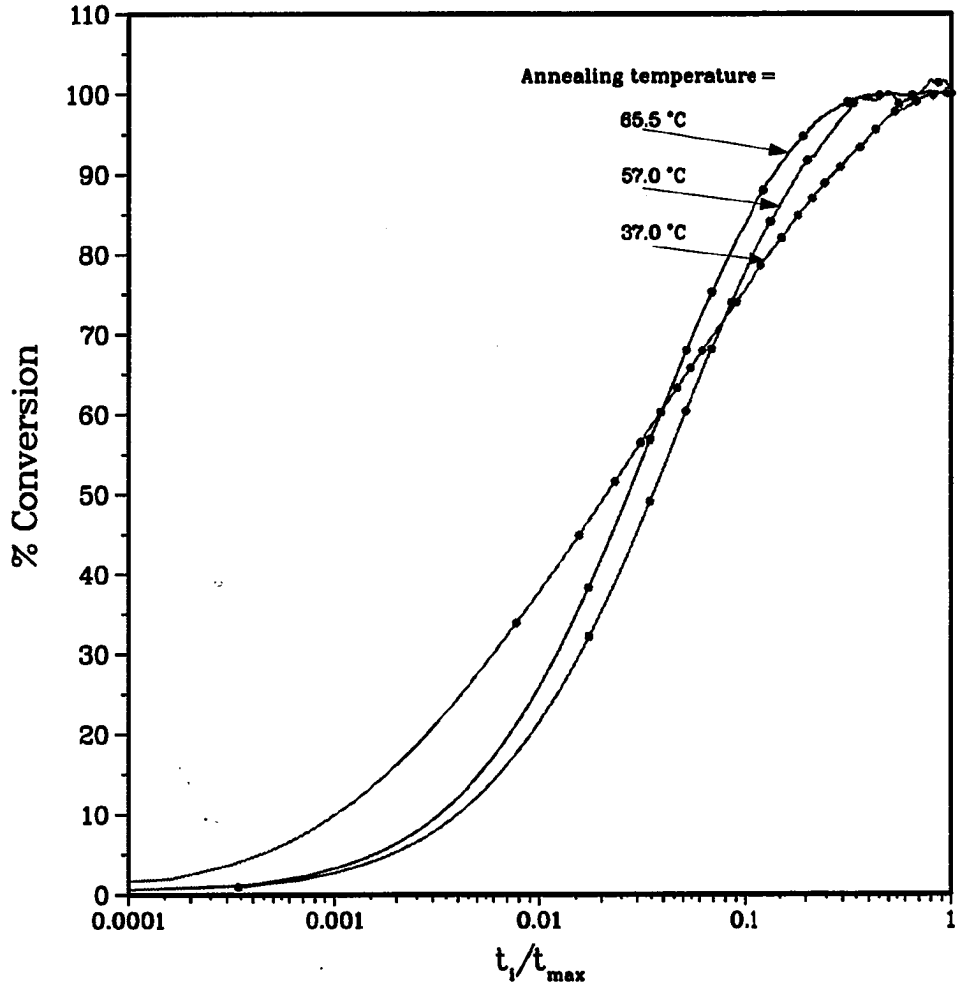

Figure 2.30: % conversion as a function of normalized annealing time for 75 wt % ZS-filled UDMA cured for 300 sec and annealed at 37.0, 57.0 and 65.5 °C.

these processes, the enthalpy changes and their rates were studied as a function of different curing times and different filler to resin ratios in an acrylate resin by means of isothermal microcalorimetric measurements. The crosslinking of these resin is accomplished by addition polymerization reactions, where the carbon double bonds on the acrylate are converted to a single bond. This process is accompanied by an exothermic heat of polymerization, which comes from the propagation reaction of free radical chains that crosslinks to an active double bond of unsaturated monomers [82]. Therefore, it can be reasonably assumed that the exothermic heat generated per unit mass and the magnitude of the exotherm can be used to follow the progress of the cure.

From the isothermal measurements, the rates of change of enthalpy and enthalpy changes of the UDMA polymer were found to be exothermic reactions and they were affected by the curing time, the filler content and the nature of the filler surface. The maximum time required for these reactions to reach equilibrium at the annealing temperatures, including body temperature, was 10^6 sec.

2.4.1 Curing Time Effect

The microcalorimetry measurements indicate that UDMA polymer and UDMA-based composites cured for longer periods of time with visible light always had higher rates of enthalpy and reaction heats than those cured for shorter periods. This suggests that annealing of resins cured for shorter times did not increase the crosslink density with time to that of the resins cured for longer, leaving more unreacted double bonds at the end of the curing and post-curing cycle and lower crosslink density. This slowing down of the curing process is due to reaching either the gel or vitrification point, which resulted in slowing the diffusion of unreacted double bonds. Thus,

this effect results in longer times required to reach equilibrium (Figures 2.3 and 2.4) and lower heat of reactions (Figures 2.17 - 2.19) in the low cured polymer and the composite resin.

At short curing times (13 and 30 sec) and high annealing temperatures (65.5 °C) for the UDMA and UDMA-based composites, the rates of enthalpy and the enthalpy changes exhibited an endothermic region at high annealing time. This observation suggests that in addition to autoacceleration, reaction occurred between the UDMA resin and other materials present in the system. These agents are possibly hydrogen-doner molecules which may be present in the system such as moisture [32]. Also, at these short curing times the reaction of the reducing agent and the camphoroquinone to form an exited complex state (exiplex) might not be complete, this endothermic reaction might be due to the reduction of the photoinitiator to form free radicals to proceed with the polymerization. In addition, it seemed that curing for 150 - 300 sec had no significant effect on the enthalpy changes, especially at low filler concentration, which might be an indication that curing for more than 90 sec with visible light did not change the crosslink density.

Although, the final conversion of the partially cured UDMA polymer and the UDMA-based composites did not reach the high conversion of those of the higher cured polymer, the conversion rates were higher at the normalized time for the lower cured polymer and composite (Figures 2.26). This contradiction can be explained by the relative number of carbon double bonds converted to single bonds which is higher in the lower cured composites, because of lower density of packing, higher diffusion rates of chain segments, and the higher availability of carbon double bonds in the lower cured composites.

2.4.2 Filler Effect

The heat of reaction of the polymer-based composite could be modified by the introduction of a plasticizer, copolymerization, or the introduction of inorganic filler. In this study, the heat of reaction of the UDMA was modified and studied by the introduction of different amounts of filler. This modification was reflected by the increase in the values of the enthalpy changes and their rates, when the filler concentration was increased to 25 % (Figures 2.21 and 2.22), while the values started to decrease at higher filler concentrations. The increases in these values at low filler concentrations were an indication of an introduction of a phase, which restricted the molecular motion of the surface layer of polymer onto filler particles, and regarded the composite as being a densely crosslinked polymer. As a result of the cross-linked structure, the thermoset was moved farther away from the glassy state and farther away from equilibrium, which caused higher enthalpy values. However, at higher filler concentrations, the enthalpy changes and their rates started to decrease. This observation might be explained by the formation of some aggregates of the filler covered with UDMA due to their high concentration [64], or it might be explained by the effect of less penetration of light which caused lower activation and the formation of free radicals. This effect may result in lower number of propagating free radicals chains, and the presence of higher number of unreacted double bonds, which leads to lower crosslink density of the composite system.

The relative conversion of the filled-UDMA is higher than the unfilled-polymer. This indicates that the lower penetration of light due to presence of the filler in the composite caused higher presence of unreacted double bonds, thus the relative number of carbon double bonds converting to single bonds is higher in highly filled-composites.

In composites containing silanated filler, the crosslink density of the composite increased as shown by the increase of the rate of change of enthalpy (Figure 2.6) and the decrease of the apparent time required to reach equilibrium. However, the change of enthalpy for samples containing silanated filler was lower than those of the unsilanated ones. Also, the overall change of enthalpy was endothermic. This observation indicates that there is breaking and forming of bonds in the system, which might be due to the dynamic equilibrium created at the interface between the filler and the polymer which serves as an internal stress reliever in the composites.

2.5 Concluding Remarks

The continual curing of the resin was monitored using microcalorimetry measurements. The rates of change of enthalpy and enthalpy changes of the UDMA polymer were found to be exothermic and they were affected by the curing time, the filler content and the nature of the filler surface. Annealing of lower cured filled- and unfilled-UDMA systems did not increase the conversion of the carbon double bonds to that of the higher cured systems. In addition, the lower cured composites may show endothermic reactions due to reduction of photoinitiators at 65.5 °C. Further, low amount of filler incorporation (25 wt %) restricts the molecular motion of the surface layer of polymer next to filler particles, and the composite can be regards as being a densely crosslinked polymer. Higher amounts of filler incorporation caused a decrease in the molecular packing of the resin, that were reflected as low enthalpy values. Finally, silanation of the filler showed a highly endothermic reaction that is probably due to breaking and forming of bonds at the interface between the organic and the inorganic phase in the composite.

CHAPTER III

THE EFFECTS OF DIFFERENT ADDITIVES ON THE DIELECTRIC RELAXATION IN URETHANE DIMETHACRYLATE POLYMER

3.1 Introduction

Polymeric-based composites, including medical and dental composites, are multi-component systems, that include pure polymers, stabilizers, plasticizers, dyes, organic and inorganic fillers. These components are usually incorporated to change and improve specific macroscopic properties such as toughness, fatigue, hardness, friction and electrical insulation. Generally, these additive components may be divided into two main physical groups: compatible and incompatible [47]. In the first group, the additives do not form a separate phase in the polymer compound, which results to some degree in a homogeneous compound (examples are plasticizers). In the second group, the additives form a separate phase that results in a heterogeneous system (examples are fillers, dyes and water inclusions), if the solubility is exceeded.

As an incompatible additive, fillers play an important role in determining and regulating properties of composites such as strength, modulus, color and durability. A wide variety of inorganic-filled polymers have been characterized quite extensively in terms of particles size, structure, density and porosity of the filler. However, what

is more difficult to characterize is the property called polymer-filler interaction. This term broadly includes the interfacial forces between the filler and the polymer, the orientation of the polymer in the vicinity of the surface filler, the formation of the interphase and other physicochemical phenomena [115]. Without knowledge of these interactions one has difficulty selecting fillers for a particular polymer system, and finding the appropriate conditions for their processing.

The polymer-filler interaction has been a topic for many researchers. It has been shown that the effect of filler incorporation as an incompatible separate phase can often interfere with the curing mechanism, either by altering the chemical environment, participating in the side reactions or simply removing active ingredients from the organic matrix by adsorption onto the filler surface [115]. Also, filler concentration as well as type and size, are statistically significant factors that affect the glass transition temperature (T_g) in silica-poly(vinyl chloride-co-vinyl acetate) system [38]. Filler presence also changes the extent and direction of the change in T_g with different thermal history in polystyrene-silica and epoxy-rubber systems [75]. Further, composite materials have higher elastic moduli and lower damping compared with unfilled resin for a range of polymeric restorative materials [109]. The presence of Aerosil and Teflon fillers in polystyrene and PMMA is reflected in changes of the maximum in dielectric side chains relaxation toward lower temperatures, and of the maximum of the T_g toward higher temperatures [61].

The effect of polymer-filler interaction can be investigated by dielectric measurements, which enables one to study and analyze the mobility of functional groups and segment chains separately. Also, dielectric measurements can detect the effects of different conditions on the different regions of the dielectric dispersion and on the different structural elements of the chains. Therefore, the purpose of this portion of

the research was to investigate, in some detail, the dielectric loss in a dental polymer, urethane dimethacrylate. Special attention is given to determine how a non-compatible inorganic phase modifies the molecular behavior of the polymer chains and how modification of this phase by silanation can affect these molecular behaviors. The dielectric dispersions and loss tangents of different filler concentrations were measured over a wide range of frequencies and temperatures for zirconia-silica-filled urethane dimethacrylate composites. In addition, the effect of different silanes and different silane concentrations used in treating the zirconia-silica was also measured under the same conditions.

3.2 Theory

The dielectric $Tan(\delta)_\epsilon$ and the mechanical $Tan(\delta)_G$ values measured as a function of temperature were fitted by least square method using polynomial curves of varying degrees (3.1).

$$\begin{aligned} y &= a_0 + a_1 x + a_2 x^2 +, \ldots, + a_n x^n \\ &= \sum_{k=0}^{n} a_k x^k \end{aligned} \tag{3.1}$$

where

y = $Tan(\delta)_\epsilon$ or $Tan(\delta)_G$

x = temperature

n = degree of polynomial

a_k = unknown coefficients to be determined

The degrees of the chosen polynomial varied between nine and thirteen for the dielectric values, while they were varied between twenty three and twenty five for the mechanical values, depending on the degree that best fit the data.

Since the polymer sample was equivalent to a capacitance (C), and was in series with a resistance (R), at a particular frequency and temperature, the dielectric permittivity ϵ' and the loss ϵ'' were calculated from the values of the measured $Tan(\delta)_\epsilon$, capacitance and empty capacitance as follows:

$$\epsilon' = \frac{C(T_i, f_j)}{C_o(f_j)[1 + (Tan\delta_\epsilon(T_i, f_j))^2]} \tag{3.2}$$

and

$$\epsilon'' = \epsilon' Tan\delta_\epsilon(T_i, f_j) \tag{3.3}$$

where

T_i = temperature (°C), $i = 1, 2, 3, \ldots, 73$

f_j = frequency (kHz), $j = 1, 2, 3, \ldots, 83$

$C(T_i, f_j)$ = measured capacitance at T_i and f_j

$C_o(f_j)$ = measured empty cell (no sample) capacitance with a gap distance between the charged plates equal to sample thickness for the specific f_j at ambient temperature

$Tan\delta_\epsilon(T_i, f_j)$ = measured dielectric loss tangent at T_i and f_j

In order to resolve the dipolar and ionic natures of the relaxation processes observed, as in the analysis of the ionic solids, the conductance and the capacitance were converted into the complex electrical modulus formalism [72],

$$M^* = (\epsilon^*)^{-1} = M' + i\, M'' \tag{3.4}$$

where the real components of the complex electric modulus, M' and the imaginary components M'' were calculated as follows:

$$M' = \frac{\epsilon'}{\epsilon'^2 + \epsilon''^2} \tag{3.5}$$

and

$$M'' = \frac{\epsilon''}{\epsilon'^2 + \epsilon''^2} \tag{3.6}$$

The change in activation energy (ΔH) and pre-exponential factor (τ_o) were determined by following the Arrhenius relation,

$$\tau = \tau_o \exp\left(\frac{-\Delta H}{RT}\right) \tag{3.7}$$

where

τ = relaxation time (Hz)

τ_o = pre-exponential factor (Hz)

ΔH = activation energy (kcal/mole)

R = universal gas constant (kcal/mole °K)

T = temperature (°K)

and,

$$\tau_o = \frac{1}{\nu}\exp\left(\frac{-\Delta S}{R}\right) \tag{3.8}$$

where ΔS is the change in the activation entropy, h is Plank's constant, k is Boltzmann's constant, and ν is related to the previously defined parameters by the following relationship:

$$\frac{1}{\nu} = \left(\frac{h}{kT}\right) \tag{3.9}$$

It is possible to calculate ΔH and τ_o by measuring $Tan(\delta)_\epsilon$ or $Tan(\delta)_G$ as a function of $\omega\ \tau$ by keeping ω constant and varying τ by varying the temperature. If $Tan(\delta)_{\epsilon,max}$ or $Tan(\delta)_{G,max}$ are the maximum value ($Tan(\delta)_{max}$) of $Tan(\delta)$, we have the relation for a single relaxation time [71],

$$\frac{Tan\delta}{Tan\delta_{max}} = \frac{2\omega\tau}{1+\omega^2\tau^2} = sech\ln\omega\tau \tag{3.10}$$

and by substituting Equation (3.7) into (3.10),

$$\frac{Tan\delta}{Tan\delta_{max}} = sech\left[\frac{\Delta H}{RT} + \ln\omega\tau_o\right] \tag{3.11}$$

and at $Tan(\delta) = Tan(\delta)_{max}$ Equation (3.11) becomes,

$$1 = sech\left[\frac{\Delta H}{RT} + \ln\omega\tau_o\right] \tag{3.12}$$

with little manipulation, Equation (3.12) follows the equation of a straight line in the form of,

$$\frac{1}{T} = \left(\frac{-R}{\Delta H}\right) \ln \omega - \left(\frac{R}{\Delta H}\right) \ln \tau_o \tag{3.13}$$

ΔH and τ_o were calculated from the slope and the intercept of the plot of the angular frequency ($\ln(\omega)$) at which the loss tangent $Tan(\delta)_\epsilon$ or $Tan(\delta)_G$ was a maximum against the reciprocal temperature.

For a single relaxation time, the total half-width of ϵ'' curve ($\Delta_{1/2}$) in decades was calculated from

$$\Delta_{1/2} = 2[f_r - f_{max}] \tag{3.14}$$

where, f_r is the frequency at which $\epsilon'' = \frac{\epsilon''_{max}}{2}$, and f_{max} is the frequency at which ϵ'' is maximum.

Finally, the thickness of adsorbed layer onto the filler was calculated using the following [115]:

$$Tan\delta_c = \frac{Tan\delta_o}{(1 + 1.5\phi_F B)} \tag{3.15}$$

where, $Tan\delta_c$ and $Tan\delta_o$ are the loss tangent of the composite and the polymer, respectively, ϕ_F is the volume fraction of the filler, and

$$B = \left(1 + \frac{\Delta R}{R_o}\right)^3 \tag{3.16}$$

where, R_o is the filler radius.

3.3 Experimental

3.3.1 Materials

Urethane dimethacrylate (UDMA) (Esschem Co., Essington PA) was used as a monomer system. Zirconia-silica (ZS) (3M Dental Products, St.Paul MN) with the same specification given previously was used as a filler. 3-methacryloxypropyl-trimethoxysilane (MAPM) and 4-aminobutyltriethoxysilane (ABTE) (Huls America, Piscataway NJ, formerly Petrarch Systems, Bristol PA) were used as a coupling agent to silanate the filler. As discussed in the previous chapter, MAPM was used because it has been shown by Craig and Mohsen [28] to be one of the most effective silanating agents for increasing the dispersion and wetting behavior of the filler particles by the monomer in this particular system, and has a carbon double bond to react with the monomer, while ABTE was shown to be not effective in wetting the filler particles by the monomer.

3.3.2 Sample Preparation

The filler was silanated as described previously by depositing the silane from an aqueous solution. The amount of silane used for the filler treatment in this part of the study was multible amounts of the minimum uniform coverage given by Equation (2.1).

Composites were formulated from UDMA, zirconia-silica and MAPM- or ABTE-silanated zirconia-silica, using *dl*-camphoroquinone as a catalyst and 2-dimethyl-aminoethylmethacrylate as an accelerator in concentrations described by Douglas, Craig and Chen [31]. The mixed composite paste was cast into thin films which were cut into discs (63.5 mm diameter and 0.5 mm thick) for dielectric measurements and was made in a form of right angle parallelepiped (54.5 mm long, 4.8 mm width and

2.9 mm thick) for mechanical measurements. The specimens were cured by visible light at 550 nm in a TRIAD II oven (Dentsply International, York, PA) for 5 min at room temperature, and then they were dried for 18 hrs in vacuum at 90 - 100 °C to remove the moisture and to insure uniform and homogeneous curing. The weight percentages of the unsilanated zirconia-silica in the composite samples were 0, 15, 45, 60 and 75 wt %, while it was 75 wt % MAPM- or ABTE-silanated zirconia-silica in the composite samples. The amount of silane used to treat the filler given by Equation (2.1), was the minimum uniform coverage (1X), three times (3X), six times (6X), ten times (10X) and thirty times that amount (30X). The weight percentage of zirconia-silica in the composite samples was 75 wt %.

3.3.3 Methods

Dielectric measurements. The sample was sandwiched between two flat edge-free capacitance plates in the assembled dielectric cell. The upper capacitance plate was pressed against the sample and bolted to the bottom plate. A micrometer was used to raise the bottom plate until the sample touched the upper plate and closed the air gap. The thickness of the sample was read from the micrometer. The dielectric cell was covered by a glass container and was flushed with dry nitrogen for 1 hr before starting the measurements to ensure the absence of moisture. Then, it was kept in the dry nitrogen environment throughout the experiment. The cell's temperature was lowered by means of liquid nitrogen.

The dielectric loss tangent ($Tan(\delta)_{\epsilon o}$) and capacitance (C) measurements were carried out over a frequency range of 0.013 to 200.000 kHz from -180 to 180 °C by means of GenRad 1693 RLC Digibridge (GenRad Inc., Concord MA), which was connected to the dielectric cell and interfaced with a Macintosh PC computer for

data collection. Also, the $Tan(\delta)_\epsilon$ and capacitance (C_o) were measured for an empty cell with the same experimental conditions and sample thickness over the frequency range at ambient temperature. The C_o measurements were used for calculations of the dielectric constant ϵ' and the loss factor ϵ'' which are discussed in section (3.2). The dielectric spectra of five replicas for each filler-monomer ratio were measured, and three replicas for each silane used as well as for each amount of silane used to treat the filler.

Mechanical measurements. The dynamic mechanical measurement was performed by means of torsion pendulum apparatus Micromecanalyseur system (INSA-METRA-VIB, Lyon France). In this particular apparatus, the lower part of the sample was clamped rigidly, whereas the upper part was connected to a vertical rod supported by a counter balance. This rod carried another horizontal one, known as the inertia rod, with weights at the end. The inertia rod was displaced slightly to twist and oscillate the sample. The decay of the oscillations was then detected by a galvanometer lamp and a scale. The assembly was immersed in liquid nitrogen for cooling to low temperatures and was heated to high temperatures gradually. The temperature of the sample was monitored by a thermocouple kept in contact with the sample. The shear modulus (G') and the mechanical loss tangent ($Tan(\delta)_G$) for the unfilled-UDMA was measured over a temperature range of -120 to 180 °C and frequency range of 0.01, 0.1 and 1.0 Hz.

3.4 Results and Discussion

3.4.1 Assignments of Dielectric Relaxations of UDMA

The mechanical loss tangent ($Tan(\delta)_G$) and the shear modulus G' for the unfilled-UDMA measured at 0.01, 0.1 and 1.0 Hz are plotted against temperature in Figure

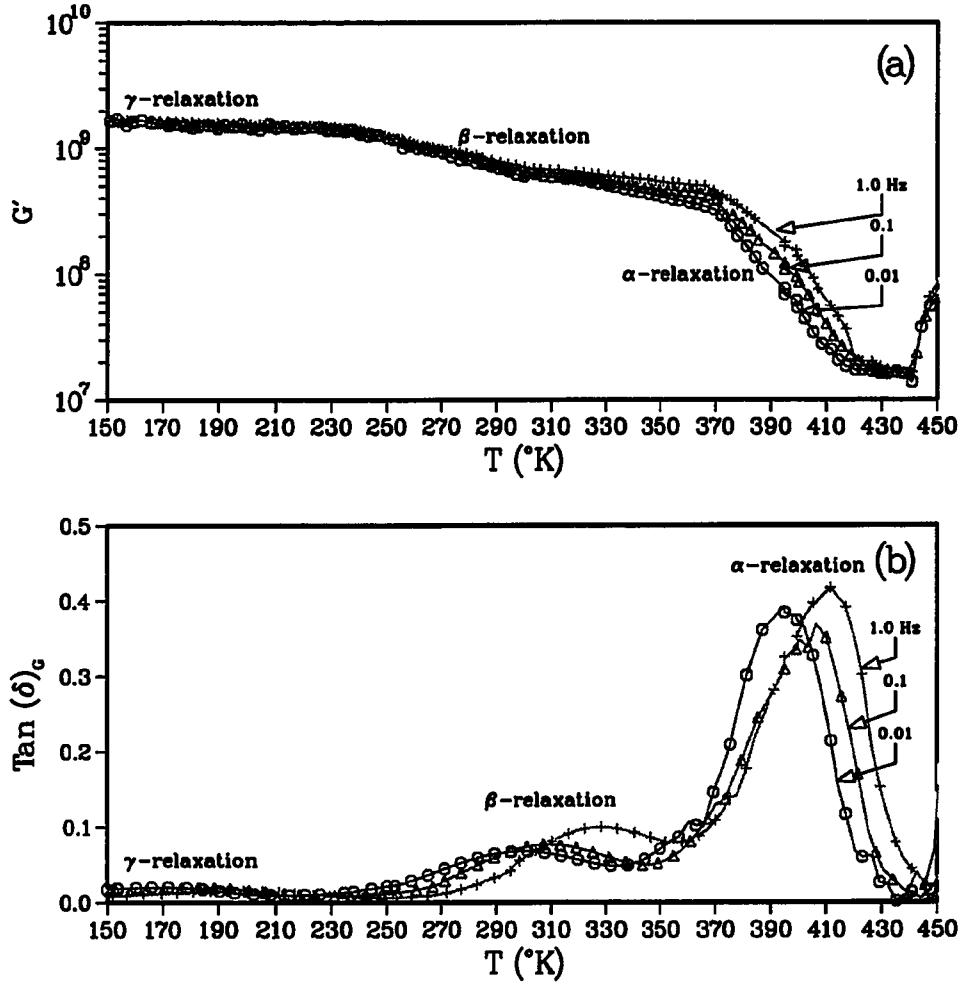

Figure 3.1: (a) G' and (b) $Tan(\delta)_G$ against temperature for unfilled-UDMA at 0.01, 0.1 and 1.0 Hz.

3.1. The G' and the $Tan(\delta)_G$ curves show three mechanical relaxations appeared as $\alpha-$, $\beta-$ and $\gamma-$peaks. For instance, at 1.0 Hz, $Tan(\delta)_G$ shows the α-relaxation peak at 414 °K with a magnitude of 0.405, while G' shows a change in magnitude of $3.85*10^8$ over the range of the relaxation. The curve also shows the β-relaxation peak at 310 °K with a magnitude of 0.077, while G' curve shows a change in magnitude of $8.5*10^8$ over the range of the relaxation. In addition, it shows the γ-relaxation peak at 183 °K with a magnitude of 0.0197, while the G' curve shows a change of magnitude of $2.5 * 10^9$ over the range of the relaxation. Since the UDMA monomer structural formula sketched in Figure 3.2(c), consists of urethane linkage (-NHCO-), separated by (-$(CH_2)_8$-) and contains methacrylate group at both ends to react by free radical polymerization to form the polymer, the main chain structure for the UDMA polymer closely resembles the polyurethanes and polyamides main chain structure (Figures 3.2(a) and 3.2(b)), respectively.

In polyurethanes and polyamides, the most pronounced dispersion corresponds to the glass-rubber transition (T_g) of the amorphous phase, the secondary relaxation (β) corresponds to rotation of unbounded amide groups or to the motion of a water-polymer complex, the third relaxation (γ) corresponds to local mode motions of the main chain [47, 71]. Mechanical losses in nylon 6, nylon 66, and urethane-acrylate oligomer have been measured by McCrum *et al.* [71], Woodward *et al.* [111] and Wadhwa and Walsh [107], respectively. In addition, the dielectric losses in nylon 66 have been measured by Boyd [14] and Rushton and Russell and whose results were reported by McCrum *et al.* [71]. The loss peaks found by these investigators are listed in Table 3.1 together with obtained mechanical and dielectric values from Figures 3.1 and 3.3, respectively. The α-relaxation has been attributed by all of the investigators to the segmental chain motion in the amorphous regions. The β-

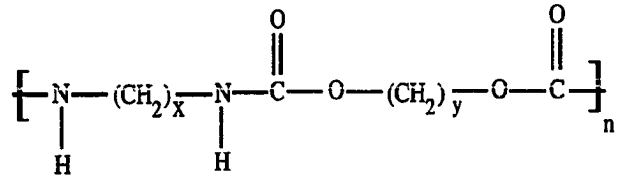

a) General Polyurethane Structure

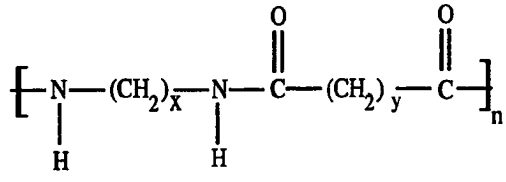

b) General Polyamide Structure

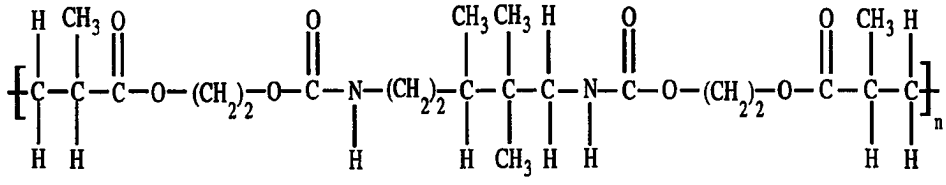

c) 2-Methyl-2-Propenoic Acid (2, 4, 4-trimethyl-1, 6-hexanediyl) bis(imino carbonyloxy - 2, 1-ethanediyl) ester (**UDMA**)

Figure 3.2: Structural formulas for (a) polyurethanes, (b) polyamides and (c) UDMA.

Type of measurement	Materials	Maximum peak (Temperature (°C) & Frequency (kHz))		
		$\alpha-$	$\beta-$	$\gamma-$
Mechanical[a]	Urethane-Acrylate	72.0 (0.1)	-40.0 (0.1)	—
Mechanical[b]	Nylon 6	78.0 (0.1)	-40.0 (0.1)	-120.0 (0.1)
Mechanical[c]	Nylon 66	77.0 (1.05)	-23.0 (0.2)	-103.0 (0.4)
Dielectric[d]	Nylon 66	50.0 (0.01)	-10.0 (0.1)	—
		72.0 (1.0)	—	—
Dielectric[e]	Nylon 66	90.0 (10.0)	10.0 (10.0)	-20.0 (1000.0)
Mechanical[f]	UDMA	141.0 (0.001)	37.0 (0.001)	-90.0 (0.001)
Dielectric[g]	UDMA	82.2 (0.053)	-71.9 (0.053)	—
		—	-38.8 (1.0)	—
		156.6 (10.0)	10.7 (10.0)	—
		—	36.8 (100.0)	—

[a] Wadhwa and Walsh (1982)[107].
[b] McCrum *et al.* (1967)[71].
[c] Woodward *et al.* (1957)[111].
[d] Boyd (1959)[14].
[e] Rushton and Russell reported by McCrum *et al.* (1967)[71].
[f] Extrapolated values Fig 1.1 from this work.
[g] Extrapolated values Fig 1.3 from this work.

Table 3.1: Comparison of mechanical and dielectric loss maximum peaks temperatures for $\alpha-$, $\beta-$ and $\gamma-$relaxations for different polymer systems.

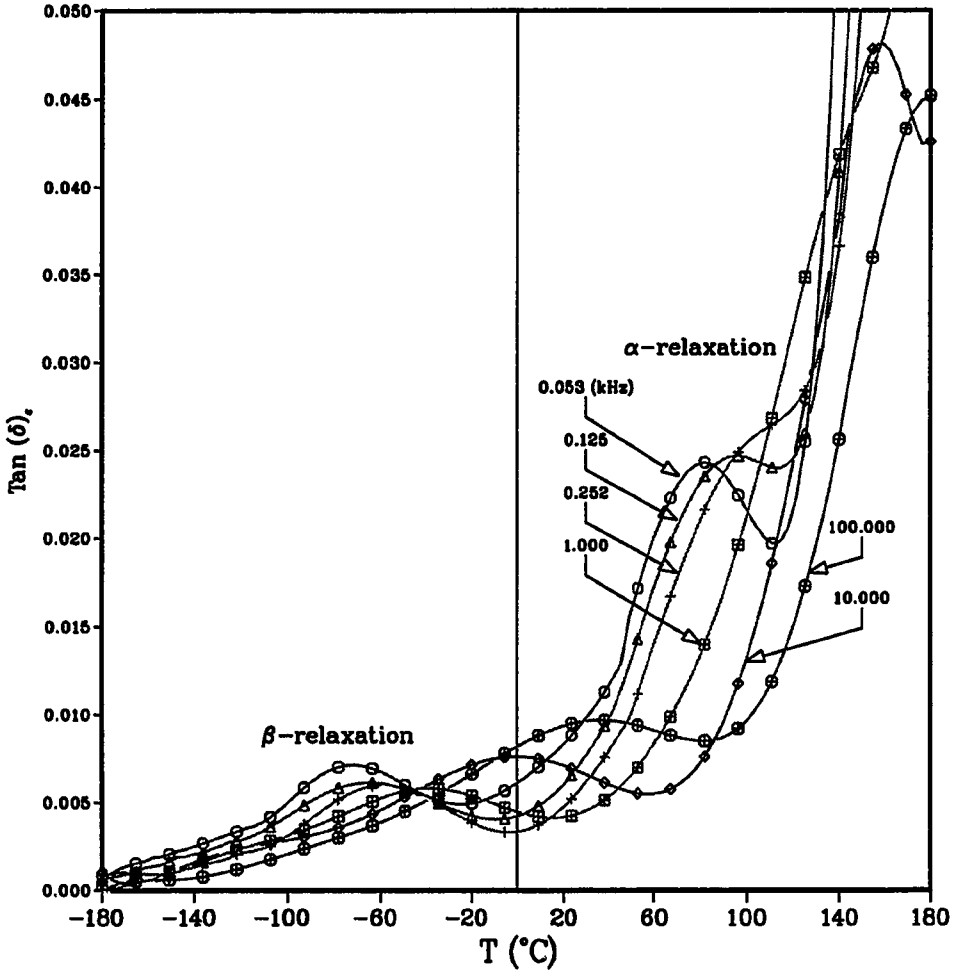

Figure 3.3: $Tan(\delta)_\epsilon$ against temperature for unfilled-UDMA at 0.053, 0.125, 0.252, 1.0, 10.0 and 100.0 kHz.

relaxation has been assigned by McCrum *et al.*, and Rushton and Russell to the motion of a water-polymer complex, or more specifically, to the motion of carbonyl groups to which water molecules are attached by hydrogen bonds. The same relaxation has been attributed by Woodward *et al.* and Boyd to the motion of unbounded amides, while it has been assigned by Wadhwa and Walsh to the rotational motion of substituent groups in the local environment. However, the γ-relaxation has been assigned by McCrum *et al.*, Woodward *et al.* and Rushton and Russell to the motion of $(CH_2)_n$ sequences. Therefore, the main peak (α-peak) in UDMA can be assigned to the T_g, the β-peak to the motion of unbound amides, since the relaxation did not disappear with vacuum drying, and the γ-peak can also be assigned to the motions of $(CH_2)_n$ sequences.

The shape of the relaxation transitions of $Tan(\delta)_G$ and the appearance of the relaxation peaks for the UDMA coincided with thermomechanical relaxations and transitions for the polyurethanes and polyamides. However, The maximum for UDMA's peaks occurred at much higher temperatures. This shift to higher temperature has been seen when the $(CH_2)_n$ sequences decreased in length, a result found for polyamides and polyurethanes, where nylon 66 has higher T_g than nylon 11 [71]. This is also true in the case of UDMA, where $n = 5$ in the $(CH_2)_n$ sequences between the urethane linkages and $n = 2$ between the urethane and the methacrylate groups. Further, the presence of methyl groups attached to the methacrylate groups and to the $(CH_2)_n$ sequences affects the mode of packing of the molecules so as to increase the density. In the absence of these bulky groups, the strict requirements of hydrogen bonds prevent the molecules from packing as closely as they would if van der Waals's forces were dominant. The presence of the bulky methyl groups lowers the number of interchain hydrogen bonds enabling the chains to pack more closely

and this could be responsible for the shift of the peaks to higher temperatures.

The dielectric loss tangent $Tan(\delta)_\epsilon$ values exhibited by the vacuum dried unfilled-UDMA measured at 0.053, 0.125, 0.252, 1.0, 10.0 and 100.0 kHz are plotted against temperature in Figure 3.3. The $Tan(\delta)_\epsilon$ curves show two dielectric relaxation peaks appeared as $\beta-$ and $\alpha-$peaks, followed by rapidly increasing loss tangent with increasing temperature. For instance, at 0.053 kHz, the β-peak occurred at -71.9 °C with a magnitude of 0.007 and the α-peak occurred at 82.2 °C with a magnitude of 0.024, while the rapid increase in $Tan(\delta)_\epsilon$ started above 110 °C.

Typical isothermal spectra of the dielectric permittivity ϵ' and the loss ϵ'' curves at low temperatures calculated from Equations (3.2) and (3.3) for vacuum dried unfilled-UDMA are plotted against $\log(f)$ in Figure 3.4. The ϵ' curves show a typical sub-T_g or β-relaxation peak, where their values increased with elevation of the measurement temperature in the range of -60 to 10 °C and with increasing the measurement frequency. For example, the β-relaxation occurred at -30.0 °C and 25 kHz. Further, the isothermal spectra of the ϵ' and ϵ'' curves at high temperatures calculated for the dried unfilled-UDMA are plotted against $\log(f)$ in Figure 3.5. In this figure, the ϵ'' curves showed a large contribution from the DC conductivity near the T_g at high temperatures and low frequencies. Such DC conductivity masked the ϵ'' peak that is due to segmental motion of the main chains, so the α-relaxation in the glass-rubber transition region could not be observed. This rise in the DC conductivity was ascribed to a mechanism involving movements of the protons in the hydrogen bonds [71]. However, by calculating the real component M' and the imaginary component M'' of the complex electrical modulus, using the relations (3.5) and (3.6) at several temperatures and plotting their values against the high frequencies in Figure 3.6, one observes the α-relaxation peaks are more pronounced than those

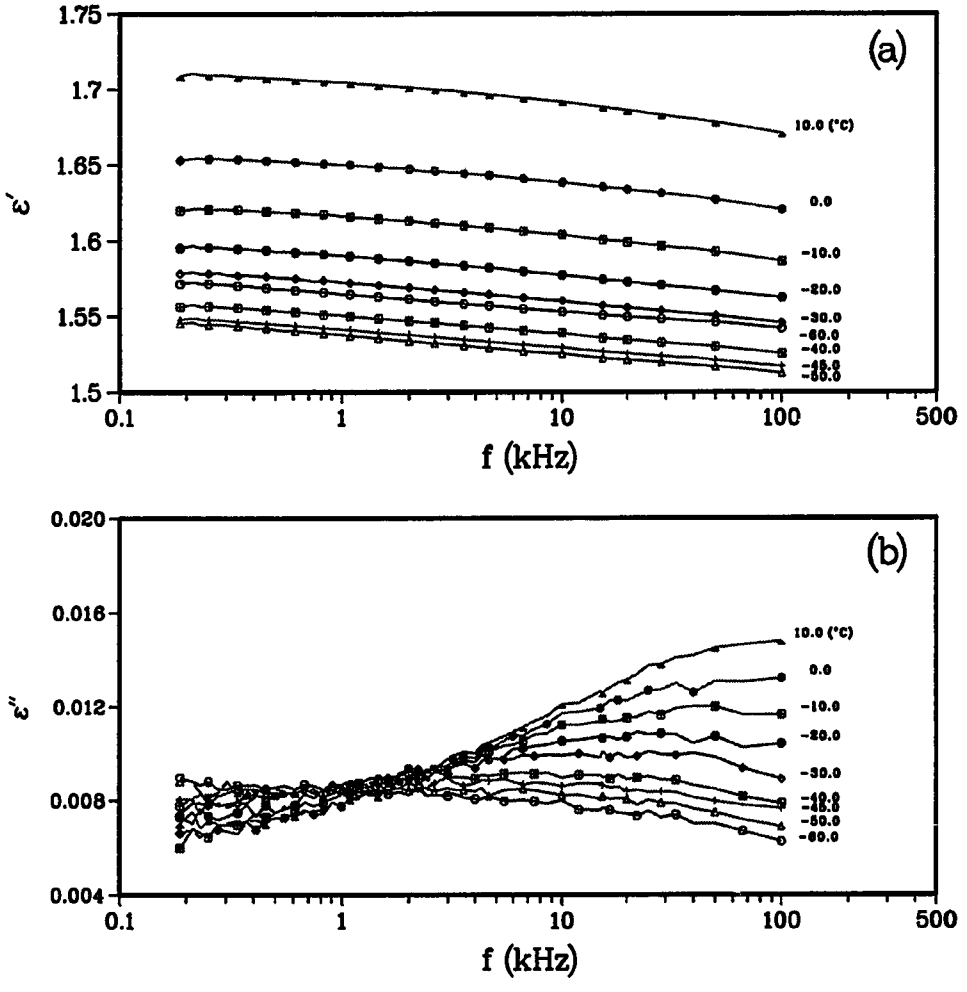

Figure 3.4: The spectra of (a) ϵ' and (b) ϵ'' against frequency for β-relaxation of unfilled-UDMA over the temperature range of -60 to 10 °C.

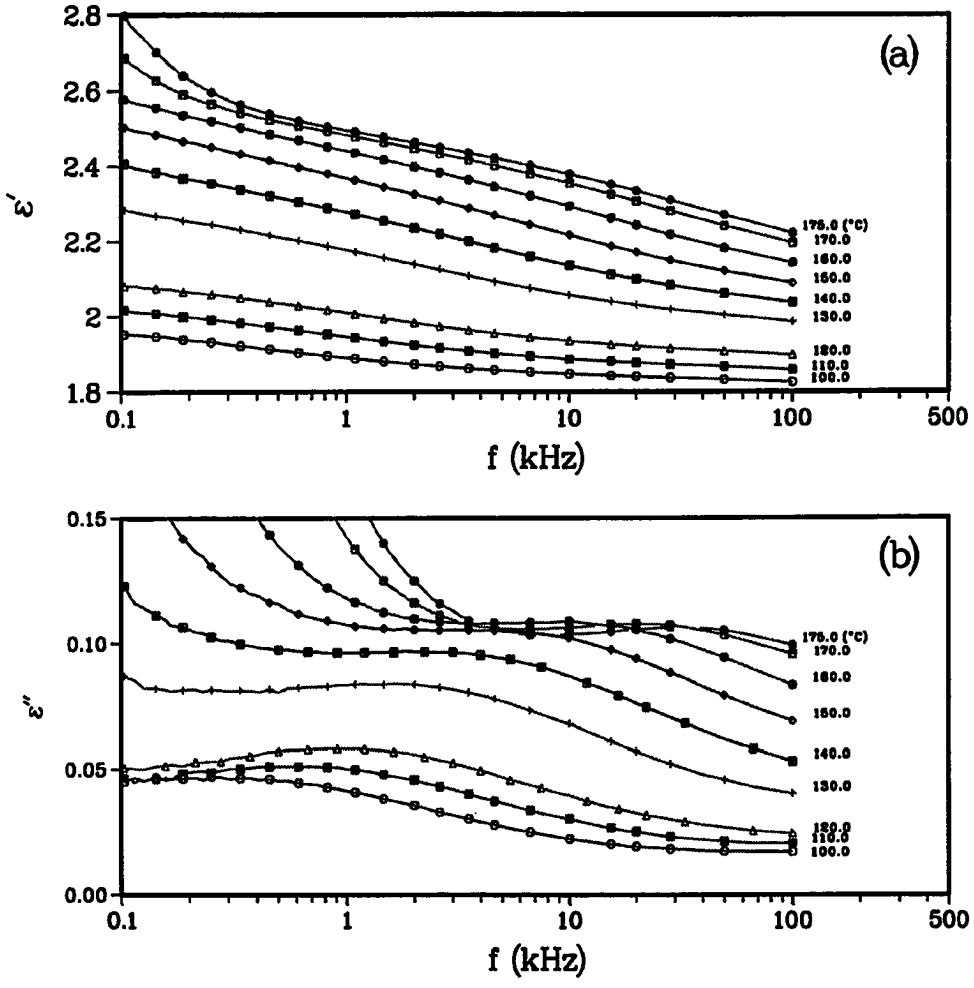

Figure 3.5: The spectra of (a) ϵ' and (b) ϵ'' against frequency for α-relaxation of unfilled-UDMA over the temperature range of 100 to 175 °C.

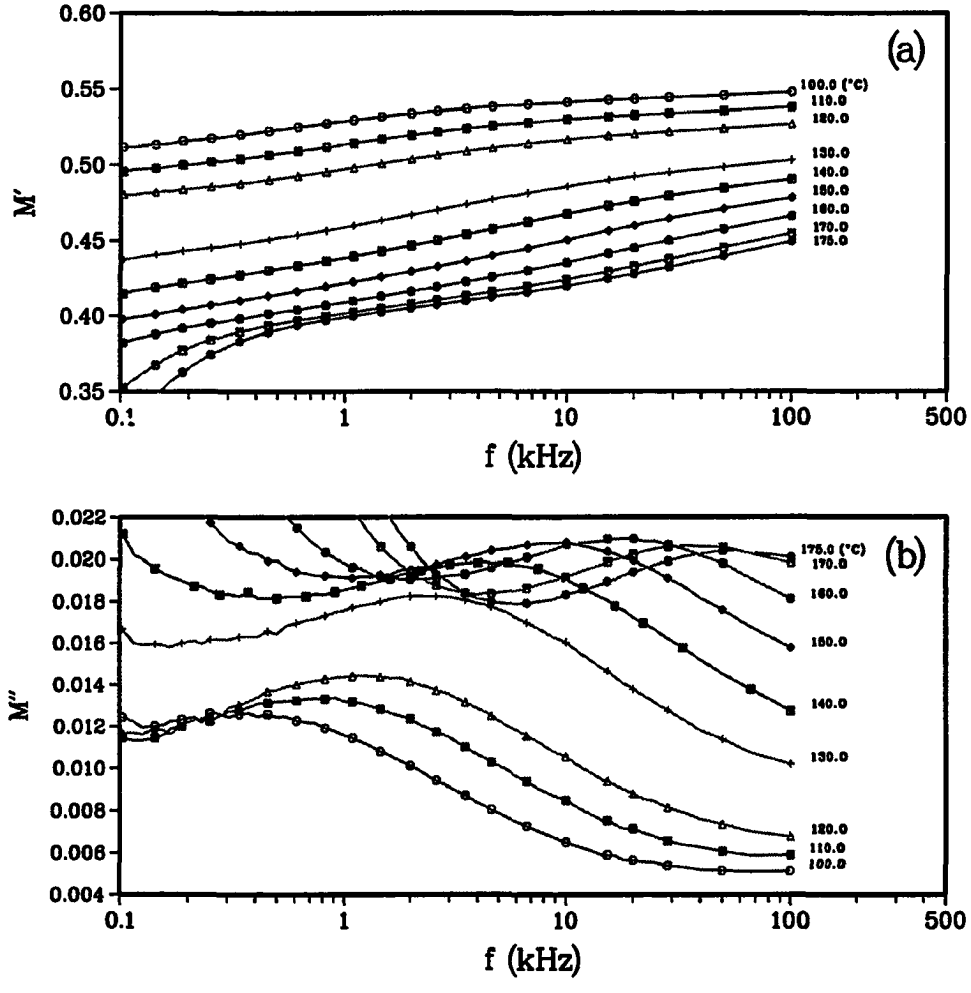

Figure 3.6: The spectra of (a) M' and (b) M'' against frequency for α-relaxation of unfilled-UDMA over the temperature range of 100 to 175 °C.

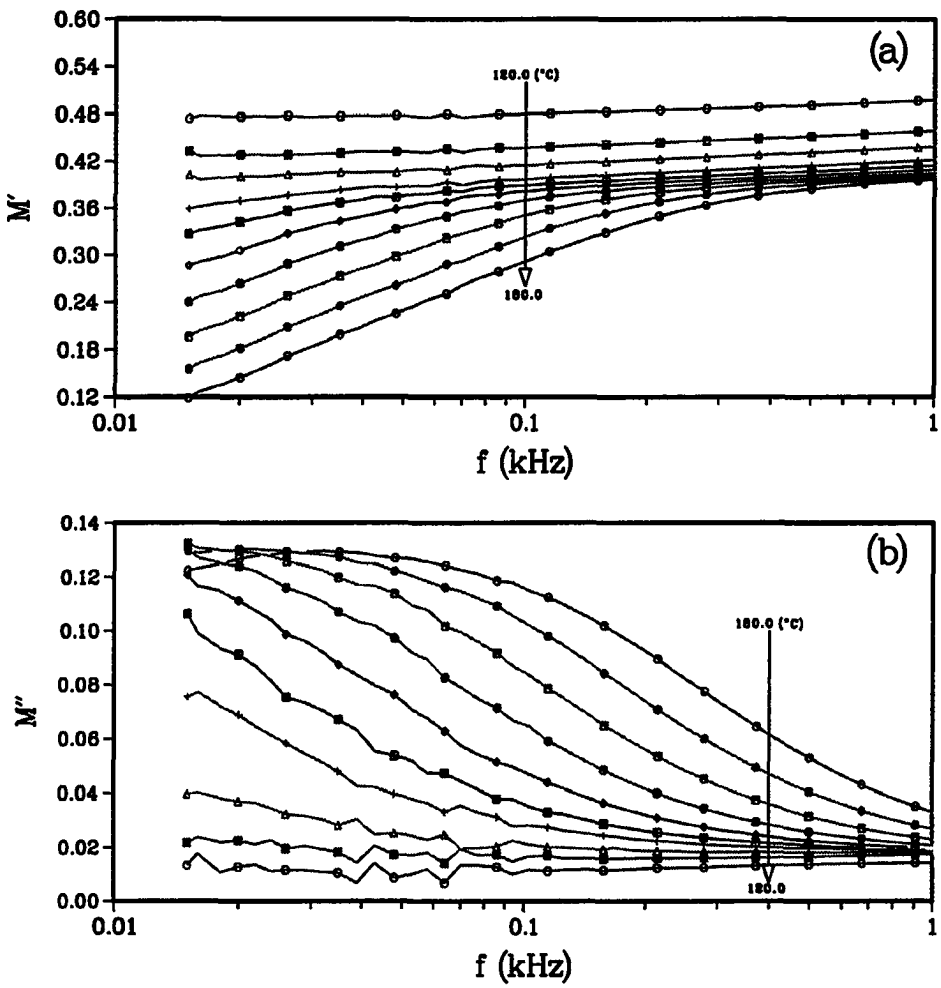

Figure 3.7: The spectra of (a) M' and (b) M'' against frequency for unfilled-UDMA over the frequency range of 0.01 to 1.0 kHz and over the temperature range of 120 to 180 °C.

of Figure 3.5. As in Figure 3.5, M'' curves show substantial increase in their values at high temperatures and low frequencies. If one looks more closely at the low frequency region, M'' curves show an onset of a new peak in Figure 3.7, which is contributed to space charge and/or Maxwell-Wagner-Sillars polarization.

With the exception of the disappearance of the γ-peak and of the elevation of $Tan(\delta)_\epsilon$ at high temperature and low frequencies, the two observed dielectric relaxation peaks for UDMA coincided with the thermomechanical relaxations in Figure 3.1. By comparing the location of these peaks with those in Table 3.1, one can give the $\alpha-$ and $\beta-$relaxations the same assignments as those observed in the mechanical measurements and those in the dielectric measurements. However, the values of the dielectric loss for UDMA are much higher probably due to the decrease of the $(CH_2)_n$ sequences length in the main chain and the increase of the density of packing of the molecule, as discussed previously.

The peaks of the angular frequency ($\ln(\omega)$), at which the loss tangent $Tan(\delta)_\epsilon$ or $Tan(\delta)_G$ was a maximum for the unfilled-UDMA were plotted against the reciprocal temperature in Figure 3.8. The activation energies and the pre-exponential factors were calculated from the slopes and intercepts of Figure 3.8 by using Equation (3.13) and the values are shown in Table 3.2. The values of the mechanical experiments are much higher than those of the dielectric measurements. This can be explained by the fact that the loss values were measured at much lower frequencies in the mechanical than the dielectric experiment. At such low frequencies, the slope of $\ln(\omega)$ against the reciprocal temperature is sharper, especially for the high temperature relaxations. Thus, one would expect higher activation energies. Further, in the dielectric experiments, the loss is measuring the net effective dipole moment in the interaction with the alternating electric field as opposed to the actual dynamic motion of the chains,

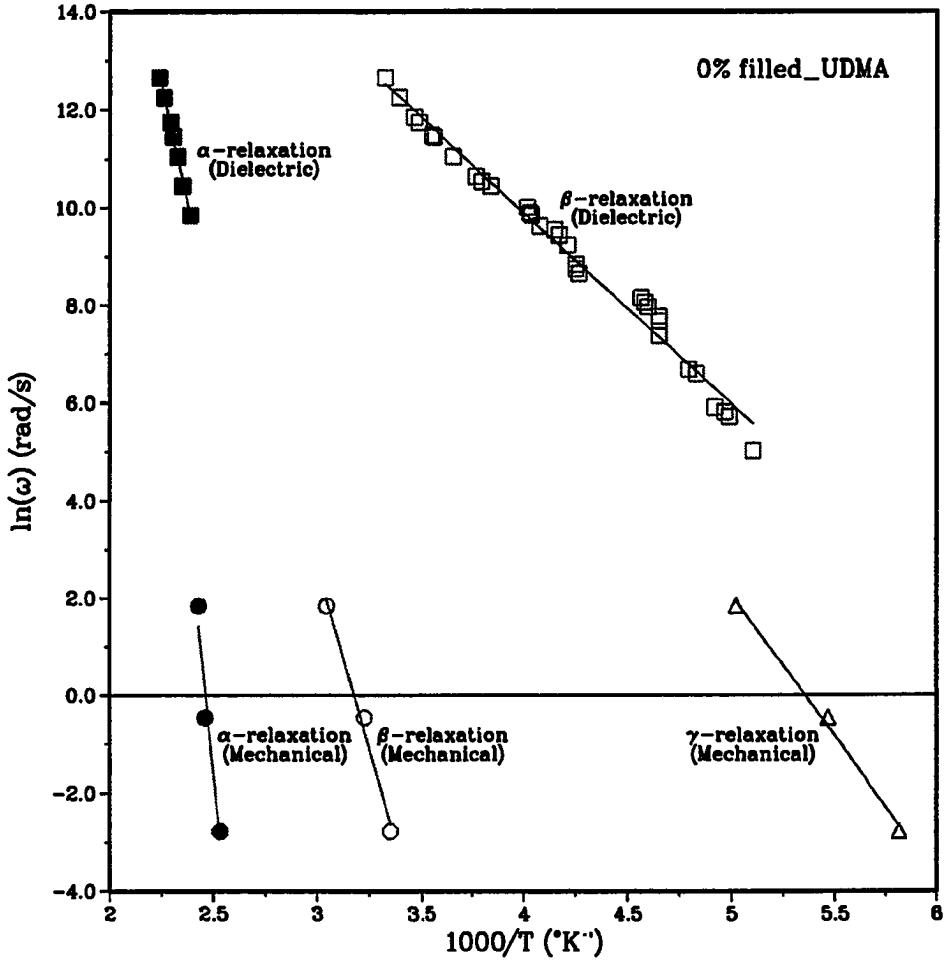

Figure 3.8: The angular frequency of $Tan(\delta)_\epsilon$ and $Tan(\delta)_G$ maximum for $\alpha-$, $\beta-$ and $\gamma-$relaxations against $\frac{1}{T}(^\circ K^{-1})$ obtained by dielectric and mechanical measurements for unfilled-UDMA.

Relaxation peak	UDMA Dielectric		UDMA Mechanical	
	Activation energy (kcal/mole)	τ_o (Hz)	Activation energy (kcal/mole)	τ_o (Hz)
$\alpha-$	40.4 ± 6.4	$5.7 * 10^{-25}$	89.1	$1.0 * 10^{-49}$
$\beta-$	7.5 ± 0.5	$3.2 * 10^{-12}$	30.1	$1.9 * 10^{-22}$
$\gamma-$	—	—	11.5	$5.3 * 10^{-12}$

Table 3.2: Activation energies and pre-exponential factors from dielectric and mechanical measurements for unfilled-UDMA polymer.

that is measured in the mechanical experiment.

Comparing the activation energies calculated from the dielectric measurements with those reported in the literature, the apparent activation energy from the α-relaxation peak reported by Boyd [14] was 46 kcal/mole for nylon 66, while those reported by Baker and Yager [11] were 24 and 42 kcal/mole for nylon 610 at low and high temperatures, respectively. These values compare well with the value of 40 kcal/mole (Table 3.2) for the α-relaxation of UDMA determined from the dielectric measurements.

Since in these types of polymers, where the polar groups are directly built in the main chain, one would expect the intensity of the dielectric loss of the α-peak to be the most dominating. This is the case for UDMA as illustrated in Figure 3.3. And with the exceptions of the disappearance of the γ-peak and the elevation of $Tan(\delta)_\epsilon$ at high temperatures and low frequencies, the two observed dielectric relaxation peaks for UDMA coincide with the thermomechanical relaxations in Figure 3.1. Further, by comparing the location of $Tan(\delta)_\epsilon$ peaks of UDMA with those reported in Table 3.1, one can give the $\alpha-$ and $\beta-$relaxations the same assignments as those observed in the mechanical and the dielectric measurements. However, the values of the dielectric loss for UDMA are higher probably due to the same reasons discussed above. So, it would be logical to assign the α-relaxation to the initiation of the micro-Brownian motion of the molecular chains from the frozen state, and the β-relaxation to the motion of the free amide groups. It would also be suitable to assign the increase of the $Tan(\delta)_\epsilon$ to the superposition of the space charge separation and the DC conductivity that is due to the movements of the protons in the hydrogen bonds of the amide groups.

3.4.2 The Effect of Filler Incorporation on the Dielectric Relaxations of UDMA

The dielectric loss tangent ($Tan(\delta)_\epsilon$) of vacuum dried UDMA filled with 0 to 75 wt % zirconia-silica were measured over the frequency range of 0.015 to 100.0 kHz, and the temperature range of -180 to 180 °C. The $Tan(\delta)_\epsilon$ exhibited by the UDMA filled with the different amount of zirconia-silica measured at 0.252 and 10.0 kHz are plotted against temperature in Figures 3.9 and 3.11. Figure 3.10 shows a magnification of the β-relaxation region to show the detail of the relaxation with increasing filler concentration. In addition, the peaks maximum temperature obtained from the measured $Tan(\delta)_\epsilon$ curves for the five replicates were averaged and their values are presented in Table 3.3. From these results, several observations can be noted as a result of filler incorporation. First, the intensity of $Tan(\delta)_\epsilon$ of the $\alpha-$ and β-relaxation decreased with increasing amounts of zirconia-silica dispersed in the UDMA. Second, the α-relaxations are shifted to higher temperatures, while the β-relaxations are shifted to lower temperatures, as illustrated in Table 3.3. The β-relaxations also became broader with the increase of filler incorporation as seen in Figure 3.10. In addition, the α-relaxation was totally obstructed with higher filler incorporation, especially at low frequencies and high temperatures, due to the increase in the DC conductivity and the shift of the α-relaxation to higher temperatures as shown in Figure 3.9.

In order to look at the above results more closely, the isothermal spectra of the M' and M'' curves of the dried UDMA filled with 0 to 75 wt % zirconia-silica were calculated and plotted against frequency over the temperature range of -180 to 180 °C. Figures 3.6 and 3.12 show the variation of M' and M'' For the 0 and 75 wt % zirconia-silica-filled UDMA with high frequency and high temperature region, while

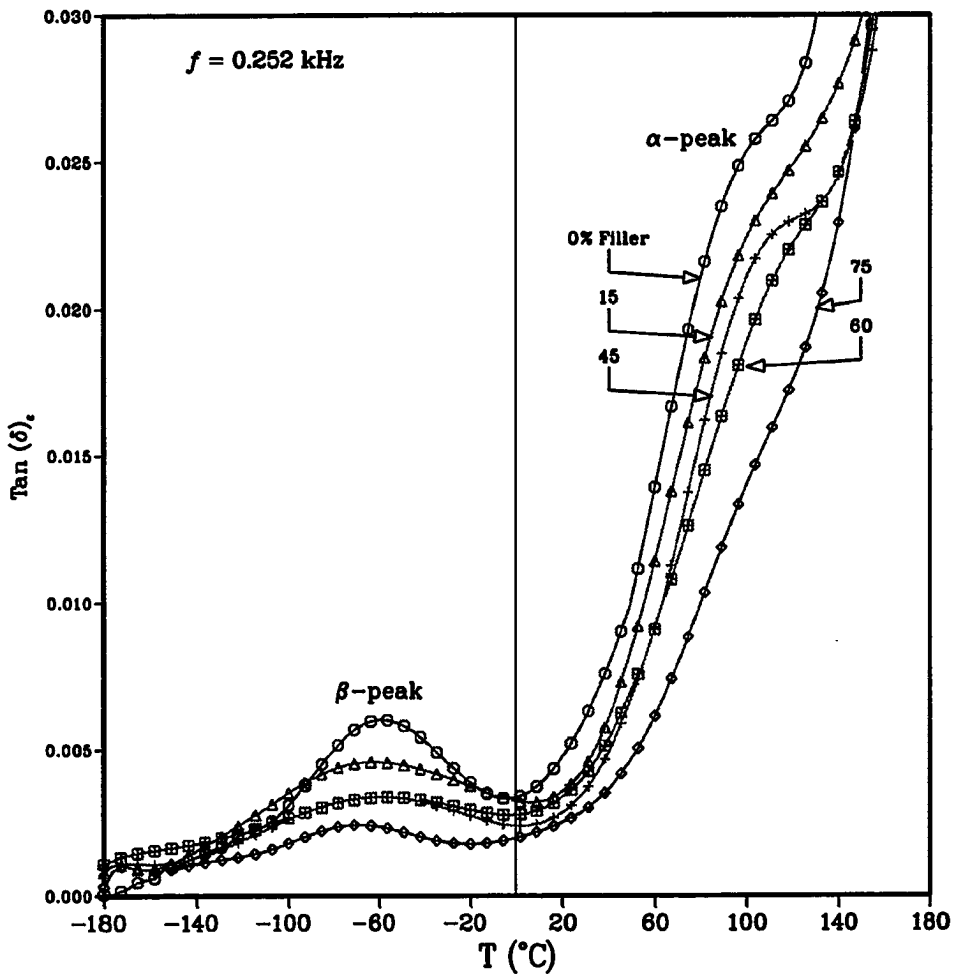

Figure 3.9: $Tan(\delta)_\epsilon$ against temperature at 0.252 kHz for 0, 15, 45, 60 and 75 wt % zirconia-silica-filled UDMA.

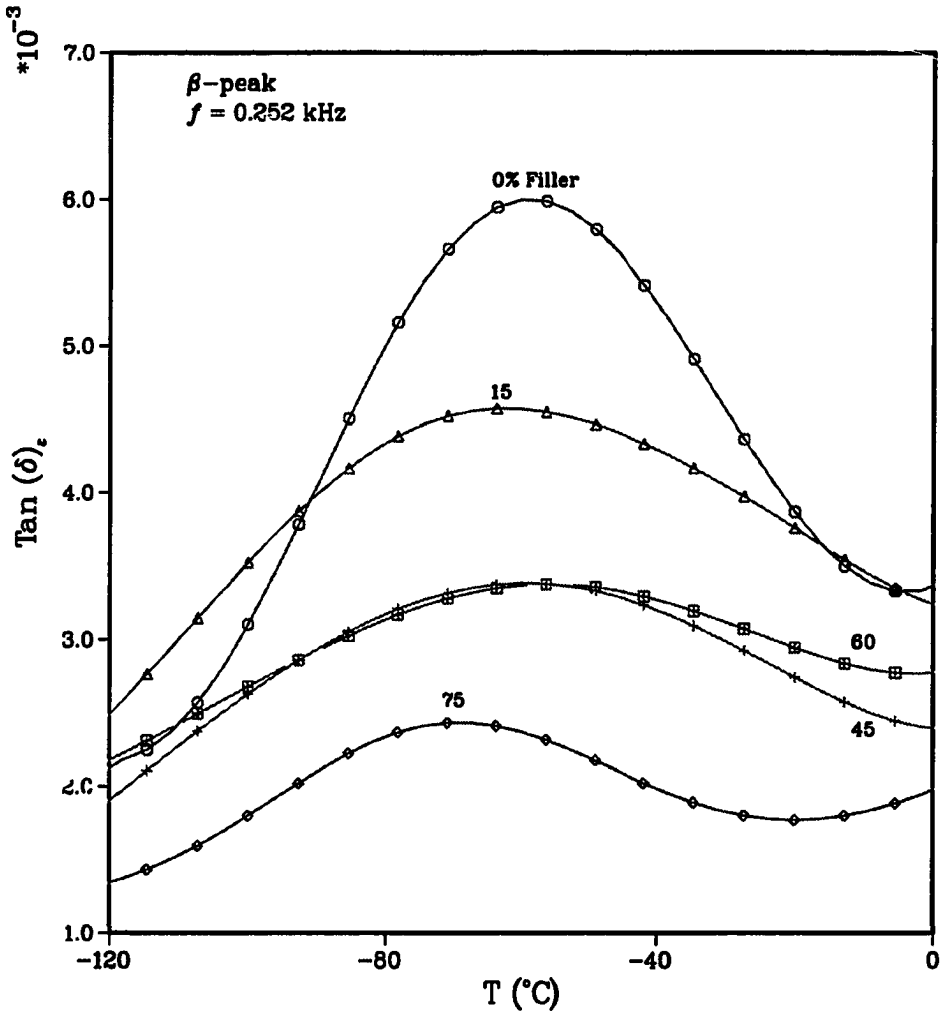

Figure 3.10: A magnification of $Tan(\delta)_\epsilon$ against temperature of the β-relaxation at 0.252 kHz for 0, 15, 45, 60 and 75 wt % zirconia-silica-filled UDMA.

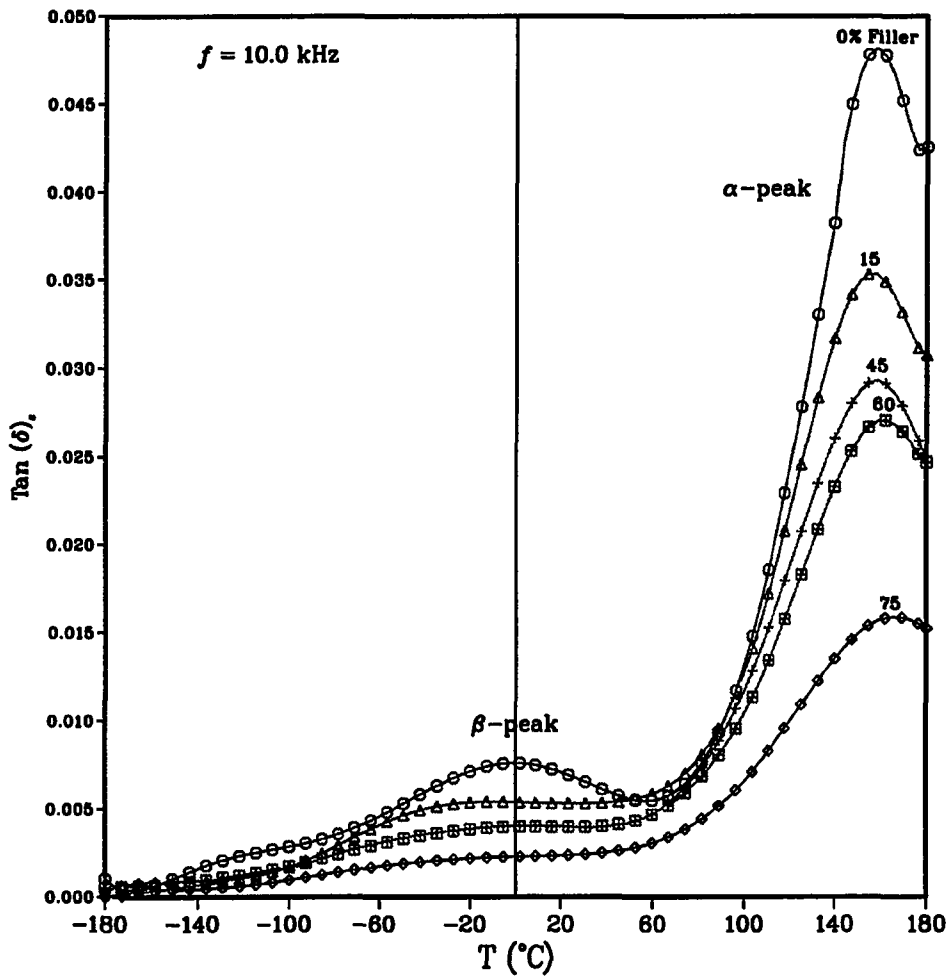

Figure 3.11: $Tan(\delta)_\epsilon$ against temperature at 10.0 kHz for 0, 15, 45, 60 and 75 wt % zirconia-silica-filled UDMA.

% Filler	Average maximum peak temperature (°C)			
	α-relaxation		β-relaxation	
	10.0 (kHz)	33.3 (kHz)	0.252 (kHz)	1.0 (kHz)
0	156.6 ± 1.6	168.9 ± 0.5	-59.8 ± 1.7	-38.8 ± 2.0
15	155.6 ± 1.1	170.5 ± 0.5	-62.6 ± 5.1	-43.2 ± 0.6
45	158.8 ± 1.2	171.7 ± 0.6	-60.0 ± 1.2	-44.2 ± 2.9
60	161.4 ± 0.4	172.4 ± 0.5	-60.0 ± 3.2	-45.0 ± 0.0
75	166.4 ± 0.5	175.0 ± 0.1	-69.1 ± 4.2	-43.3 ± 0.9

Table 3.3: Average maximum peaks temperatures (°C) from $Tan(\delta)_\epsilon$ measurements for different amount of zirconia-silica dispersed in UDMA for $\alpha-$relaxations at 10.0 and 33.3 kHz and for $\beta-$relaxations at 0.252 and 1.0 kHz.

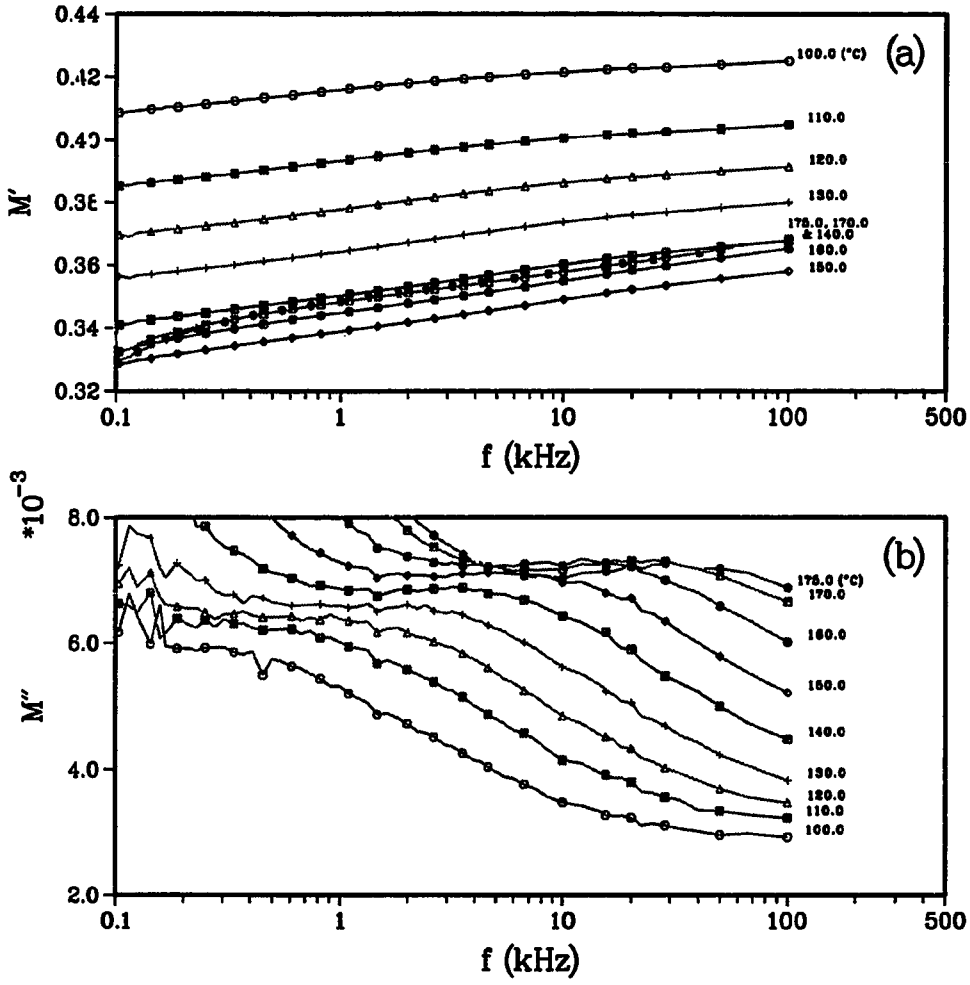

Figure 3.12: The spectra of (a) M' and (b) M'' against frequency for α-relaxation of the 75 wt % zirconia-silica-filled UDMA over the temperature range of 100 to 175 °C.

Figures 3.7 and 3.13 show the variations with low frequency and high temperature. The M' values of these figures show the typical behavior of them decreasing with elevating the measurement temperature in the range of 100 to 175 °C and with lowering the measurement frequency. The M'' curves showed a peak that had been assigned earlier to the large scale segmental chain motion and has decreased to lower frequency with increasing filler incorporation. For example, at 140 °C the maximums of the peaks were found at 4.3 and 3.2 kHz when obtained from Figures 3.6(b) and 3.12(b) for 0 and 75 wt % zirconia-silica-filled UDMA, respectively. To compare the effect of filler concentration on the relaxations of the backbone chains, M' and M'' at 170 °C for 0 to 75 wt % zirconia-silica-filled UDMA are plotted in Figures 3.14(a) and 3.14(b). The M' values and slopes of the curves of the large scale segmental motion decreased with an increase in the amount of filler dispersed in the UDMA, and the M'' values decreased and shifted to lower frequencies. Regardless of filler concentration the DC conductivity still exists, however it seems to appear at much lower frequency than for the unfilled-UDMA as illustrated in Figure 3.15.

The ϵ' and ϵ'' spectra of the 0 and 75 wt % zirconia-silica-filled UDMA against frequency and over the temperature range of -60 to 10 °C are shown in Figures 3.5 and 3.16, respectively. These curves show the onset of a peak, which was assigned earlier to the motion of the free amide groups.

To show the effect of filler incorporation on the β-relaxation , the M' and M'' are plotted against frequency in Figure 3.17 at -40 °C for 0, 15, 45, 60 and 75 wt % zirconia-silica-filled UDMA. In general, the M' values followed the same trend as those of the $\alpha-$relaxation's. That is the values and slopes of the curve decreased with an increase in the filler concentration as shown in Figure 3.17(a) at -40 °C. However, the M'' curves followed the opposite trend, where the maximum of M'' values shifted

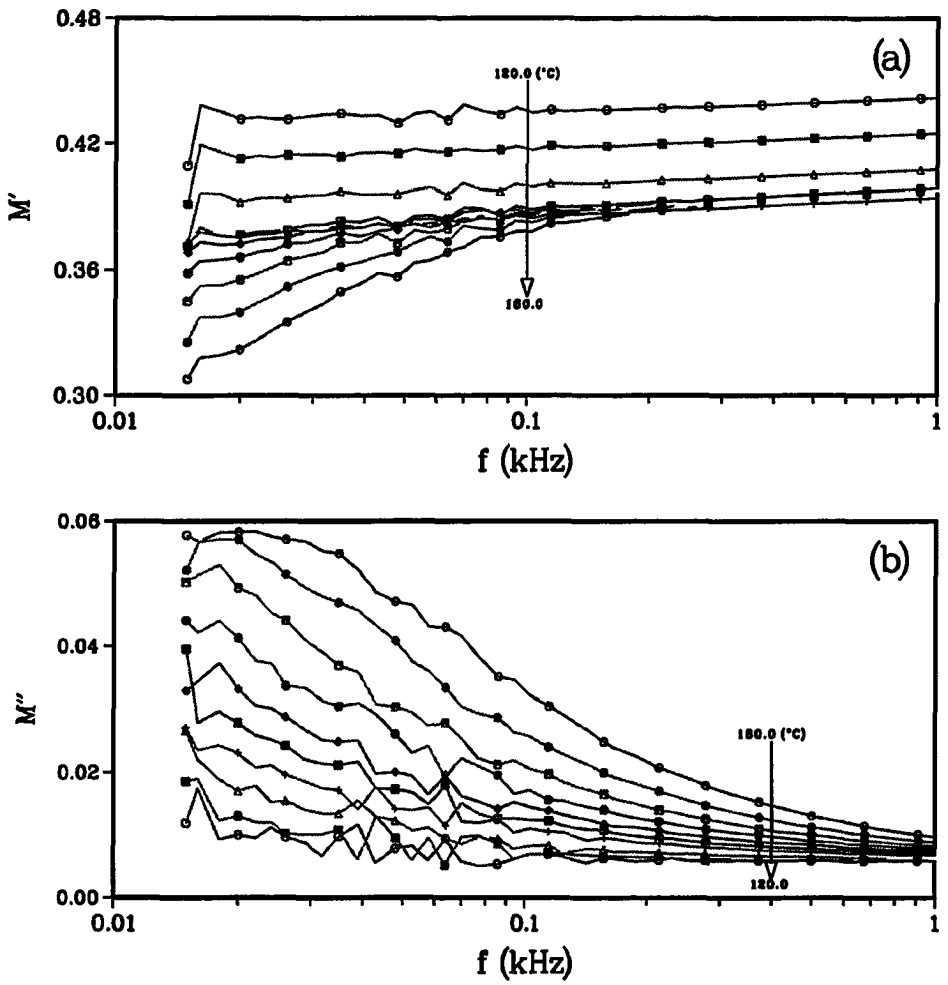

Figure 3.13: The spectra of (a) M' and (b) M'' against frequency for 75 wt % zirconia-silica-filled UDMA over the frequency range of 0.01 to 1.0 kHz and over the temperature range of 120 to 180 °C.

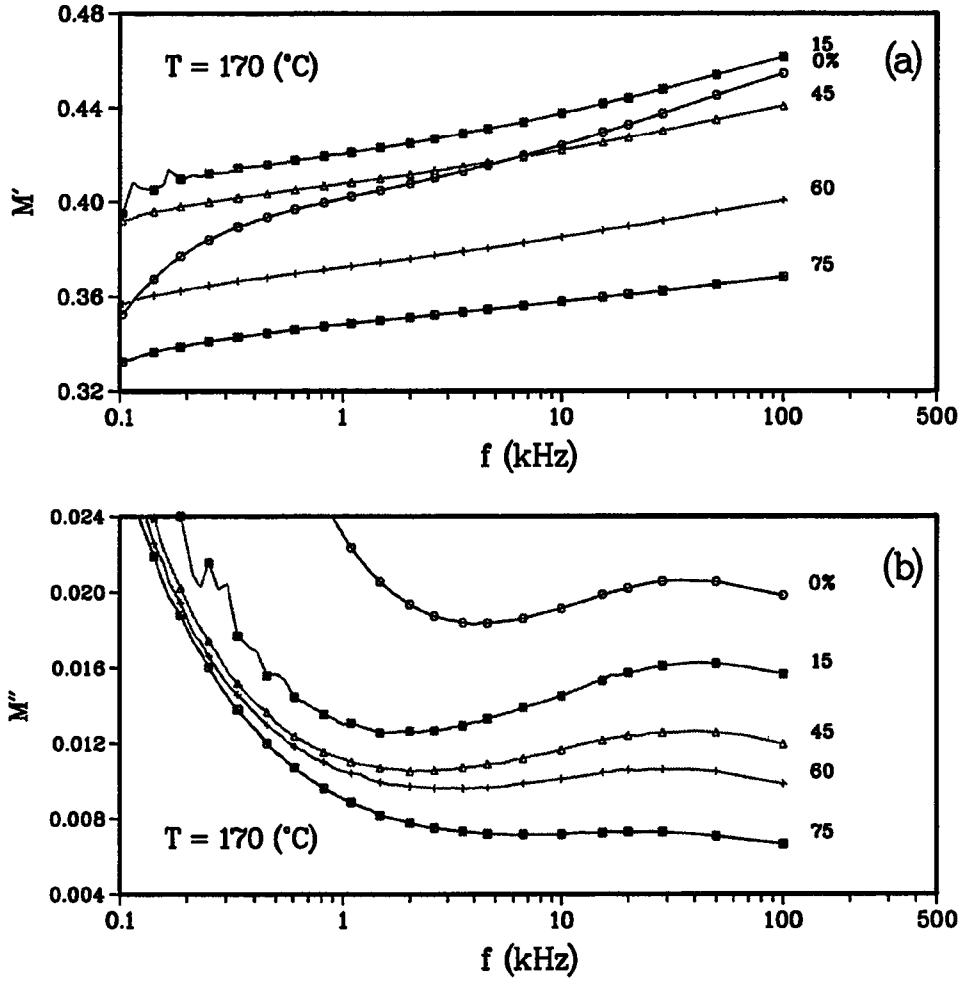

Figure 3.14: The spectra of (a) M' and (b) M'' against frequency for 0, 15, 45, 60 and 75 wt % zirconia-silica-filled UDMA at 170 °C.

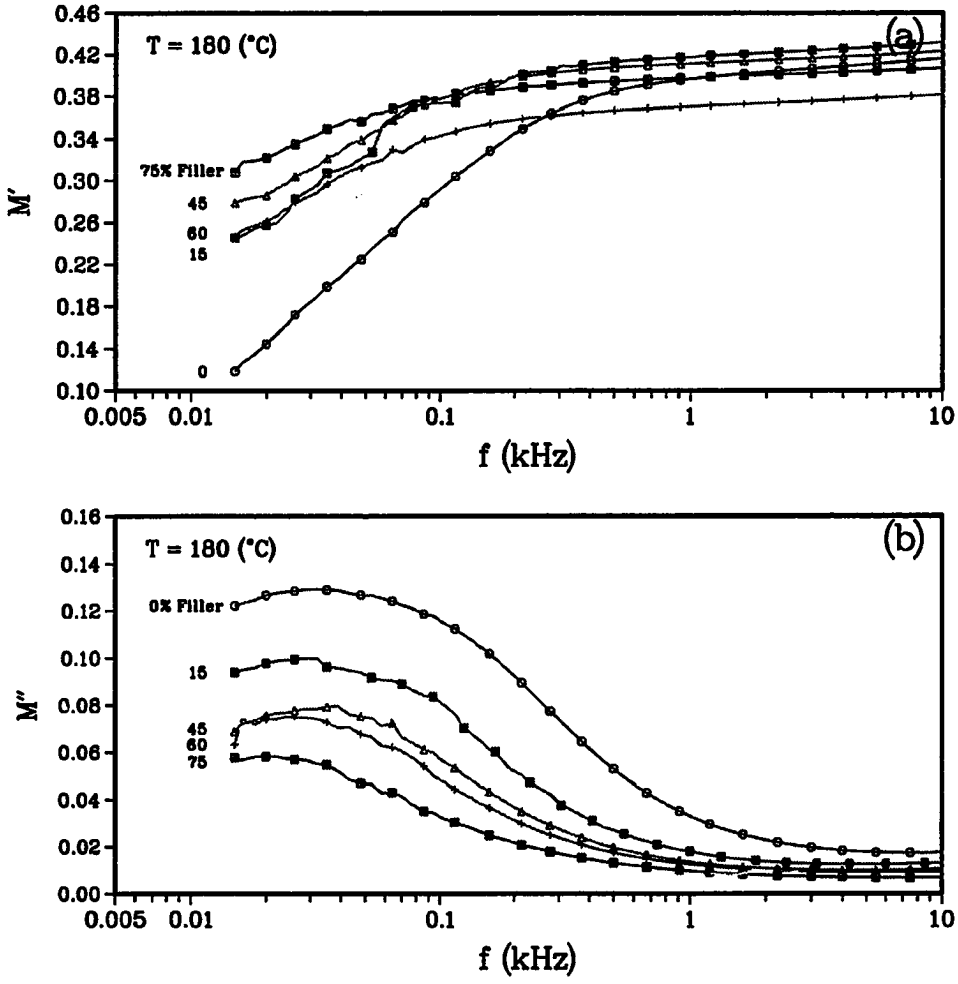

Figure 3.15: The spectra of (a) M' and (b) M'' against frequency for 0, 15, 45, 60 and 75 wt % zirconia-silica-filled UDMA at 180 °C and over the frequency range of 0.01 to 1.0 kHz.

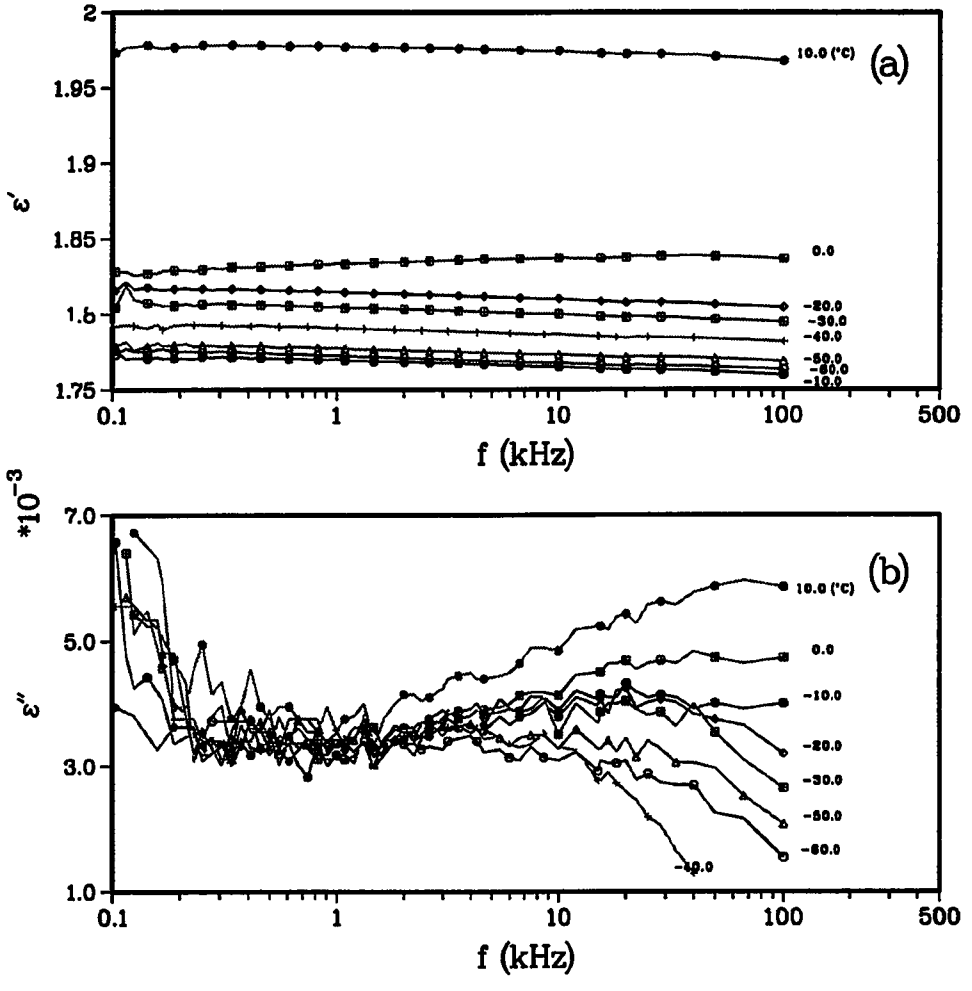

Figure 3.16: The spectra for (a) ϵ' and (b) ϵ'' against frequency for β-relaxation of 75 wt % zirconia-silica-filled UDMA over the temperature range of -60 to 0 °C.

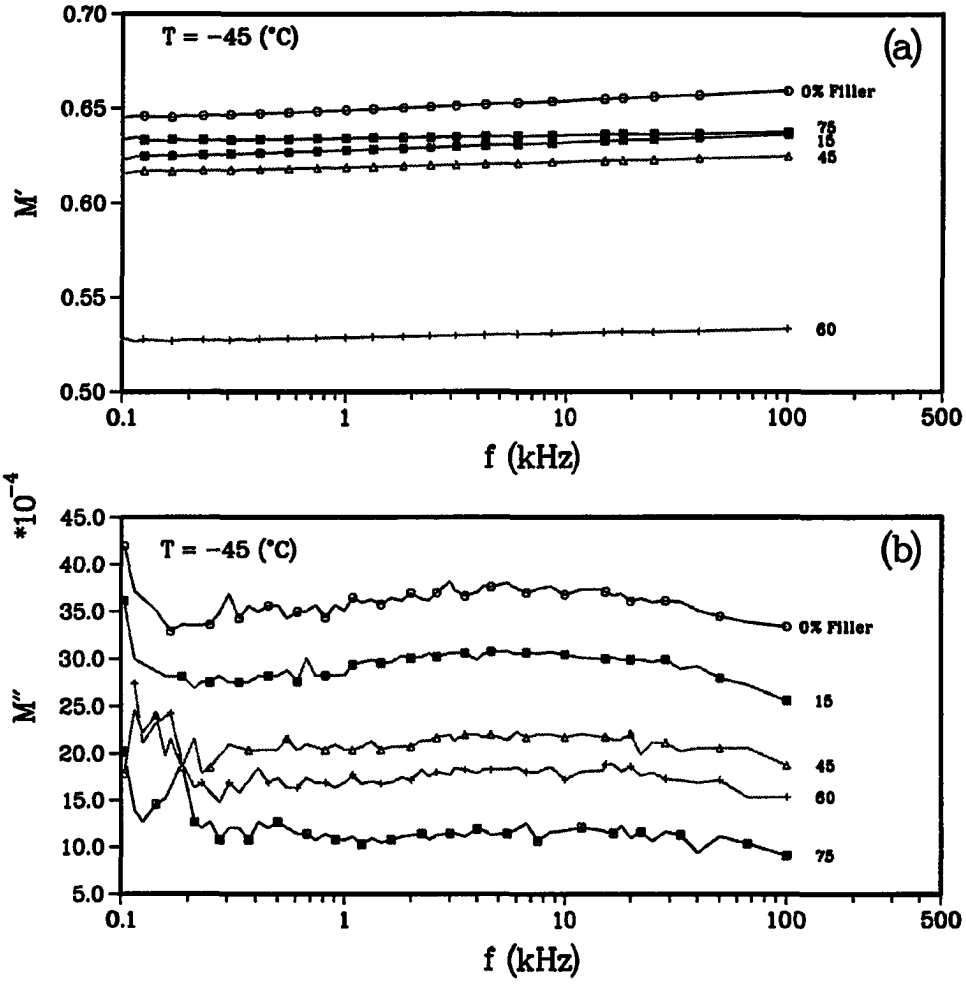

Figure 3.17: The spectra of (a) M' and (b) M'' against frequency for 0, 15, 45, 60 and 75 wt % zirconia-silica-filled UDMA at -40 °C.

to higher frequencies.

The Effect of the Filler on the α-relaxation

It was observed from the above results that the existence of an interface brings about substantial changes in the relaxation behavior of the glass transition. When the matrix was reinforced with zirconia-silica, the filled polymer consisted of particles bearing on their surface polymer layers of various thicknesses. As the filler concentration increased, the thickness of the surface layer decreased with the increase in filler concentration as was shown in Table 3.4. As the thickness of the surface layer decreased, the glass transition was shifted to higher temperature or lower frequency, if the variable was the temperature or the frequency, respectively. Further, the intensities of the $Tan(\delta)_e$ decreased with the decrease of the surface layer thickness. The increase of the glass transition temperature to higher values indicates a decrease and restriction of the main chain mobility in the layers of the polymer close to the vicinity of the filler surface, while the decrease in the intensities indicates fewer chains are involved in the relaxation. This can be explained by the stiffness of the interfacial region due to the existence of strong linkages between the silica and the polymer and/or due to changes in conformation of the surface layer at the interface. If the restriction of the mobility occurred only in the surface in direct contact with the filler, one cannot observe a change in the T_g, because the amount of layer in direct contact with the filler and its mobility is very small compared to the bulk. This supports that the filler not only affected the polymer layer in direct contact with it, but also the more remote layers. Lipatov *et al.* [61] argued that the glass transition is a cooperative process and for this reason restriction of mobility due to the presence of the filler applies to both to molecules bounded onto the surface and molecules

% Filler	Temperature (°C)	$Tan\delta_c$ at 20.0 (kHz)	ϕ_F	ϕ_e	Δr (μm)
0	170.9	0.04774	—	—	—
15	162.2	0.03369	0.066	0.278	0.459
45	165.6	0.02245	0.248	0.751	0.335
60	166.9	0.02185	0.376	0.931	0.264
75	171.9	0.01793	0.547	1.187	0.221

Table 3.4: Thickness of the adsorbed UDMA layer onto the filler as a function of concentration of the dispersed phase.

bonded into aggregates and other superstructure. So, the increase in the T_g in the presence of the filler is due to the restriction of the mobility of the chains close to the surface, which in turns restricts the mobility of other chains in the aggregates. However, in the filled polymer, the presence of a separate transition for the interface due to the surface layer or to interfacial polarization was not observed. One reason for not observing the separate transition for the surface layer is due to the low content of filler and that the difference between the transition temperature of the surface and that of the bulk is insignificant so both transitions showing as one transition shifted to higher temperature [61]. Another reason for not observing the separate transition that characterizes the interface and is due to the interfacial polarization, is because the dielectric constant and conductivity of the polymer and the filler do not differ substantially from each other, which is a requirement for detecting the interfacial polarization [91].

The increase in the T_g indicates a considerable chain stiffness, which is caused by the existence of conformational restrictions, energetic interactions or both. The conformational restriction caused by the entropic factors in the boundary layer, while the energetic interaction is caused by the formation of additional bonds between the silica and the polymer at the interface. To evaluate the contribution of these factors on the change of the molecular motion at the interface, activation energies (ΔH) and activation entropies (ΔS) were calculated using Equations (3.13) and (3.8). The dependencies of ΔH and ΔS on the increase of filler concentration, *i.e.* the decrease in the thickness of the surface layer, are presented in Table 3.5. A considerable increase in the activation entropy changes of the surface layer as compared to the bulk has been observed for the main chain relaxation (α-relaxation). The increase in ΔS indicates that the entropy is an important factor in changing the properties

% Filler	α-relaxation			β-relaxation		
	ΔH $\left(\frac{kcal}{mole}\right)$	ΔS $\left(\frac{kcal}{mole^oK}\right)$	τ_o (Hz) $*10^{-26}$	ΔH $\left(\frac{kcal}{mole}\right)$	ΔS $\left(\frac{kcal}{mole^oK}\right)$	τ_o (Hz) $*10^{-12}$
0	40.4 ± 6.4	0.167	57.0	7.5 ± 0.5	0.107	3.2
15	39.7 ± 2.9	0.171	8.0	7.9 ± 0.3	0.109	1.2
45	42.0 ± 1.6	0.176	0.45	7.5 ± 0.5	0.107	3.3
60	45.3 ± 3.3	0.181	0.049	7.2 ± 0.3	0.106	4.5
75	49.9 ± 0.6	0.184	0.011	6.7 ± 0.2	0.105	7.3

Table 3.5: Activation energies (ΔH), pre-exponential factors (τ_o) and activation entropies (ΔS) for $\alpha-$ and $\beta-$dielectric relaxation processes at 432 and 232 °K, respectively, as a function of percent filler dispersion in UDMA.

of the polymer and their molecular mobility in the surface layer. This increase of the activation entropy can be explained by the requirement of greater conformational changes in the case of stiff chains than of flexible ones for the transition of molecular segments from one position to another during the relaxation [61, 62]. So one would observe more conformational changes in a relaxation process which is reflected by an increase in the activation entropy at the surface layer due to its greater stiffness to achieve the relaxation, than a similar movement in the bulk.

The activation energies and the pre-exponential factors (τ_o) are determined from the slopes of the curves in Figure 3.18, and their values as a function of the increase in filler concentration are shown in Table 3.5. These results show an increase in the change of the activation energy and a decrease in the pre-exponential factor. The increase in the activation energy is an indication of the decrease in the main chain mobility due to the increase in the chain rigidity with the increase in filler concentration. Fabulyak *et al.* [33] showed an increase of the activation energy values of the oligomer as the flexibility of its molecular chain decreases. So the filler will act as a cross-linking agent which will restrict the polymer motion by adsorption of the polymer onto its surface and is reflected as an increase in the activation energy values. On the contrary, the reduction of the pre-exponential factor in the presence of the hard particles is due to the reduction of the density of packing in the surface layer, and an increase in the free volume [61].

The decrease in the intensity of $Tan(\delta)_\epsilon$ might be due to the decrease of the concentration of the polymer, which in turns reduces the concentration of the polar group. However, it might further support that the filler acts as a cross-linking agent, that causes a decrease in the motion of the polar groups which is manifested by the decrease in the $Tan(\delta)_\epsilon$ intensities.

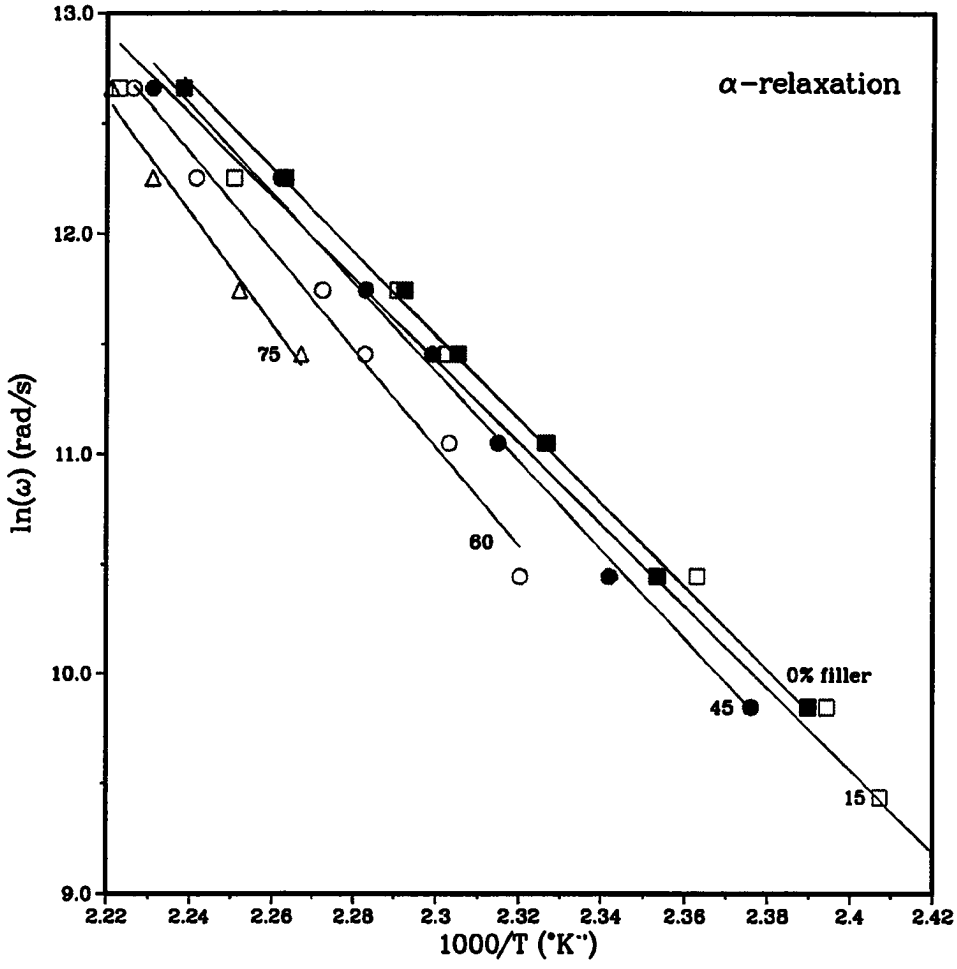

Figure 3.18: The angular frequency ($\ln(\omega)$) of $Tan(\delta)_e$ for the α-relaxation against $\frac{1}{T}(^{\circ}K^{-1})$ obtained by dielectric measurements for 0, 15, 45, 60 and 75 wt % zirconia-silica-filled UDMA.

In summary, the incorporation of the filler causes the polymer to adsorb onto the surface of the filler to create a thin layer with different thickness depending on the amount of the filler concentration. This layer has different properties than the bulk, which are reflected by the entire relaxation behavior of the composites. In the layer close to the filler and in the remote layers, the restriction of the chain mobility is due to conformational restrictions imposed by the surface that lowered the chain flexibility. These effect dominate the reduction of the density of packing and other factors, and all these factors are reflected by an increase of the α-relaxation towards higher temperatures.

The Effect of the Filler on the β-relaxation

The β-peak corresponds to the side group relaxation (β-relaxation) of the polymer and is shifted to lower temperature with the increase of the filler concentration. This indicates an increase in the mobility of the side groups at the interface, which is due to the reduction of the density of packing. To support this statement, the theory of polymer adsorption on solid surfaces shows that only portions of the chains are directly bounded to the surface, while the rest remain free [63]. In addition, the activation energy values calculated from the slopes of the curves of Figure 3.19 are shown in Table 3.5. Their values decreased with the presence of filler in the low relaxation region, which supports the explanation of the free movement of molecules due to the reduction of the density of packing in the boundary layer. These results show that the energetic factors are insignificant. Otherwise, one will observe indications of the restriction of the mobility of the side groups due to the formation of the additional bonds between the silica and the polymer at the interface. Further, the activation entropy showed insignificant changes and decreased to lower values, indicating that

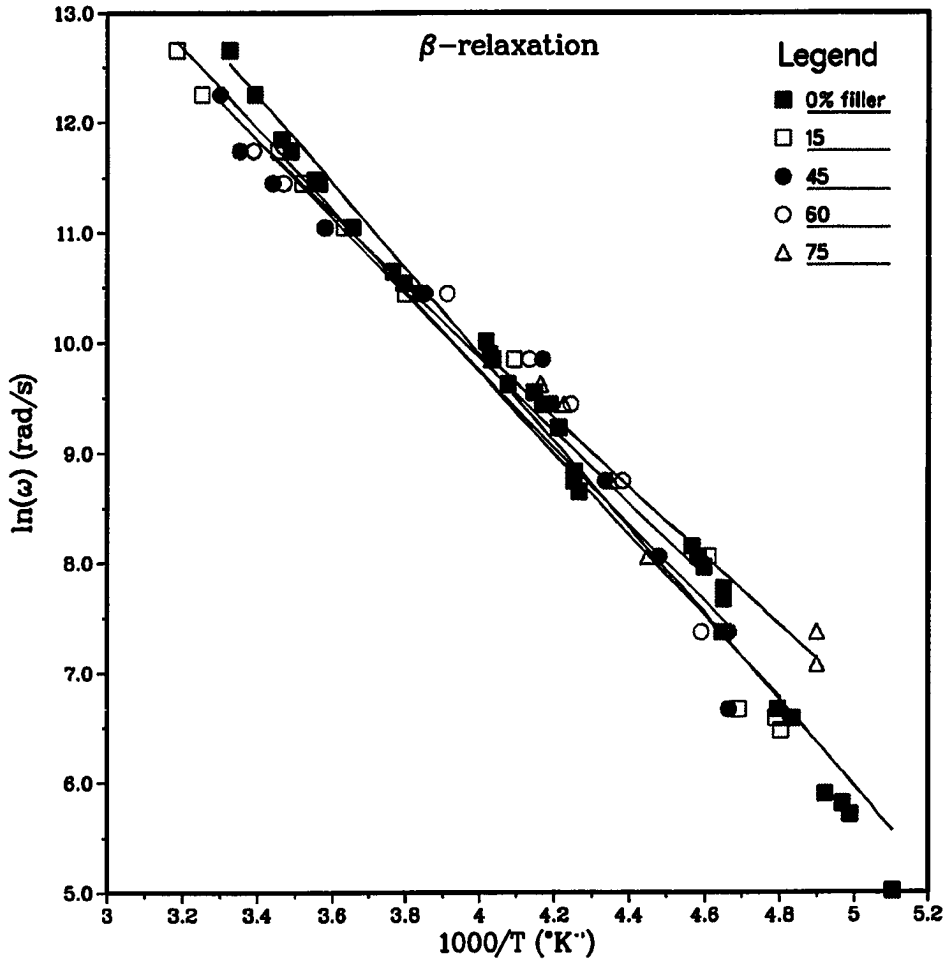

Figure 3.19: The angular frequency ($\ln(\omega)$) of $Tan(\delta)_\epsilon$ for the β-relaxation against $\frac{1}{T}(^\circ K^{-1})$ obtained by dielectric measurements for 0, 15, 45, 60 and 75 wt % zirconia-silica-filled UDMA.

the conformational changes do not also play a major role in the conformations of the β-relaxation . As a result the formation of large number of relaxant, the broadening of the β-relaxation (Figure 3.10), and the increase in the mobility of functional groups of the chains and of small units that are not bounded to the surface, further supports the above statement.

3.4.3 The Effect of Silanation of Filler on the Dielectric Relaxations of UDMA

The $Tan(\delta)_\epsilon$ of vacuum dried UDMA filled with 75 wt % MAPM-silanated zirconia-silica were measured over the frequency range of 0.015 to 100.0 kHz and the temperature range of -180 to 180 °C. The $Tan(\delta)_\epsilon$ exhibited by the UDMA containing zirconia-silica treated with different amounts of MAPM at different frequencies are plotted against temperature in Figures 3.20 and 3.22. To show the details of these relaxations as a function of silane concentrations, Figure 3.21 shows an enlargement of the β-relaxation region at 0.252, while Figure 3.23 shows a magnification of the α-relaxation region at 10.0 kHz. The temperature values of the peak's maxima for the $\alpha-$ and $\beta-$relaxations obtained from these figures are shown in Table 3.6. From these results, one can observe a definite trend as a result of increasing MAPM treatment. That is, the α-relaxations were shifted to higher temperatures at 1X, then shifted to lower temperatures at higher concentrations of MAPM. In addition, the β-relaxations were shifted to higher temperatures when the filler was treated with low amounts of silane, and then were shifted back to lower temperatures with high amounts of silane. Further, the M' and M'' isothermal spectra at 160 °C for the UDMA filled with zirconia-silica treated with different amounts of MAPM were calculated and are plotted against frequency in Figure 3.24. In this figure, the M'' frequency values at the peaks maximum were shifted to lower frequencies with

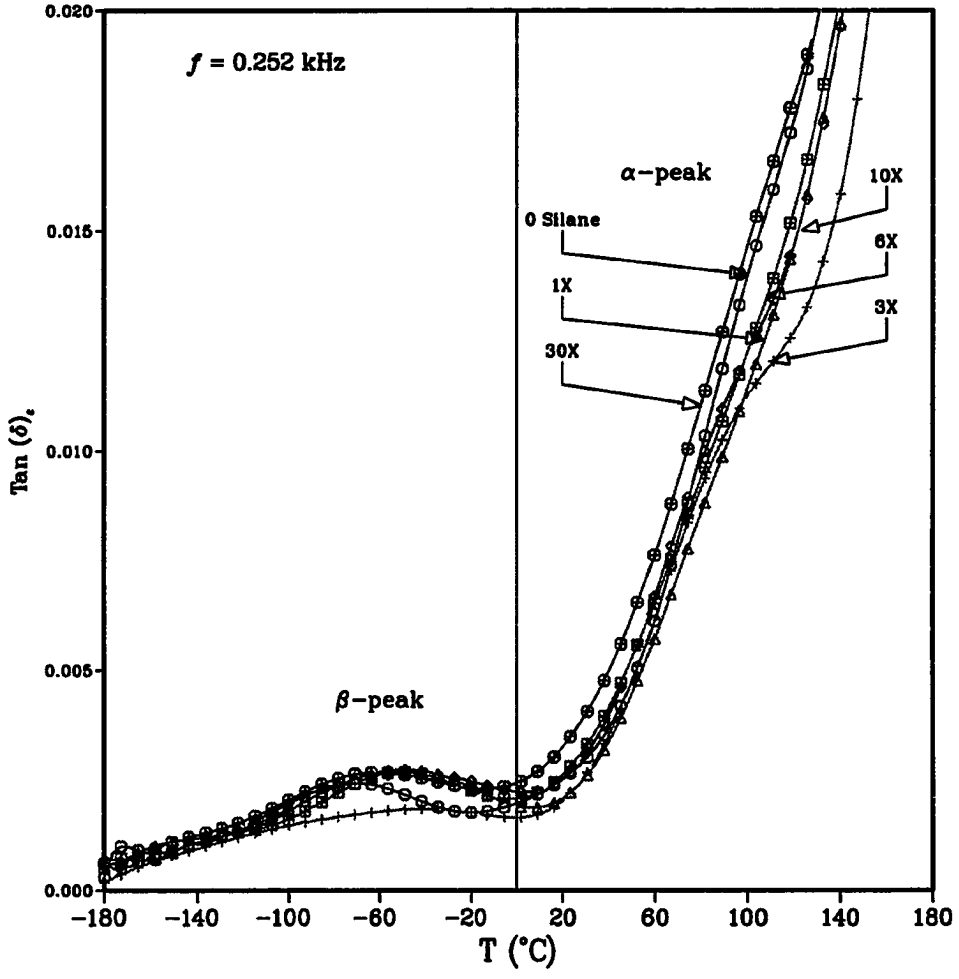

Figure 3.20: $Tan(\delta)_\epsilon$ against temperature at 0.252 kHz for 0, 1X, 3X, 6X, 10X and 30X MAPM-treated zirconia-silica-filled UDMA.

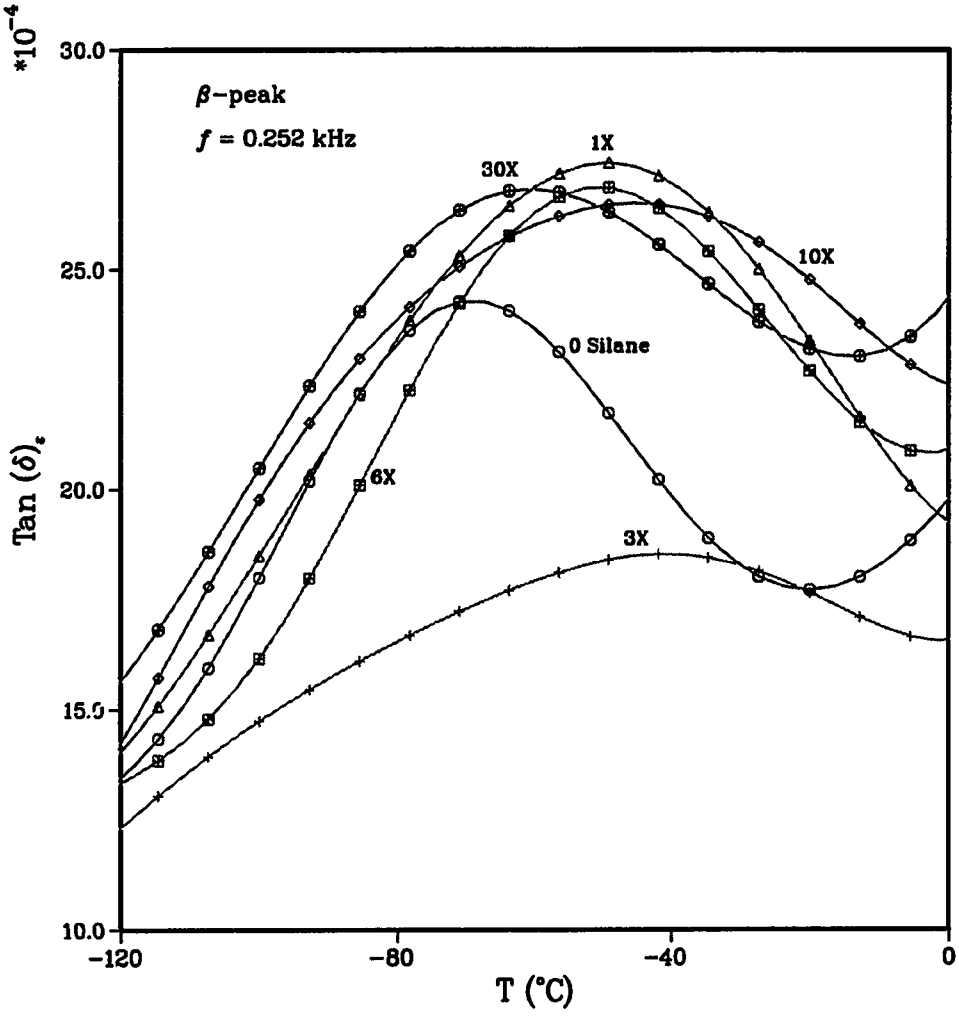

Figure 3.21: A magnification of $Tan(\delta)_\epsilon$ against temperature of the β-relaxation at 0.252 kHz for 0, 1X, 3X, 6X, 10X and 30X MAPM-treated zirconia-silica-filled UDMA.

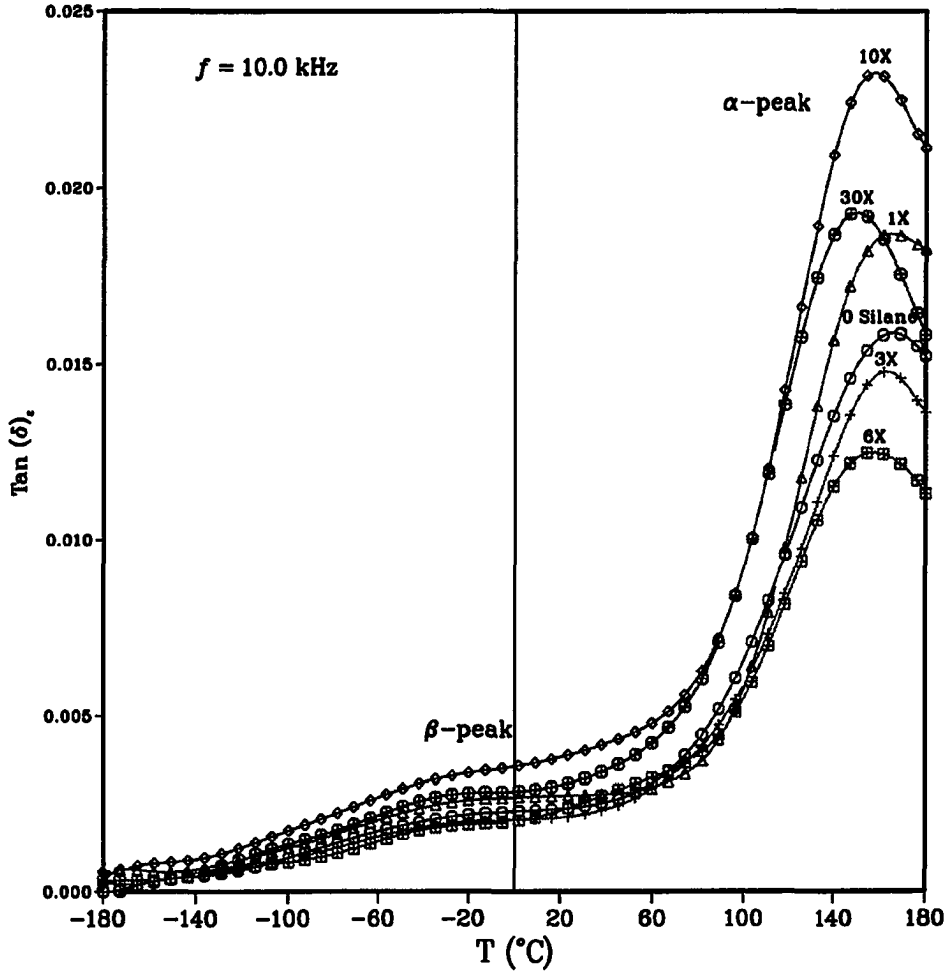

Figure 3.22: $Tan(\delta)_\epsilon$ against temperature at 10.0 kHz for 0, 1X, 3X, 6X, 10X and 30X MAPM-treated zirconia-silica-filled UDMA.

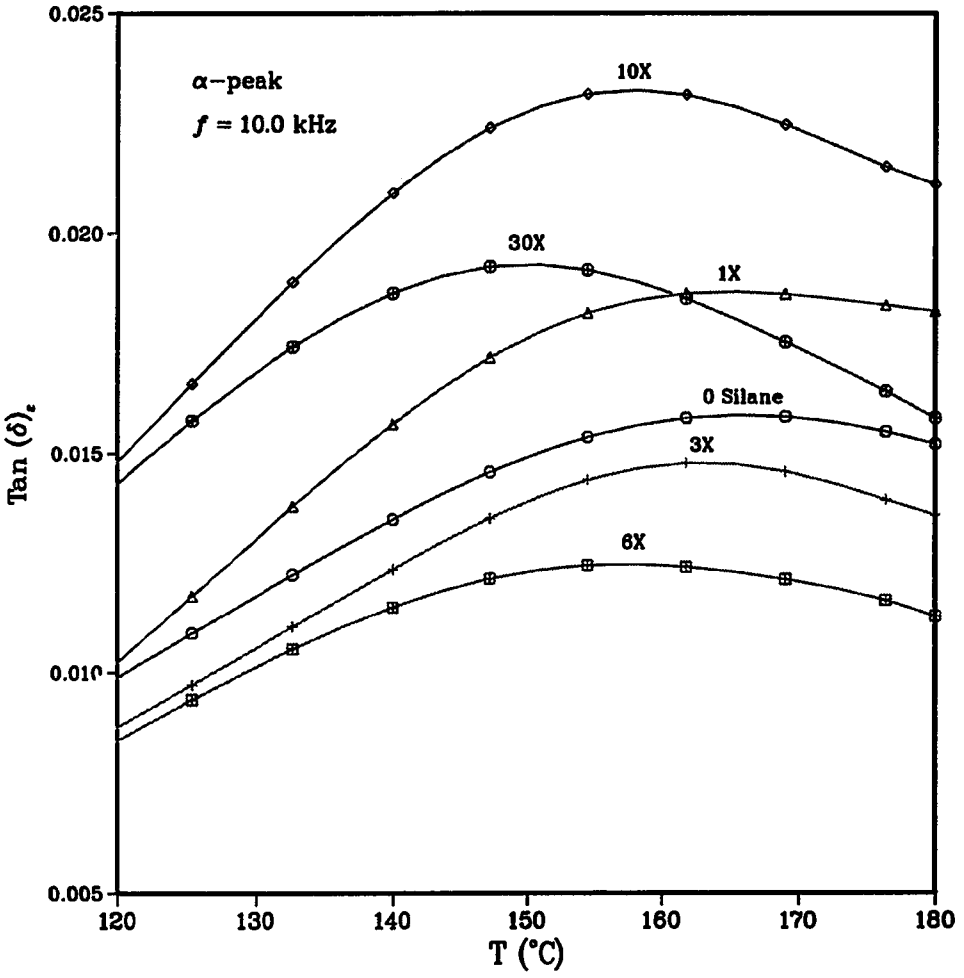

Figure 3.23: A magnification of $Tan(\delta)_\epsilon$ against temperature of the α-relaxation at 10.0 kHz for 0, 1X, 3X, 6X, 10X and 30X MAPM-treated zirconia-silica-filled UDMA.

MAPM Amount	Average maximum Peak temperature (°C)			
	α-relaxation		β-relaxation	
	5.5 (kHz)	33.3 (kHz)	0.252 (kHz)	1.0 (kHz)
0	165.4 ± 0.5	175.0 ± 0.5	-69.1 ± 4.2	-43.3 ± 0.9
1X	163.8 ± 2.0	176.0 ± 2.0	-49.1 ± 6.0	-38.5 ± 3.5
3X	160.5 ± 3.0	172.9 ± 1.5	-39.9 ± 6.5	-33.0 ± 5.0
6X	158.5 ± 3.0	169.9 ± 3.5	-43.0 ± 4.8	-38.2 ± 5.9
10X	155.0 ± 2.3	169.5 ± 2.8	-54.5 ± 5.7	-39.7 ± 2.7
30X	145.3 ± 6.1	162.2 ± 5.8	-60.0 ± 6.2	-50.0 ± 3.4

Table 3.6: Average maximum peaks temperatures (°C) from $Tan(\delta)_\epsilon$ measurements for different amount of MAPM treatment of 75 wt % zirconia-silica dispersed in UDMA for α−relaxations at 5.5 and 33.3 kHz and for β−relaxations at 0.252 and 1.0 kHz.

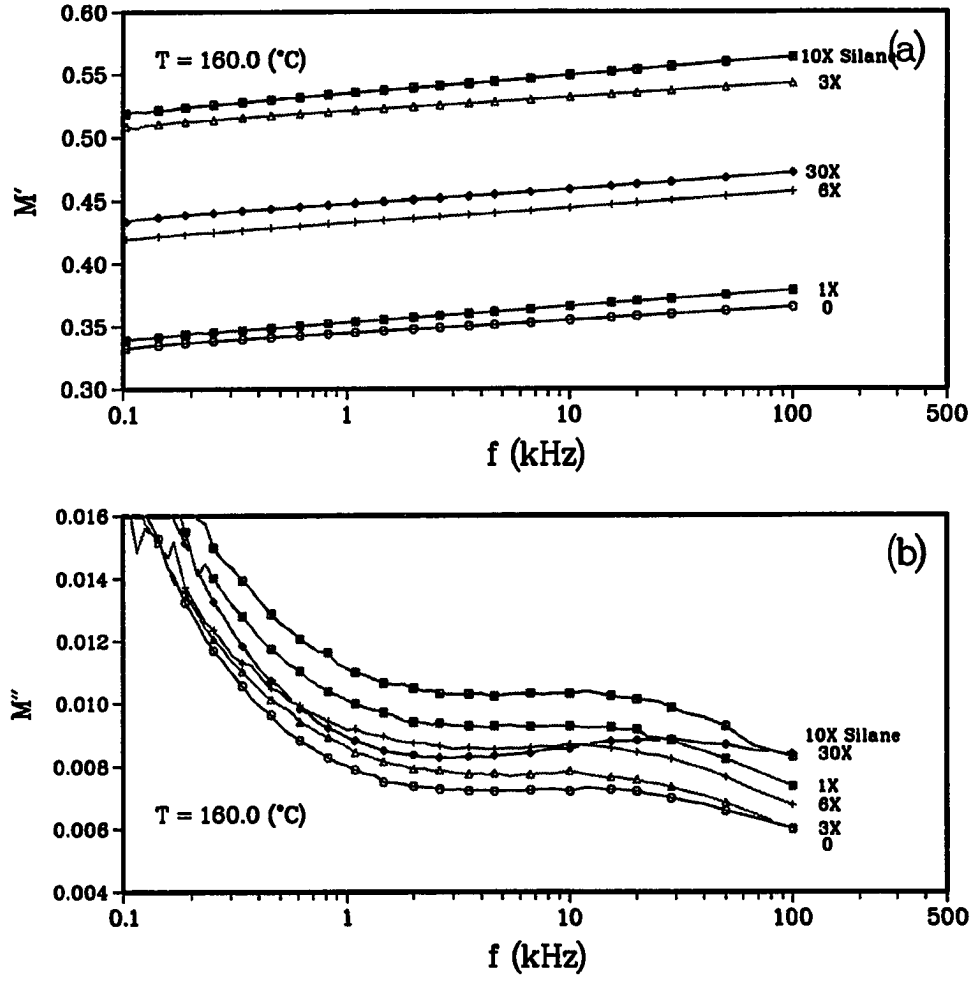

Figure 3.24: The spectra of (a) M' and (b) M'' against frequency for α-relaxation of 0 to 30X MAPM-treated zirconia-silica-filled UDMA at 160 °C.

increases in the amount of silane in treating the filler. A comparison of the M' and M'' isothermal curves at 180 °C over the low frequency range are plotted in Figure 3.25 for the unfilled-, 75 wt % filled-, and 75 wt % filled-UDMA with MAPM-silanated filler with the different amounts. This figure shows that the presence of the silane between the filler and the polymer reduces the effect of space charge separation that accumulates due to incompatibility of the interface. However, the silane presence did not prevent the rapid increase of the $Tan(\delta)_\epsilon$ and M'' values at low frequencies and high temperatures. This observation further supports the presence of the DC conduction mechanism due to the motion of hydrogen protons which act as current carriers.

The $Tan(\delta)_\epsilon$ of vacuum dried UDMA filled with 75 wt % ABTE-silanated zirconia-silica were measured over the frequency range of 0.015 to 100.0 kHz and the temperature range of -180 to 180 °C. The $Tan(\delta)_\epsilon$ exhibited by the UDMA containing zirconia-silica treated with different amount of ABTE are plotted against temperature in Figures 3.26 and 3.27. The temperature values of the peak's maxima for the $\alpha-$ and $\beta-$relaxations obtained from the measured $Tan(\delta)_\epsilon$ are shown in Table 3.7. In general, these results show shifts of the $\alpha-$ and $\beta-$relaxations to lower temperatures with the increase in filler silanation with ABTE. Further, an extra peak emerged in the high temperature region, when the filler was silanated with 30 times the minimum uniform coverage (30X) (Figure 3.27). This new peak was superimposed on the α-relaxation which appeared as a shoulder around 70.0 °C.

To resolve the ionic and dipolar nature of the relaxation, the M' and M'' of the 3X ABTE-silanated zirconia-silica-filled UDMA was calculated over the temperature range of 120.0 to 180.0 °C and are plotted against the high frequency range in Figure 3.28, and against the low frequency range in Figure 3.29. In addition, the M'

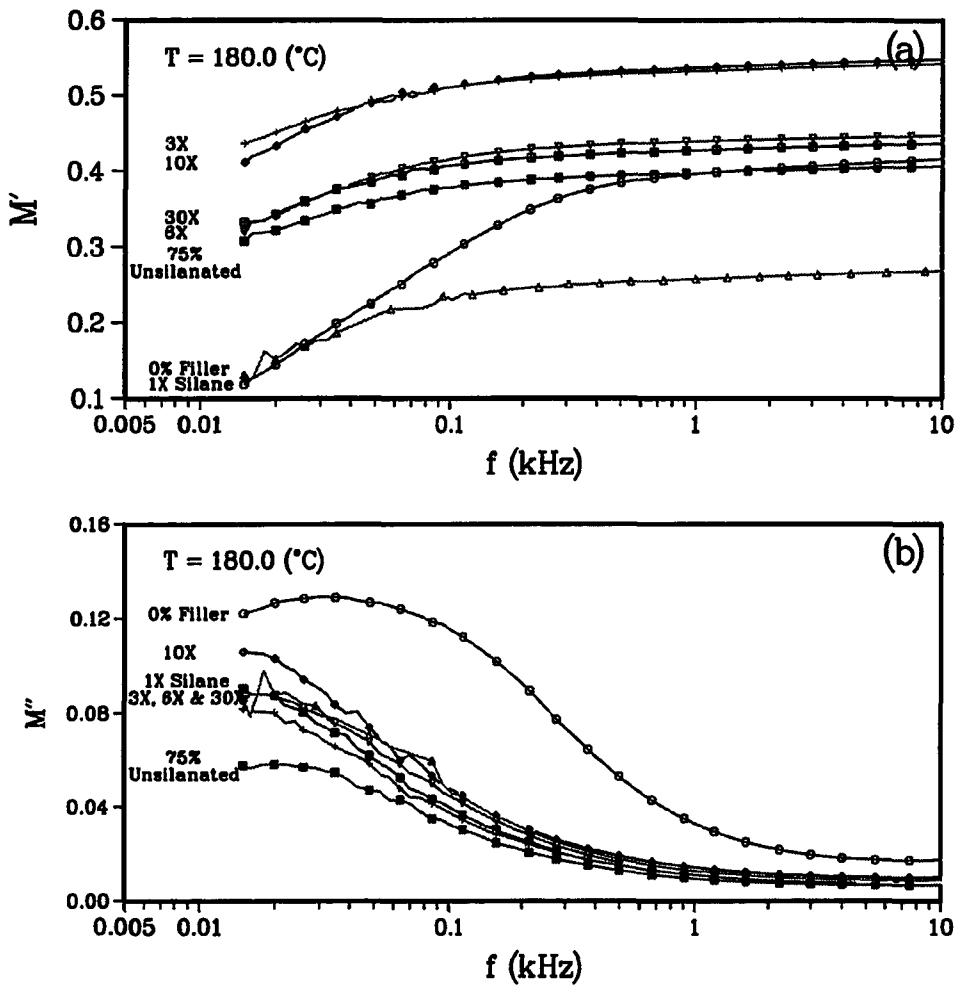

Figure 3.25: The spectra of (a) M' and (b) M'' against frequency for α'-relaxation of Unfilled-UDMA and 0 to 30X MAPM treated zirconia-silica-filled UDMA at 180 °C and the frequency range of 0.01 to 1.0 kHz.

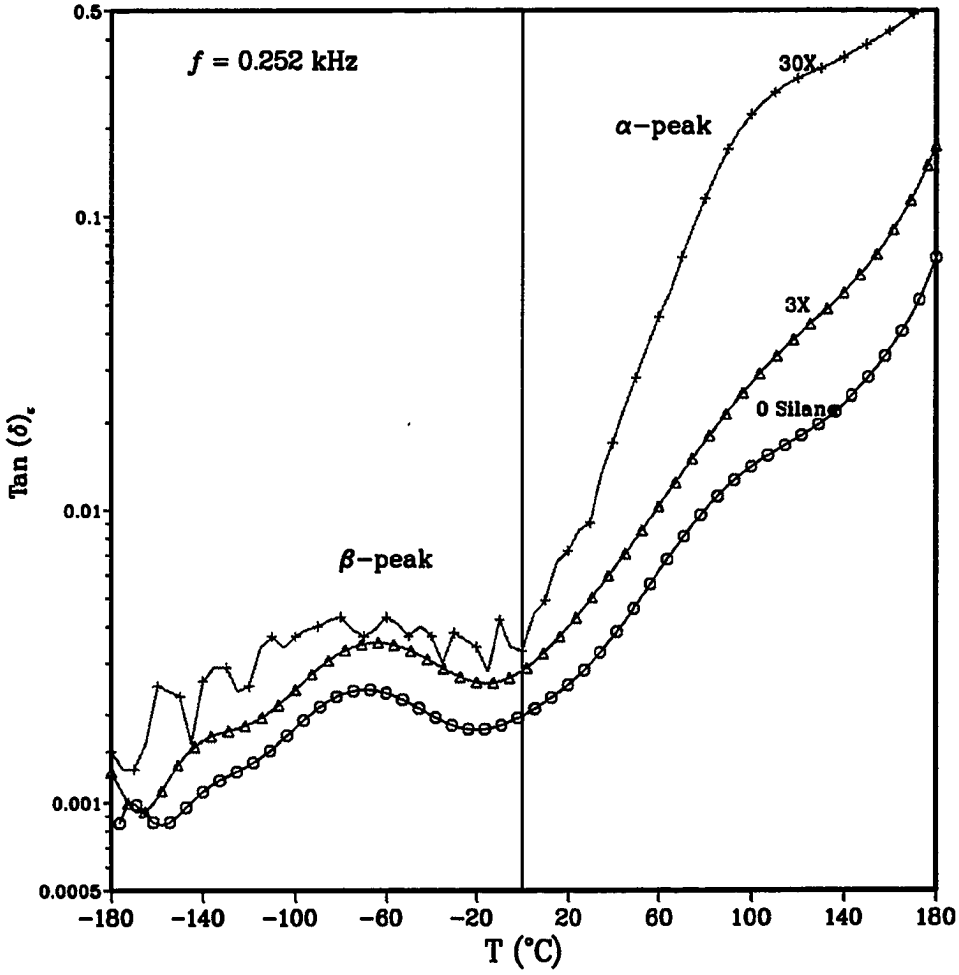

Figure 3.26: $Tan(\delta)_\epsilon$ against temperature at 0.252 kHz for 0, 3X and 30X ABTE-treated zirconia-silica-filled UDMA.

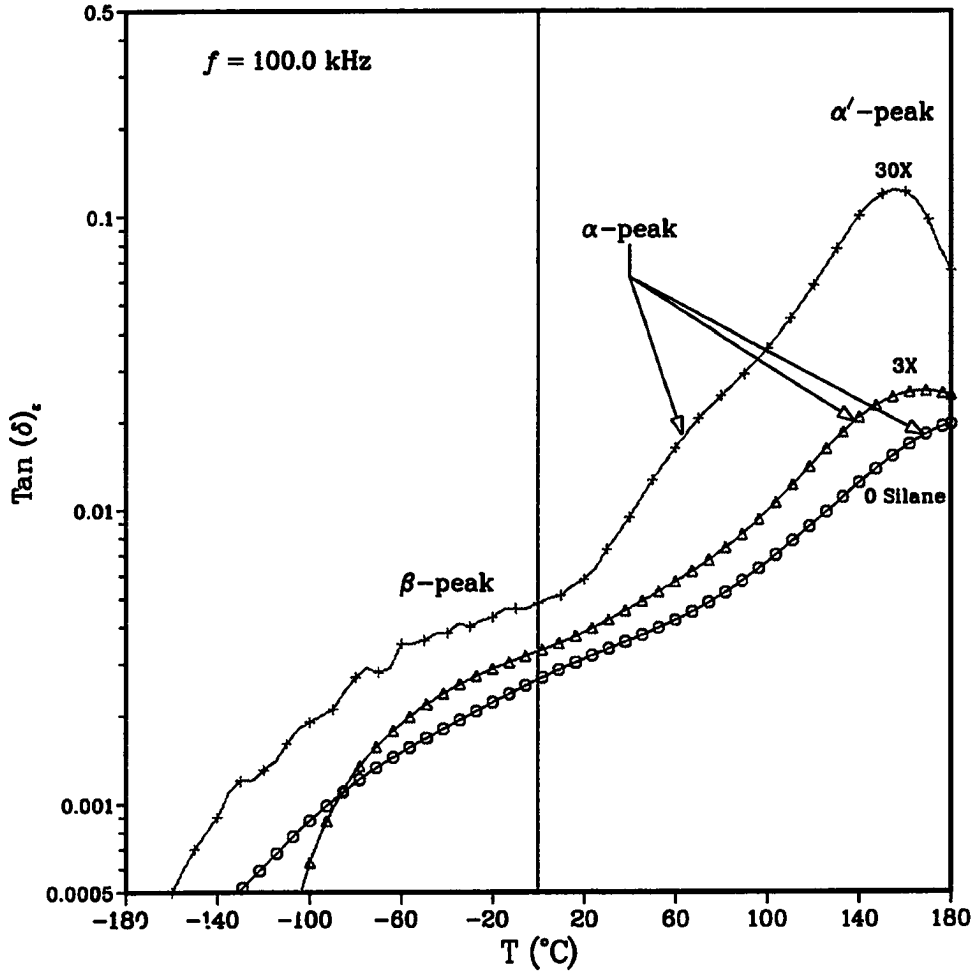

Figure 3.27: $Tan(\delta)_\epsilon$ against temperature at 100.0 kHz for 0, 3X and 30X ABTE-treated zirconia-silica-filled UDMA.

ABTE Amount	Average maximum peak temperature (°C)			
	α-relaxation		β-relaxation	
	10.0 (kHz)	33.3 (kHz)	0.252 (kHz)	1.0 (kHz)
0	166.4 ± 0.5	175.0 ± 0.5	-69.1 ± 4.2	-43.3 ± 0.9
3X	155.0 ± 3.2	159.4 ± 1.7	-63.6 ± 1.8	-50.7 ± 2.3
30X	—	—	-70.0 ± 3.1	-62.5 ± 1.6

Table 3.7: Average maximum peaks temperatures (°C) from $Tan(\delta)_\epsilon$ measurements for different amount of ABTE treatment of 75 wt % zirconia-silica dispersed in UDMA for $\alpha-$relaxations at 10.0 and 33.3 kHz and for $\beta-$relaxations at 0.252 and 1.0 kHz.

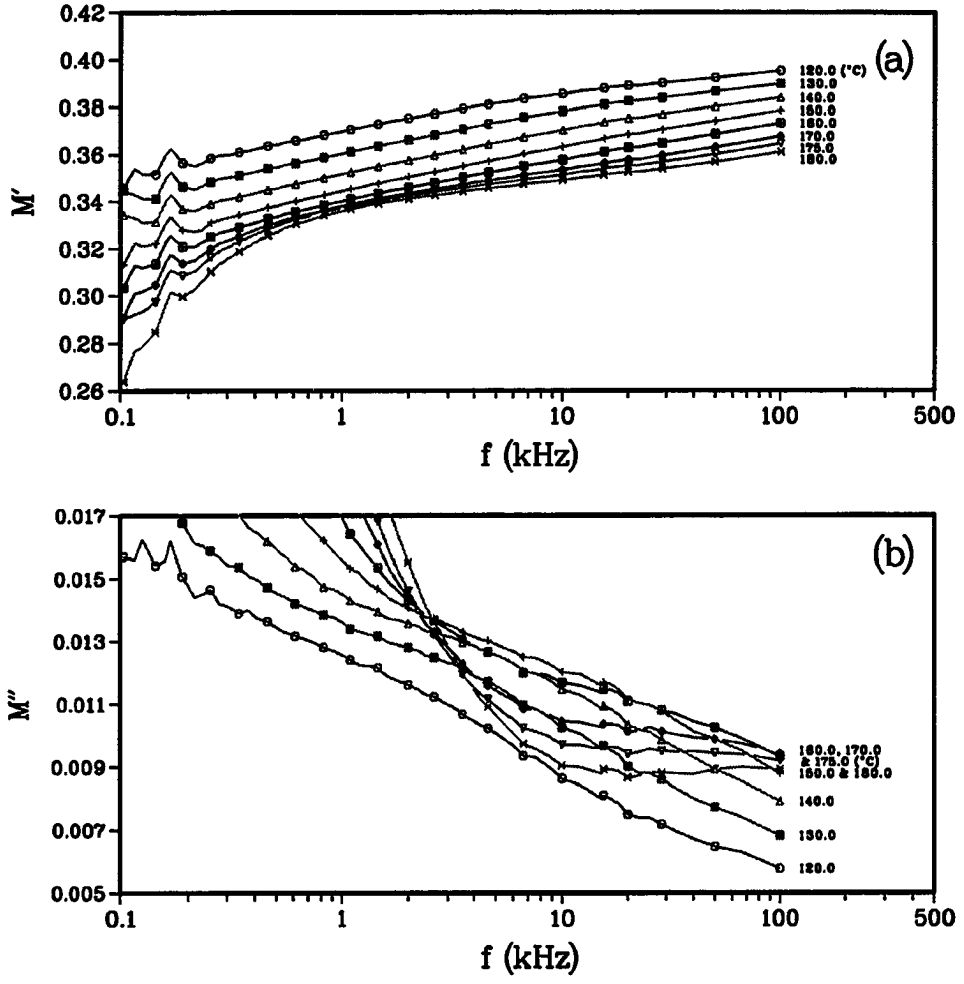

Figure 3.28: The spectra of (a) M' and (b) M'' against frequency for α-relaxation of 3X ABTE-treated zirconia-silica-filled UDMA over the temperature range of 120.0 to 180 °C and over the frequency range of 0.1 to 100 kHz.

and M'' of the 30X ABTE-silanated zirconia-silica-filled UDMA were calculated over the temperature range of 120.0 to 180.0 °C and are plotted against the entire frequency range in Figure 3.30. These results show increasing values of M'' at the low frequency region in Figure 3.28 that blocked the onset of the α-relaxation . These rising values were due to an onset of a new peak that started to develop at high temperatures and low frequencies when the filler was silanated with 3X ABTE (Figure 3.29). This new peak is further enhanced and is shown more clearly in Figure 3.30, which was attributed to space charge separation at the interface.

The activation energies (ΔH) for MAPM-treated filler were determined from the slopes of the curves in Figures 3.31 and 3.32 for the $\alpha-$and $\beta-$relaxations, respectively, and their values are shown in Table 3.8. In addition, the half-width of the bands ($\Delta_{1/2}$) for both relaxations are calculated from equation (3.14) and the values are also presented in Table 3.8 as a function of silane concentration in the filler treatment. Further, the intensities of $Tan(\delta)_\epsilon(\lambda)$ for the $\beta-$ and $\alpha-$relaxations at 0.252 and 10.0 kHz were obtained from Figures 3.20 and 3.22, respectively, and their values are shown in Table 3.9. Finally, the dielectric increments ($\Delta\epsilon$) were calculated from Figures 3.24 and 3.33 at 180.0 and -30.0 °C for the $\alpha-$ and $\beta-$relaxations, respectively, and the values are also shown in Table 3.9 as a function of increasing MAPM concentration in treating the filler.

The values of ΔH, τ_o and ΔS for ABTE-treated filler as a function of the increase in the silane concentration are shown in Table 3.10. In addition, the values of λ at 10.0 kHz and $\Delta\epsilon$ values calculated from Figures 3.28 and 3.30 at 160 °C are shown in Table 3.11.

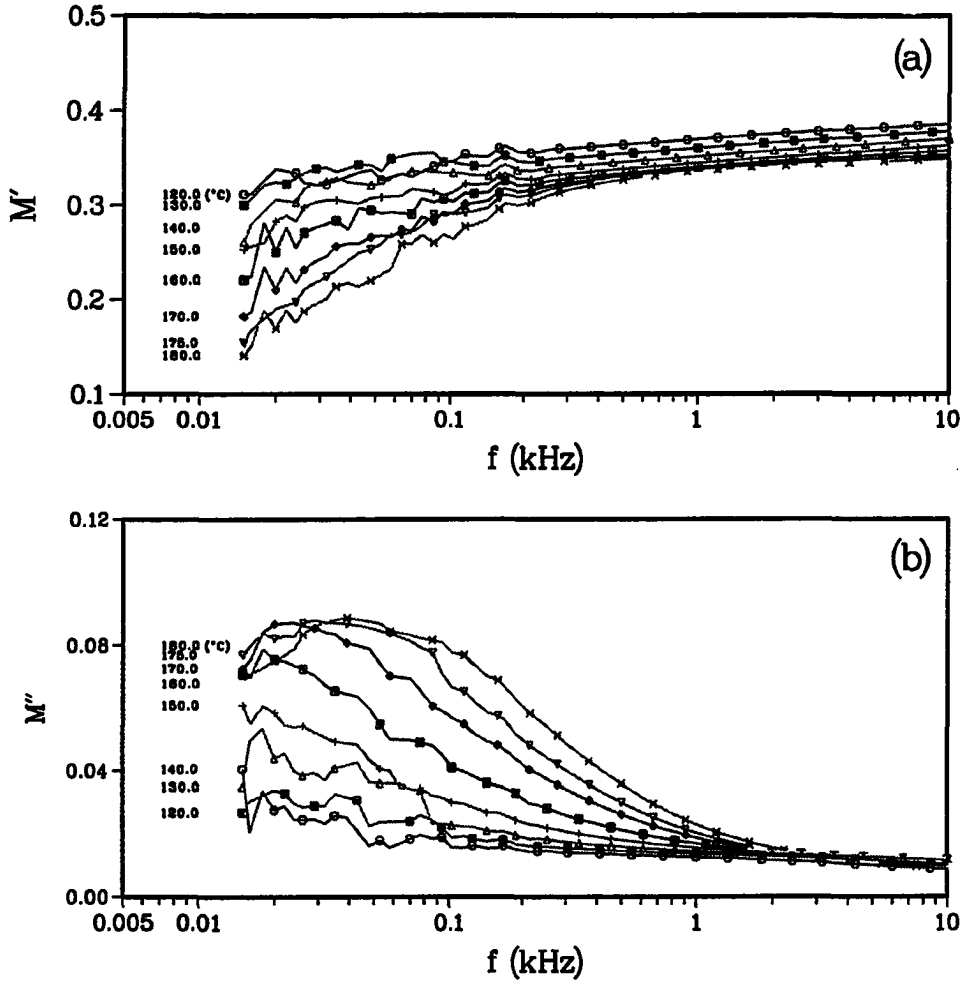

Figure 3.29: The spectra of (a) M' and (b) M'' against frequency for α'-relaxation of 3X ABTE-treated zirconia-silica-filled UDMA over the temperature range of 120.0 to 180 °C and over the frequency range of 0.01 to 10 kHz.

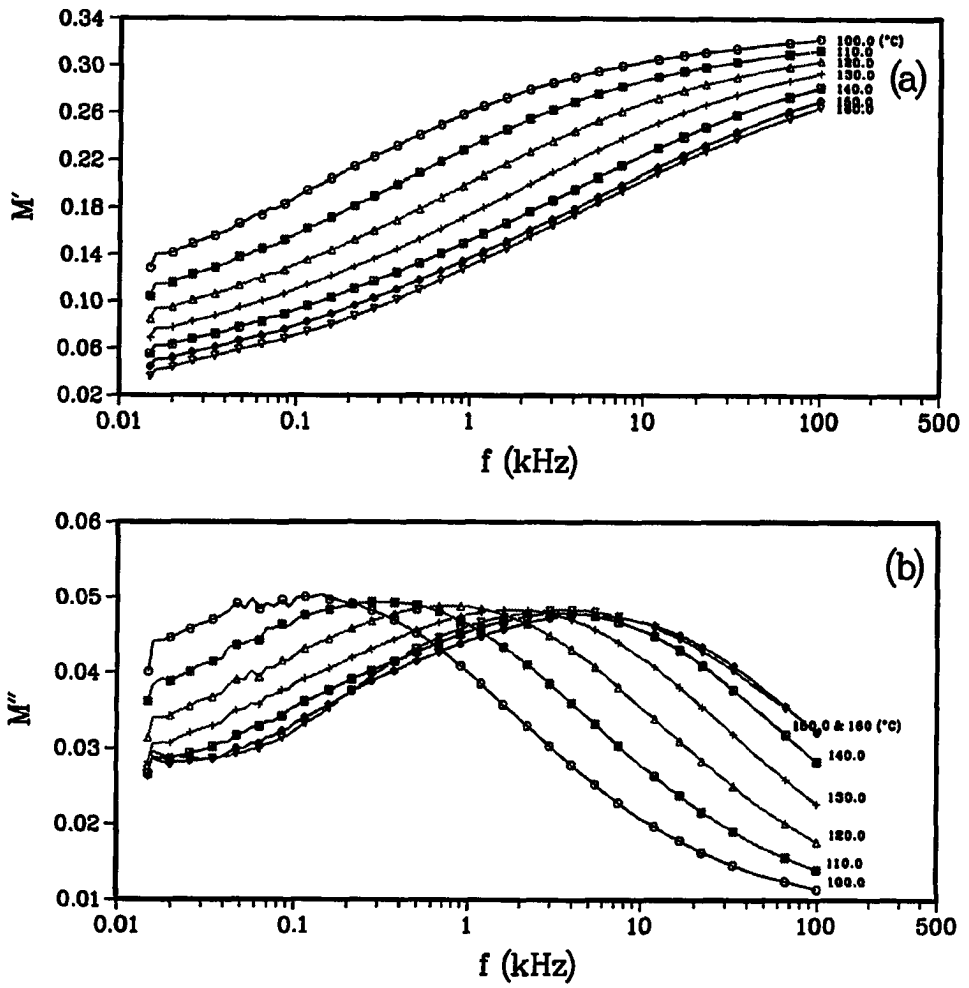

Figure 3.30: The spectra of (a) M' and (b) M'' against frequency for α'-relaxation of 30X ABTE-treated zirconia-silica-filled UDMA over the temperature range of 120.0 to 180 °C and over the frequency range of 0.01 to 100 kHz.

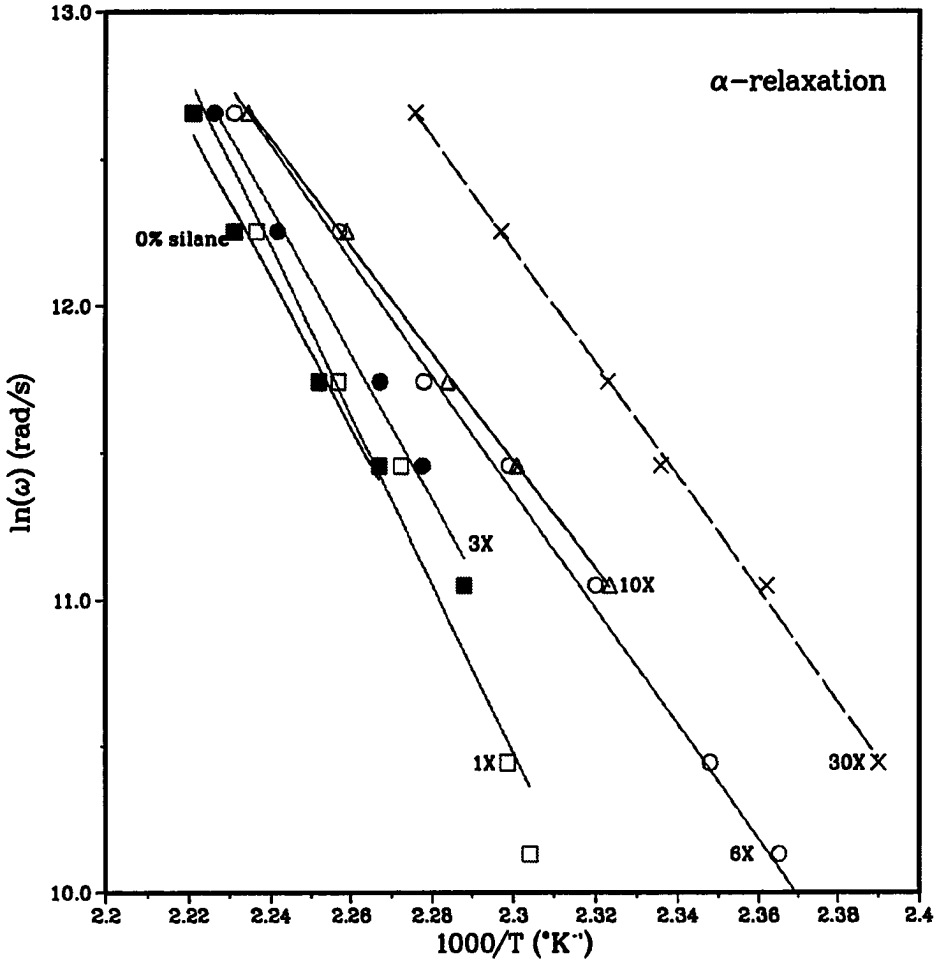

Figure 3.31: The angular frequency ($\ln(\omega)$) of $Tan(\delta)_\epsilon$ for the α-relaxation against $\frac{1}{T}(^\circ K^{-1})$ obtained from dielectric measurements for 0, 1X, 3X, 6X, 10X and 30X MAPM-treated zirconia-silica-filled UDMA.

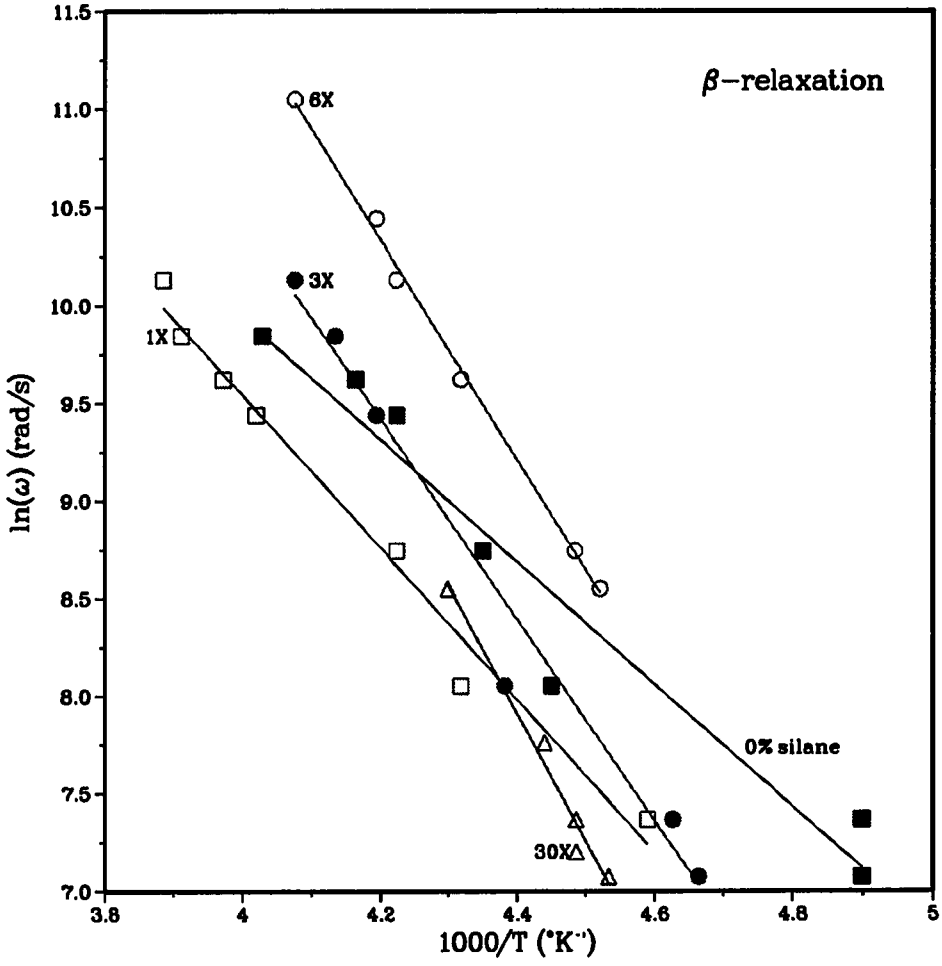

Figure 3.32: The angular frequency ($\ln(\omega)$) of $Tan(\delta)_\epsilon$ for the β-relaxation against $\frac{1}{T}(^\circ K^{-1})$ obtained from dielectric measurements for 0, 1X, 3X, 6X, 10X and 30X MAPM-treated zirconia-silica-filled UDMA.

MAPM Amount	α-relaxation		β-relaxation	
	ΔH $\left(\frac{kcal}{mole}\right)$	$\Delta_{1/2}$ (decades)	ΔH $\left(\frac{kcal}{mole}\right)$	$\Delta_{1/2}$ (decades)
0	49.9 ± 0.6	4.95	6.7 ± 0.2	5.49
1X	57.2 ± 2.5	5.25	7.7 ± 0.4	4.69
3X	48.5 ± 1.6	4.17	10.5 ± 1.2	4.24
6X	41.8 ± 2.7	3.73	11.3 ± 0.6	4.89
10X	43.6 ± 6.4	3.82	7.5 ± 0.2	5.01
30X	42.3 ± 0.8	5.65	8.6 ± 0.4	5.04

Table 3.8: Activation energies (ΔH) from $Tan(\delta)_\epsilon$ measurements and half-width of bands ($\Delta_{1/2}$) for $\alpha-$ and $\beta-$relaxations at 120 and 10 °C, respectively, as a function of different amount of MAPM treatment of 75 wt % zirconia-silica dispersed in UDMA.

MAPM Amount	α-relaxation		β-relaxation	
	λ 10.0 (kHz)	$\Delta\epsilon$ 180 (°C)	λ 0.252 (kHz)	$\Delta\epsilon$ -30 (°C)
0	0.016	0.85	0.0024	0.0098
1X	0.019	0.49	0.0027	0.0260
3X	0.015	0.49	0.0019	0.0094
6X	0.012	0.77	0.0027	0.0135
10X	0.023	0.65	0.0027	0.0104
30X	0.019	0.93	0.0027	0.0173

Table 3.9: Intensities (λ) of $Tan(\delta)_\epsilon$ at 10.0 kHz and dielectric increments ($\Delta\epsilon$) for $\alpha-$ and $\beta-$relaxations at 180 and -30 °C, respectively, as a function of increasing MAPM concentration in treating 75 wt % zirconia-silica dispersed in UDMA.

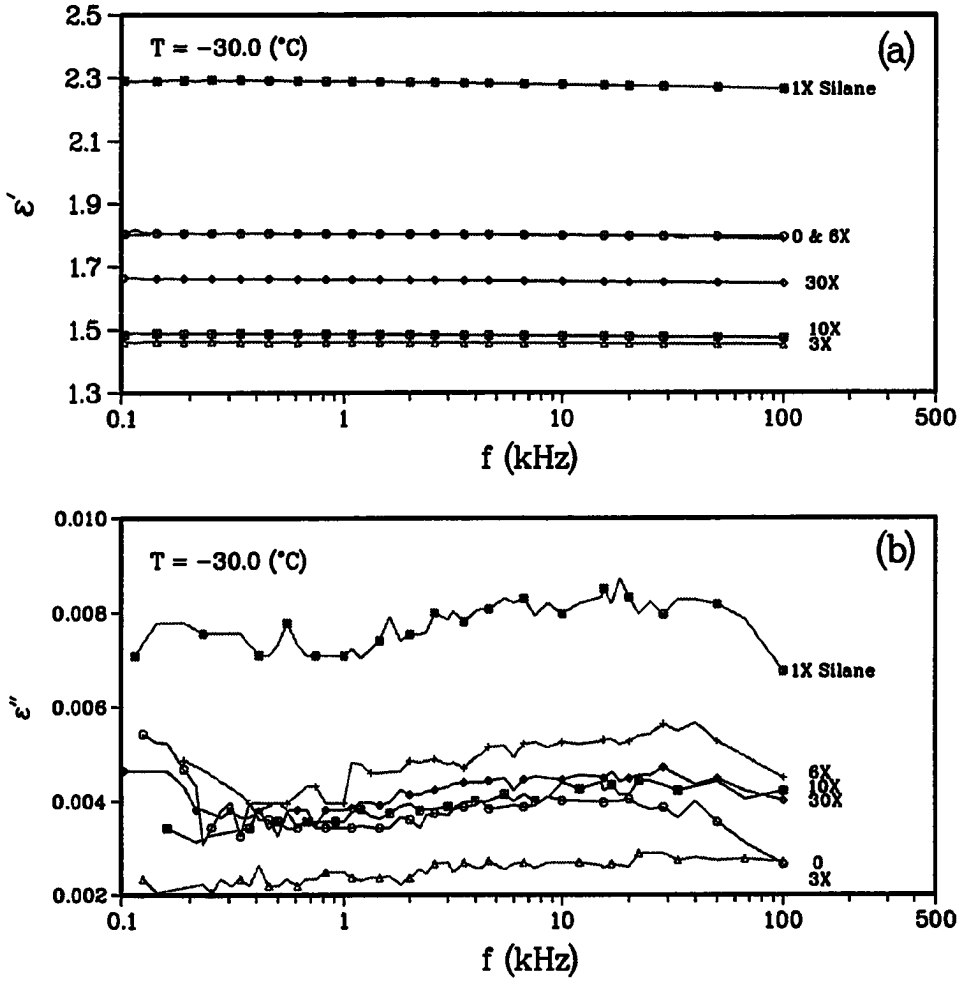

Figure 3.33: The spectra of (a) ϵ' and (b) ϵ'' against frequency for α-relaxation of 0 to 30X MAPM-treated zirconia-silica-filled UDMA at -30 °C.

ABTE Amount	α-relaxation			β-relaxation		
	ΔH $\left(\frac{kcal}{mole}\right)$	ΔS $\left(\frac{kcal}{mole^oK}\right)$	τ_o (Hz) $*10^{-29}$	ΔH $\left(\frac{kcal}{mole}\right)$	ΔS $\left(\frac{kcal}{mole^oK}\right)$	τ_o (Hz) $*10^{-12}$
0	49.9 ± 0.6	0.184	67.0	6.7 ± 0.2	0.105	46.0
3X	46.1 ± 0.2	0.143	2.4	9.0 ± 0.3	0.116	0.27
30X	—	—	—	8.9 ± 0.1	0.117	0.13

Table 3.10: Activation energies (ΔH), pre-exponential factors (τ_o) and activation entropies (ΔS) for $\alpha-$ and $\beta-$dielectric relaxation processes at 432 and 232 °K, respectively, as a function of different amount of ABTE treatment of 75 wt % zirconia-silica dispersed in UDMA.

ABTE Amount	α-relaxation		β-relaxation	
	λ 10.0 (kHz)	$\Delta\epsilon$ 160 (°C)	λ 0.252 (kHz)	$\Delta\epsilon$ -30 (°C)
0	0.016	0.34	0.0024	0.0098
3X	0.033	1.87	0.0035	0.0071
30X	—	23.87	0.0040	0.0048

Table 3.11: Intensities (λ) of $Tan(\delta)_\epsilon$ at 10.0 kHz and dielectric increments ($\Delta\epsilon$) for $\alpha-$ and $\beta-$relaxations at 160 and -30 °C, respectively, as a function of increasing ABTE concentration in treating 75 wt % zirconia-silica dispersed in UDMA.

The Effect of the Silane on the α-relaxation

Since Lipatov [62] postulated that the nature of the interface is independent of the chemical nature of the surface unless there is a specific interaction between the filler surface and the matrix, the above results show a dependence of the interface on the chemical nature of the silanated filler. For instance, when the matrix was reinforced with zirconia-silica treated with MAPM at the minimum uniform coverage of the silane, the α-relaxation shifted to higher temperatures, however, at the higher MAPM concentrations the α-relaxation shifted to lower temperatures. The increase of the peak's maxima to higher temperature is indicative of the decrease of the main chain mobility in the vicinity of the filler surface. This effect can be explained by the stiffness of the interfacial region due to the existence of strong linkages between the silane and the filler, and between the silane and the matrix. Since the specific interaction between the silane and the surface of the filler does not extend beyond the second layer, when the thickness of the silane layer increases, the relative contribution of the first layer decreases [49]. One may assume that at the low concentration of MAPM the contributions of the chemical interactions between the zirconia-silica and the silane and between the silane and the resin dominate and are reflected as increases in the α-relaxation temperatures. This conclusion is further supported by the increase of ΔH values from 49.9 kcal/mole for the unsilanated zirconia-filled UDMA to 57.2 kcal/mole for the MAPM-silanated zirconia-filled UDMA. Further, it has been shown by Plueddemann [80] that the amount of silanes deposited on the mineral surfaces from an aqueous solution increases rapidly as the concentration increases to certain transition concentration, and above this concentration the silane increases more slowly. The transition concentration that was given by Plueddemann for MAPM is 0.4 wt %, which is equivalent to the minimum uniform coverage (1X)

that is given by equation (2.1).

The fact that there was no indication of a new peak above the transition concentration, implies the non-existence of a separate phase that is due to space charge separation that characterizes an interface. This proves that MAPM is a compatible plasticizer to the UDMA system. Such a compatibility manifested itself in the shift of the $\alpha-$relaxations toward lower temperatures as well as the decrease of the activation energy values. These results showed increases in the main chain mobility and in the free volume of the polymer which are positive determination of the plasticizer efficiency [47]. In addition, the increase in the $\Delta_{1/2}$ values implied broadening in the $\alpha-$relaxations by increasing MAPM concentration, indicating wider distribution of relaxation times. Also, λ and $\Delta\epsilon$ showed a general increase in their values which indicates ease of polar groups mobility in the polymer. This ease of mobility developed by attaching the MAPM molecules strongly enough to the chains of the polymer so as to contribute to the polarization involved in the mechanism. Such a contribution appeared as an enhancement to the strength of the polymer's dipole moment rather than appearing as separate losses.

Silanation of zirconia-silica with ABTE at 3X showed the same effect on the α-relaxation of the composite. That is, the $\alpha-$peaks shifted to lower temperatures, and the activation energies, entropies and relaxation times decreased to lower values. These results also confirmed the above behavior of increasing the flexibility of the adsorbed layer as its thickness increases due to the increase of silane concentration in filler treatment beyond the transition concentration. However, at the low concentration of ABTE (3X) a new peak started to emerge at very low frequencies (Figure 3.29) and developed to a complete peak (α'-peak) at the very high concentration (30X) (Figure 3.30). The α'-peak obstructed the $\alpha-$peak which was shifted

to a very low temperature and appeared as a shoulder at 70.0 °C (Figure 3.27). This newly emerged peak appeared at lower frequencies and disappeared at higher frequencies (above 6 kHz) and had an activation energy of 28.9 kcal/mole. This peak was attributed to part of the silane that could not penetrate the polymer and formed a separate phase incompatible with it. Also, the λ and $\Delta\epsilon$ values showed definite increase with ABTE concentration, indicating that the effective dipole moment also has been affected.

From these results one can gain insights into the interactions between the polymer and the silane. It seems that in the presence of a compatible silane, the composite exhibited a single glass transition dispersion in the dielectric spectra, while in the presence of an incompatible silane a new dispersion transition was separately observed. This new relaxation characterizes the interphase. In the presence of the compatible silane, the mechanism of its effect on the composite behavior depends on its concentration at the interface. For instance, with small amount of the silane specific molecular interactions occurred between the filler surface and the matrix which caused restriction in the motion of the surface layer. These molecular interactions are due to chemical linkages between the silanetriol and the silica surface as well as the carbon double bond in the MAPM and the UDMA. In addition, with large amounts of the silane, intermediate flexible layers started to develop in the vicinity of the filler due to the formation of loosely adsorbed layers [2] composed of condensed polysiloxane with uncondensed silanetriol. However, in the presence of the incompatible silane, the interphase that started to form is due to the formation of solvating layers in the polymer and spontaneous aggregation of the low molecular weight compound molecules [13]. These low molecular weight compounds are composed of mixtures of structures where the charge separations characterizes their

nature. Such structures will be discussed in the next subsection.

The Effect of the Silane on the β-relaxation

Adding small amounts of MAPM up to about three times the minimum uniform coverage restricted the mobility of the free amide groups. This was reflected by the increase in the activation energy values and the shifts of the peak maxima for the β-relaxation toward higher temperatures. Also, the $\Delta_{1/2}$ values decreased with increasing MAPM concentration showing narrowing of the distribution of relaxation times. Further, narrowing of the distribution of relaxation times reflects the decrease in the different number of different environments of amide groups in the system implying that higher amounts of free amide groups are reacted and having similar relaxation times. This seems to support that low concentration of MAPM (about 3X) is enough to decrease the mobility of amide groups probably by increasing the density of molecular packing at the interface between the filler and the polymer, thus decreasing the the distance between the molecules and augmenting the chance of interchain coupling that existed in the polymer network.

However, adding high amounts of MAPM increased the mobility of the free amide groups. This was seen by the decrease in the activation energy values and the shift of the peak maxima for the β-relaxation toward lower temperatures, along with the broadening of the relaxation times. These results imply that the increase in the amide groups mobility resulted from the reduction of interchain coupling by breaking of the amide-hydrogen bond that exists in the polymer network and increasing the segmental mobility by dilution. This breaking occurred by the MAPM molecule through unreacted silanetriols that might replace the amide-hydrogen bonds. These unreacted silanetriols are attached strong enough to the amide groups so they move

the chains as they change configuration and hence increase the dipole moment of the amide groups.

The $\Delta_{1/2}$, the activation energies and the peak maxima temperatures at 0.252 and 1.0 kHz exhibited maxima at about 3X MAPM content. This concentration seems to be optimum with respect of the efficiency of MAPM.

The hydrolysed aminosilane may exist in two structural forms and they are shown in Figures 3.34(a) and 3.34(b). Both structures can probably be found in equilibrium. One of these structures is an open extended form (Figure 3.34(a)), where the amino groups exist as free NH_2 or strongly hydrogen bound to the silica, while the other structure is a cyclic hydrogen-bonded amine structure (Figure 3.34(b)), where a partial proton transfer exists ($SiO \ldots H \ldots NH_{2+}$) in the ring structure [49, 80]. The open extended structure seems to predominate in low concentrated solution, while the low molecular cyclic structures are favored in concentrated solution [80]. These two structures can be seen to influence the behavior of the dielectric dispersions of UDMA. For instance, adding different amounts of ABTE shifted the peak maximum temperatures for the β-relaxation toward lower values and caused the new separate loss to occur. The lowering of the β-relaxation temperature indicates that the ABTE plasticized the polymer by increasing the segmental mobility and the reduction of the interchain bonding. Such interchain bonding occurred by replacement of the hydrogen bonding exists in the original polymer to the hydrogen bonding between the ABTE's free amino groups or the unreacted silanetriol and the amine or carbonyl groups exist in the UDMA. This seems to occur at very low concentrations of ABTE and it is only limited to the first few monolayers of the silane. However, at the high concentration of ABTE the occurrence of the new peak indicates the existence of a

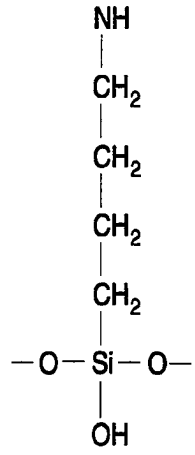

a) Open extended structure

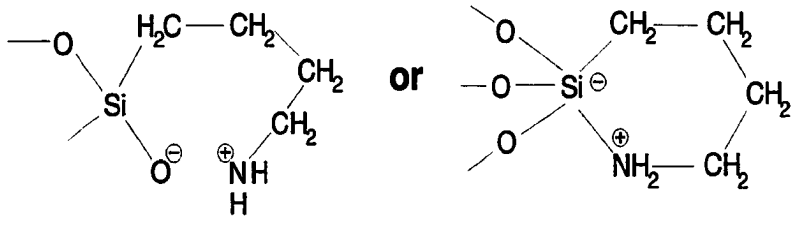

b) Cyclic structure

Figure 3.34: Proposed models of amino functional silane in water, (a) open extended model and (b) cyclic model.

separate interphase that has space charge separations which oscillates and moves with alternating electric field and resembles the interfacial polarization. This supports the existence of the cyclic structure with a partial proton transfer formed by the aminosilane, especially at the high concentration. Such structure could not react or form any chemical links with the UDMA, and was forced into a separate phase. This seems to be the dominate effect on the dielectric spectra, since there is an over all increase in the intensity of the $Tan(\delta)_\epsilon$ values.

The activation energy values increased slightly and became independent of the ABTE concentration. Such independence indicated that ABTE contributes slightly to this loss mechanism, and the hydrogen bonding described above occurred only at the first few monolayers and became irrelevant at higher concentrations. This was further supported by the decrease in the dielectric increment of the $\beta-$relaxation (Table 3.11), which indicated the decrease in the effective dipole moment. Such decrease implied the restriction of the amino group motion and/or the decrease in the number of the free amide groups available, which were depleted by H-bonding to the amino groups of the silane. These results further supported that the above assignment of the β-relaxation is indeed due to the relaxation of the free unbounded NH_2 groups in UDMA.

3.5 Concluding Remarks

UDMA shows three relaxations $\alpha-$, $\beta-$ and $\gamma-$relaxations. The α-relaxation is attributed to the segmental motion of the main chains, the β-relaxation to the motion of free amide groups, and the γ-relaxation to the local motion of $(CH_2)_n$.

Adding zirconia-silica to the UDMA shows pronounced effect on the behavior and on the thickness of the boundary layer at the interface. Increasing filler concentration

restricts the mobility of the main chains and decreases the thickness of the surface layer, while allowing more movement to the local chains in the loosely packed layer. These changes near the interface are due to the reduction of the conformational numbers and the need of more conformational changes of the main chains for the transition of molecular segments from one position to another to occur during the relaxation.

MAPM was shown to be a compatible silane with the zirconia-silica and UDMA system. Such compatibility was observed through the effectiveness of the chemical linkage of the silane to the filler and the polymer without forming separate interphase. The effective chemical bonds formed between the coupling agent and the composite depends on the concentration of the silane. In the case of MAPM-silanated zirconia-silica-filled UDMA, the optimum silane concentration is about three times the minimum uniform coverage given by Equation (2.1). Above this concentration, high plasticization effects starts to develop.

ABTE was shown to be an incompatible silane for zirconia-silica-filled UDMA system. The incompatibility was seen by the occurrence of a new peak that characterizes an interphase. This interphase is made of low molecular unreactive cyclic amino structures that contain protonated amines. These amines cause charge separation upon the application of the electric field and were shown as a separate dispersion.

CHAPTER IV

THE EFFECT OF MOISTURE ON THE DIELECTRIC RELAXATION IN URETHANE DIMETHACRYLATE POLYMER AND COMPOSITES

4.1 Introduction

Since synthetic polymers are now extensively used in the biological environment, there is considerable concern about the nature of the interaction between the water in such environment and the polymer. The water-polymer interaction is often beneficial or detrimental to the performance of the synthetic polymer. For successful performance of these polymers in these environments, it is of great interest to augment our knowledge and understanding of the changes in the molecular dynamics of the polymer in the presence of water and in the states of the water molecules in the presence of polymers.

The state of water that can found in polymers consists of bound and bulk water. Bound water is the portion of water that interacts so strongly with polymers that it becomes associated with it, while bulk water is the portion of water that is not associated or bound with the polymer [29]. The bound water readily supercools without crystallization, while the bulk water crystallizes to ice [73].

Water interaction with bulk polymer was first described by Starkweather in Nylon 66 as being tightly bound, nonfreezing, and uniformly distributed [99]. When water is first absorbed into the polymer, water molecules are believed to hydrogen bond between two amides groups, acting as crosslinks at low temperatures but plasticizing at elevated temperatures because of greater thermal mobility of water compared to segments of the polymer chains. Water molecules were also found to hydrogen bond to esters and carboxyl groups in amorphous acrylic polymers by Brown [16]. However, above a characteristic level of water for each kind of polymer, the water appears in a second form generally called "clusters" [16]. These clusters consist of an average of three molecules bonded at polar sites [99] or a separate phase of water in a less polar polymer [53].

Early investigations of the effect of water on dielectric low temperature relaxations of polyamides [14], polyurethanes [71] and polycarbonate [53] were shown to enhance the height of these relaxations by the presence of unassociated nonfreezing water. In addition, a secondary dielectric loss peak associated with frozen clustered water occurred in polycarbonate about 40 °C below its β-relaxation [53]. Further, liquid clustered water at 23 °C yielded a loss mechanism in the MHz region in polyethylene and in the kHz region for polycarbonate that was interpreted as a Maxwell-Wagner-Sillars (MWS) polarization [53]. Such an effect is due to the existence of free charges in solid material at the interface that develop from the presence of water inclusions.

The Maxwell-Wagner-Sillars (MWS) polarization, which is also known as interfacial polarization arises from the accumulation of charges at the interface between two phases whose conductivities and permittivities differ [39, 47, 91]. The occurrence of the MWS peak depends on the permittivity of the inclusion. If the inclusion has a low permittivity ($\epsilon' = 1$ - 5), the relaxation will appear at low frequencies ($f_m = 10^{-2}$ Hz)

and may only appear as a steeply increasing conductivity in an alternating current (AC) measurements. As the permittivity of the inclusions increases, so does the the frequency of the relaxation and with water ($\epsilon' = 76.8$) [39] it may occur up to 100 kHz and a characteristic peak may develop [47, 91, 104].

Therefore, the purpose of this part of the study was to examine the effect of moisture sorption on the molecular dynamics of a dental polymer by dielectric measurements in order to understand the behavior of water-polymer interaction. In addition, the effect of moisture on a dental composite containing treated and untreated filler with a silane coupling agent was investigated to elucidate the effect of moisture on the stability of the interface. Finally, a mechanism of water interaction with the polymer was proposed.

4.2 Experimental

4.2.1 Materials

Urethane dimethacrylate (UDMA) (Esschem Co., Essington PA) was used as a monomer system. Zirconia-silica (ZS) (3M Dental Products, St.Paul MN) with the same specification given previously was used as a filler. 3-methacryloxypropyltrimethoxysilane (MAPM) (Huls America, Piscataway NJ, formerly Petrarch Systems, Bristol PA) was used as a coupling agent to silanate the filler.

4.2.2 Sample Preparation

The filler was silanated as described previously by depositing the silane from an aqueous solution. The amount of silane used for the filler treatment in this part of the study was three times (3X) the minimum uniform coverage given by Equation (2.1). The polymer was formulated from UDMA using *dl*-camphoroquinone catalyst and 2-dimethylaminoethylmethacrylate accelerator in concentrations described by Douglas,

Craig and Chen [31]. Composites were formulated from UDMA, zirconia-silica, and MAPM-silanated zirconia-silica using the accelerator and the catalyst. The polymer and the composites were cast into thin discs and cured as described earlier. All samples were dried in vacuum at 100 °C for 72 hrs to remove the moisture.

Sorption of water vapor was carried out by exposing the samples over vapors of distilled water, until they were conditioned to equilibrium and no more moisture could be sorbed. Moisture sorption by the unfilled-UDMA was lower than the the sorption of the ZS-filled UDMA, which was higher than the sorption of the silanated ZS-filled UDMA. Moisture content (MC) was defined as grams of sorbed moisture per 1 gram of dried polymer. The maximum moisture sorption attained by the UDMA was 3.72 wt % and it was 7.32 and 6.0 wt % for unsilanated ZS-filled UDMA and MAPM-silanated ZS-filled UDMA, respectively.

4.2.3 Dielectric Measurements

The dielectric apparatus was described earlier in section (3.3.3). The dielectric loss tangent ($\mathrm{Tan}(\delta)_\epsilon$) and capacitance ($C$) measurements were carried out over a frequency range of 0.015 to 100 kHz from -180 to 180 °C. In addition, the $\mathrm{Tan}(\delta)_\epsilon$ and capacitance (C_o) were measured for an empty cell with the same experimental conditions and sample thickness over the frequency range at ambient temperature.

4.3 Results and Discussion

The effect of moisture on the dielectric behavior of UDMA, ZS-filled UDMA and MAPM-silanated ZS-filled UDMA is discussed in sections (4.3.1), (4.3.2) and (4.3.3), respectively. Then, a mechanism of moisture in UDMA is proposed in section (4.3.4). At the beginning of these sections, the experimental results are presented and discussed to show the general behavior of the effect of moisture on the dielectric

relaxation of the particular system. Then, the effect of moisture on each transition relaxation ($\alpha-$ and $\beta-$relaxations) is discussed thoroughly and an attempt to explain the mechanisms responsible for such behavior are also presented.

4.3.1 The Effect of Moisture on the Dielectric Behavior of UDMA

The dielectric loss tangents ($\mathrm{Tan}(\delta)_\epsilon$) for the UDMA with MC of 0, 0.69, 1.0, 1.83, 3.0 and 3.72 wt % measured at 1.0 kHz are plotted against temperature in Figure 4.1. The $\mathrm{Tan}(\delta)_\epsilon$ curves show a sub-T_g or β-relaxation peak, an α-relaxation peak and a substantial increase in the values of $\mathrm{Tan}(\delta)_\epsilon$ at high temperatures with MC $\leq$ 1.83 wt %. The curves also show the α-relaxation was obstructed by a new peak (α') which appeared as shoulder at 100 °C with MC $\geq$ 1.83 wt %. The maximum temperatures of the $\alpha-$ and $\beta-$peaks obtained from the $\mathrm{Tan}(\delta)_\epsilon$ curves measured at different frequencies are shown in Table 4.1. Figure 4.1 and Table 4.1 show the α-relaxation is shifted to slightly lower temperatures at the very high moisture content (MC of $\geq$ 3.0 wt %) due to plasticization effect of the moisture, while its intensity slightly increased. The results also show the β-relaxation is shifted to slightly higher temperature with MC of 0.69 wt %, while it shifted back to lower temperatures with MC $>$ 0.69 wt %. Finally, the relaxation shifted to higher values with MC $\geq$ 1.83 wt %.

The dielectric permittivity ϵ' and loss ϵ'' calculated from Equations (3.2) and (3.3) for the moistened UDMA with MC of 0 and 3.72 wt % are plotted against temperature in Figures 4.2 and 4.3, respectively. The ϵ'' spectra show the same behavior as those described above. The ϵ' values increased in the β-relaxation region from 1.562 to 1.656 with MC of 3.72 wt %, which was more than twice the height of the sub-T_g peak. For temperatures above the T_g, $\mathrm{Tan}(\delta)_\epsilon$, ϵ' and ϵ'' continuously increased

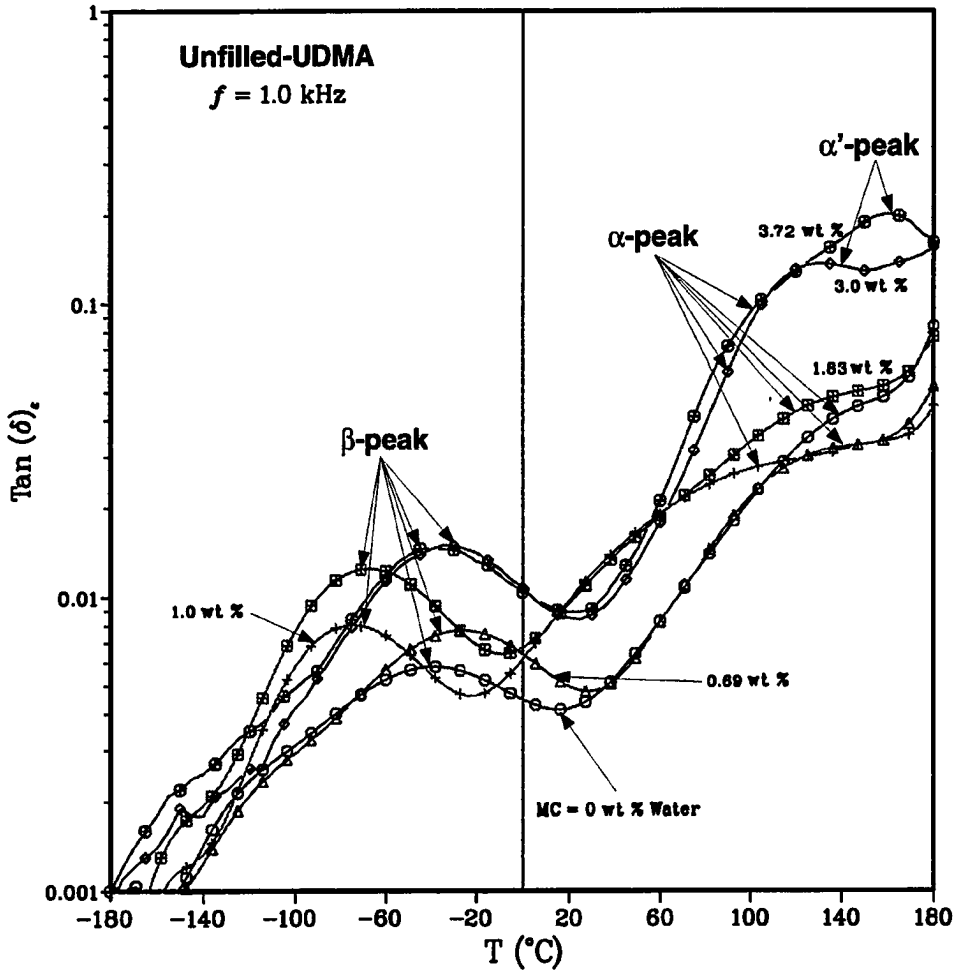

Figure 4.1: Tan(δ)$_\epsilon$ against temperature measured at 1.0 kHz for UDMA with MC of 0, 0.69, 1.0, 1.83, 3.0 and 3.72 wt %.

MC wt %	Maximum peaks temperature (°C)					
	α-relaxation			β-relaxation		
	5.5 (kHz)	10.0 (kHz)	33.3 (kHz)	0.252 (kHz)	1.0 (kHz)	10.0 (kHz)
0.0	156.4	158.2	168.5	-58.2	-38.8	0.4
0.69	152.4	157.4	172.2	-36.1	-25.5	6.4
1.00	157.4	160.6	171.1	-81.8	-74.2	-51.5
1.83	154.8	159.8	—	-79.8	-66.7	-42.4
3.00	136.5	—	—	-45.3	-32.5	-3.5
3.72	—	—	—	-50.0	-40.0	-4.9

Table 4.1: Maximum peaks temperatures (°C) from $\mathrm{Tan}(\delta)_\epsilon$ measurements for different amount of moisture content in UDMA polymer for α—relaxations at 5.5, 10.0 and 33.3 kHz and for β—relaxations at 0.252, 1.0 and 10.0 kHz.

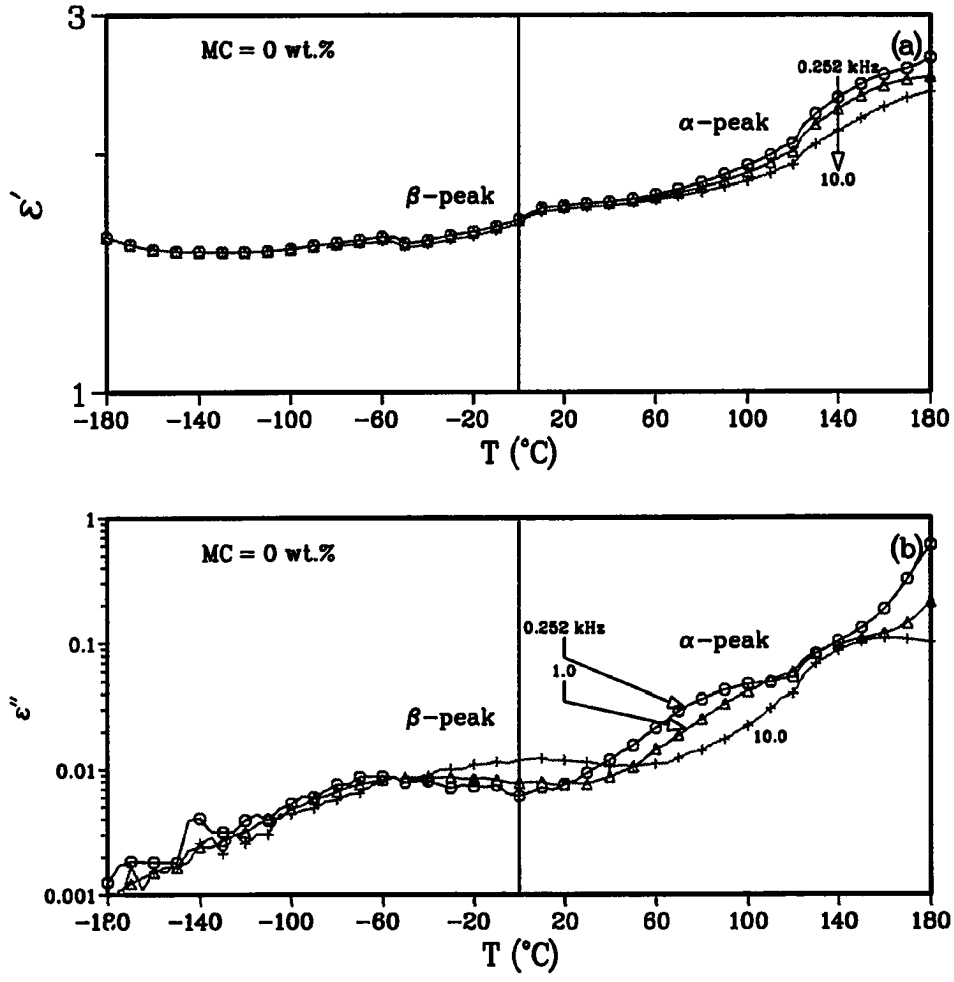

Figure 4.2: The temperature dependence of (a) ϵ' and (b) ϵ'' calculated for vacuum dried UDMA at 0.252, 1.0 and 10.0 kHz.

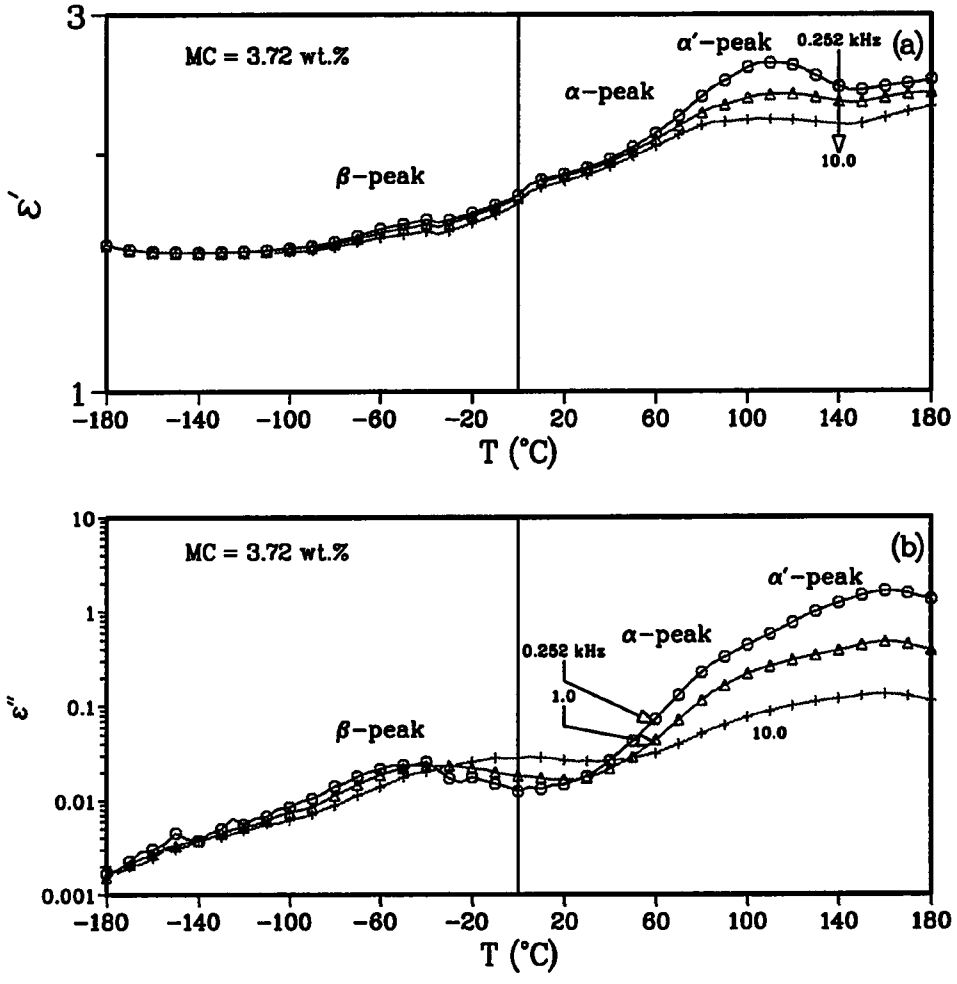

Figure 4.3: The temperature dependence of (a) ϵ' and (b) ϵ'' calculated for UDMA with MC of 3.72 wt % at 0.252, 1.0 and 10.0 kHz.

on heating from 100 to 180 °C.

Typical isothermal spectra of ϵ' and ϵ'' at several temperatures for the $\beta-$process of UDMA with MC of 0.69, 1.83 and 3.72 wt % are shown in Figures 4.4, 4.5 and 4.6, respectively. These plots suggest the persistence of the sub-T_g segmental mobility of the UDMA, which was assigned in the previous chapter to the mobility of the free amide groups. The feature of this relaxation is similar to those of the local mode motions in polymers and molecular glasses [73], namely, that there is an increase in the height of the ϵ'' peak with increasing temperature, a decrease in the half-width and an Arrhenius dependence of the rate on temperature with relatively low activation energy (Table 4.2). However, such an increase in the height of ϵ'' decreased with an increase in the moisture content in UDMA. For instance, for vacuum dried UDMA, the height of ϵ'' peak increased by 74 % over the temperature range of -60 to 10 °C, while it increased by 46 % and 40 % with MC of 0.69 and 3.72 wt %, respectively, in the same temperature range. The dielectric strength also increased with increasing moisture content and their values are presented in Table 4.3. In addition, the intensity (λ) of ϵ'' and $\text{Tan}(\delta)_\epsilon$ values increased with increasing MC, while those of the half-width decreased. Both quantities are listed in Table 4.4.

To compare the effect of moisture content on the amide group mobility, isothermal spectra of ϵ' and ϵ'' at -45 °C for UDMA with MC of 0, 0.69, 1.0, 1.83, 3.0 and 3.72 wt % are plotted in Figure 4.7. As in Figure 4.1, the ϵ'' peaks for the different amount of moisture in Figure 4.7 showed similar trends as those exhibited by the $\text{Tan}(\delta)_\epsilon$ peaks. Namely, the β-relaxation increased in intensity, as stated above, and shifted toward higher frequencies (i.e lower temperatures) with MC > 0.69 wt %, then it shifted back to lower frequencies (i.e higher temperatures) with MC $\geq$ 1.83 wt %.

Theoretically, the relaxed permittivity (ϵ_o) is measured at $f = 0$ kHz,

while the unrelaxed permittivity (ϵ_∞) is measured in the optical frequency range. However, experimentally, such extremes were not attainable due to the limitations of the instrument used. Therefore, and throughout this dissertation, what is referred to as ϵ_o is actually ϵ calculated at $f = 0.01$ kHz, i.e., $\epsilon_o = \epsilon_{0.01}$. Similarly, ϵ_∞ is actually ϵ calculated at $f = 200$ kHz, i.e., $\epsilon_\infty = \epsilon_{200}$. The above holds true for all other variables calculated at such extreme frequencies, e.g., M_o and M_∞.

Because of the large contribution to ϵ'' from the DC conductivity at temperature near the T_g which masked the ϵ'' peak due to dipolar reorientation, the α-relaxation in the glass-rubber transition region could not be observed. Therefore, the analysis for ionic solids was used, i.e., the conductance and capacitance were converted into complex electrical modulus formalism [73] by Equation (3.4), where M' and M'' are calculated by Equations (3.5) and (3.6). The isothermal spectra of M' and M'' at several temperatures through the T_g are plotted against frequency for UDMA with MC of 0, 0.69, 1.83 and 3.72 wt % in Figures 3.6 and 4.8 - 4.10. These plots show an onset of a second peak at low frequencies, that masked the T_g at high moisture content. The height of M'' peak increased slightly with temperature on the high frequency side. The reciprocal of the M_∞ and M_o determined from the M' relaxation peak, i.e., the reciprocal of the high- and low-frequency values of ϵ' to give the values of ϵ_∞ and ϵ_o at 175 °C, respectively, along with the dielectric increment determined from these values are presented in Table 4.3. For example, the M' high frequency process is 0.4494 at 175 °C, which gives $\epsilon_\infty = 2.22$ for the UDMA without moisture content. The ϵ_∞ value is in agreement with the values of ϵ_o of the sub-T_g obtained from Figure 3.5.

To look at the new peak that developed, M' and M'' for UDMA with MC of 0,

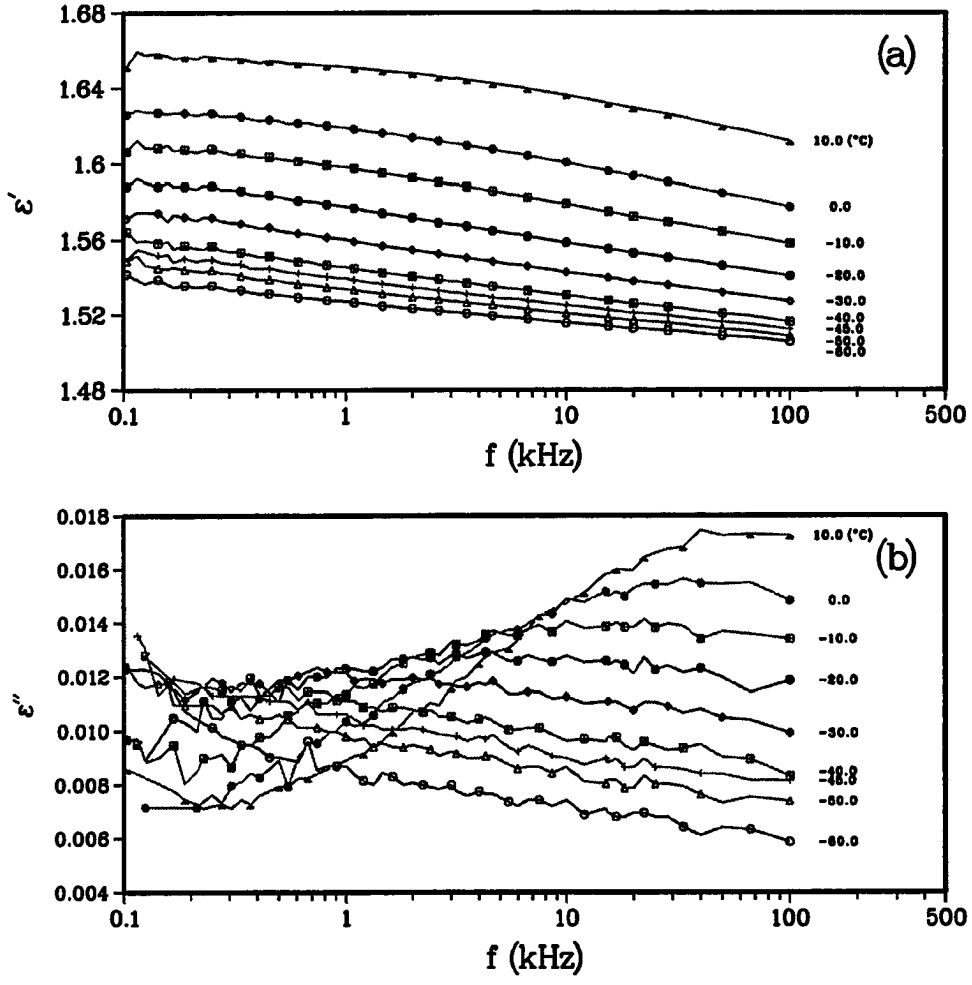

Figure 4.4: The frequency dependence of (a) ϵ' and (b) ϵ'' calculated over the temperature range of -60 to 10 °C for β-relaxation of UDMA polymer with MC of 0.69 wt %.

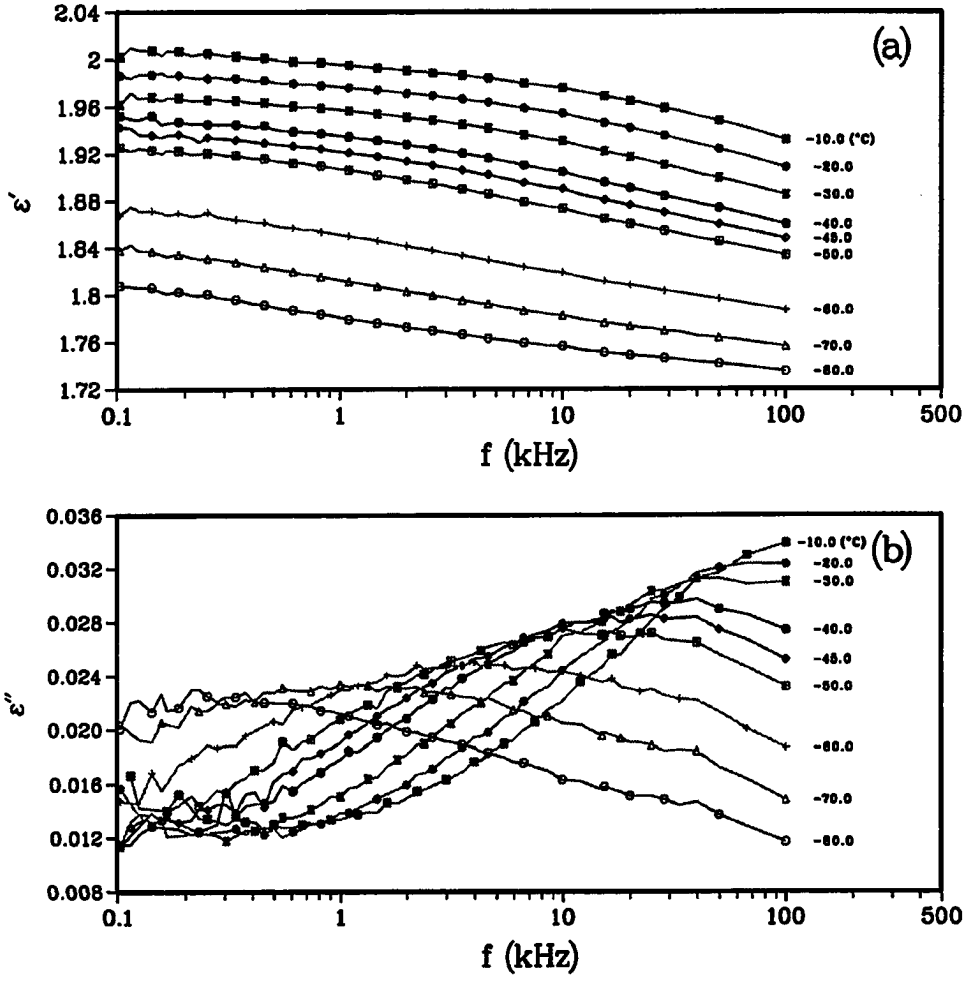

Figure 4.5: The frequency dependence of (a) ϵ' and (b) ϵ'' calculated over the temperature range of -80 to -10 °C for β-relaxation of UDMA polymer with MC of 1.83 wt %.

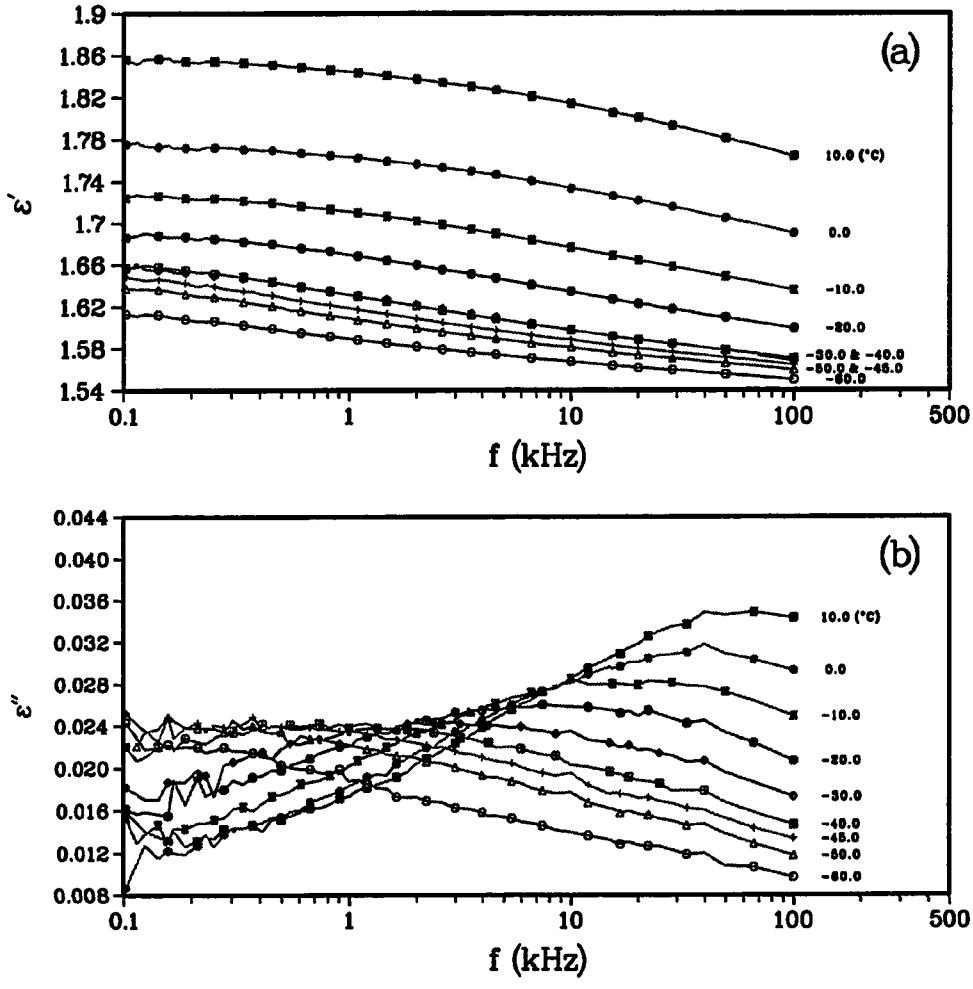

Figure 4.6: The frequency dependence of (a) ϵ' and (b) ϵ'' calculated over the temperature range of -60 to 10 °C for β-relaxation of UDMA polymer with MC of 3.72 wt %.

MC wt %	α-relaxation		α'-relaxation		β-relaxation	
	ΔH $\left(\frac{kcal}{mole}\right)$	τ_o (Hz)	ΔH $\left(\frac{kcal}{mole}\right)$	τ_o (Hz)	ΔH $\left(\frac{kcal}{mole}\right)$	τ_o (Hz)
0.0	40.4	$5.7 * 10^{-25}$	30.9	$1.1 * 10^{-18}$	7.5	$3.2 * 10^{-12}$
0.69	36.4	$9.7 * 10^{-25}$	39.5	$5.1 * 10^{-23}$	12.2	$5.4 * 10^{-16}$
1.00	38.6	$8.9 * 10^{-26}$	39.5	$5.1 * 10^{-23}$	9.2	$2.5 * 10^{-15}$
1.83	33.9	$2.2 * 10^{-23}$	26.9	$6.5 * 10^{-17}$	8.9	$1.0 * 10^{-14}$
3.00	21.3	$1.0 * 10^{-17}$	8.0	$2.5 * 10^{-08}$	10.6	$7.0 * 10^{-15}$
3.72	11.6	$6.2 * 10^{-11}$	8.2	$1.0 * 10^{-08}$	10.6	$4.9 * 10^{-15}$

Table 4.2: Activation energies and pre-exponential coefficients for $\alpha-$, $\alpha'-$ and $\beta-$dielectric relaxation processes as a function of moisture content (wt %) in UDMA polymer.

MC wt %	α-relaxation			β-relaxation		
	ϵ_o	ϵ_∞	$\Delta\epsilon$	ϵ_o	ϵ_∞	$\Delta\epsilon$
0.0	3.07	2.23	0.84	1.584	1.546	0.038
0.69	2.67	2.20	0.47	1.571	1.527	0.044
1.00	2.18	1.85	0.33	1.509	1.468	0.042
1.83	3.17	2.37	0.80	1.972	1.885	0.087
3.00[a]	70.46	2.58	67.88	1.944	1.832	0.111
3.72[b]	130.10	2.14	127.96	1.661	1.562	0.093

[a] ϵ_o , ϵ_∞ and $\Delta\epsilon$ of α'-relaxation
[b] ϵ_o , ϵ_∞ and $\Delta\epsilon$ of α'-relaxation

Table 4.3: Low (ϵ_o) and high (ϵ_∞) frequency limiting values of ϵ' as well as dielectric increments ($\Delta\epsilon$) for $\alpha-$ and $\beta-$relaxations at 175 and -30 °C as a function of moisture content (wt %) in UDMA polymer.

	α-relaxation		β-relaxation		α'-relaxation
MC	λ	$\Delta_{1/2}$	λ	$\Delta_{1/2}$	$\Delta_{1/2}$
wt %	0.252 (kHz)	100 (°C)	0.252 (kHz)	0 (°C)	180 (°C)
0.0	0.016	2.94	0.0060	4.38	2.13
0.69	0.024	3.14	0.0074	3.30	1.34
1.00	0.022	3.82	0.0074	3.32[a]	—
1.83	0.027	—	0.0118	3.38[b]	1.87
3.00	—	—	0.0146	3.65	1.26
3.72	—	—	0.0146	3.65	1.26

[a] half-width at -40 °C
[b] $\Delta_{1/2}$ at -40 °C

Table 4.4: Intensities (λ) of $\mathrm{Tan}(\delta)_\epsilon$ at 0.252 kHz and half-widths of $\epsilon''(\Delta_{1/2})$ (decades) for $\alpha-$, $\beta-$ and $\alpha'-$relaxations at 100, 0 and 180 °C, respectively, as a function of moisture content (wt %) in UDMA polymer.

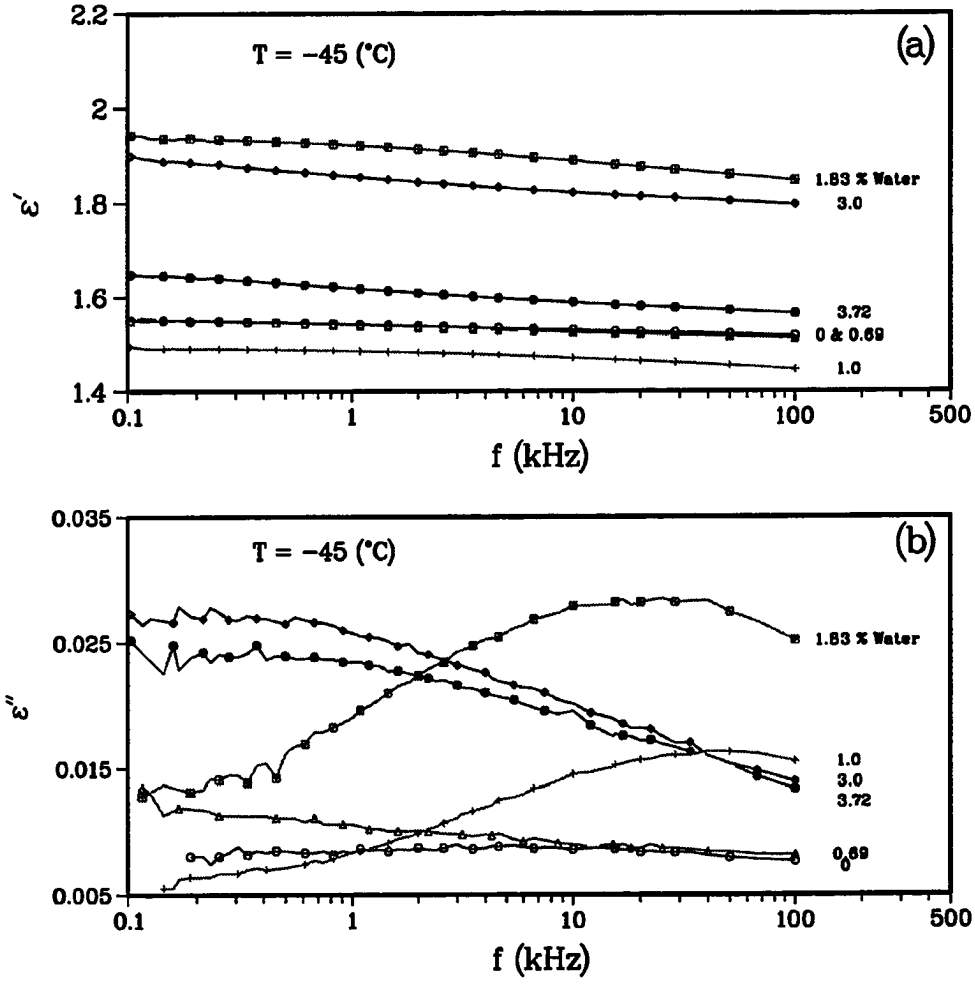

Figure 4.7: The frequency dependence of (a) ϵ' and (b) ϵ'' calculated at -45 °C for β-relaxation of UDMA polymer with MC of 0, 0.69, 1.0, 1.83, 3.0 and 3.72 wt %.

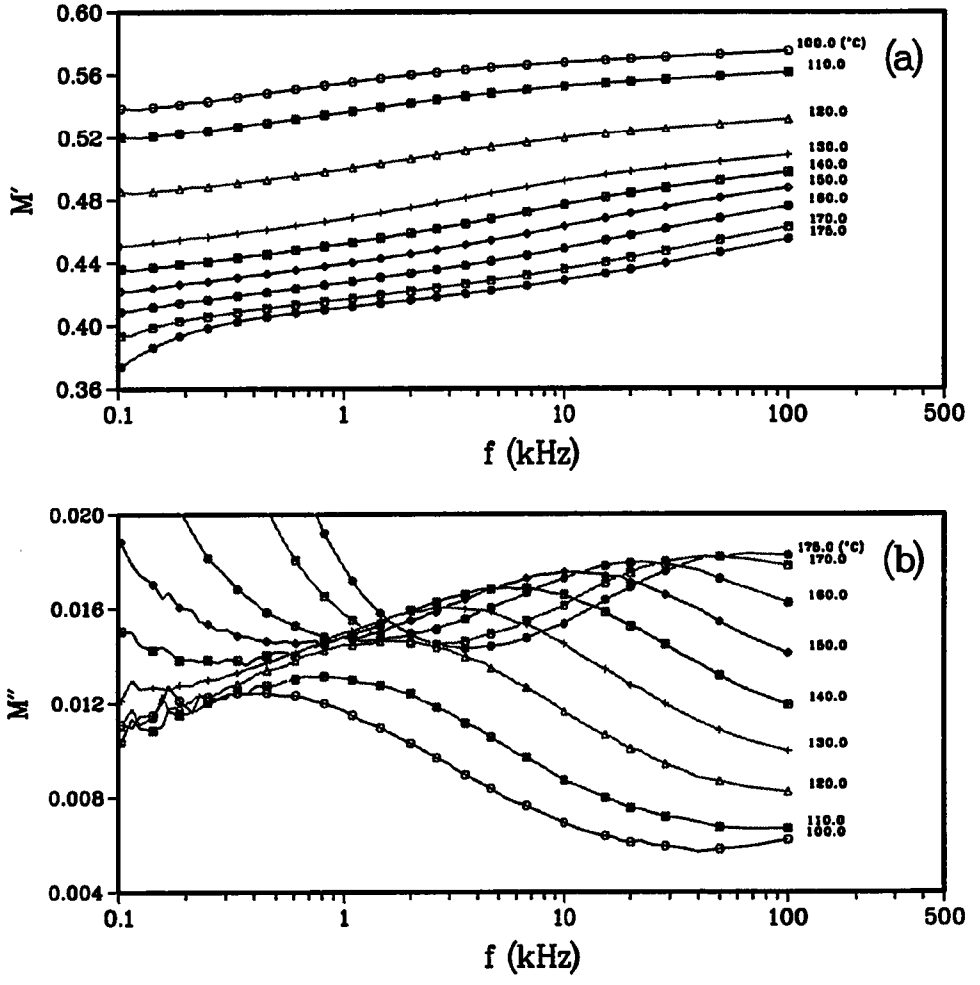

Figure 4.8: The frequency dependence of (a) M' and (b) M'' calculated over the temperature range of 100 to 175 °C for α-relaxation of UDMA polymer with MC of 0.69 wt %.

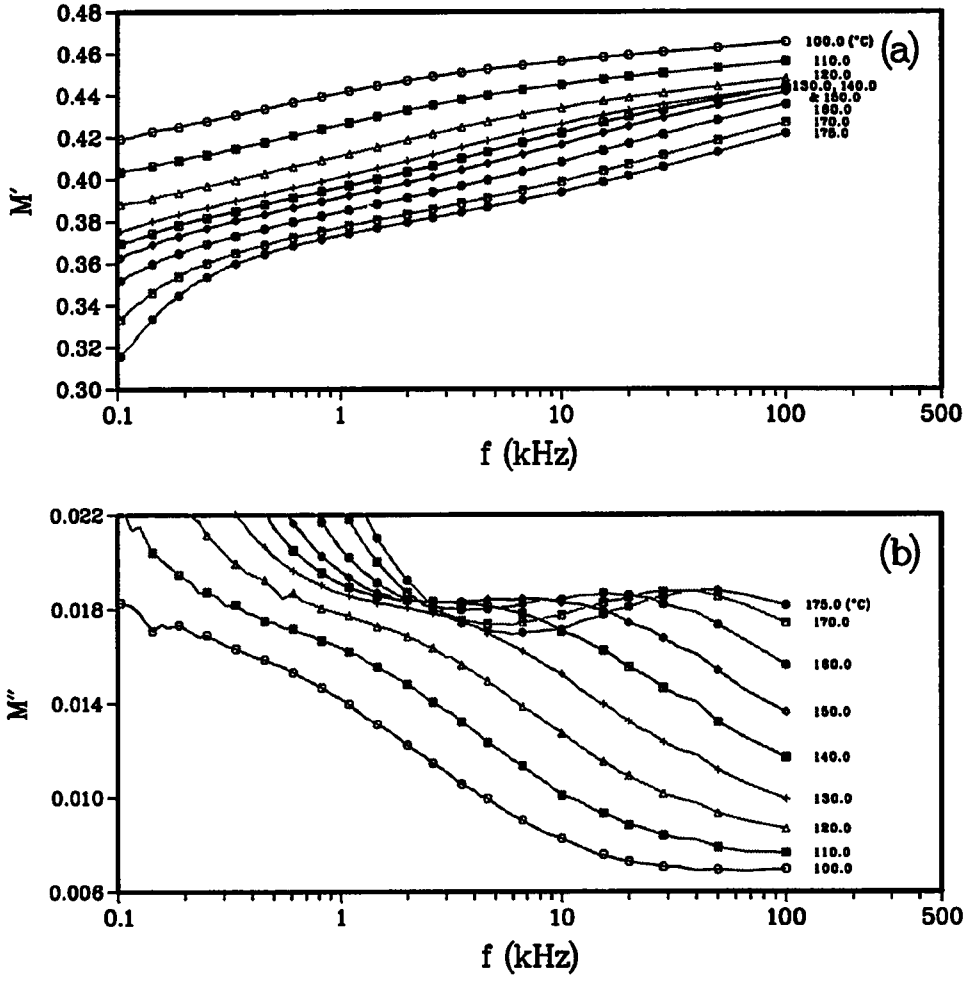

Figure 4.9: The frequency dependence of (a) M' and (b) M'' calculated over the temperature range of 100 to 175 °C for α-relaxation of UDMA polymer with MC of 1.83 wt %.

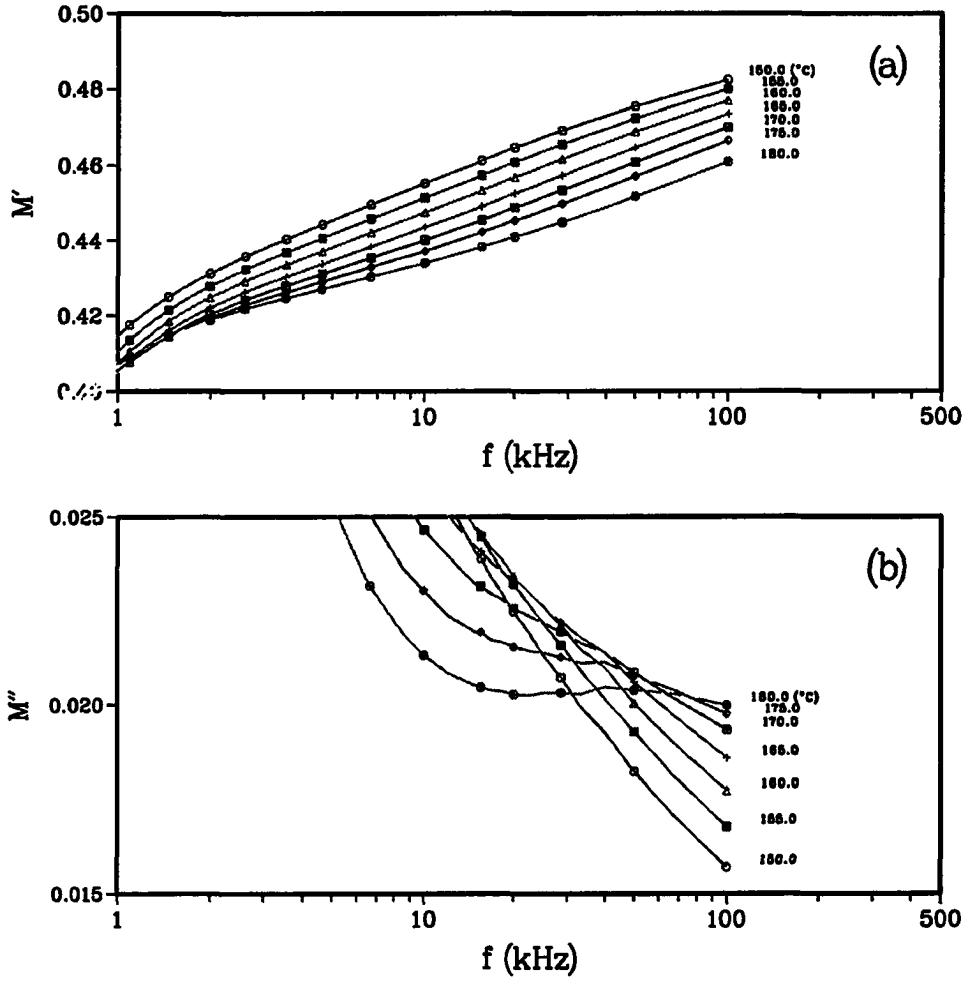

Figure 4.10: The frequency dependence of (a) M' and (b) M'' calculated over the temperature range of 150 to 180 °C for α-relaxation of UDMA polymer with MC of 3.72 wt %.

0.69, 1.83 and 3.72 wt % at several temperatures are plotted against low frequency range (0.01 - 1 kHz) in Figures 3.7, 4.11 - 4.13. These figures along with Figure 4.14 show clearly how the low frequency peak developed with increasing moisture content.

The half-width for the $\alpha-$ and $\alpha'-$relaxations are presented in Table 4.4 at 100 and 180 °C, respectively. The $\Delta_{1/2}$ values for the α-relaxation increased with moisture content, which indicates broadening of the distribution of relaxation times. However, the $\Delta_{1/2}$ values for the α'-relaxation decreased with moisture content indicating narrowing of relaxation times until it approached a limiting value of 1.26 decades. This value is little higher than the half-width of a single relaxation time (1.14 decades), also indicating the presence of a slight widening of the distribution.

The activation energies and pre-exponential factors were calculated from the slopes and intercepts of the plots of the frequencies at which the maximum peaks of $\mathrm{Tan}(\delta)_\epsilon$ appeared against reciprocal temperature and the values are presented in Table 4.2.

To summarize these results, The $\mathrm{Tan}(\delta)_\epsilon$ spectra measured at different temperatures, the ϵ' and ϵ'' spectra calculated at different frequencies for the low temperature processes, and the M' and M'' spectra calculated at different frequencies for the high temperature processes, are all clear evidence for the presence of the three relaxation peaks; The low temperature process corresponds to the mobility of the free amide groups. The high temperature process that occurred in the high frequency region corresponds to the backbone motions, while the new process that occurred at high temperature in the low frequency region corresponds to a combination of ionic and Maxwell-Wagner-Sillars polarization. These processes behaved differently with the presence of different moisture content. These behaviors will be discussed based upon the results that have been presented in the preceding paragraphs in the following

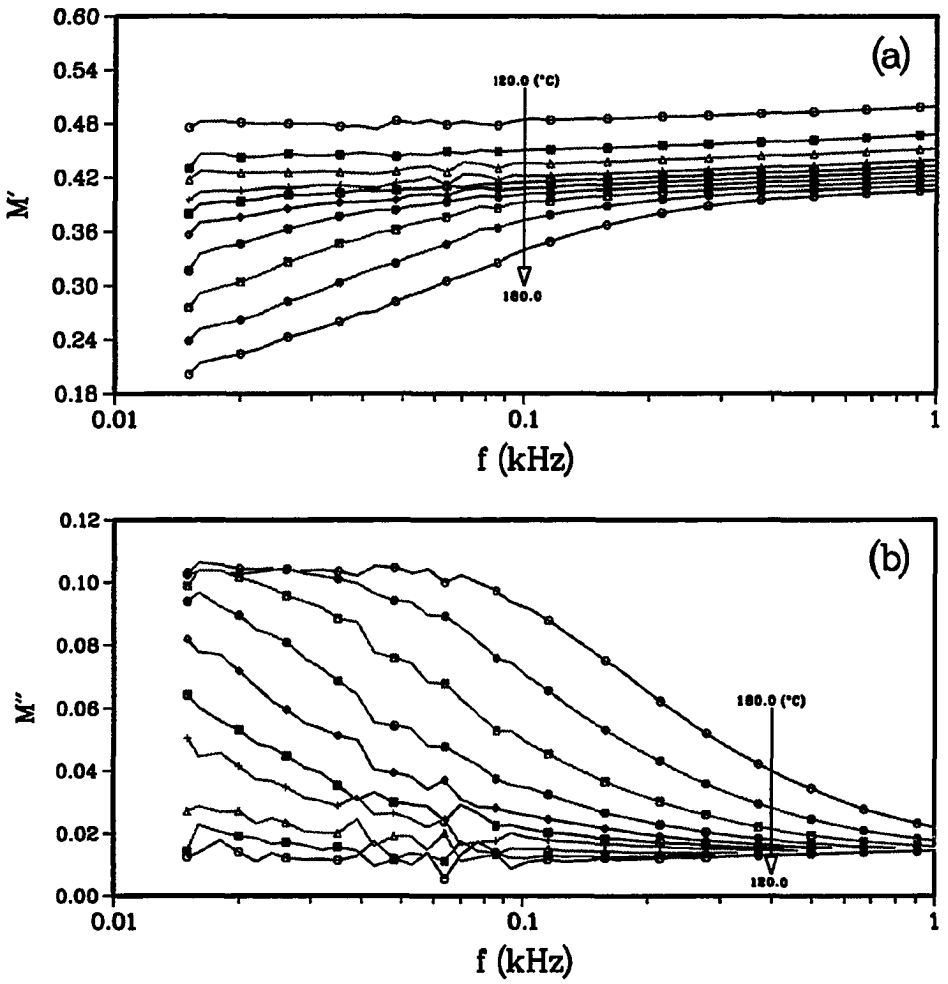

Figure 4.11: The spectra of (a) M' and (b) M'' against the frequency range of 0.01 to 1.0 kHz calculated over the temperature range of 120 to 180 °C for α'-relaxation of UDMA polymer with MC of 0.69 wt %.

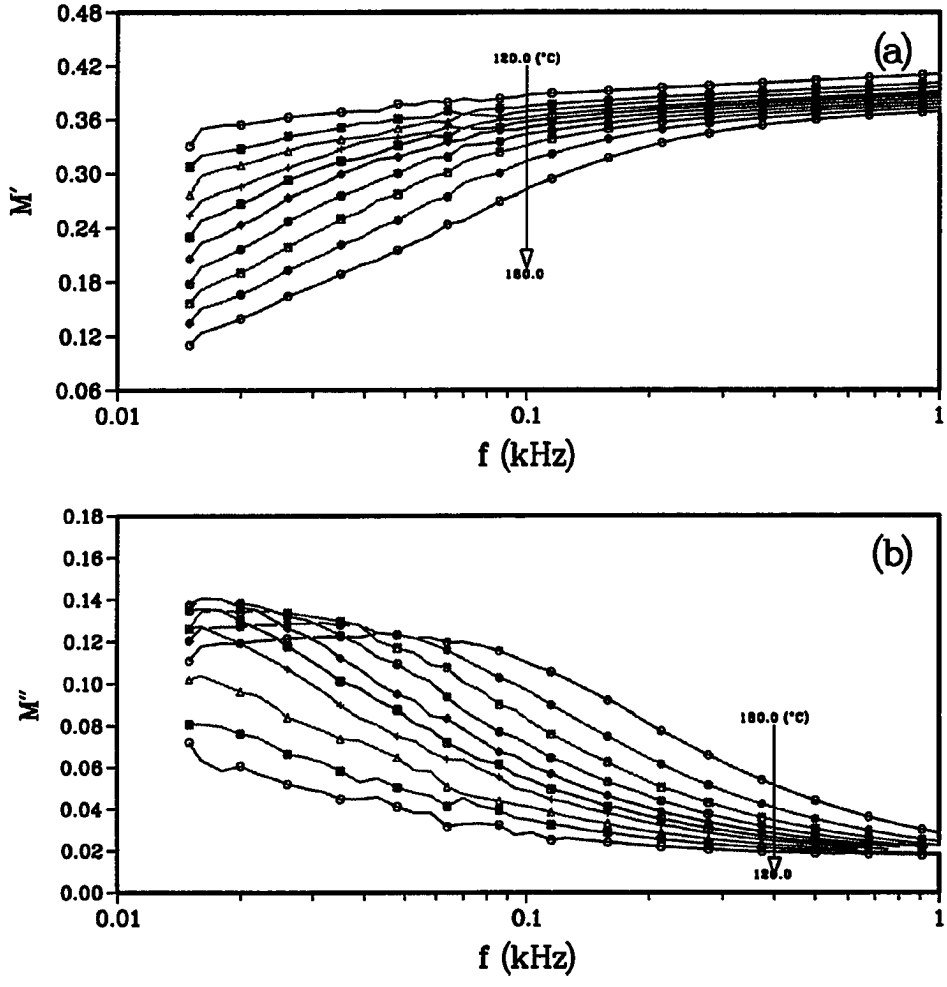

Figure 4.12: The spectra of (a) M' and (b) M'' against the frequency range of 0.01 to 1.0 kHz calculated over the temperature range of 120 to 180 °C for α'-relaxation of UDMA polymer with MC of 1.83 wt %.

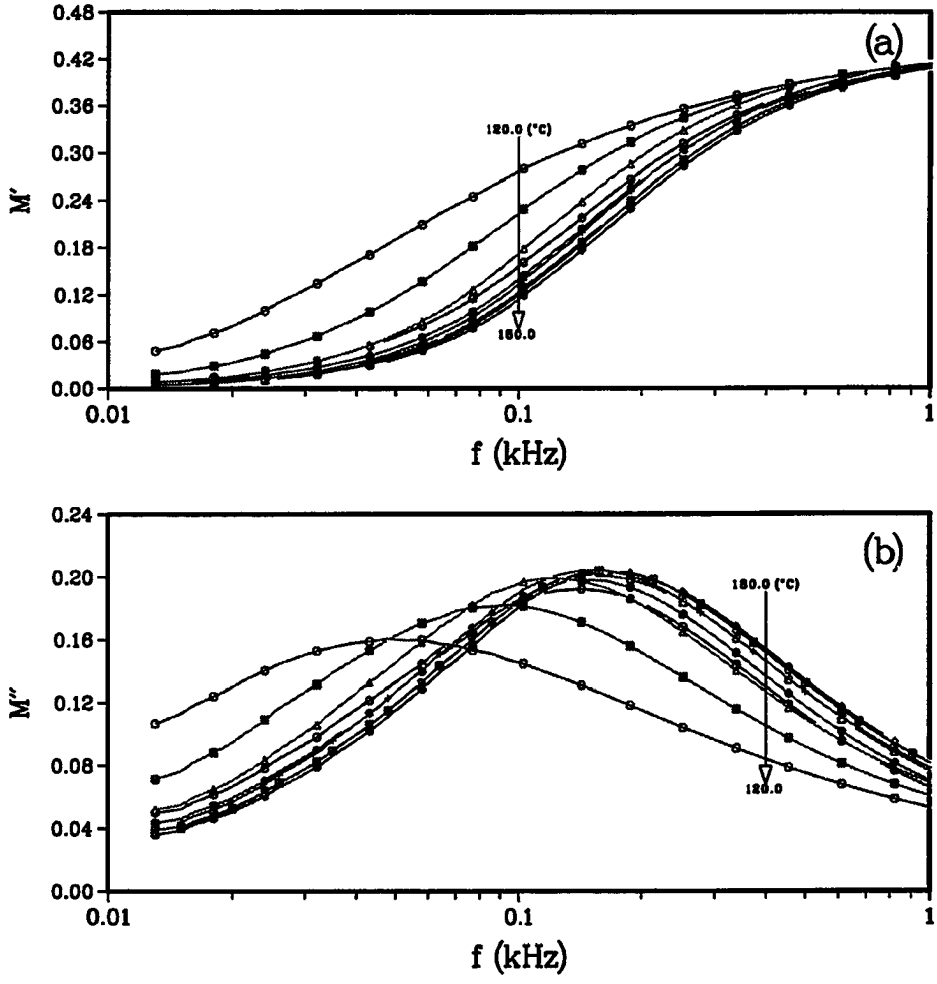

Figure 4.13: The spectra of (a) M' and (b) M'' against the frequency range of 0.01 to 1.0 kHz calculated over the temperature range of 120 to 180 °C for α'-relaxation of UDMA polymer with MC of 3.72 wt %.

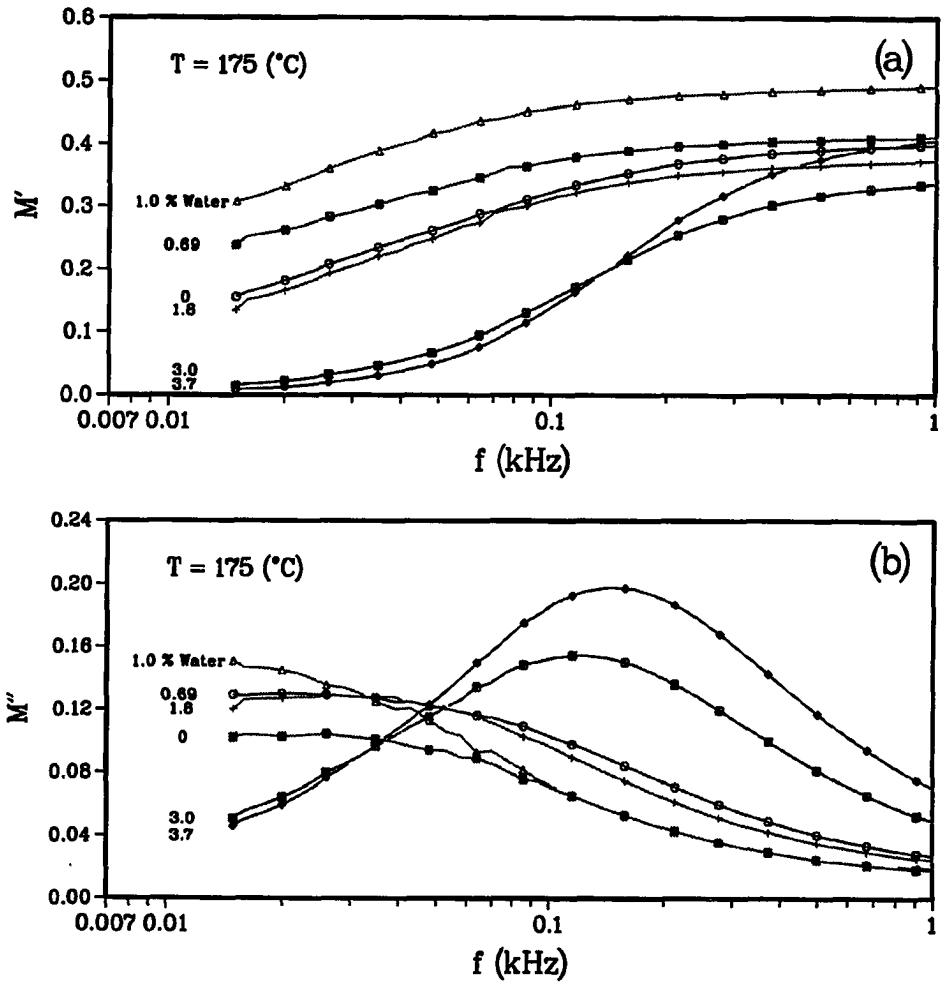

Figure 4.14: The spectra of (a) M' and (b) M'' calculated over the frequency range of 0.01 to 1.0 kHz and at 175 °C for α'-relaxation of UDMA polymer with MC of 0, 0.69, 1.0, 1.83, 3.0 and 3.72 wt %.

two subsections.

The effect of moisture on the β-relaxation

The maximum peaks of $\text{Tan}(\delta)_\epsilon$ shifted gradually to higher temperature with sorption of small amount of moisture until it reached a maximum temperature of -36.1 °C at MC of 0.69 wt % and 0.252 kHz. Then, it shifted to lower temperature rapidly to approach a limiting value of -81.8 °C at MC of 1.0 wt %. Further, the maximum peaks shifted again to higher values to reach a maximum temperature of -50.0 °C at MC of 3.72 wt %.

At low amounts of MC, the first shift of the peak to higher temperatures indicates that the mobility of the free amide groups is suppressed as a result of the moisture sorption in the lower range of MC $\leq$ 0.69 wt %. Such suppression of the free amide groups in the polymer network implies that the water molecules increased the number of intermolecular bonds in the polymer [81] by replacing the hydrogen bonds with water-amide hydrogen bonds [14]. A study of sorption and desorption isotherms of water in polyamides has revealed that water molecules form a H-bond between two CO groups (firmly bound water) and forms H-bonds between the CO and the NH groups (loosely bound water) [81]. Another study based on heat capacity measurements of water sorption in proteins has shown that the first water added interacts predominantly with ionizable groups and restores the normal pK order among groups perturbed strongly through dehydration [85]. Further, mechanical losses where the magnitude of the β-relaxation increased showed the stiffening effect of water in polyamides [55]. Therefore, it was concluded that the first amount of water added interacted with the CO groups to form firmly bound water that causes stiffening of the polymer network.

Subsequent sorption of moisture content caused more water molecules to break the hydrogen bonding existing in the polymer network, forcing the chains to large mutual distances and exerting its plasticizing effect. This results in an increase in the number of free amide groups and an increase in their mobility. Such an effect is observed by the shift of the β-relaxation peak to low temperatures in the medium range of MC $>$ 0.69 to $<$ 3.0 wt %. However, at high amounts of MC, the β-relaxation shifted to higher temperatures, which might be due to either higher density of packing or due to the motion of moisture itself or both. The increase in the density is due to the presence of hydrogen bound water molecules, which also hydrogen bond to the amide groups of the UDMA. Since in the absence of water molecules the steric hindrance of the hydrogen bonds prevent the molecules from packing as closely as they would if Van der Waals' forces were dominant. So bonded water molecules lower the number of interchain hydrogen bonds to allow the molecules to pack more closely, thus increasing the polymer density. The motion of moisture is due to frozen and clustered water that forms a supercooled liquid or ice [73]. The reason for the anticipation of the motion of ice or quasi-ice structure in UDMA with MC $>$ 1.83 wt % is because the peak maximum shifted to -40 °C at 1.0 kHz. At this temperature usually the emulsified water crystallizes to hexagonal ice at T $\leq$ -40 °C during cooling [73]. The validity of this anticipation along with the possibility of the higher density of packing at the high moisture content will be discussed below.

In general, the low frequency permittivity (ϵ_o) for the β-relaxation of the UDMA with the different moisture content increased with increasing temperature. For instance, the ϵ_o of the UDMA with MC of 0.69 wt % is between 1.542 and 1.651 and about 1.571 at -30 °C. The magnitude of the dielectric increment of the disper-

sion ($\Delta\epsilon$) is thus about 0.044, which is higher than the dielectric increment of the dried UDMA (Table 4.3). Such a higher value of $\Delta\epsilon$ for moistened UDMA with low amounts of water implies that the water molecules are attached strongly to the chain by hydrogen-bonding, so that they contribute to the polarization involved by moving the chains as they change their configuration and hence increase the dipole moment of the amide groups, thus creating strongly bound water. In addition, the $\Delta\epsilon$ for UDMA with the different moisture content increases rather rapidly and with the shift of the β-relaxation from -38.8 °C at 1.0 kHz for the dried UDMA polymer to -74.2 °C for the moistened UDMA with MC at 1.0 wt % and confirms the overcoming of interchain coupling, since water has spread more onto the surface of the polymer and plasticized it. Thus it forces the chains to go further apart and increased the average interchain distance between the H-bonded crosslinks. This situation will increase the number of free amides groups and increase their mobility [14]. Further, the $\Delta\epsilon$ for UDMA with the high MC $\geq$ 1.83 showed a new behavior with increasing temperature which is presented in Figure 4.15. The $\Delta\epsilon$ showed an increase followed by a temperature independent region. From this behavior it seems that a change which is thermodynamic in nature has occurred that disappears at low temperature.

To look into the temperature independence of the $\Delta\epsilon$ more closely, one would suspect that the thermodynamic change is a phase transition of the water molecule to crystal or supercooled liquid. Usually, if a micron-size droplets existed, one would observe a dispersion around -138 °C due to the T_g of a hyperquenched glassy water, and upon heating a second dispersion at -43 °C might appear due to water crystillization to ice [73]. The first dispersion is lacking in our measurements, while the later dispersion can be observed with MC > 1.83 wt %.

To examine the nature of the later dispersion one can look at the change in the

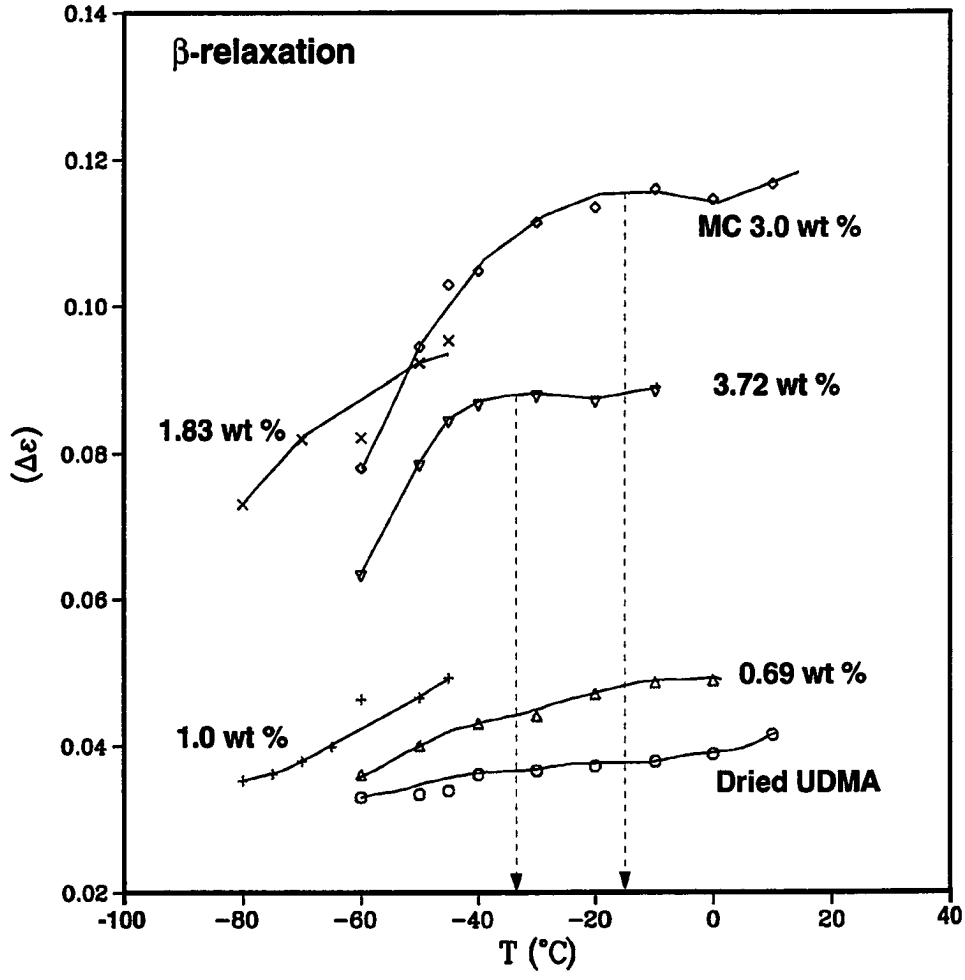

Figure 4.15: Dielectric increments of β—relaxations against temperature for UDMA polymer with MC of 0, 0.69, 1.0, 1.83, 3.0 and 3.72 wt %.

dielectric increment, ϵ_o and ϵ_∞ during the process, and compare them to those of ice clathrates. For instance, the $\Delta\epsilon$ increased rapidly and reached a limiting magnitude of 0.094 with MC of 3.72 wt % at -30 °C. This magnitude is more than twice the value of 0.038 measured for vacuum dried UDMA at the same temperature. A $\Delta\epsilon$ of about 40 would require that all the water in the material has crystallized to ice, for example, the dielectric increments for hexagonal ice and structural I and II clathrates hydrates at these temperature are about 117 [51] and 50 [74], respectively. Since the $\Delta\epsilon$ for moistened UDMA with MC of 3.72 wt % is much less than these values, one can assume that the water molecules in the H-bonded network have not crystallized to any phases of ice and they have much lower degree of rotational freedom. However, the dielectric increments as stated above (Figure 4.15) showed an independent temperature region at MC $>$ 1.83 wt % which is similar to a transition to a different structural state. This behavior implies slowness of the orientational correlation factor and the dielectric permittivity. Such behavior indicates the formation of disordered structures composed of monomers or dimers and/or the assembly of higher disordered nonfreezing clusters of water bonded to the amide groups which restricted their motion, although the amide groups of the UDMA are less restricted than those bonded by the tightly H-bound water molecules with the lowest moisture content.

The high frequency permittivity ϵ_∞ of 1.832 at -30 °C for high moisture content represents a combined magnitudes of the corresponding values of ϵ_∞ of the hydrogen-bonded water and of the UDMA network structures. The open H-bonded structures formed by the water molecules, have ϵ_∞ values much less than 3.0 and for the various phases of ice are between 3 and 3.6 [73]. Since ϵ_∞ of the UDMA at -30 °C is 1.546 which is 18.5 % lower than that of the moistened UDMA, it would seem that the

network structure of water in UDMA has started to form into fragments of small units of nonfreezing disordered water structures. In addition, The values of ϵ_o and ϵ_∞ for the $\alpha-$and $\beta-$processes provide an insight as to whether crystallization occurs in moistened UDMA. At -30 °C, ϵ_o is about 1.661 for the β-relaxation (Table 4.3 and Figure 4.6), while the α-relaxation has a value of about 2.14 at 175 °C. Since the ϵ_o of the β-relaxation increases slightly with increasing temperature and no other relaxation process was observed, one may compare these values and observe that they are continuous and no abrupt change in their values occurs. This implies that moistened UDMA does not undergo any phase transition in this relaxation. Therefore, this behavior along with the shifting of this region of change toward higher temperatures and the presence of abundant water molecules, might imply two mechanisms that are happening simultaneously. The first mechanism is that the water molecules tend to hydrogen bond with each other to form fragments of clusters of water molecules. These fragments lack freezing and crystallinity and bind to the amide groups to restrict their motion. The second mechanism is that the water molecules replace the hydrogen bonds existing between the amide groups thus lowering the number of interchain hydrogen bonds in the polymer to allow the molecules to pack more closely and increasing the polymer density.

Although the half-width ($\Delta_{1/2}$) of the β-process became narrower on the addition of small amount of moisture to the UDMA, the typical features of the half-width of the local mode motions persisted. That is the spectra broaden with decreasing temperature in the normalized loss factor plots against frequency as shown in Figures 4.16(a) and 4.16(b) and the heights of ϵ'' decreased as shown in Figures 4.4, 4.5 and 4.6. For instance, the half-width of the β-relaxation spectrum decreased from 4.38 decades for dried UDMA to 3.30 decades for UDMA with MC of 0.69 wt % at

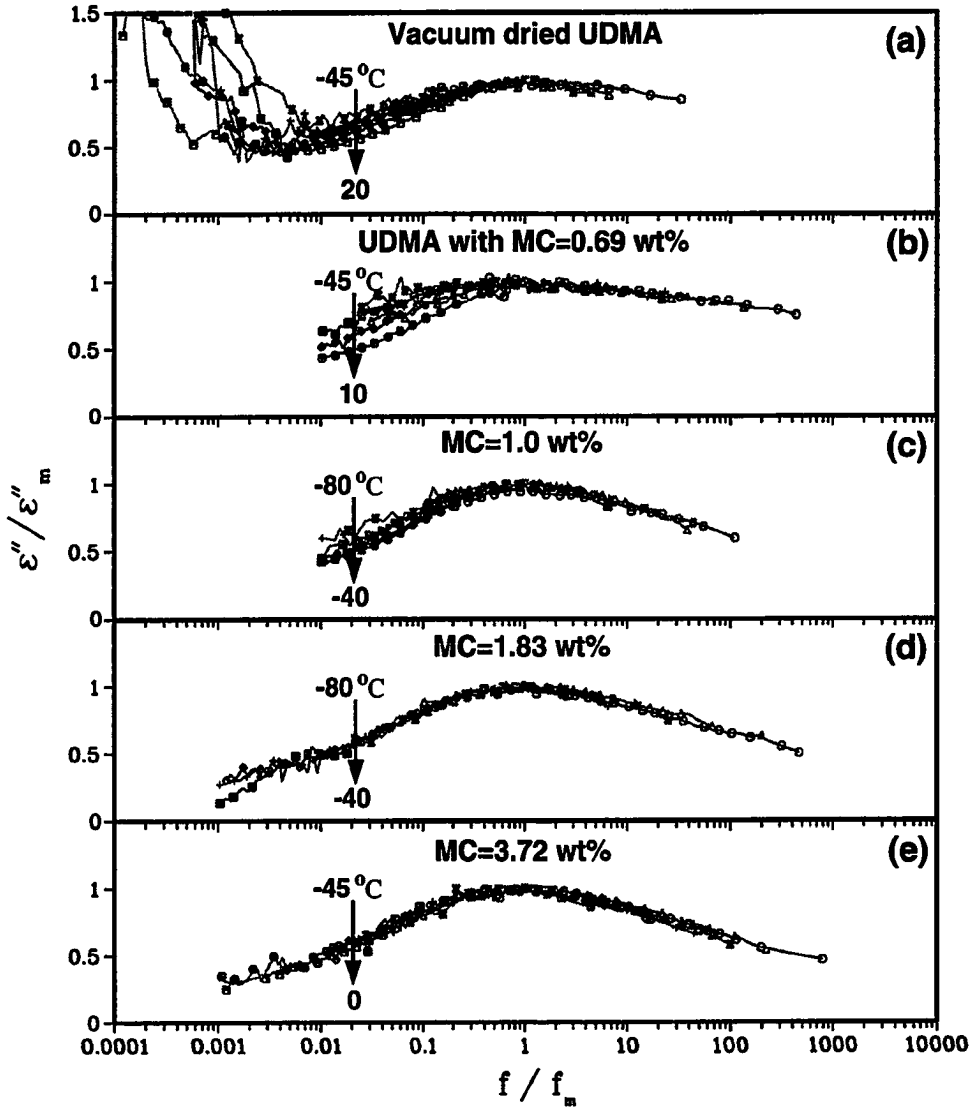

Figure 4.16: Normalized plots of the β-relaxation spectra over the temperature range of -80 to 20 °C for (a) vacuum dried UDMA, (b) 0.69 wt % moistened UDMA, (c) 1.0 wt % moistened UDMA, (d) 1.83 wt % moistened UDMA, and (e) 3.72 wt % moistened UDMA.

0 °C. This decrease in the half-width indicates that the mobility of the local chain motion is more restricted with the addition of small amount of moisture. Subsequent addition of moisture decreased the $\Delta_{1/2}$ to 3.32 decades for the UDMA with MC of 1.0 wt % at 0 °C and both the shape of the spectrum and the $\Delta_{1/2}$ became independent of temperature (Figure 4.16(c)). This feature differs from that of the β−relaxations normally observed in polymers as stated previously, which implies that the distribution of the dipolar environment is much smaller in the moistened UDMA than the dry UDMA. Finally, the $\Delta_{1/2}$ increased to a limiting value of 3.65 decades and kept its temperature independence for the UDMA with MC $\geq$ 3.0 wt % (Table 4.4, Figures 4.16(d) and 4.16(e)). This result is higher than the 1.5 decades observed for ice [74] and indicates the broadening of the distribution of the relaxation times due to different environments of water molecules. Also, it might contain the different distribution times due to differently plasticized local chains in the polymer network.

The intensity of $\mathrm{Tan}(\delta)_\epsilon(\lambda)$ of the β-relaxation peak at 0.252 represented in Table 4.4 increased on the addition of moisture to the UDMA. The λ of the β-relaxation increased by a factor of two, which means that an increase occurred in the total number of dipoles or in the dipole moment of molecules or both, that are involved in the process. Thus the moisture effect is dominated by the hydrogen bonds between the water molecules themselves and between the water molecules and the amino as well as the carbonyl groups in the UDMA.

The change in the apparent activation energy (ΔH) of the β-relaxation increased to higher values with the addition of a small amount of moisture. The ΔH increased from 7.5 kcal/mole for pure UDMA to 12.2 kcal/mole for UDMA with MC of 0.69 wt %. Such an increase further supports the increase in interchain coupling

and chain stiffening due to tightly bound hydrogen bonds that occur between the water molecules and the amide groups. The activation energy of the relaxation process decreased to lower values upon the further addition of water showing the ease of motions of the local chains due to the plasticization effect of water. Finally, the change in energy increased to a limiting value of 10.6 kcal/mole for the UDMA with MC $\geq$ 3.0 wt %. This increase in the values is due to the restriction of the motion of amide groups due to closely packed polymer and closely packed regions around the amide groups of the UDMA that are created by the hydrogen-bonded water molecules.

The effect of moisture on the α-relaxation

Since the α-relaxation is due to large segmental motion of the molecular chains in the UDMA polymer, their loosening or stiffening controls the orientation of the amide groups. Logically, the effect of moisture on these large segments should correlate with those of the $\beta-$relaxations. Therefore, the effect of moisture on the dielectric parameters of the α-relaxation for UDMA, that was measured and calculated, will be discussed in terms of the relationship to the orientation of the amide groups in the following paragraphs. Further, the effect of moisture content $\geq$ 3.0 wt % on the dielectric parameters of the α-relaxation could not be resolved due to its obstruction by the appearance of a new peak, whose origin will also be discussed in the following paragraphs.

The main feature of the effect of moisture on the dielectric spectrum was the occurrence of a new separate loss peak that obstructed the observation of the α-relaxation (Figure 4.1). This loss peak started to manifest itself in the low frequency and high temperature region for the moistened UDMA with MC $\geq$ 1.83 wt % (Figures 4.12 and 4.13) and developed completely for the UDMA with MC $\geq$ 3.0 wt %

(Figures 4.13 and 4.14). For instance, the peak maximum occurred at 0.143 kHz and 175 °C for the moistened UDMA with MC 3.72 wt %. This loss peak was attributed to the interfacial or MWS polarization, which is developed due to charge mobility at the interface between the polymer and water inclusions. This peak only developed after the formation of a certain size of water droplets that are not stabilized yet by hydrated polar groups. These water droplets started to form an interphasal hydrated structures on the amide groups of the UDMA and developed an interfacial monolayers of surface active agents. This same interfacial monolayer, that is composed of hydrated water molecules that are hydrogen bonded to each other and to the amide groups, caused the restriction of the motion of the amide groups as was discussed previously.

To look at the characteristics of the MWS polarization (α'), the relevant measured and calculated parameters will be examined. These parameters are $\Delta\epsilon$, half-width, activation energy, and pre-exponential factors. For instance, the $\Delta\epsilon$ values for this relaxation have a maximum when plotted against temperature in the region of the relaxation as is shown in Figure 4.17. The peak maximum of the $\Delta\epsilon$ for the UDMA with MC of 3.0 wt % appeared at 170 °C, while it appeared at 160 °C for the UDMA with MC of 3.72 wt %. This means that the maximum peaks of the loss should appear at higher frequency for the MC of 3.72 wt % and lower frequency for the MC of 3.0 wt %, which is consistent with the results in Figure 4.14. The peak of the $\Delta\epsilon$ for the moistened UDMA with temperature might be explained by an ordering and disordering mechanism of the dipole arrangements of the hydrated structures on the amide groups are similar to those that occur in the glass transition region [9, 47]. That is, since the application of the electric field reduces the disorder of the dipole by aligning it with the field, which in the absence of a field would be

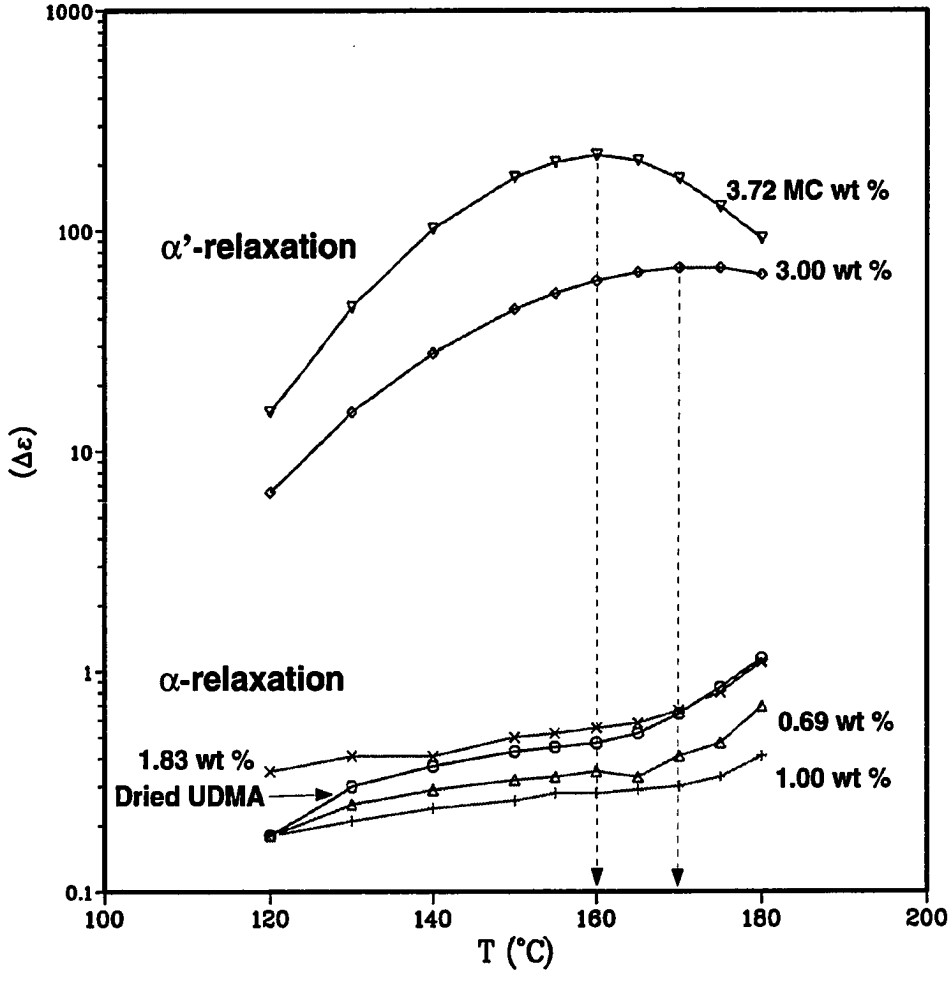

Figure 4.17: Dielectric increments of $\alpha-$ and $\alpha'-$relaxations against temperature for UDMA with MC of 0, 0.69, 1.0, 1.83, 3.0 and 3.72 wt %.

at random, it decreases the configuration entropy of the system. However, increasing the temperature before reaching the $\Delta\epsilon$ peak maximum would increase the configuration entropy and the disorder of the dipole arrangement with the electric field in the system, until the field has no effect on the entropy and the peak maximum isreached. Upon further increasing the temperature, the field starts to decrease the entropy by orienting some of the dipole. Further, the $\Delta\epsilon$ values for this relaxation increased with moisture content. The values were very high and they almost double from 70.46 for the UDMA with MC 3.0 wt % to 120.10 with MC of 3.72 wt %. Such high values are due to high mobility and high deformation of the dispersed water droplets. The difference in the $\Delta\epsilon$ values between 3.0 wt % and 3.72 wt % moistened UDMA is due probably to the size of the dispersed water droplets.

The half-width of this relaxation decreased with the increase in moisture content and reached a limiting value of 1.26 decades for the UDMA with MC of 3.72 wt % (Table 4.4). This value is higher than the value of 1.14 decades for the single relaxation behavior. This observation suggests that some distribution of relaxation times may be found due to non-uniformity of conductivity of the hydrated structures on the amide groups. In addition, the activation energy values were reduced with the increase in moisture content of the UDMA and reached a limiting value of 8.0 kcal/mole (Table 4.2).

The glass transition temperature (T_g) of the α-relaxation was affected slightly with the addition of small amount of moisture to the UDMA (Table 4.1 and Figure 4.1). However, the T_g decreased severely with high moisture content, and it decreased from 156.4 °C for the dried UDMA to 136.5 for the UDMA with MC of 3.0 wt %. This effect has been interpreted to be an increase in the free volume with increasing temperature and the consequent loosening of the interchain and/or

intrasegmental motion as reported by Chan *et al.* [19], thus plasticizing the polymer and increasing the number of the free amide groups.

In general, the dielectric increment of the glass transition region reaches a maximum value when plotted against temperature [9, 47]. The $\Delta\epsilon$ in UDMA, however, increased slightly with temperature as is shown in Figure 4.17 after a temperature independence region. This temperature independence region is equivalent to the onset of the maximum with increasing temperature, which could not be resolved probably due to the inaccuracy of determining $\Delta\epsilon$. This inaccurate determination is due to the obstruction of the α-relaxation by the DC conductivity. Although such behavior persisted for the moistened UDMA, the $\Delta\epsilon$ values decreased with small amount of moisture content and then increased with higher amount (Table 4.3). On one hand, the decrease in the $\Delta\epsilon$ values along with the change of the T_g values (Table 4.1) for the UDMA with low MC confirms that the stiffening of the main chains had occurred which is due to the tightly bound water molecules to the amide groups, thus decreasing the dipole moment of the chains. On the other hand, the increase in the $\Delta\epsilon$ values for the UDMA with high MC indicates that the water molecules attached to the chain through hydrogen bonding at the amide groups are contributing to the polarization.

The relaxation spectrum of the α-process became broader and the intensity of the $\mathrm{Tan}(\delta)_\epsilon$ increased on the addition of water to the UDMA as shown in Figure 4.18. The half-width and the intensity of the α-relaxation spectrum increased from 2.94 decades and 0.016, respectively, for the dried UDMA to 3.82 decades and 0.022 for the UDMA with MC of 1.0 wt %. These results suggest the broadening of the distribution of relaxation times and the increase in the dipole moments due to the polymer chains or the water molecules.

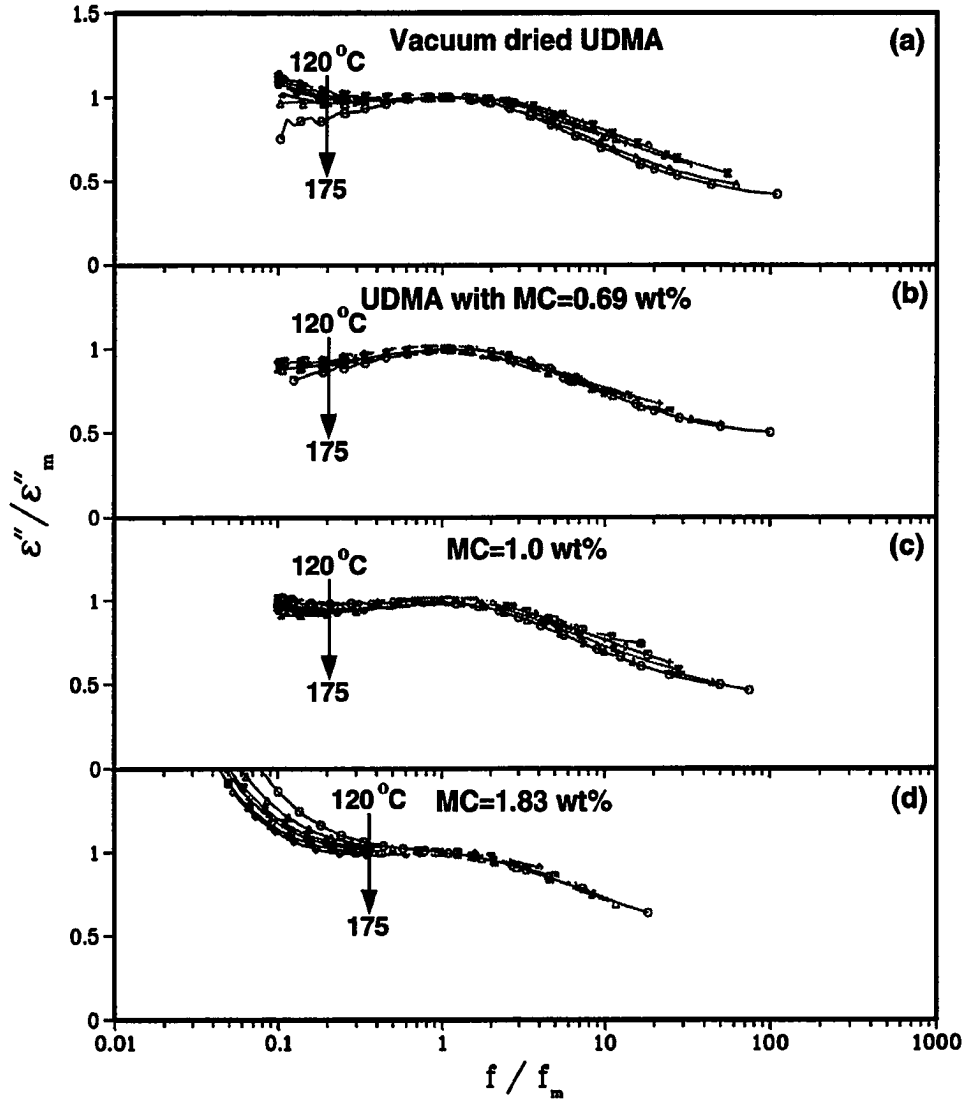

Figure 4.18: Normalized plots of the α-relaxation spectra over the temperature range of 120 to 175 °C for (a) vacuum dried UDMA, (b) 0.69 wt % moistened UDMA, (c) 1.0 wt % moistened UDMA, and (d) 1.83 wt % moistened UDMA.

However, the normalized loss against frequency plots of water-UDMA mixtures in Figure 4.18 show that the half-width of the α-relaxation remain nearly constant with changing temperature.

Finally, the moisture has a strong plasticizing action as evidenced by the reduction in the activation energy (Table 4.2). The reduction of the activation energy was highly noticed with the introduction of large amounts of moisture. The plasticization may be due to two effects, the reduction of interchain bonding by the replacement of amide-amide hydrogen bonds and increasing the mobility of the segmental chains by dilution.

In summary, moisture first sorbed in UDMA forms tightly bound water molecules by replacing the hydrogen bonds existing in the network with water-amide hydrogen bonds thus increasing the number of intermolecular bonds causing an overall stiffening of the polymer. Subsequent moisture sorption causes massive breaking of hydrogen bonding of the network allowing a drastic loosening of the chains and an overall plasticization effect. Further moisture sorption causes water molecules to hydrogen bind to each other forming clusters and fragments that bind to the amide groups thus restricting their motion and creating an interphasal layer with unbalanced surface active agents.

4.3.2 The Effect of Moisture on the Dielectric Behavior of ZS-Filled UDMA

The dielectric loss tangent ($\mathrm{Tan}(\delta)_\epsilon$) for the 75 wt % ZS-filled UDMA with MC of 0, 2.5, 4.0, 6.0 and 7.32 wt % measured at 0.020 kHz are plotted against temperature in Figure 4.19. The $\mathrm{Tan}(\delta)_\epsilon$ curves show almost the same behavior as those shown by the UDMA polymer, namely a sub-T_g or β-relaxation peak, an α-relaxation peak and a substantial increase at high temperature. The increase of the $\mathrm{Tan}(\delta)_\epsilon$ values

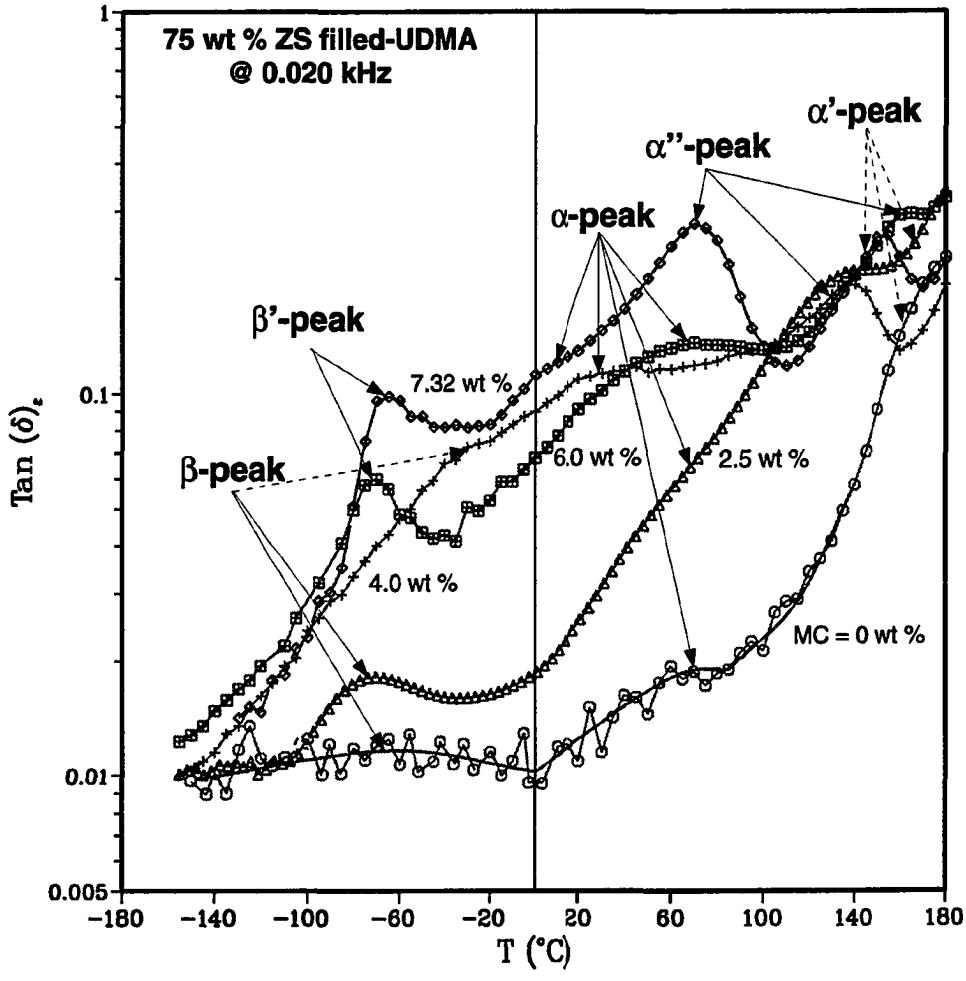

Figure 4.19: Tan$(\delta)_\epsilon$ against temperature measured at 0.020 kHz for 75 wt % zirconia-silica-filled UDMA polymer with MC of 0, 2.5, 4.0, 6.0 and 7.32 wt %.

at high temperature are due to proton transfer and interfacial polarization, which were shown clearly at the low amount of moisture content (MC = 2.5 wt %). The curves also show that the α-relaxation was obstructed by a new peak (α'') which appeared as shoulder. For example, the α-peak appeared at 70 and 20 °C with MC of 6.0 and 7.32 wt %, respectively, and it disappeared completely with MC > 2.5 wt % at high frequencies. The new peak appeared clearly for the composite with MC $\geq$ 4.0 wt %. The maximum of the $\alpha-$ and $\beta-$peaks obtained from the Tan$(\delta)_\epsilon$ curves measured at different frequencies are shown in Table 4.5. Figure 4.19 and Table 4.5 show the α-relaxation is shifted to lower temperatures due plasticization effect of the moisture, while its intensity increased. The curves also show the β-relaxation is shifted to higher temperatures with MC $\geq$ 2.5 wt %, while it shifted back to lower temperatures with MC of 6.0 wt %. Finally, the relaxation started to shift slightly to higher temperatures with MC > 6.0 wt %.

To enhance the appearance of the β-relaxation , M' and M'' was calculated by Equations (3.5) and (3.6) for moistened 75 wt % ZS-filled UDMA. The isothermal curves for M' and M'' at several temperatures for the moistened UDMA composite with MC of 2.5 and 7.32 wt % are shown in Figures 4.20 and 4.21, respectively. These plots suggest the persistence of the sub-T_g segmental mobility of the UDMA, which was assigned earlier in the previous chapter to the mobility of the free amide groups. Like the pure UDMA, the feature of this relaxation shows similar behavior to those of the typical local mode motions in polymers and molecular glasses with low moisture content (MC $\leq$ 4.0 wt %). Namely, as discussed above, there is an increase in the height of the M'' peak by 31.5 % over the temperature range of -45 to 20 °C, a decrease in the half-width and an Arrhenius dependence of the rate on temperature with relatively low activation energy as in Table 4.6. Unlike the pure

MC wt %	Maximum peaks temperature (°C)					
	α-relaxation			β-relaxation		
	0.5 (kHz)	5.5 (kHz)	10.0 (kHz)	0.252 (kHz)	1.0 (kHz)	10.0 (kHz)
0.0	—	164.9	165.9	-69.1	-43.3	—
2.5	122.8	140.0	155.0	-50.0	-40.0	10.0
4.0	—	—	—	10.0	20.0	—
6.0	115.0	—	—	-62.5	-55.0	-45.0
7.32	70.0	—	—	-52.5	-45.0	-30.0

Table 4.5: Maximum peaks temperatures (°C) from $\mathrm{Tan}(\delta)_\epsilon$ measurements for different moisture content in 75 wt % zirconia-silica-filled UDMA for $\alpha-$relaxations at 0.5, 5.5 and 10.0 kHz and for $\beta-$relaxations at 0.252, 1.0 and 10.0 kHz.

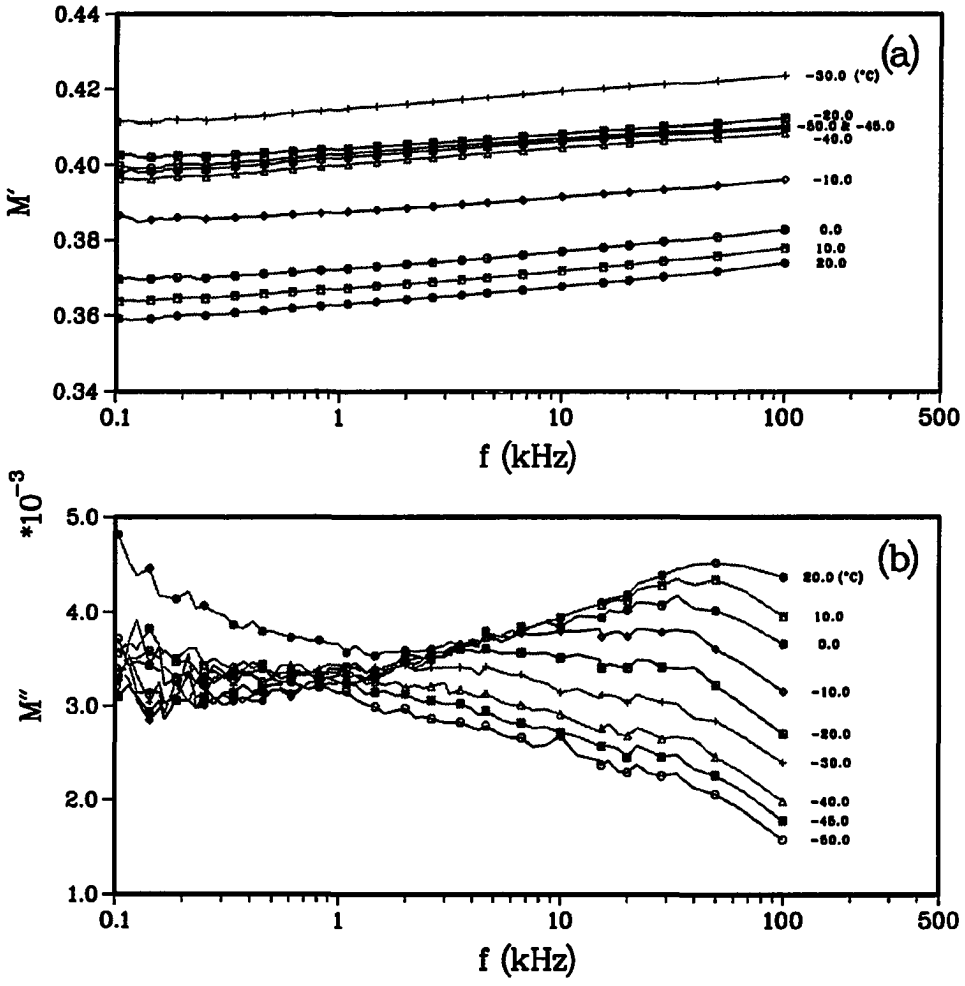

Figure 4.20: The frequency dependence of (a) M' and (b) M'' calculated over the temperature range of -50 to 20 °C for β-relaxation of 75 wt % zirconia-silica-filled UDMA with MC of 2.5 wt %.

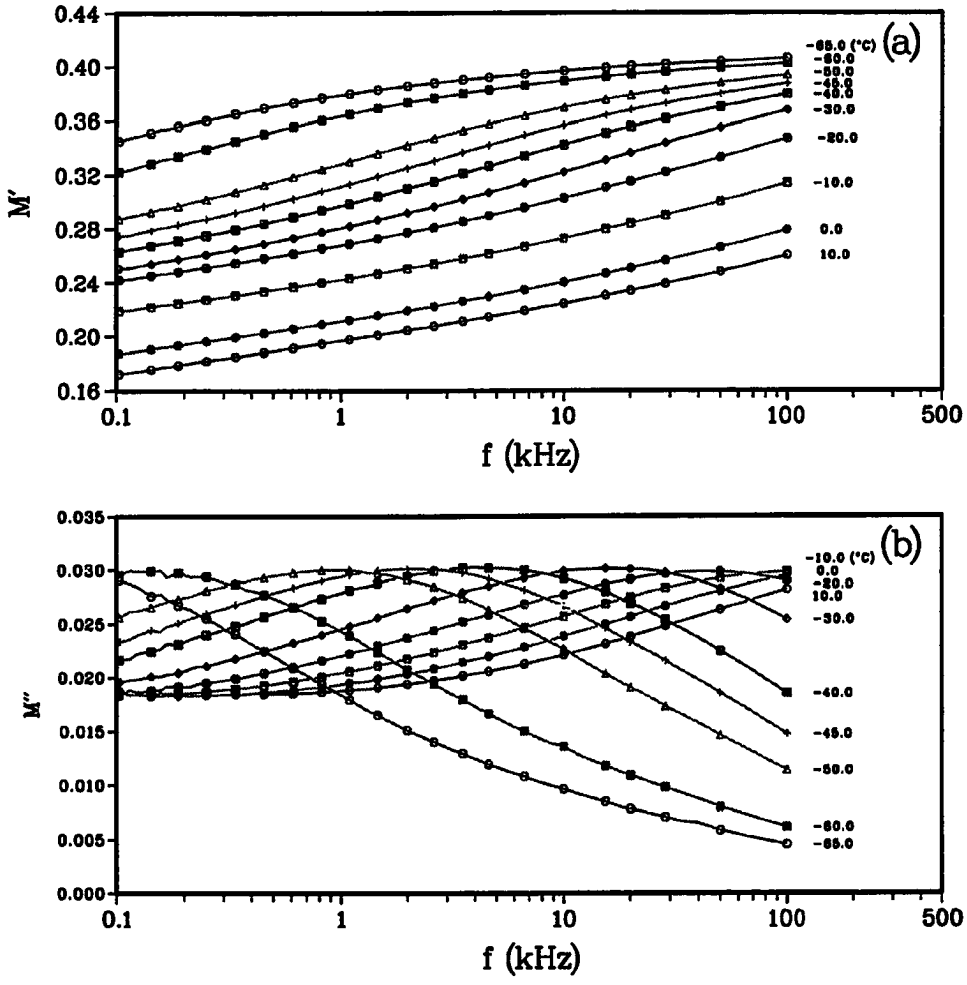

Figure 4.21: The frequency dependence of (a) M' and (b) M'' calculated over the temperature range of -65 to 10 °C for β'-relaxation of 75 wt % zirconia-silica-filled UDMA with MC of 7.32 wt %.

MC wt %	α-relaxation		β-relaxation	
	ΔH $\left(\frac{kcal}{mole}\right)$	τ_o (Hz)	ΔH $\left(\frac{kcal}{mole}\right)$	τ_o (Hz)
0.0	49.9	$4.6 * 10^{-31}$	6.7	$3.0 * 10^{-11}$
2.5	27.4	$1.9 * 10^{-20}$	6.9	$1.4 * 10^{-11}$
4.0	16.4	$5.2 * 10^{-14}$	15.9	$3.2 * 10^{-17}$
6.0	21.7	$5.4 * 10^{-18}$	19.6	$6.7 * 10^{-16}$
7.32	17.4	$1.3 * 10^{-14}$	17.9	$2.0 * 10^{-22}$

Table 4.6: Activation energies and pre-exponential coefficients for $\alpha-$ and $\beta-$dielectric relaxation processes as a function of moisture content (wt %) in 75 wt % zirconia-silica-filled UDMA.

UDMA, this feature did not persist with high moisture content (MC $\geq$ 6.0 wt %). For example, the height of M'' decreased by 4.4 % over the temperature range of -60 to 0 °C with MC 7.32 wt %. To distinguish this peak from the regular sub-T_g peaks, this peak will be called $\beta'-$ for the 75 wt % ZS-filled UDMA with MC of $\geq$ 6.0. To compare the effect of moisture content on the amide group mobility, isothermal spectra of M' and M'' at -45 °C for 75 wt % ZS-filled UDMA with MC of 0, 2.5, 4.0, 6.0 and 7.32 wt % are plotted in Figure 4.22. The M'' peaks for the different amount of moisture in this figure show similar trends to those of the UDMA polymer. Namely, the β-relaxation increased in intensity and shifted toward lower frequencies (i.e higher temperatures) with MC $\geq$ 2.5 wt %, then it shifted to higher frequencies (i.e lower temperatures) with MC $\geq$ 6.0 wt %. Finally, the β-relaxation shifted to lower frequencies with MC $\geq$ 7.32 wt %.

To look at the effect of moisture content on the α-peak more closely, the isothermal spectra of of M' and M'' at several high temperatures for 75 wt % ZS-filled UDMA with MC of 2.5 and 7.32 wt % are plotted in Figures 4.23 and 4.24, respectively. In addition, the M' and M'' for the α-relaxation at medium range temperature (20 - 120°C) and low frequencies for the filled-UDMA with MC of 6.0 and 7.32 wt % are plotted in Figures 4.25 and 4.26, respectively. These figures show two important features due to moisture effect. The first feature is the plasticization effect of the moisture, where the T_g decreased drastically from about 60 to 20 °C at 0.020 kHz. The second feature is the accumulation of the moisture at the interface, where it continues to disappear at higher temperatures as is shown in Figures 4.27 - 4.29.

The properties ϵ_∞, ϵ_o and $\Delta\epsilon$ for $\beta-$and $\alpha-$processes as a function of moisture content are presented in Table 4.7, while the values of λ of $\mathrm{Tan}(\delta)_\epsilon$ and $\Delta_{1/2}$ are shown in Table 4.8.

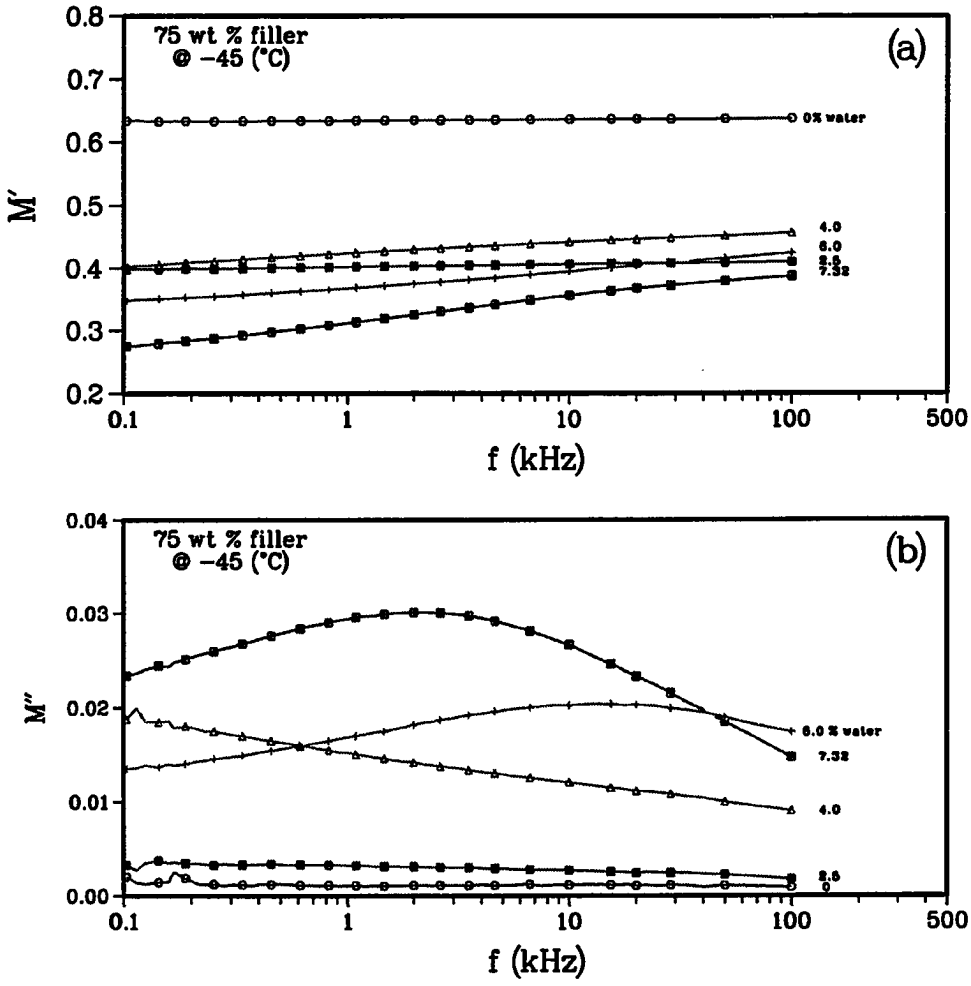

Figure 4.22: The frequency dependence of (a) M' and (b) M'' calculated at -45 °C for $\beta-$ and $\beta'-$ relaxations of 75 wt % zirconia-silica-filled UDMA with MC of 0, 2.5, 4.0, 6.0 and 7.32 wt %.

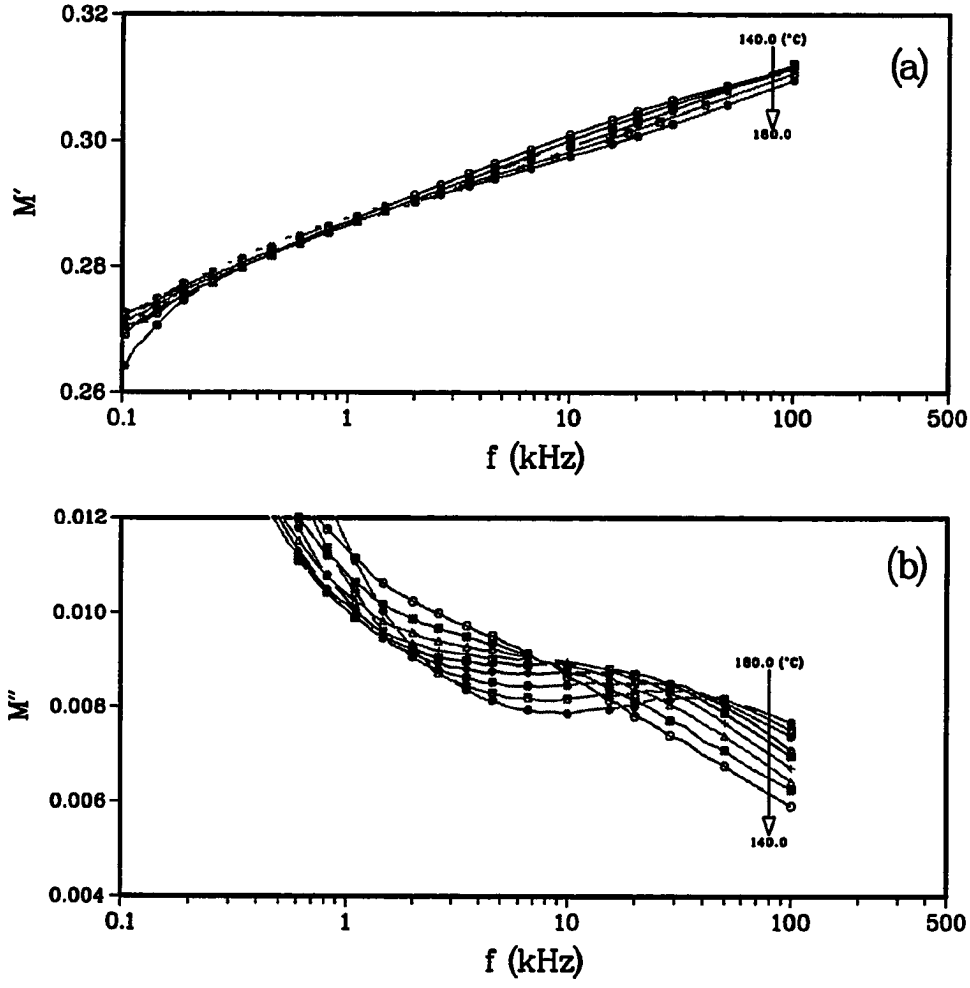

Figure 4.23: The frequency dependence of (a) M' and (b) M'' calculated over the temperature range of 140 to 180 °C for α-relaxation of 75 wt % zirconia-silica-filled UDMA with MC of 2.5 wt %.

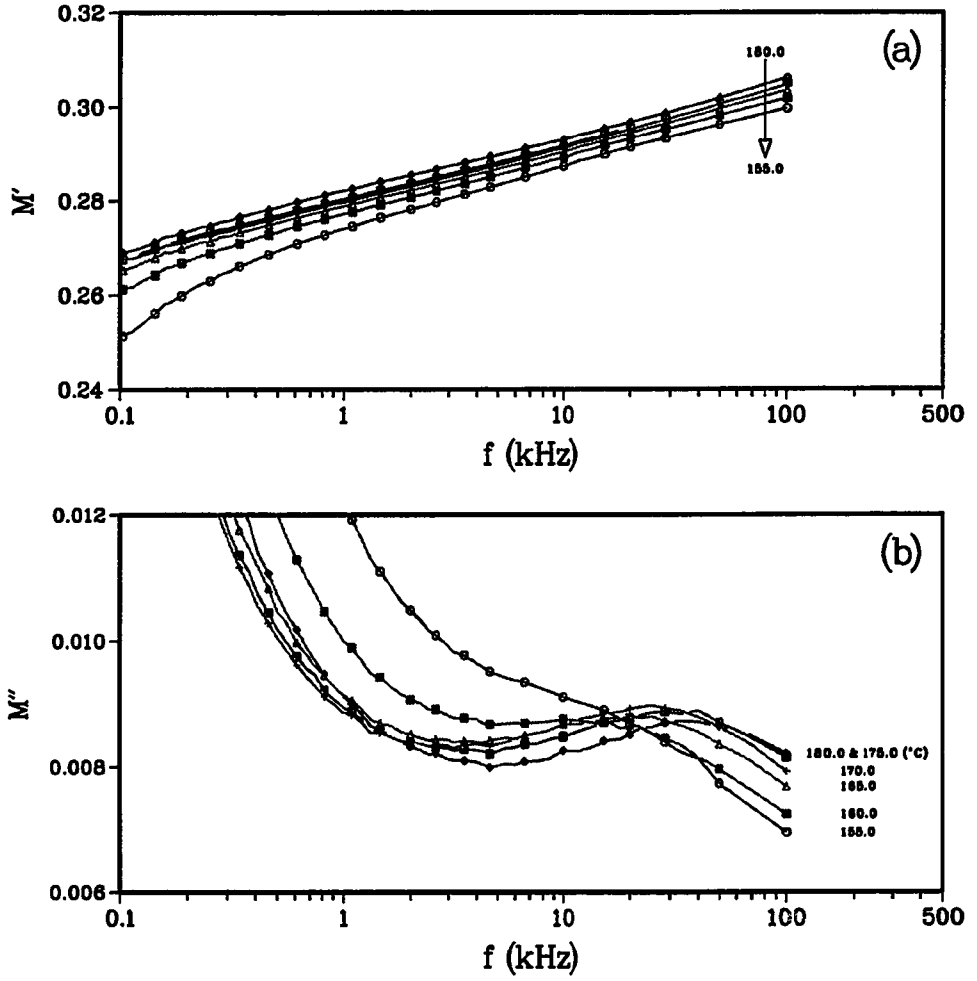

Figure 4.24: The frequency dependence of (a) M' and (b) M'' calculated over the temperature range of 155 to 180 °C for α-relaxation of 75 wt % zirconia-silica-filled UDMA with MC of 7.32 wt %.

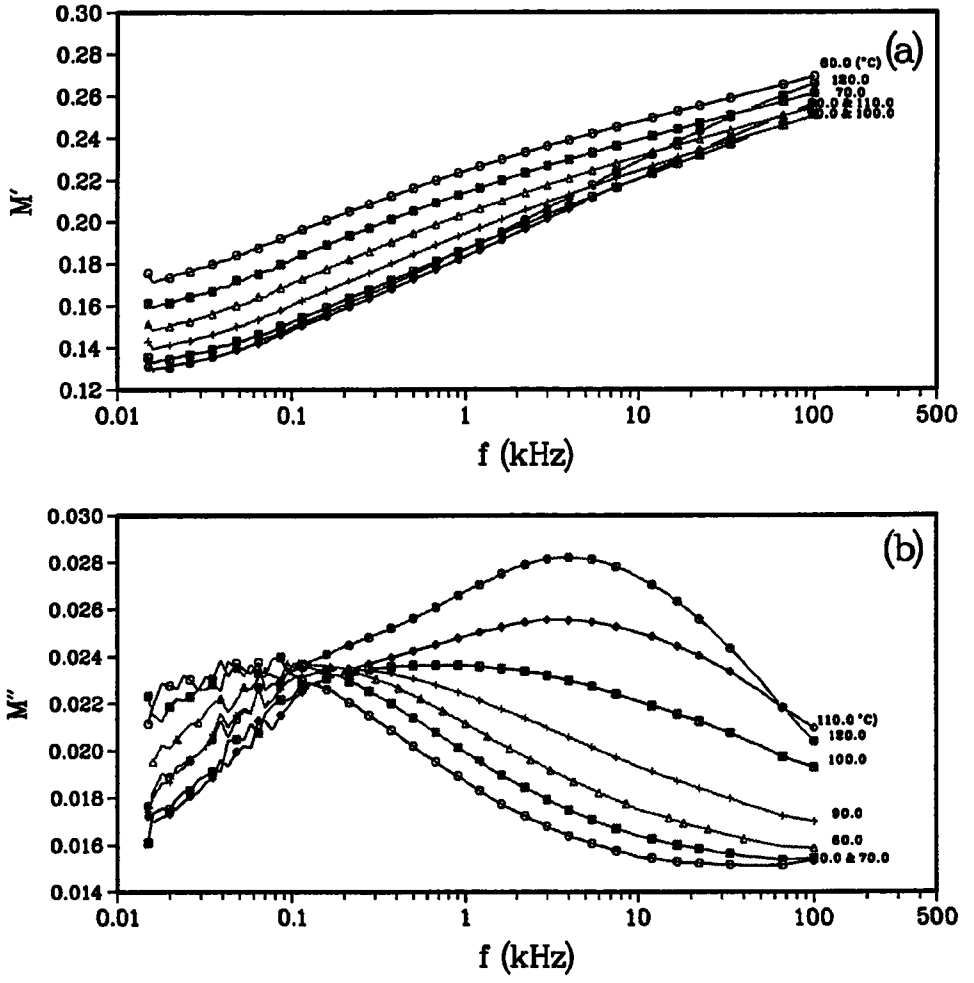

Figure 4.25: The frequency dependence of (a) M' and (b) M'' calculated over the temperature range of 60 to 120 °C for α-relaxation of 75 wt % zirconia-silica-filled UDMA with MC of 6.0 wt %.

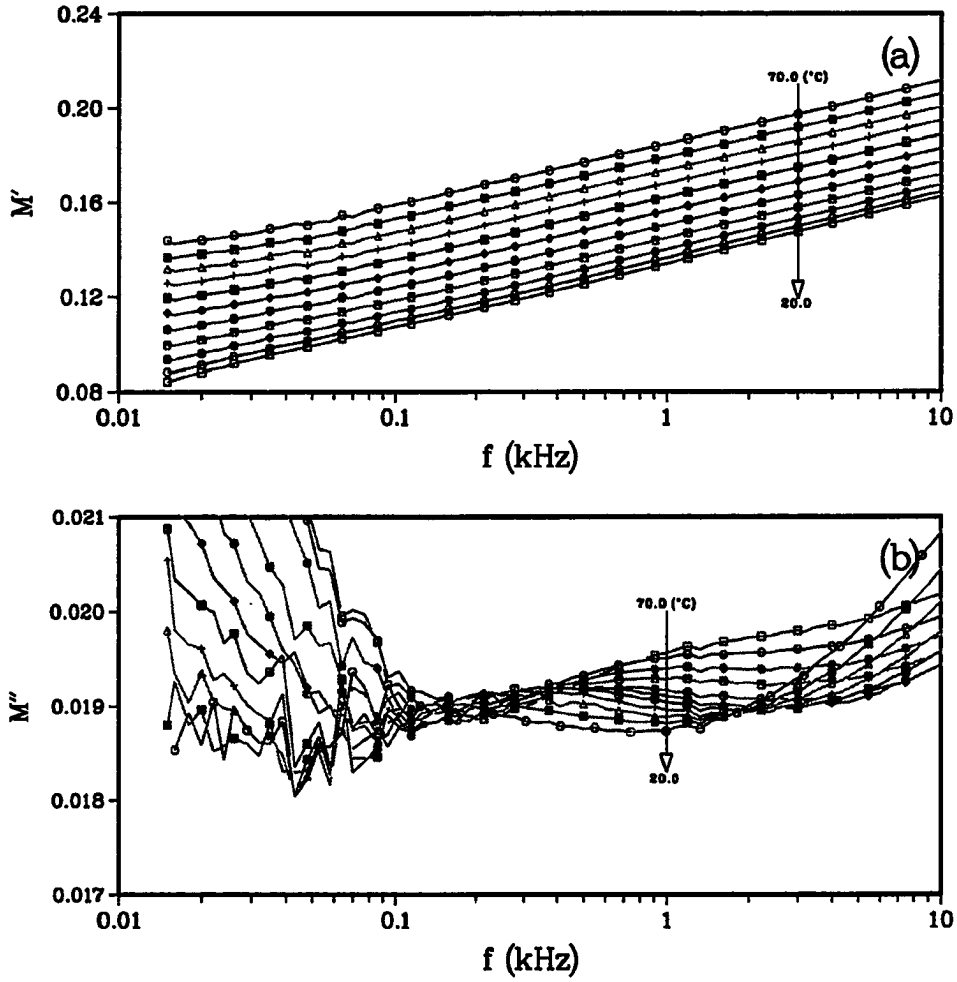

Figure 4.26: The frequency dependence of (a) M' and (b) M'' calculated over the temperature range of 20 to 70 °C for α-relaxation of 75 wt % zirconia-silica-filled UDMA with MC of 7.32 wt %.

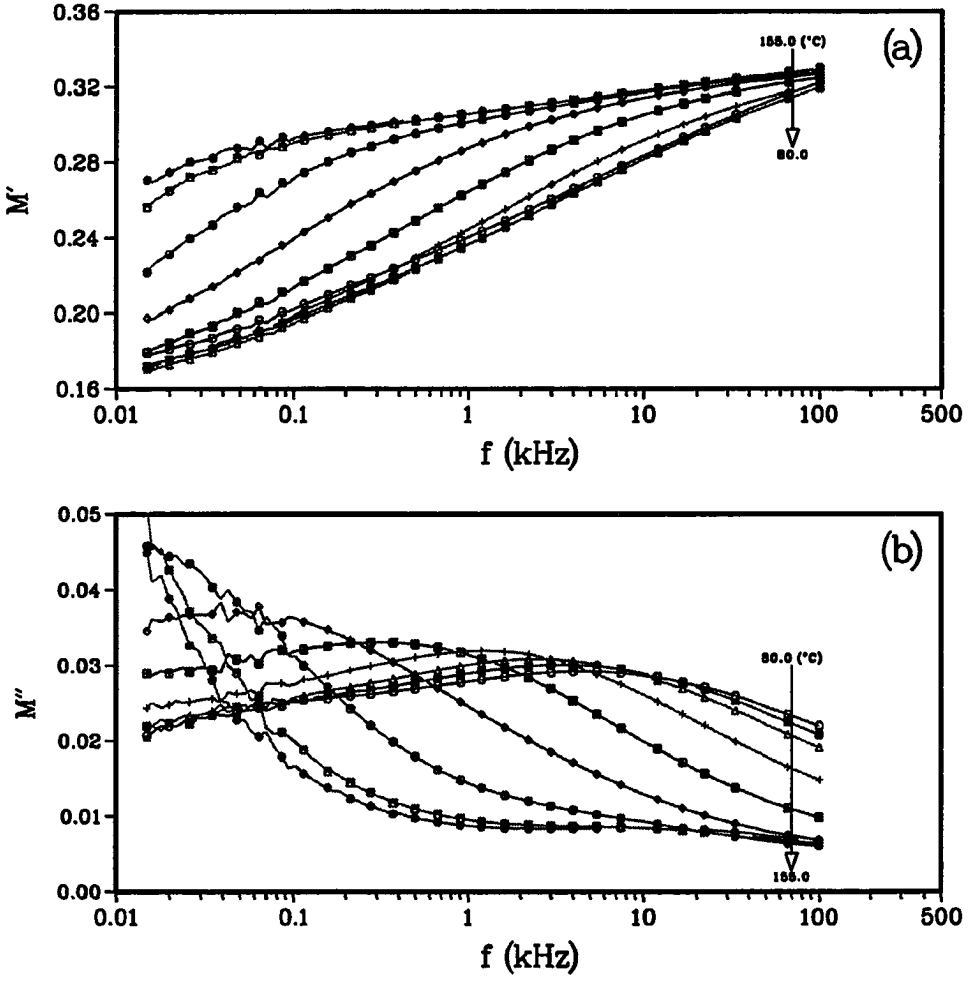

Figure 4.27: The frequency dependence of (a) M' and (b) M'' calculated over the temperature range of 80 to 155 °C for α''-relaxation of 75 wt % zirconia-silica-filled UDMA with MC of 4.0 wt %.

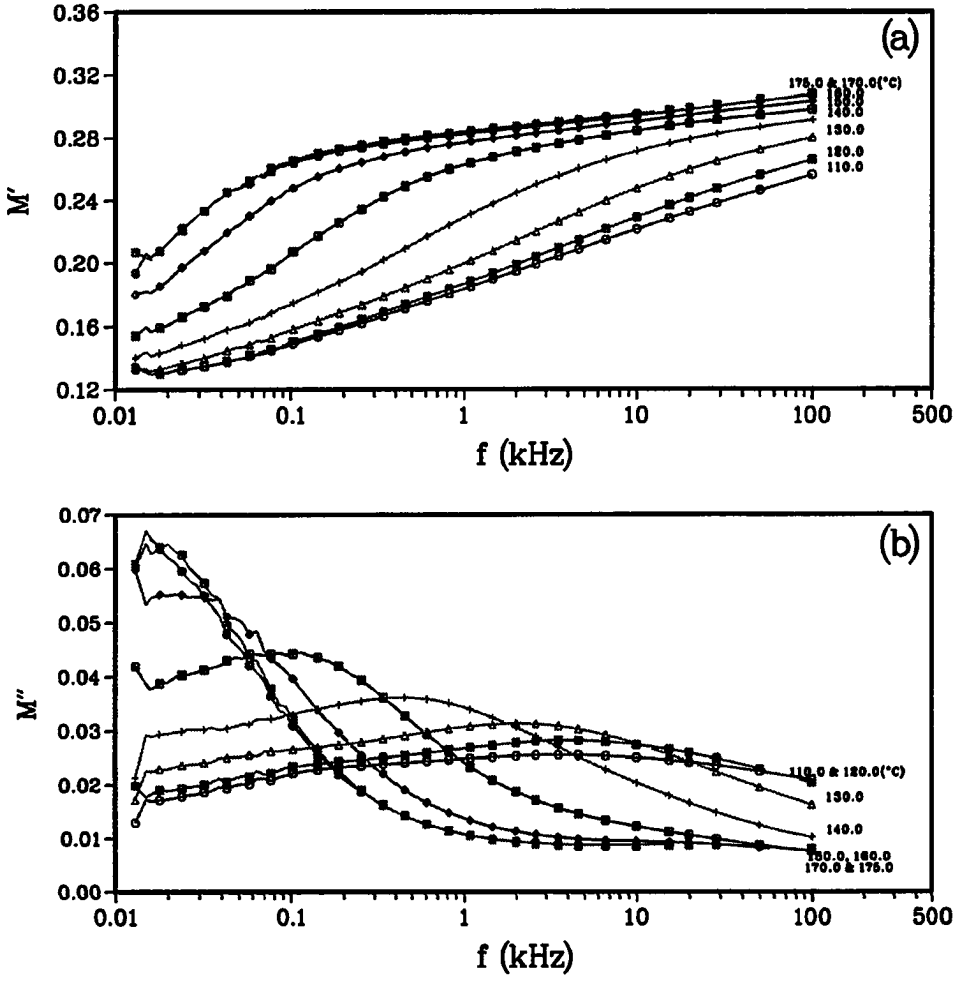

Figure 4.28: The frequency dependence of (a) M' and (b) M'' calculated over the temperature range of 110 to 175 °C for α''-relaxation of 75 wt % zirconia-silica-filled UDMA with MC of 6.0 wt %.

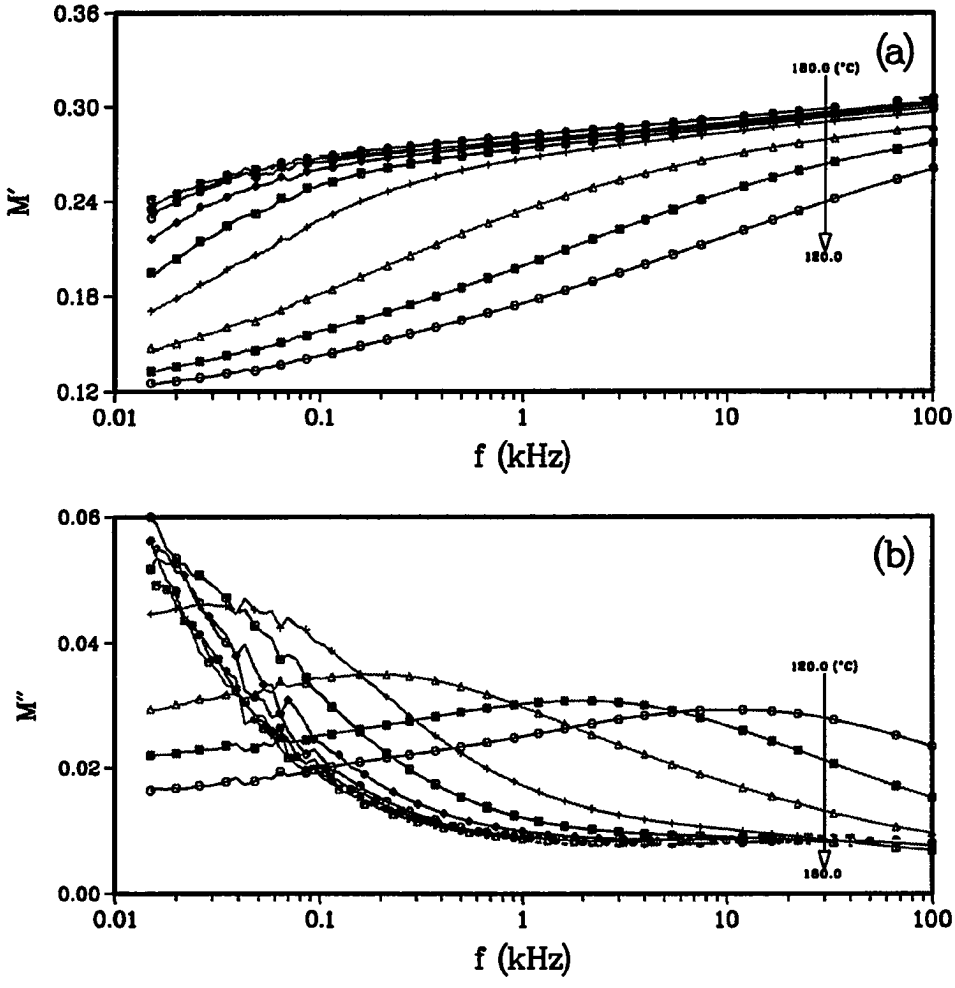

Figure 4.29: The frequency dependence of (a) M' and (b) M'' calculated over the temperature range of 120 to 180 °C for α''-relaxation of 75 wt % zirconia-silica-filled UDMA with MC of 7.32 wt %.

MC wt %	α-relaxation			β-relaxation		
	ϵ_o	ϵ_∞	$\Delta\epsilon$	ϵ_o	ϵ_∞	$\Delta\epsilon$
0.0	3.033	2.715	0.318	1.810	1.795	0.015
2.5	3.744	3.219	0.525	2.431	2.361	0.071
4.0	3.427	3.039	0.387	2.604	2.193	0.411
6.0	3.767	3.242	0.525	3.064	2.533	0.508
7.32	3.738	3.278	0.460	3.988	2.730	1.268

Table 4.7: Low (ϵ_o) and high (ϵ_∞) frequency limiting values of ϵ' as well as dielectric increments ($\Delta\epsilon$) for $\alpha-$ and $\beta-$relaxations at 175 and -30 °C as a function of moisture content (wt %) in 75 wt % zirconia-silica-filled UDMA.

	α-relaxation		β-relaxation		α'-relaxation
MC	λ	$\Delta_{1/2}$	λ	$\Delta_{1/2}$	$\Delta_{1/2}$
wt %	0.252 (kHz)	165 (°C)	0.252 (kHz)	-45 (°C)	135 (°C)
0.0	0.0146	4.40[a]	0.0024	3.10	1.47[b]
2.5	0.0625	3.40	0.0083	5.11	1.61[c]
4.0	—	3.78	—	6.48[d]	2.74
6.0	0.1413	4.72	0.0514	4.19[e]	3.31
7.32	0.1613	—	0.0931	3.31[f]	3.56

[a] $\Delta_{1/2}$ for α-peak at 140 °C
[b] $\Delta_{1/2}$ for α'-peak at 180 °C
[c] $\Delta_{1/2}$ for α'-peak at 180 °C
[d] $\Delta_{1/2}$ for β-peak at -10 °C
[e] $\Delta_{1/2}$ for β'-peak at -45 °C
[f] $\Delta_{1/2}$ for β'-peak at -45 °C

Table 4.8: Intensities (λ) of $\mathrm{Tan}(\delta)_\epsilon$ at 0.252 kHz and half-widths of $\epsilon''(\Delta_{1/2})$ (decades) for $\alpha-$, $\beta-$ and α' -relaxations at 165, -45 and 135 °C, respectively, as a function of moisture content (wt %) in 75 wt % zirconia-silica-filled UDMA.

Further, the activation energies and pre-exponential factors calculated from the slopes and intercepts of plots of frequencies at which the $\text{Tan}(\delta)_\epsilon$ maximum peaks appeared for $\beta-$and $\alpha-$processes against the reciprocal temperatures are listed in Table 4.6.

The effect of moisture on the β-relaxation

At low moisture content, the results presented above for the β-relaxation of the 75 wt % ZS-filled UDMA resemble those of the UDMA. That is, the sorbed moisture restricted the motion of the amide groups by increasing the intermolecular bond in the polymer network. Such restriction was achieved by the water molecules, when they form tight hydrogen-bonds between two CO groups in the polymer and loose hydrogen-bonds between CO and NH groups. This was concluded from the following results: (1) the gradual shift of the peak maximum of $\text{Tan}(\delta)_\epsilon$ to higher temperatures with sorption of small amount of moisture until it reached a maximum temperature of 10.0 °C for MC of 4.0 wt % at 0.252 kHz (Table 4.5), (2) the $\Delta\epsilon$ increased gradually with temperature (Figure 4.30) and rapidly with moisture content (Table 4.7) indicating that the orientation of the dipole of the composite increased with temperature and with moisture, (3) the half-width of the local motion persisted, i.e broadening with decreasing temperature, while their values increased with moisture content (Table 4.8) indicating the increase in the distribution of relaxation time, thus implying the presence of diverse species of water molecules that have different relaxation times with higher moisture content, (4) the increase in the intensity of the $\text{Tan}(\delta)_\epsilon$ almost equal to those for the UDMA values (Tables 4.4 and 4.8), and (5) the increase in the change of the activation energy from 6.7 kcal/mole for 75 wt % ZS-filled UDMA with MC of 0 wt % to 15.9 kcal/mole with MC of 4.0 wt % (Table 4.6).

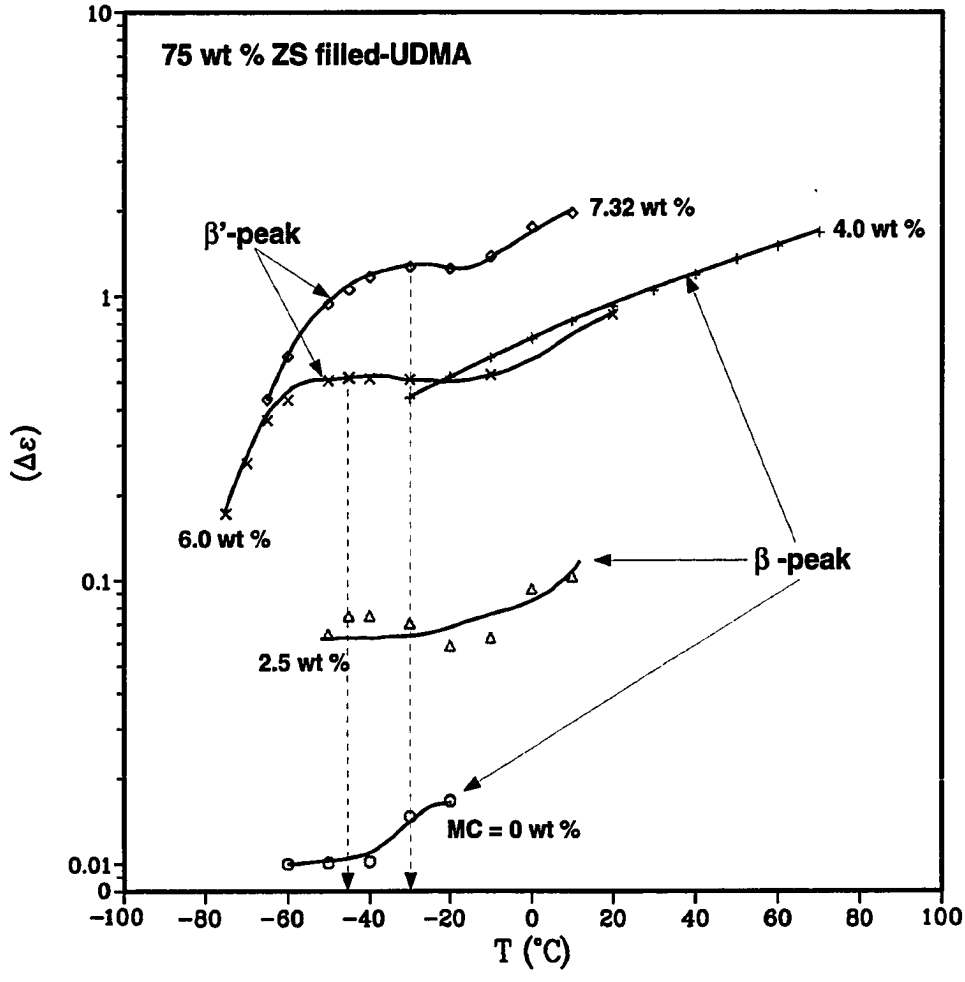

Figure 4.30: Dielectric increments of $\beta-$relaxations against temperature for 75 wt % zirconia-silica-filled UDMA polymer with MC of 0, 2.5, 4.0, 6.0 and 7.32 wt %.

At high moisture content, the results show resemblances and differences in the behavior of the β-relaxation for the 75 wt % ZS filled-UDMA compared to those of the unfilled-UDMA. Like the unfilled-UDMA, the peak maximum of the $\mathrm{Tan}(\delta)_\epsilon$ for the composite shifted to lower value of -62.5 °C with MC of 6.0 wt % at 0.252 kHz and then increased to approach a limiting value of -52.5 °C with MC of 7.32 wt % at the same frequency. In addition, the $\Delta\epsilon$ values increased with increasing moisture concentration and with increasing temperature until they reached a temperature independent region for the composite with MC $\geq$ 6.0 wt %. Further, the $\Delta_{1/2}$ reached similar values of 3.31 decades for the 75 wt % ZS-filled UDMA at -45.0 °C and the intensities of the $\mathrm{Tan}(\delta)_\epsilon$ also increased with moisture content. These results indicate that the water molecules tend to plasticize the polymer by separating the chains, which result in increasing the number of free amide groups and their mobility. However, the shift of the relaxation to higher temperature for the composite with MC of 7.32 wt % indicates (1) the restriction of the amide groups mobility due to higher density of packing of the polymer, and (2) the formation of fragments of clusters of water molecules that are hydrogen bonded to each other and to the amide groups as discussed earlier.

Unlike the unfilled-UDMA, the low frequency dielectric constant (ϵ_o) for the composite with MC of 7.32 wt % is 3.988 and is increased by 55 % from the value of the dried composite, indicating that the orientational correlation of the dipole moments has increased drastically for the moistened composite. However, such magnitude is lower than the values estimated for ice on the basis of the data presented in the literature [50, 73, 101]. In addition, the high frequency dielectric constant (ϵ_∞) of 2.7 at -30 °C for the high moisture content represents statistically the combined magnitudes of the corresponding values of ϵ_∞ of a hydrogen-bonded water structure

and of the UDMA network structures. As indicated earlier, the open H-bonded structures formed by the water molecules such as those in clathrates, have ϵ_∞ values much less than 3.0 [50, 73]. The present results show that the combined magnitudes of the hydrogen-bonded water structure and of the UDMA network structures are in fact < 3. Further, the values of ϵ_o and ϵ_∞ for $\alpha-$ and $\beta'-$ processes provide an insight into the state of the water that occurs in the composite. At 0 °C, ϵ_o is about 5.3 for the β-process (Figure 4.21), while the α-process has a value of about 4.1 for ϵ_∞ at 20 °C (Figure 4.26). Since no other relaxation processes are observed between 0 and 20 °C, the lower the value of 4.1 for the ϵ_∞ for the α-relaxation compared with 5.3 for ϵ_o for the β-relaxation implies that their is some phase transition that has undergone in the composite over this temperature range. Also, the ϵ_∞ increases from 4.8 at 50 °C to about 5.2 at 70 °C. These observations suggest that there is melting of partially crystallized ice that continues with increasing temperature. Since this behavior was not seen in the unfilled-UDMA system and moisture sorption of the filled-UDMA was higher than the sorption in the unfilled-UDMA, this suggests that the additional moisture and the partially crystallized ice are located in the region of the interface between the polymer and the filler and/or at the micro-voids and cracks in the composite or both.

Although the dielectric increment for the β-relaxation is a monotonous function of the temperature, i.e. at the transition temperature no maximum is exhibited [47], the $\Delta\epsilon$ values increased as a function of temperature to reach a maximum above the transition of the $\beta'-$ relaxation for the 75 wt % ZS-filled UDMA with MC $\geq$ 6.0 wt % (Figure 4.30). For instance, The maximum value for $\Delta\epsilon$ was achieved at -45 °C for the composite with MC of 6.0 wt %, while it was achieved -30 °C for the MC of 7.32 wt %. This observation indicates a persistence of a thermodynamic change that

is taking place in this region and a gradual onset of a decrease in $\Delta\epsilon$ beginning at these temperatures and a beginning of a transition to a more ordered structural state of low dielectric permittivity. Such a transition might be due to ordering and disordering mechanism of the hydrogen-bonded water structures and their fragmented clusters to form partially ordered ice structures. This transition is similar to phase transition of ice III $\rightarrow$ IX transition where a gradual decrease in the orientational polarization occurs, and at all temperatures in the transformation range ice III is partially disordered [74]. Further, the shift of the maximum of the $\Delta\epsilon$ values and the peak of the $\mathrm{Tan}(\delta)_\epsilon$ values to higher temperatures with the increase of moisture content indicates that more partial ordering might be occurring. This proposal is supported by Jain and Johari who showed that crystallization of H-bonded structures in amorphous aqueous poly(vinylpyrrolidone) shifted the dispersion's peak to higher temperature [50].

The half-width of β-relaxation for the 75 wt % ZS-filled UDMA is decreased 3.10 decades of frequency (Table 4.8) with an increase of temperature over the range of -50 to 10 °C, as is seen in Figure 4.31(a). As water content increased in the mixture, the half-width became constant over the temperature range of -50 to 10 °C (Figures 4.31(b)-4.31(d)) and broadened until a maximum value was reached of 6.48 decades with MC of 4.0 wt %. Eventually, the $\Delta_{1/2}$ became narrower and reached a value of 3.31 decades of frequency with MC of 7.32 wt % and the intensity of the relaxation increased from 0.0514 for the composite with MC of 6.0 wt % to 0.0931 with MC of 7.32 wt % at 0.252 kHz (Table 4.8). The widening of the half-widths of the spectra indicates broadening of distribution of relaxation time at low moisture content, while the narrowing indicates restraining of the distribution due to the decrease of the number of the different water environments. Although the $\Delta_{1/2}$ value

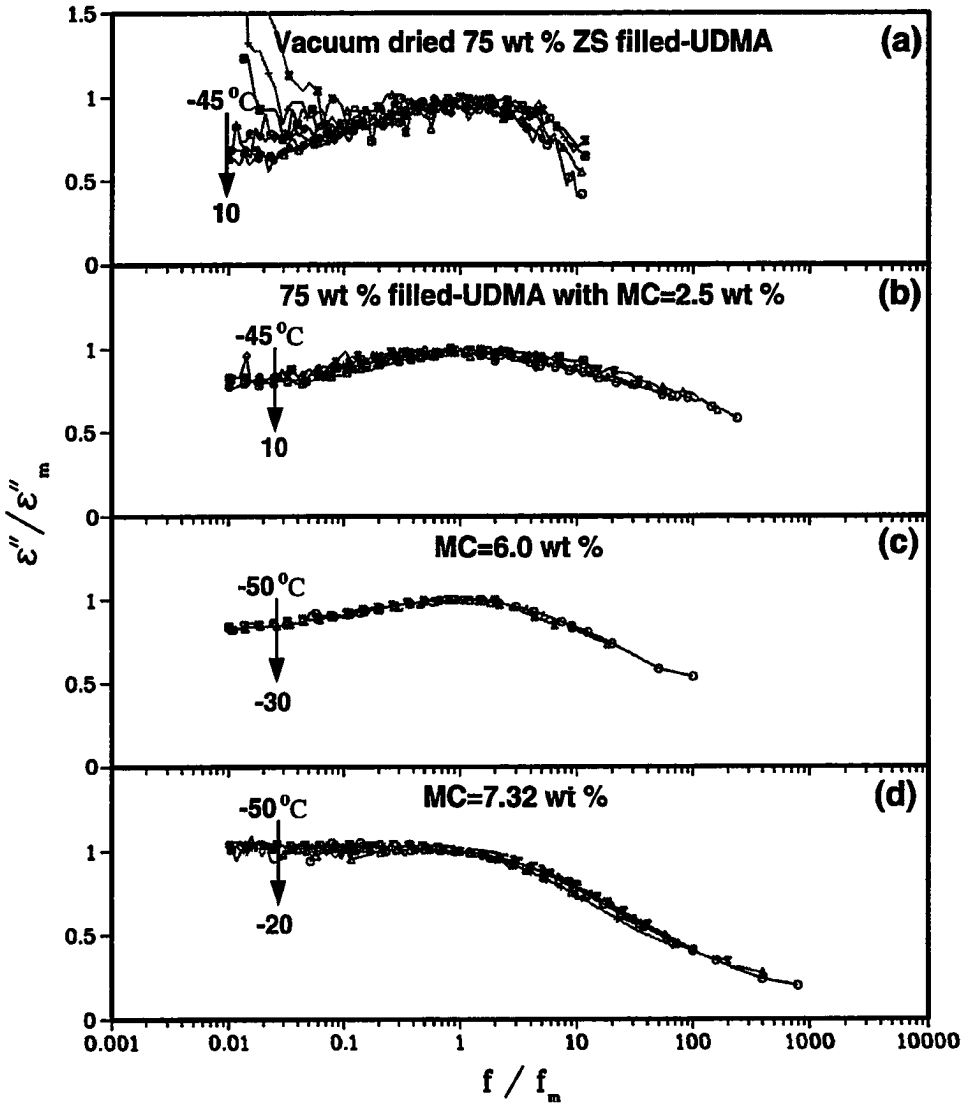

Figure 4.31: Normalized plots of the β-relaxation spectra over the temperature range of -50 to 10 °C for (a) vacuum dried 75 wt % ZS-filled UDMA, (b) a 2.5 wt % moistened filled-UDMA, (c) a 6.0 wt % moistened filled-UDMA, (d) a 7.32 wt % moistened filled-UDMA.

of 3.31 decades for the composite with MC of 7.32 wt % is lower than the $\Delta_{1/2}$ of the moistened composite with MC of 6.0 wt %, it is still higher than the dried composite and much higher than the 1.5 decades observed for the ice [74], as stated earlier. Part of the increased half-width may be due to the fact that the composite contained several different environments of water molecules, such as randomly oriented disordered crystals at the interface, nonfreezing fragments of water clusters in the polymer phase and hydrogen bonded water molecules with each other and with the amide groups. These different environments of reorienting water molecules may cause such a wide distribution of the spectra.

The activation energy also increased and then decreased to a value of 17.9 kcal/mole for the reorientation of water molecules in the UDMA composite. Such a value is much higher than activation energy found for ice clathrates (13 kcal/mole) [50, 73, 74, 101]. But in H-bonded structures with disordered arrangements of water molecules, as in aqueous poly(vinylpyrrolidone) glasses [50, 51], glucose and water mixture [19] and glassy water [73, 74], the activation energy is higher than the 13 kcal/mole. This seems to indicate further that most of the water molecules are in fact disordered, nonfreezing and open hydrogen bonded structures.

The effect of moisture on the α-relaxation

The main feature of the effect of moisture on the dielectric spectrum of the composite was the occurrence of the α'' peak with MC $\geq$ 4.0 wt %. This peak was attributed to superposition of the effects of the interfacial polarization and phase transition. The phase transition was associated with moisture evaporation that existed in the region of the interface. The α'' peak differs from the α' peak that occurred for the moistened unfilled-UDMA, because of its shift to lower frequency and the in-

crease in its height with the increase in the temperature as well as the superposition of the dc conductivity, the peak seemed to disappear (Figures 4.27 - 4.29). This conclusion will be discussed in details in the following.

The dielectric increment for the α'' processes increased as a function of temperature to reach a peak maximum value of about 4.0 at 125 °C for the 75 wt % ZS-filled UDMA with MC $\geq$ 6.0 wt % as is seen in Figure 4.32. This result further supports the existence of a phase transition which is the evaporation of water at this high temperature. In addition, the values of ϵ_o and ϵ_∞ for the α-process before and after the occurrence of the α'' -process for the composite with MC 7.32 wt % provide an insight into the evaporation that occurs in the interface region of the composites. Since the α'' -relaxation occurs over the temperature range of 70 to 150 °C, the ϵ_o value is 11.9 at 70 °C (Figure 4.26), while the ϵ_∞ of the α-relaxation is 3.3 at 155 °C (Figure 4.24). This low value of 3.3 for ϵ_∞ for the high temperature region of the α-relaxation as compared with 11.9 for ϵ_o for the low temperature region implies that the moisture at the interface has undergone a phase transition in this temperature range. This observation was also reflected by the decrease in values of the dipole moment of the α-relaxation as a function of temperature in Figure 4.33. With the evaporation of water molecules one would expect to see a decrease in the dielectric increment for the α-relaxation which is clearly obvious from the results in Table 4.7 and Figure 4.33.

The half-width of the M'' peak for the α'' relaxation for the composite with MC of 7.32 wt % at 120 and 130 °C are 5.87 and 3.40, respectively, (Figure 4.29). The decrease of the half width from 5.87 decades to 3.40 decades for an increase of 10 °C further indicates that the dipolar processes have different sensitivities to temperature.

In general, the moisture does not only occupy the interfacial region in the composite, but also it plasticizes the UDMA polymer. Such an effect is reflected by

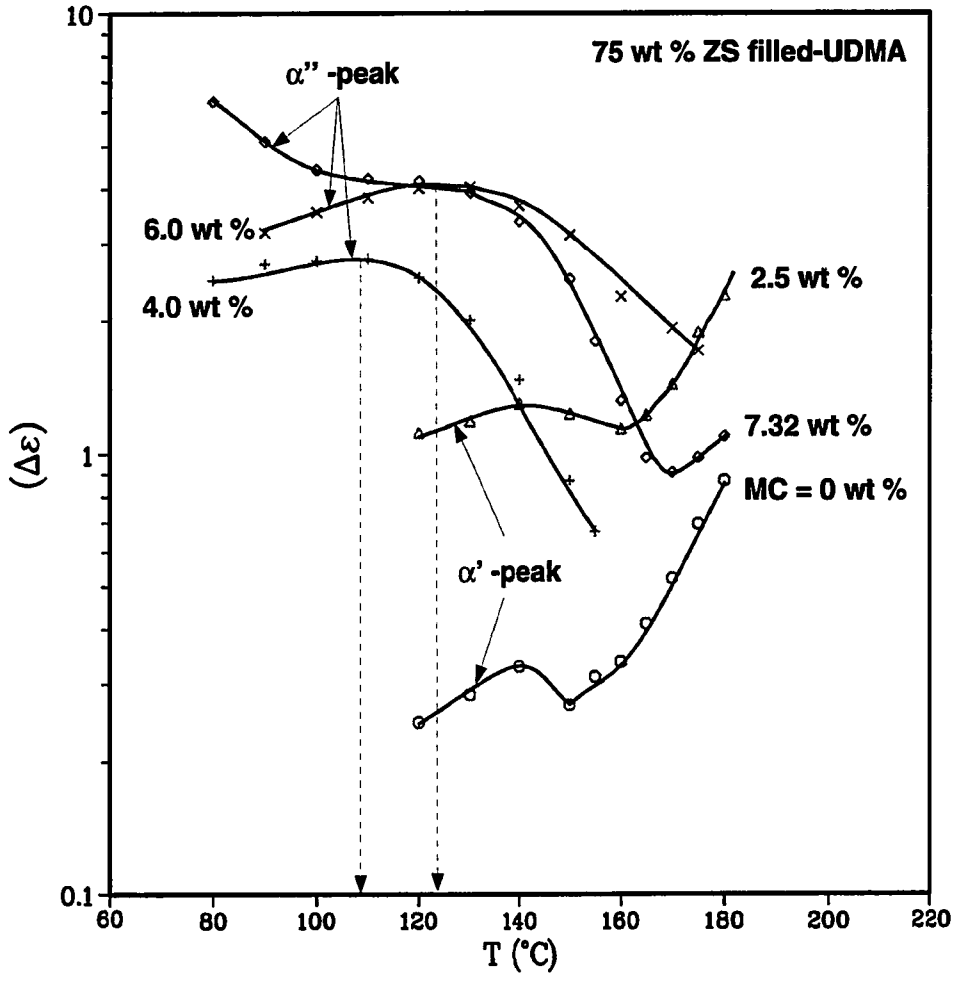

Figure 4.32: Dielectric increments of α'' - and α' -relaxations against temperature for 75 wt % zirconia-silica-filled UDMA with MC of 0, 2.5, 4.0, 6.0 and 7.32 wt %.

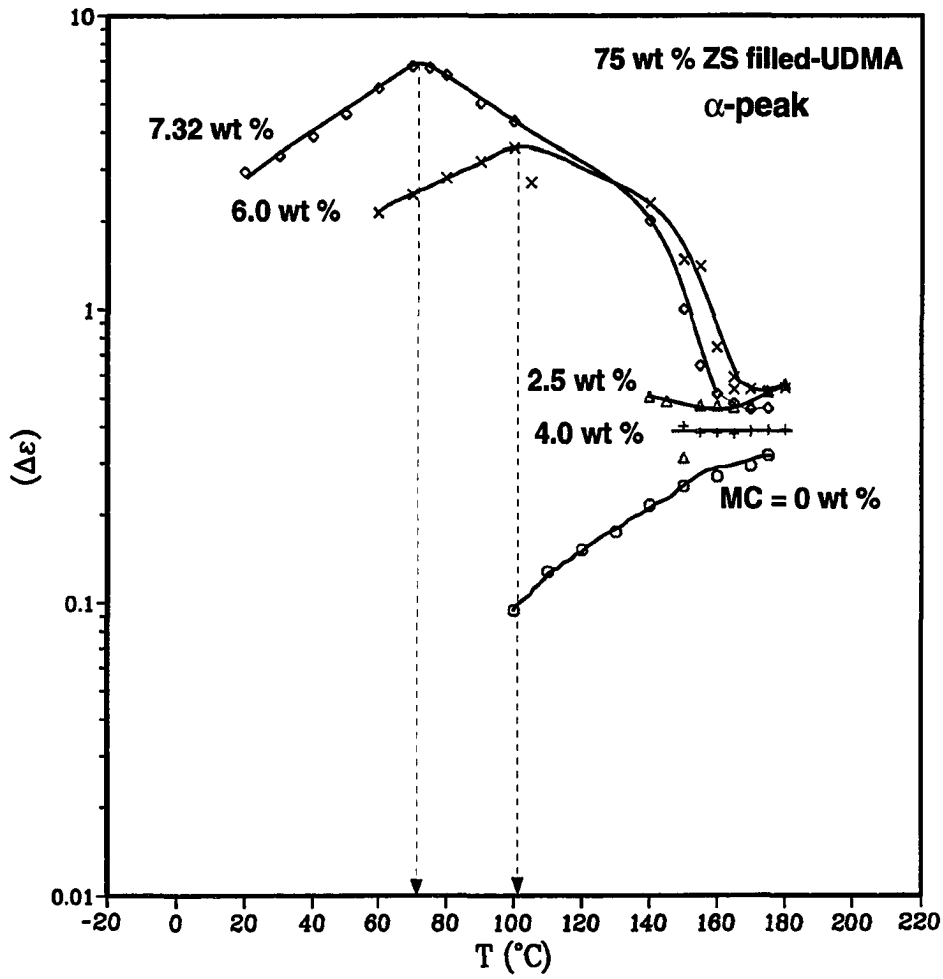

Figure 4.33: Dielectric increments of α-relaxation against temperature for 75 wt % zirconia-silica-filled UDMA polymer with MC of 0, 2.5, 4.0, 6.0 and 7.32 wt %.

the shift of the peak maximum of the $\text{Tan}(\delta)_\epsilon$ for the α-relaxation to lower temperature (Table 4.5), the increase in the intensity of $\text{Tan}(\delta)_\epsilon$ values, the increase of $\Delta_{1/2}$ (Table 4.8) and the decrease in the activation energy from 49.9 kcal/mole for the dried composite to 17.4 kcal/mole for the moistened composite with MC of 7.32 wt % (Table 4.6). These results show an increase in the free volume and the consequent loosening of the segmental chain motion.

Since the maximum amount of moisture content that can be sorbed for the composite is 7.32 wt % and the maximum for the UDMA polymer is 3.72 wt %, one would assume that the extra moisture that was sorbed by the composite is found in the interface region and/or at the voids. This assumption implies that plasticization effect in the polymer part of the composite will be equivalent to that of the polymer. However, by looking at the different results such as the shift of the α-relaxation peak temperature to lower values and the decrease in the activation energy values, one notices that the values for the moistened composites are drastically more affected than the values for the moistened UDMA. For instance, the peak maximum of the $\text{Tan}(\delta)_\epsilon$ was shifted to lower values by 20 °C for the unfilled-UDMA with MC of 3.00 wt % at 5.5 kHz (Table 4.1), while it decreased by about 25 °C with the small introduction of moisture and decreased by about 50 °C over the entire moisture content at 0.5 kHz for the moistened composites (Table 4.5). In addition, the activation energy values decreased by about 28.8 kcal/mole for the moistened unfilled-UDMA from the value of the dried UDMA, while it was decreased by about 32.5 kcal/mole for the moistened composites from the value of the dried composites. These results suggest that the filler in the composites, as discussed in the previous chapter, decreases the density of packing of the polymer at the boundary layer, thus facilitating more water molecules to enter between the chains and exposing more chains to re-

act with the water. This condition might result in a larger increase in the distance between the chains and consequently more loosening of the network.

In summary, the polymer in the ZS-filled UDMA composite forms similar interactions with moisture to those of the unfilled-UDMA In addition to these interactions, more moisture is sorbed in the composites than the polymer. This additional moisture occupies the interface between the filler and the polymer, and/or the micro-voids and cracks in the composites or both. This interfacial moisture undergoes phase transition to disordered ice structures upon lowering the temperature, and it evaporates when elevating the testing temperature. Further, filler incorporation enhances the plasticization effect in the polymer by the moisture because of the decrease in the density of packing of the polymer at the boundary layer that is created by the filler in the composite.

4.3.3 The Effect of Moisture on the Dielectric Behavior of MAPM-Silanated ZS-Filled UDMA

The dielectric loss tangent ($\mathrm{Tan}(\delta)_\epsilon$) for the 75 wt % MAPM-silanated ZS-filled UDMA with MC of 0, 2.5, 4.0 and 6.0 wt % measured at 0.053 kHz are plotted against temperature in Figure 4.34. The $\mathrm{Tan}(\delta)_\epsilon$ curves show the same behavior as those shown by the UDMA polymer, namely a sub-T_g or β-relaxation peak, an α-relaxation peak and a substantial increase of the values of $\mathrm{Tan}(\delta)_\epsilon$ at high temperature. The increase of the $\mathrm{Tan}(\delta)_\epsilon$ values at high temperature continues to form a new peak (α') with higher moisture content (MC $\geq$ 4.0 wt %). This new peak obstructed the appearance of the α-relaxation as it did previously for the UDMA polymer. The maximum of the $\alpha-$ and $\beta-$peaks obtained from the $\mathrm{Tan}(\delta)_\epsilon$ curves measured at different frequencies are shown in Table 4.9. Figure 4.34 and Table 4.9

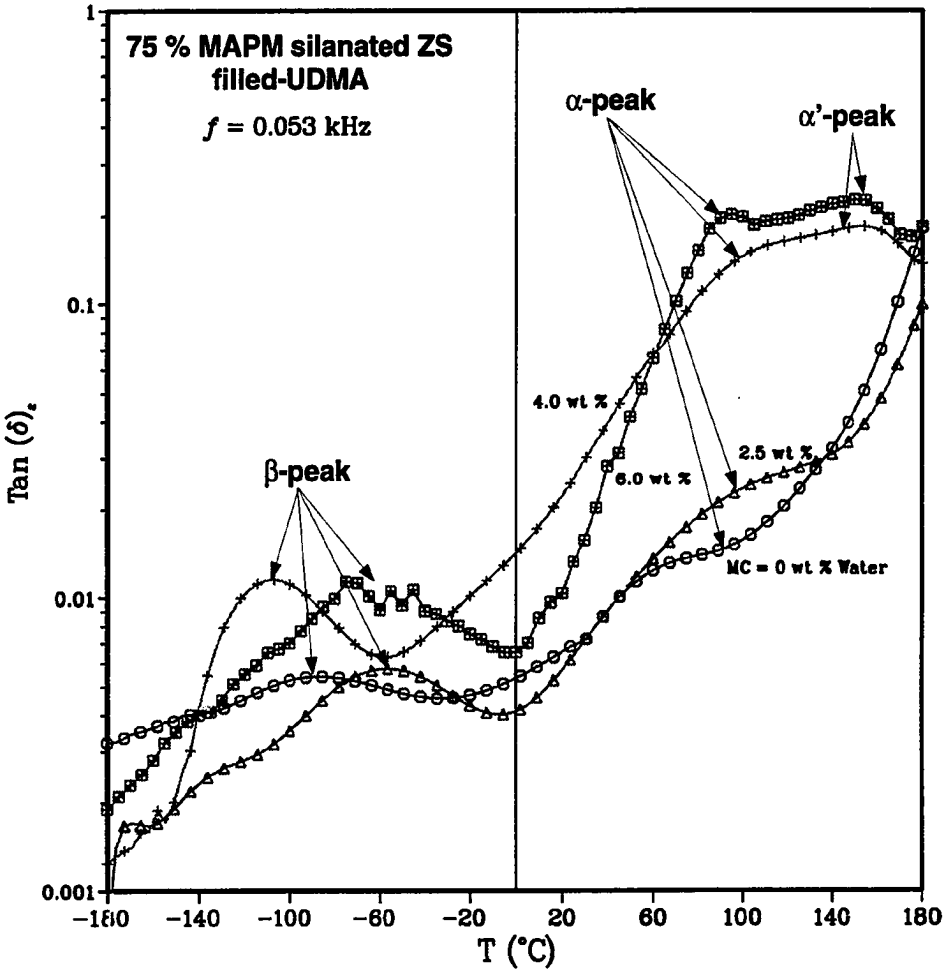

Figure 4.34: Tan$(\delta)_\varepsilon$ against temperature measured at 0.053 kHz for 75 wt % MAPM-silanated zirconia-silica-filled UDMA with MC of 0, 2.5, 4.0 and 6.0 wt %.

MC wt %	Maximum peaks temperature (°C)					
	α-relaxation			β-relaxation		
	5.5 (kHz)	10.0 (kHz)	33.3 (kHz)	0.252 (kHz)	1.0 (kHz)	10.0 (kHz)
0.0	—	163.8	172.9	-39.9	-33.0	—
2.5	150.1	156.6	173.5	-45.7	-31.7	-3.8
4.0	135.0	138.0	143.6	-92.5	-90.0	-61.9
6.0	129.9	131.5	134.0	-58.9	-49.3	-35.9

Table 4.9: Maximum peaks temperatures (°C) from $\mathrm{Tan}(\delta)_\epsilon$ measurements for different moisture content in 75 wt % MAPM-silanated zirconia-silica-filled UDMA for $\alpha-$relaxations at 5.5, 10.0 and 33.3 kHz and for $\beta-$relaxations at 0.252, 1.0 and 10.0 kHz.

show shifts of the α-relaxation peak maximum to lower temperatures due to the plasticization effect of the moisture, and the β-relaxation showed the same trends of peaks shifts as for the moistened UDMA.

M' and M'' values were calculated at several temperatures by Equations (3.5) and (3.6) for moistened 75 wt % MAPM-silanated ZS-filled UDMA with MC of 2.5 to 6.0 wt %. The isothermal curves of M' and M'' for the moistened composite with MC of 2.5 and 6.0 wt % are plotted against frequency in Figures 4.35 and 4.36 for the β-process, in Figures 4.37 and 4.38 for the α-process, and in Figures 4.39 and 4.40 for the α'-process.

The properties ϵ_∞, ϵ_o and $\Delta\epsilon$ for $\beta-$and $\alpha-$processes as a function of moisture content are presented in Table 4.10, while the $\Delta\epsilon$ values for both processes against temperature are plotted in Figures 4.41 and 4.42, respectively. In addition, the values of λ of $\text{Tan}(\delta)_\epsilon$ and $\Delta_{1/2}$ as a function of moisture content are listed in Table 4.11. The activation energies and pre-exponential factors are calculated from slopes and intercepts of the plots of frequencies at which the $\text{Tan}(\delta)_\epsilon$ peaks maximum appeared for $\beta-$ and $\alpha-$processes against reciprocal temperatures are listed in Table 4.12.

The effect of moisture on the β-relaxation

The β-process for the composite (75 wt % MAPM-silanated ZS-filled UDMA) shows exactly the same behaviors as those of the UDMA polymer. Namely, with small amount of moisture, an over all stiffening of the composite occurred due to bonding of the water molecules to the amide groups to create intermolecular bonds that hold the chains tightly together which results in the restriction of their motion. This effect is observed by the shift of the β-peak maximum of the $\text{Tan}(\delta)_\epsilon$ to higher temperatures (Table 4.9), the decrease of the half-width of the bands from 6.60

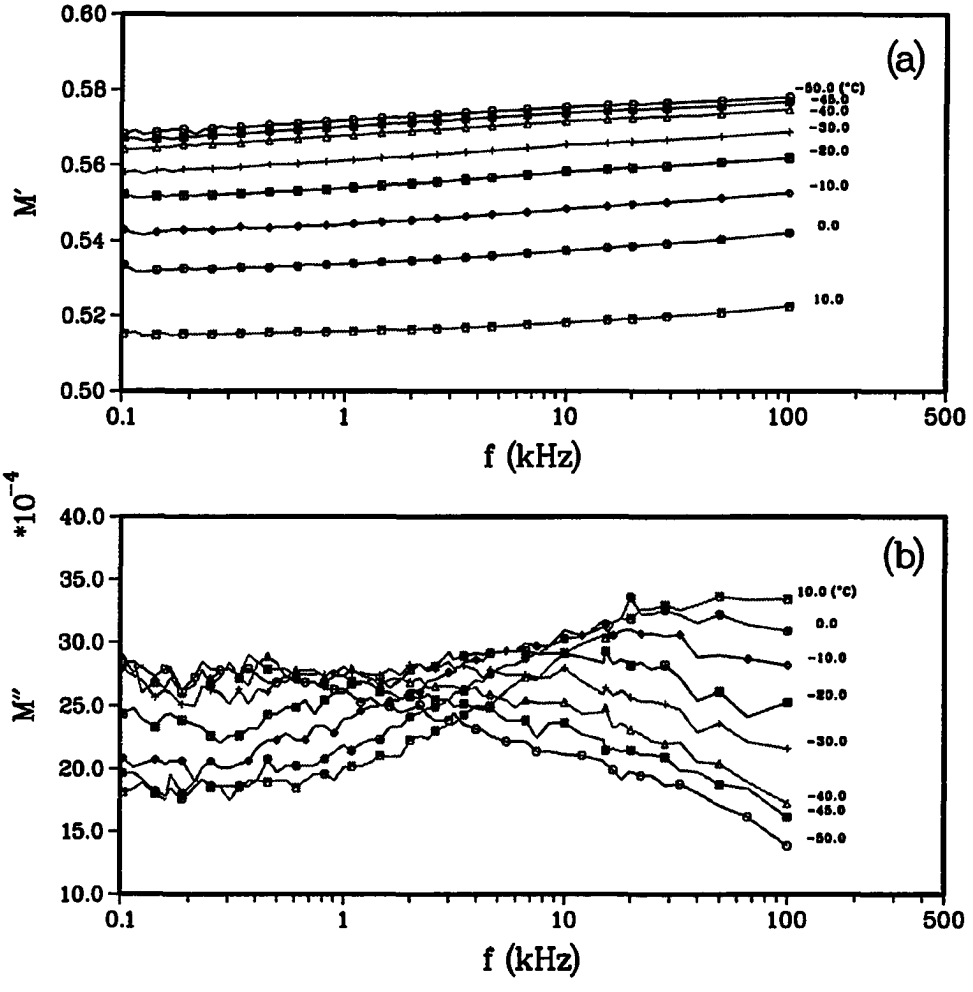

Figure 4.35: The frequency dependence of (a) M' and (b) M'' calculated over the temperature range of -50 to 10 °C for β-relaxation of 75 wt % MAPM-silanated zirconia-silica-filled UDMA with MC of 2.5 wt %.

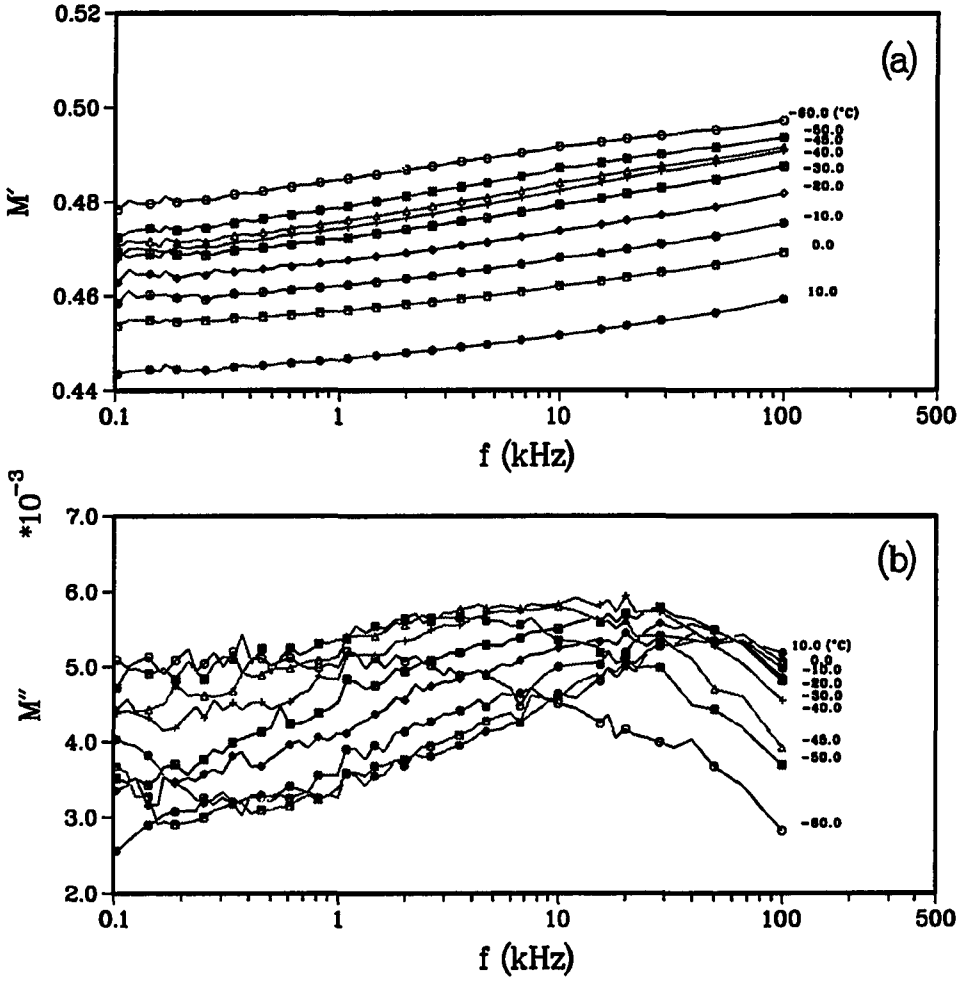

Figure 4.36: The frequency dependence of (a) M' and (b) M'' calculated over the temperature range of -60 to 10 °C for β-relaxation of 75 wt % MAPM-silanated zirconia-silica-filled UDMA with MC of 6.0 wt %.

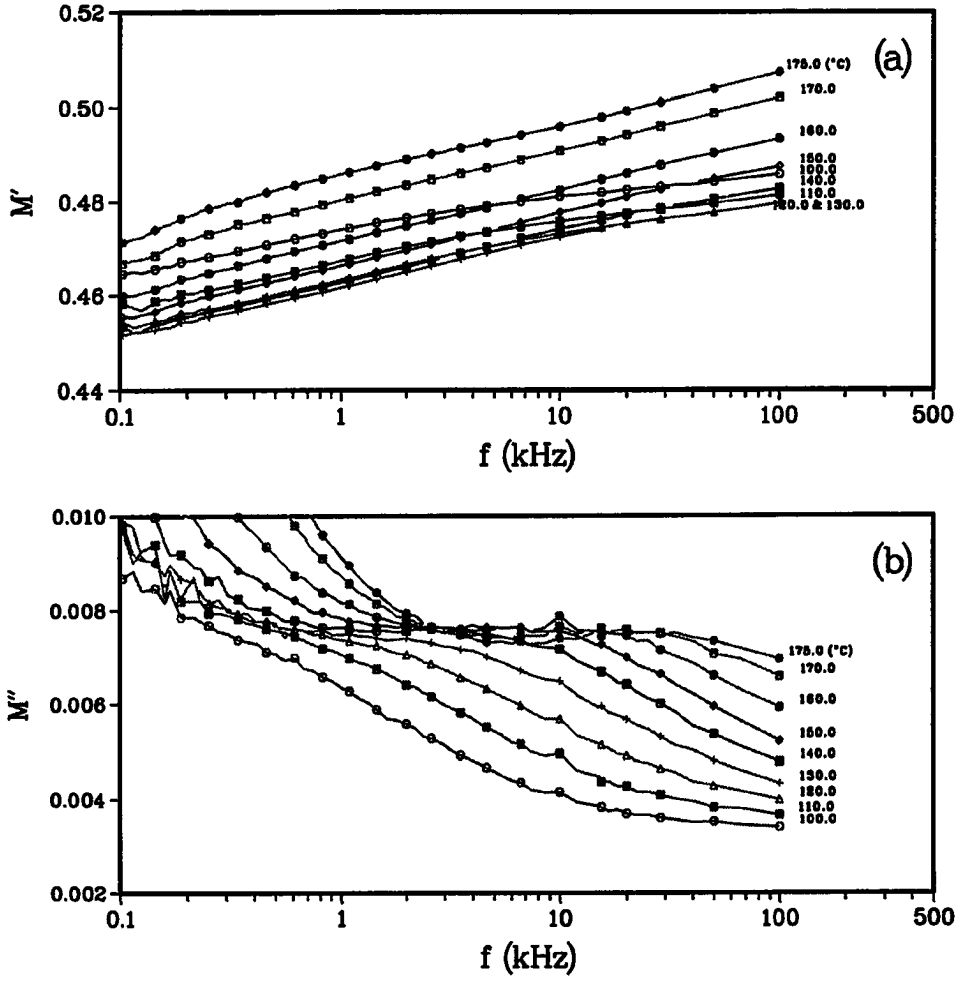

Figure 4.37: The frequency dependence of (a) M' and (b) M'' calculated over the temperature range of 100 to 175 °C for α-relaxation of 75 wt % MAPM-silanated zirconia-silica-filled UDMA with MC of 2.5 wt %.

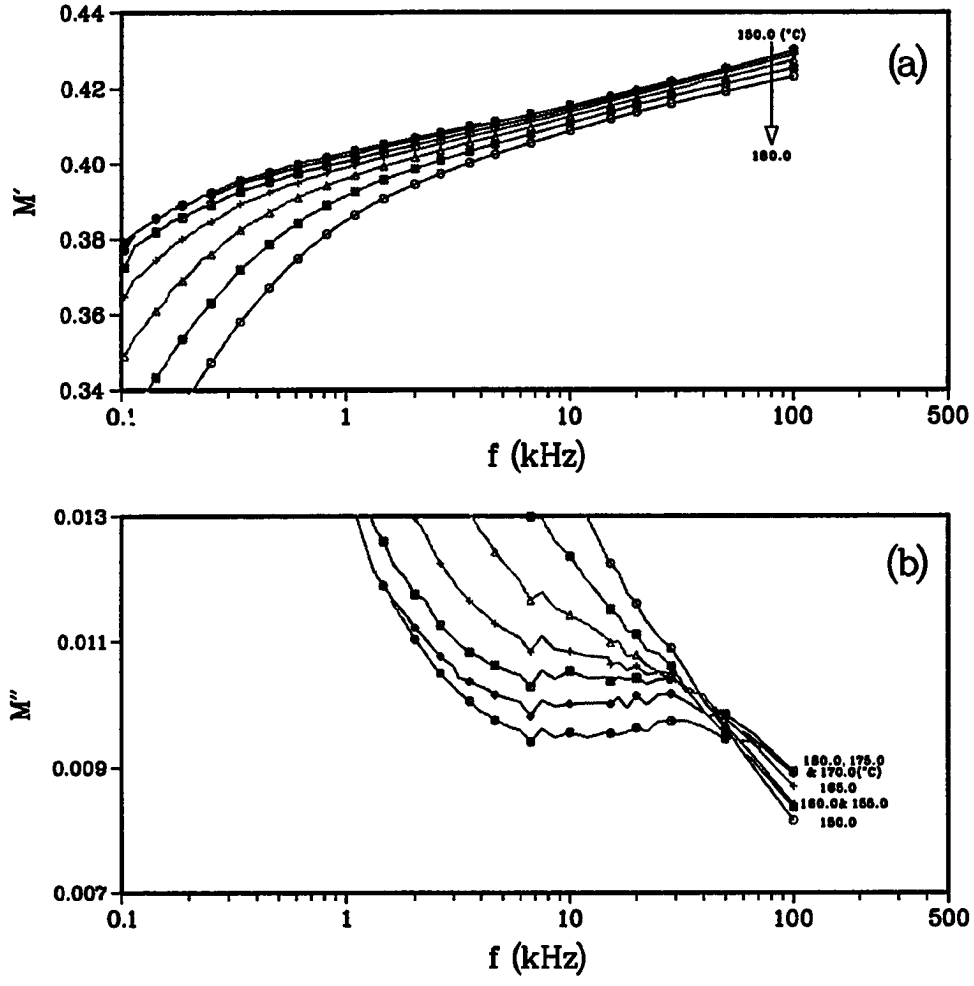

Figure 4.38: The frequency dependence of (a) M' and (b) M'' calculated over the temperature range of 150 to 180 °C for α-relaxation of 75 wt % MAPM-silanated zirconia-silica-filled UDMA with MC of 6.0 wt %.

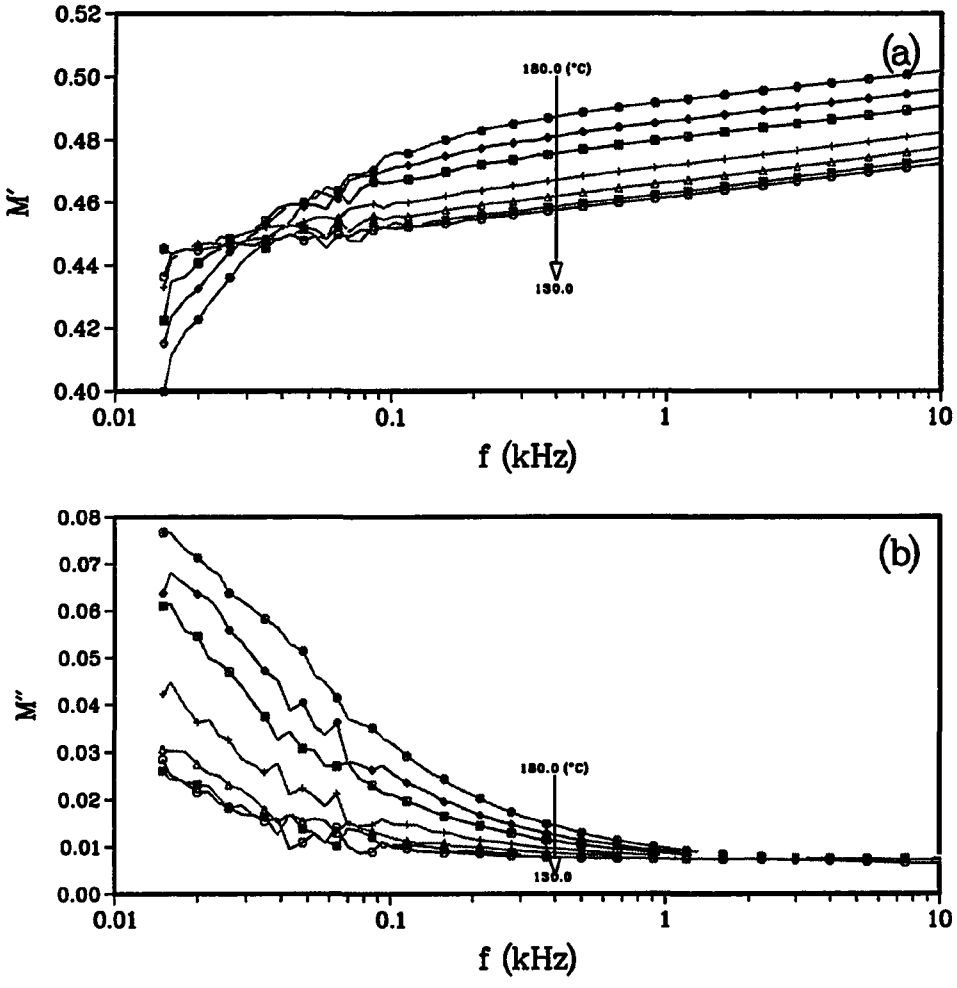

Figure 4.39: The frequency dependence of (a) M' and (b) M'' calculated over the temperature range of 130 to 180 °C for α'-relaxation of 75 wt % MAPM-silanated zirconia-silica-filled UDMA with MC of 2.5 wt %.

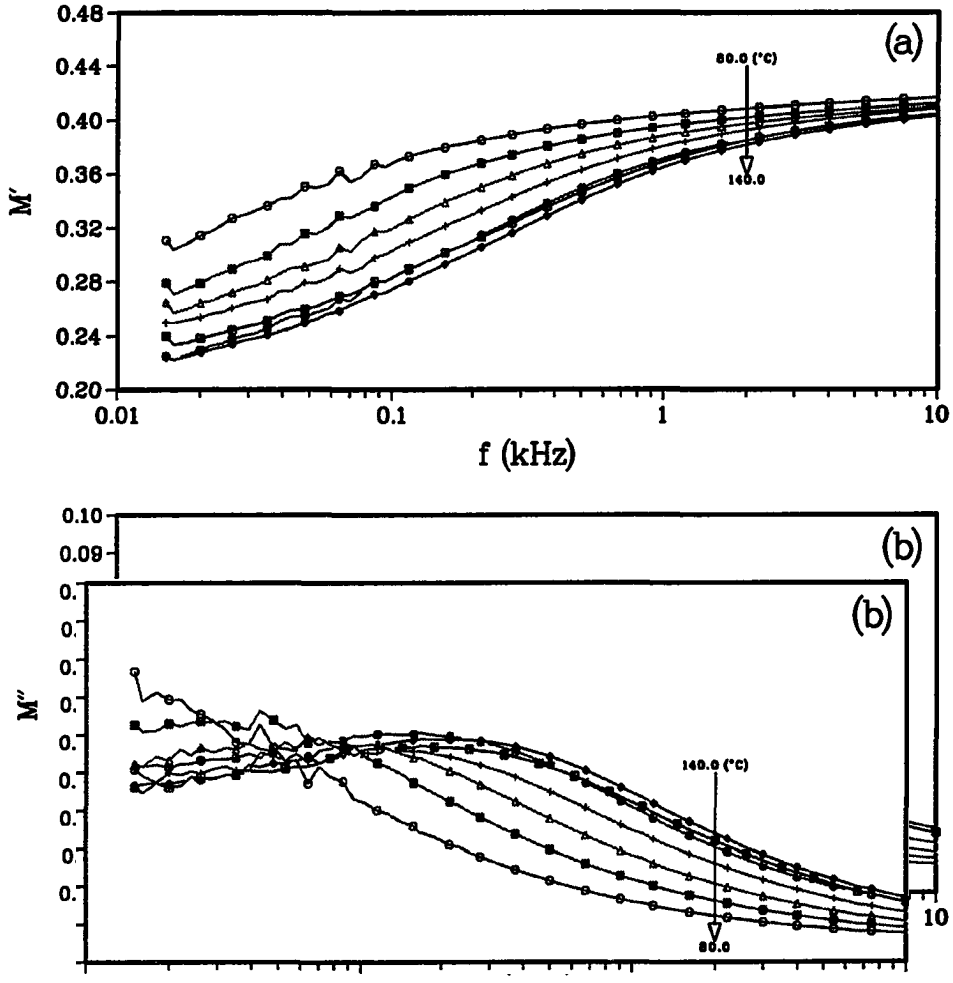

Figure 4.40: The frequency dependence of (a) M' and (b) M'' calculated over the temperature range of 80 to 140 °C for α'-relaxation of 75 wt % MAPM-silanated zirconia-silica-filled UDMA with MC of 6.0 wt %.

MC wt %	α-relaxation			β-relaxation		
	ϵ_o	ϵ_∞	$\Delta\epsilon$	ϵ_o	ϵ_∞	$\Delta\epsilon$
0.0	2.466	2.210	0.210	1.998	1.978	0.018
2.5	2.142	1.992	0.150	1.793	1.758	0.034
4.0	2.555	2.226	0.328	2.139	2.072	0.066
6.0	2.685	2.327	0.357	2.130	2.051	0.079

Table 4.10: Low- (ϵ_o) and high- (ϵ_∞) frequency limiting values of ϵ' as well as dielectric increments ($\Delta\epsilon$) for $\alpha-$ and $\beta-$relaxations at 170 and -30 °C as a function of moisture content (wt %) in 75 wt % MAPM-silanated zirconia-silica-filled UDMA.

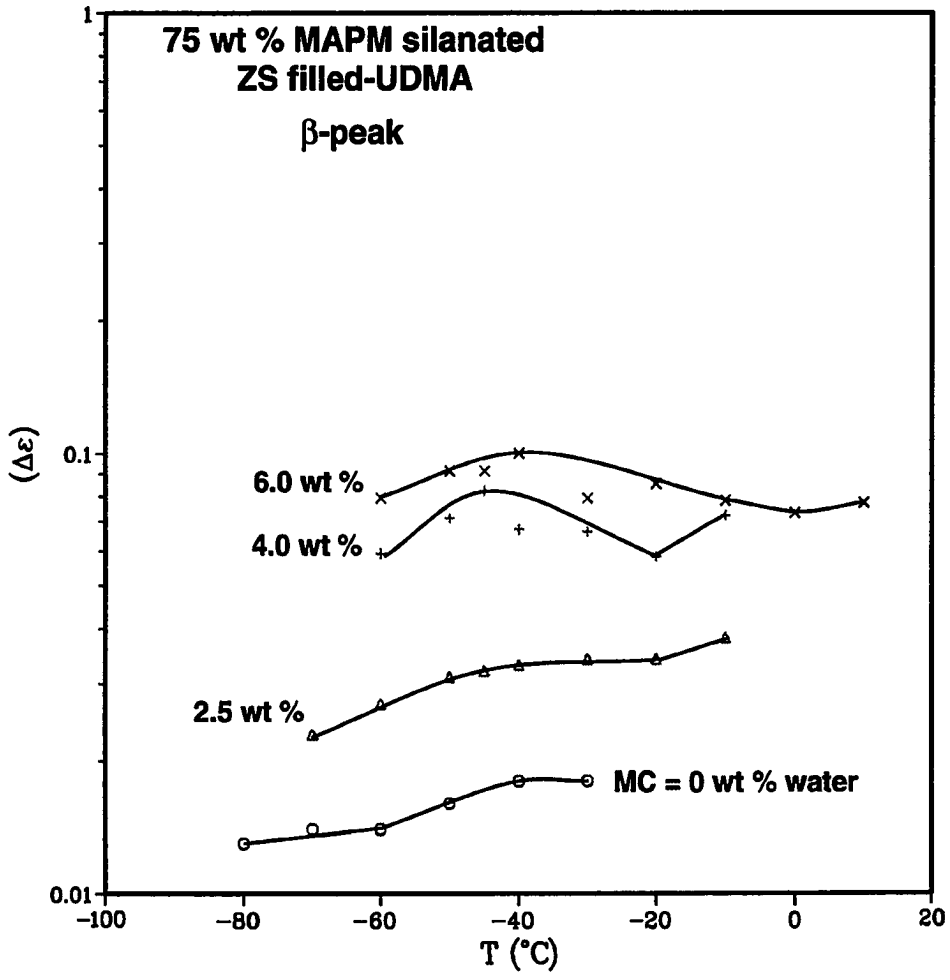

Figure 4.41: Dielectric increments of β−relaxations against temperature for 75 wt % MAPM-silanated zirconia-silica filled-UDMA with MC of 0, 2.5, 4.0, and 6.0 wt %.

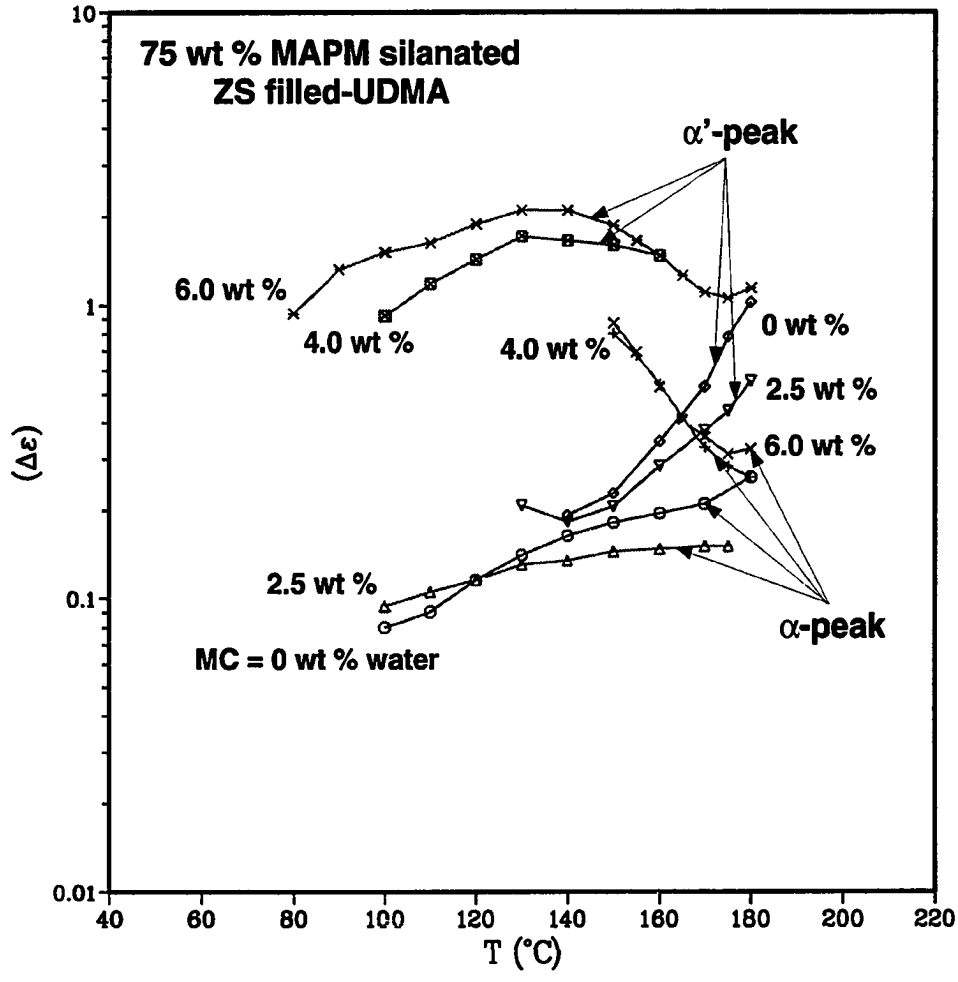

Figure 4.42: Dielectric increments of $\alpha-$ and $\alpha'-$processes against temperature for 75 wt % MAPM-silanated zirconia-silica filled-UDMA with MC of 0, 2.5, 4.0, and 6.0 wt %.

	α-relaxation		β-relaxation		α'-relaxation
MC	λ	$\Delta_{1/2}$	λ	$\Delta_{1/2}$	$\Delta_{1/2}$
wt %	0.252 (kHz)	170 (°C)	0.252 (kHz)	-45 (°C)	135 (°C)
0.0	0.0120	4.35	0.0019	6.60	—
2.5	0.0177	3.32	0.0047	5.08	—
4.0	0.1554	2.70	0.0086	4.69	2.25
6.0	0.1880	2.76	0.0101	2.95	2.32

Table 4.11: Intensities (λ) of $\mathrm{Tan}(\delta)_\epsilon$ at 0.252 kHz and half-widths of $\epsilon''(\Delta_{1/2})$ (decades) for $\alpha-$, $\beta-$ and α' -relaxations at 170, -45 and 135 °C, respectively, as a function of moisture content (wt %) in 75 wt % MAPM-silanated zirconia-silica-filled UDMA.

	α-relaxation		β-relaxation	
MC	ΔH	τ_o	ΔH	τ_o
wt %	$\left(\frac{kcal}{mole}\right)$	(Hz)	$\left(\frac{kcal}{mole}\right)$	(Hz)
0.0	48.5	$1.3 * 10^{-30}$	10.5	$3.1 * 10^{-15}$
2.5	38.6	$5.7 * 10^{-26}$	10.6	$9.1 * 10^{-15}$
4.0	20.6	$6.8 * 10^{-16}$	5.4	$1.3 * 10^{-11}$
6.0	32.4	$2.5 * 10^{-23}$	16.0	$5.5 * 10^{-21}$

Table 4.12: Activation energies and pre-exponential coefficients for $\alpha-$ and $\beta-$dielectric relaxation processes as a function of moisture content (wt %) in 75 % MAPM-silanated zirconia-silica-filled UDMA.

decades for the dried composites to 5.08 decades for the moistened composite with MC of 2.5 wt % (Table 4.11), and the insignificant increase in the change of the activation energy (Table 4.12). In addition, one would expect a decrease in the dielectric increment and the intensity of the $\mathrm{Tan}(\delta)_\epsilon$ values, however, one would see exactly the opposite effect (Tables 4.10 and 4.11, respectively), because of high orientational correlation of the dipole moment of the water molecules.

With more moisture sorption, the water molecules starts to replace more H-bonds in the composite by binding to the CO and NH groups of the amide groups and to each other. Thus, forcing the chains to separate and create larger distance between them which result in increasing the number of free amide groups and increasing their mobility. This result was observed mainly by the shift of the β-peak maximum value from -31.7 °C for the moistened composite with 2.5 wt % to -90.0 °C for the moistened composite with 4.0 wt % at 1.0 kHz, and the decrease of their activation from 10.6 to 5.4 kcal/mole, respectively.

When the maximum amount of moisture sorption is achieved, the water molecules tend to bind with each other to form water fragments and clusters between the polymer chains, thus restricting the chain motion. Also, as more water molecules bind to the amide groups replacing the hydrogen bonds that exist between them, the number of interchain hydrogen bonds are lowered allowing the molecules to pack more closely and increasing the polymer density. This effect was observed by the increase of the peaks maximum to higher temperatures, an increase in the values of the activation energies, and a narrowing of the distribution of the relaxation times, as depicted from the decrease of $\Delta_{1/2}$ values (Table 4.11).

The effect of moisture on the α-relaxation

In general, the over all effect of moisture was to plasticize the polymer by breaking its interchain coupling. This was also the case in the UDMA polymer system, although not as severe plasticization occurred, as discussed previously, which was seen from the decrease of the α-peak by about 20 °C for the moistened UDMA with 3.0 wt % from the dried UDMA at 5.5 kHz. This slight plasticization effect in the UDMA polymer was attributed to the breaking of the interchain couplings that are formed by the amide groups. However, in the composite with unsilanated filler, as well as silanated filler, the plasticization was more severe than for the pure UDMA polymer, especially for the composite containing unsilanated filler, since the shift in the α-peak was at least 50 °C at 0.5 kHz. In the case of the composite with unsilanated filler the high plasticization was attributed, logically, to presence of the filler. As discussed in the previous chapter, filler presence causes a decrease in the density of packing at the interface thus exposing more amide groups to water molecules. Such exposure will increase the chances of the amide groups breaking the hydrogen bond existing in the network and replacing them with water hydrogen bonds. In the case of composite with silanated filler, water plasticization was less severe than the plasticization of the composite with unsilanated filler and more severe than the polymer. This observation may be attributed to the breakage of the siloxane bonds that are formed between the filler and the silane or it may be due to water molecules attacking the filler surface at sites incompletely covered by the silane molecules or both. This situation may result in dilution and the formation of less packed layer at the boundary thus increasing the segmental mobility.

Like the polymer, a new peak (α') was developed (Figures 4.39 and 4.40) that obstructed the α-relaxation . This peak was attributed to the separation of charges

that occurred between the water droplets and the hydrated polar groups to form an interfacial monolayer of surface active agent.

In general, the quantities such as $\Delta\epsilon$ and $\Delta_{1/2}$ show that their is more non-uniformity of the hydrated structures on the amide groups in the interfacial monolayer for the composite than those for the polymer. For instance, the $\Delta\epsilon$ of the α'-relaxation increased with the increase in moisture content and formed a peak maximum with temperature about 135 °C (Figure 4.42) for the composite with silanated filler and it was about 125 °C for the composite with unsilanated filler (Figure 4.32). This result implies that the ordering and disordering of the dipole arrangement in the composite is much easier than pure UDMA ($\Delta\epsilon$ peak maximum = 160 °C) with temperature and with the electric field. In addition, The half-width was 2.32 decades of frequency with MC of 6.0 wt % for the composite with silanated filler (Table 4.11) and it was 3.56 decades for the composite with unsilanated filler, while it was 1.26 decades for the UDMA with MC of 3.72 wt % (Table 4.4).

In summary, the MAPM-silanated ZS-filled UDMA behaved similarly to the UDMA polymer with the presence of moisture. That is, low moisture addition caused restriction of the mobility of the amide groups due to tightly bound water molecules. Subsequent addition of moisture caused substantial plasticization effect due to massive replacement of hydrogen bonds that existed in the polymer network with hydrogen-bonding with water molecules. High addition of moisture caused water clusters to form around the amide groups thus restricting their motion. Unlike the UDMA polymer, the composite with silanated filler was more plasticized primarily due to the attack on siloxane bonds at the interface by the water molecules thus creating weak layers which facilitate chains mobility.

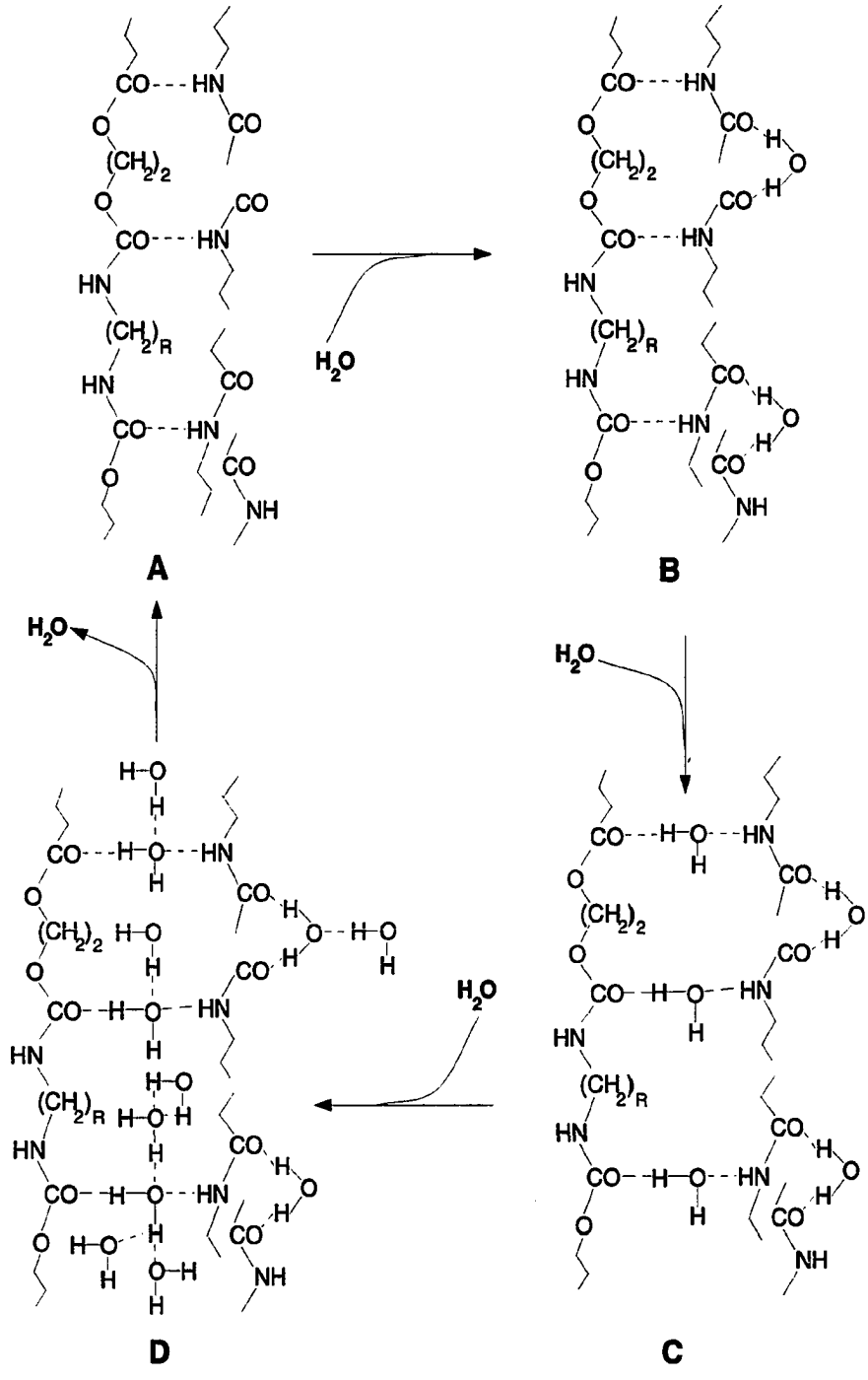

Figure 4.43: Representation of the events of water sorption process in UDMA polymer. Letters correspond to discussion in the text.

4.3.4 The Mechanism of Moisture in UDMA Polymer and Composite

The previous discussion of the various results of the water sorption process in dry UDMA fits the following picture, which follow closely a description by Puffer and Šebenda [81] and which is illustrated in Figure 4.43. (A) The dry UDMA polymer molecule makes few contacts with neighboring molecules. (B) The first water added interacts predominantly with the carbonyl groups forming tight bonds. This strongly bound water (MC = 0.69 wt %) is dispersed about the UDMA surface. It constitutes about 18.5 wt % of the moisture sorbed in the polymer. (C) At higher water content, the water molecules start to break and replace the hydrogen bonds that exists between the amino and carbonyl groups forming loosely bound water. This type of water causes loosening of the chains and increases the number of free amide groups. (D) At about 49 wt % of the sorbed moisture in the polymer, clusters develop presumably around the polar groups. This proposal was established from the variability of the hydrogen bonding arrangements in the polymer as was seen in the broadening of the distribution of relaxation time (Table 4.4), the development of MWS polarization indicating the presence of interphasal monolayer that contains unstable hydrated polar groups, and the restriction of the amide groups mobility. In UDMA polymer, the maximum water that can be sorbed into the polymer is MC of 3.72 wt % at 100 °C, indicating that water can only forms clusters in the UDMA polymer and does not form a monolayer or become bulk water.

In the ZS-filled UDMA, additional moisture is sorbed and it accumulates at the interface between the filler and polymer or at the cracks and micro-voids in the polymer or both, forming an interfacial layer. This layer contains different hydrogen bonding environments that mesh well with bulk water that can undergo phase transitions. These phase transitions were seen from the abrupt changes in the $\Delta\epsilon$ values

due to melting and evaporation of the bulk water. With increasing temperature, the bulk water causes major plasticization of the composites thus lowering the T_g severely.

In the MAPM-silanatated ZS-filled UDMA, the composites behaved more readily like the polymer, except with increasing temperature it is more plasticized than the polymer with increasing moisture content. Such plasticization is not as severe as for the composite with unsilanated filler. This plasticization is attributed to the breaking of the siloxane bonds that forms between the filler and the silane coupling agent and/or the water molecules attacking the filler surface at sites incompletely covered by the silane molecules.

4.4 Concluding Remarks

A proposed model was described for water sorption in UDMA polymer. From the model, it can be concluded that water can only be found as fragments of water molecules that form nonfreezing clusters. These water clusters contain charges that are not stabilized by the hydrated amide groups. However, in UDMA based-composites containing unsilanated filler, bulk water can exist at the interface between the filler and the polymer. This type of water can form disordered structures of ice at low temperatures and can evaporate at high temperatures. Further, the UDMA-based composites that contain silanated filler behave more or less like the UDMA polymer in the presence of moisture at low temperatures, but it is more plasicized than the polymer at high temperatures. Finally, it was seen that the dielectric apparatus is a good instrument for detecting phase transitions in a system and investigating water-polymer interactions.

CHAPTER V

BIOCOMPATIBILITY OF URETHANE DIMETHACRYLATE COMPOSITE BEFORE AND AFTER AGING AND LEACHING

5.1 Introduction

Light-cured composites resins are being extensively used in restorative dentistry. Although the physical and mechanical properties of these materials have been shown to be superior to silicate cements and room temperature curing acrylic resins, clinical studies have shown notable shortcomings. One of these shortcoming is the irritation of pulpal tissues which may lead to inflammation. One reason for a pulp response to these materials is the release of uncured chemicals components of the composites. Another reason is their lack of adhesion to the teeth which may leads to bacterial leakage. Also, the presence of oxygen that inhibits the polymerization reaction which leads to an increase in the percentage of unreacted components at the surface. These unreacted components may also result from a limited depth of cure due to attenuation of the radiation by the composite itself or not enough time of exposure to radiation to fully cure the material. Studies have shown that manufactures specifications for curing time for a specific depth are not enough to ensure complete polymerization [69].

The incomplete polymerization not only causes mechanical and physical failure of the restoration, but it can invoke severe tissue reactions. For instance, Spangberg *et al.* [97] showed that uncured materials *in situ* caused severe tissue reactions. In addition, Anderson *et al.* [3] revealed that the combination of different components of composites elicited cytotoxic response *in vitro* and they suggested that components of unpolymerized resin may leach from restoration and exert a severe cytotoxic response in cell culture [4]. However, in a later study by the same investigators, they proposed a conflicting explanation suggesting that bacterial microleakage might be the primary cause of pulpal inflammation *in vivo* [5]

In general, two different explanations were proposed by investigators for the cause of these pulpal reactions. The first explanation was chemical compounds that were released from resins were responsible for these pulpal responses, while the second explanation claimed that microleakage of bacteria around the restorative material was the primary cause of these reactions rather than the composites themselves.

In support of chemical proposal, Tobias and associates [103] have shown that a significant inflammatory response was elicited from a composite resin when it was used without lining in a dental cavity, and attributed such a response to ingredients that are toxic to the pulp. Hanks *et al.* [42] concluded that the toxicity of resin composites might be caused by either new toxic products which arise upon setting of the material or by toxic products resulting from incomplete setting. Caughman and coworkers [18] indicated that the degree of cytotoxicity of light-cured composites was inversely related to curing time. They also stated that the degree of tissue reaction depended on the degree that luting agents affected the cells and were functions of degree of polymerization, percentage of filler, and cells type. Rathbun *et al.* [83] showed that a 90 % reduction in toxicity was attained when the leachable components

were removed as compared to non-extracted Bis-GMA composites. Stanley and associates [98] in 1979 tested the eight individual compounds of the composites resins in cavity preparations, with varying dentin thicknesses, in monkey's teeth for 21 days. While most components were not significantly irritating, three components 2-hydroxy-4 methoxy-benzophenone, the methyl ester of benzoin, and the methyl peroxide, were toxic in deep cavity preparation in the absence of bacteria.

In support of bacterial contamination, Brännström and associates [15] have shown that bacteria was a more serious threat to the pulp than irritation by chemicals. Inokoshi *et al.* [48] concluded that microleakage of bacteria was responsible for most of pulp irritation observed, because a greater pulpal response was found in response to a component when no etching was done to enamel and dentin, and less severe pulpal response was found with their total etching. Cox *et al.* [24] also found that pulpal inflammation in monkeys was associated with bacterial contaminants and stated that bacteria were more significant pulpal irritants than chemicals from composites resin. It is presently thought that pulpal response to these resins may be a combination of bacterial microleakage and diffusion of unpolymerized resins.

Therefore, it was the purpose of this part of the research to investigate the effects of different curing- and post-curing times on the cytotoxicity of UDMA based-composites in cell culture before and after leaching and polishing the composites, and to identify the major components that might be responsible for cells reactions.

5.2 Experimental

5.2.1 Materials

Urethane dimethacrylate (UDMA) (Esschem Co., Essington PA) was used as a monomer system. Zirconia-silica with a surface area of 1.6 m^2/g and an average

diameter of 1.5 μm (3M Dental Products, St.Paul MN) was used as a filler. 3-methacryloxypropyltrimethoxysilane (MAPM) (Huls America, Piscataway NJ, formerly Petrarch Systems, Bristol PA) was used as a coupling agent to silanate the filler. Teflon^R (Bel-Art products, Peuanneck, New Jersey), a known non-toxic material was used as a negative control.

5.2.2 Sample Preparation

The filler was silanated as described previously by depositing the silane from an aqueous solution of 75 % ethanol (190 % proof) and 25 % silane (weight ratio). The amount of silane used for the filler treatment in this part of the study was three times (3X) the minimum uniform coverage given by Equation (2.1). The polymer was formulated from UDMA using *dl*-camphoroquinone (CQ) catalyst and 2-dimethylaminoethylmethacrylate (DMAEMA) accelerator in concentrations described by Douglas, Craig and Chen [31]. Composites were formulated from UDMA zirconia-silica and MAPM silanated zirconia-silica using the accelerator and the catalyst.

The mixed composite paste was placed in Teflon disk-shaped molds (6.0 mm diameter and 3.5 mm thick). The Teflon controls were punched out in a similar shape and dimension. The composite paste was made in two layers and each cured by visible light in a TRIAD II oven (Dentsply International,York, PA) for 13, 30, 90, 150 and 300 sec at room temperature. The samples were then aged for another 0, 24, 72, 144, 216 and 288 hrs at 57 °C in vacuum oven. Immediately after being cured and aged, the samples were weighed on an analytical balance (initial weight). For each curing and aging condition, the samples were either untreated, polished, or extracted with different solvents. Polishing of the samples was carried out by polishing each

side with 600 grit silicon carbide paper and then smoothing both sides with 1200 grit silicon carbide paper. Extraction of the samples was carried out by placing them in vials containing 10 mL of either distilled water or a mixture of 75 % ethanol/water (volume ratio), representing poor and good solvents, respectively, for composites. The samples were extracted for 48 hrs at ambient temperatures, since it was found by Ferracane and Condon [35] that elution of nearly all the leachables components was complete within the first 24 hr period in either solvents. After the different treatments, all samples and controls were ultrasonically cleaned, rinsed thoroughly in double distilled, deionized water and dried to a constant weight for 8 - 12 hrs in a vacuum desiccator (dry weight). Six replicates were made for each of the testing conditions to be evaluated for cytotoxicity. The percent leachables were calculated as follows [35]

$$\% \; Leachables \; = \; \frac{W_i - W_d}{W_i} * 100 \tag{5.1}$$

where,

W_i = initial weight (gm)

W_d = dry weight (gm)

For identification of leachables, the UDMA based composites resin were extracted using the mixture of 75 % ethanol/water. The composite paste was transferred in the Teflon molds and was made in two layers. Each layer was cured by the visible light for 30 sec. The polymerized samples were ground with mortar and pestle to maximize the surface area for extraction. The ground composite powder was weighed and placed in 10 mL of solvent at ambient temperature for 48 hrs. The solvent was

pipetted out carefully and replaced with 5 mL of fresh solvent and the powder was extracted for additional 24 hrs. Throughout the extraction process, the vials were covered to prevent solvent evaporation and were kept in light-free environment. After the third day, the vials were uncovered and the solvent was removed and combined with the older extract (total of 15 ml). The powder was then weighed after it was vacuum dried for 48 hrs at 80 °C.

The resultant extract was first quantified by evaporating the solvent at ambient temperature and pressure. Three replicates of powder extraction were made to quantify the amount of extract, while one replica was used to identify the leachables.

5.2.3 Cell Culture

All samples, cured and aged for different times, and then untreated, extracted or polished, as well as Teflon controls were centered in 24-well dishes of polystyrene (Costar, Cambridge MA). Teflon holders were made to hold the samples in place as shown in Figure 5.1. Then the wells were plated with Balb/c 3T3 embryonic mouse fibroblasts derived from clone A31 (ATCC CCL 163: anchorage dependent, aneuploid, and contact inhibited fibroblasts, Rockville MD).

The medium used for maintaining the cell culture consisted of Dulbecco's minimum essential medium (DMEM) without glutamine, 3 % Nu-Serum (Collaborative Research, Bedford MA), 28 mM HEPES (N-2-hydroxy-ethyl-piperazine-N'-2-ethane-sulfonic acid, pH = 7.2), and supplements (2 mmol/L glutamine, 125 units/mL penicillin, 125 μg/mL streptomycin and 10 μg/mL gentamycin; Gibco, GrandIsland NY). HEPES buffer was added to control the pH of the medium.

The stock cells were grown to confluency and were treated for 4 min at 37 °C with a sterile trypsin/EDTA solution that consisting of 0.05 % trypsin and 0.02 %

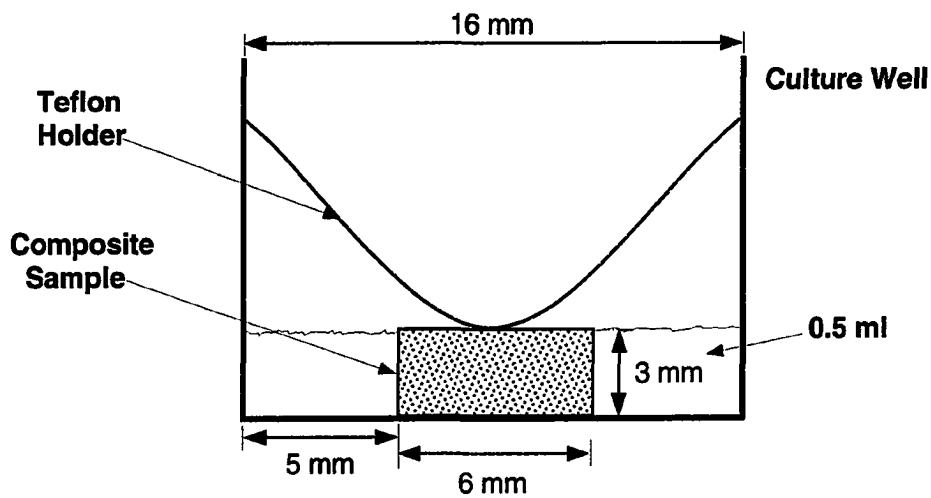

Figure 5.1: Sketch of cross section of a well in the culture dish with the composite held in position with a teflon holder.

EDTA in phosphate buffered silane (PBS) to harvest the cells. After trypsinization, the cells were collected by centrifuging at 750 rpm for 4 min, resuspended in cell culture medium and diluted to 25,000 cells/cm^2 with the medium. One-half mL of cell suspension was added to each culture well of the 24-well dish which contained the sample. Care was taken to make sure that the cell suspension would cover the area around the sample evenly. The dishes were incubated at 37 °C in 95 % air, 5 % CO_2 and 85 % relative humidity for 48 hrs. At this time the dishes were processed to evaluate the cytotoxic effects of the composites. The cytotoxicity effect was calculated as a percent of the Teflon control. Six replicate wells were used for each composite/condition tested. Analysis of variance for a general factorial design was used to determine whether the effects of resin-aging and curing times on the different treatments were significant at the 95 % confidence level.

5.2.4 Measurements of Cytotoxicity

To test for cytotoxicity, MTT-formazan production was used to evaluate succinic dehydrogenase activity in the mitochondria of the cells, which is a reflection of cell viability. The medium was suctioned off the cells and the cells were washed with PBS. One-half mL of histochemical staining/disodium succinate medium was added to each well and was incubated for 90 min at 37 °C. This medium consists of 10 mL of 2.5 mL molal disodium succinate with 90 mL of the dye solution containing 100 mg MTT, 25 mL of 0.2 M Tris-HCl, 10 mL of 0.005 M $MgCl_2$, 5.0 mL of 0.05 M $CoCl_2$, 55 mL of H_2O and 80 μL of 10 N HCl. After the incubation for 1 - 1 1/2 hrs at 37.0 °C to permit the color reaction to develop, the staining medium was suctioned off, and the cells were fixed in Tris-HCl-buffered 4 % formalin for 5 min, rinsed twice with distilled water and dried in air. To dissolve the formazan dye, one-half mL of

6.25 % v/v 0.1 mol/L NaOH in dimethylsulfoxide (DMSO) was added to each well. The amount of formazan was quantified by measuring its optical density at 560 nm.

5.2.5 Identification of Leachables

High performance liquid chromatography (HPLC) was used to separate samples of the extract, UDMA monomer and the UDMA mixed with the initiator and catalysts at ambient temperature. The HPLC unit was a Rainin High Performance Liquid Chromatographer with an ultra detector set at 220 nm. The samples were diluted with 0.1 % TFA in 80 % CH_3CN. The solution was injected into a C18 column (3.9 x 300 mm) at a flow rate of 1 mL/min and sampling interval of 0.1 sec for 60 min.

Mass spectroscopy (MS) with a direct probe was used to analyze the most intense fractions of the extract. The fractions were dried, to a constant weight, prior to analysis.

5.3 Results

5.3.1 Evaluation of Cytotoxicity

The effects of different exposure times on curing of composites by visible light are shown in Figures 5.2 - 5.5. The percent of Balb/c 3T3 cell viability for untreated, polished, ethanol and water extracted composites, respectively, are given for the cells exposed to composites light cured for 13 - 300 sec and then aged for 0 - 288 hrs at 57 °C. In these figures, error bars are shown graphically which represent of one standard error of the mean (n = 6). In the study of the influence of different curing times of the treated as well of the untreated composite on the cell viability, there was a statistically significant difference (p = 0.05) in the cell viability when they were exposed to composites that were cured by visible light for different times. In general,

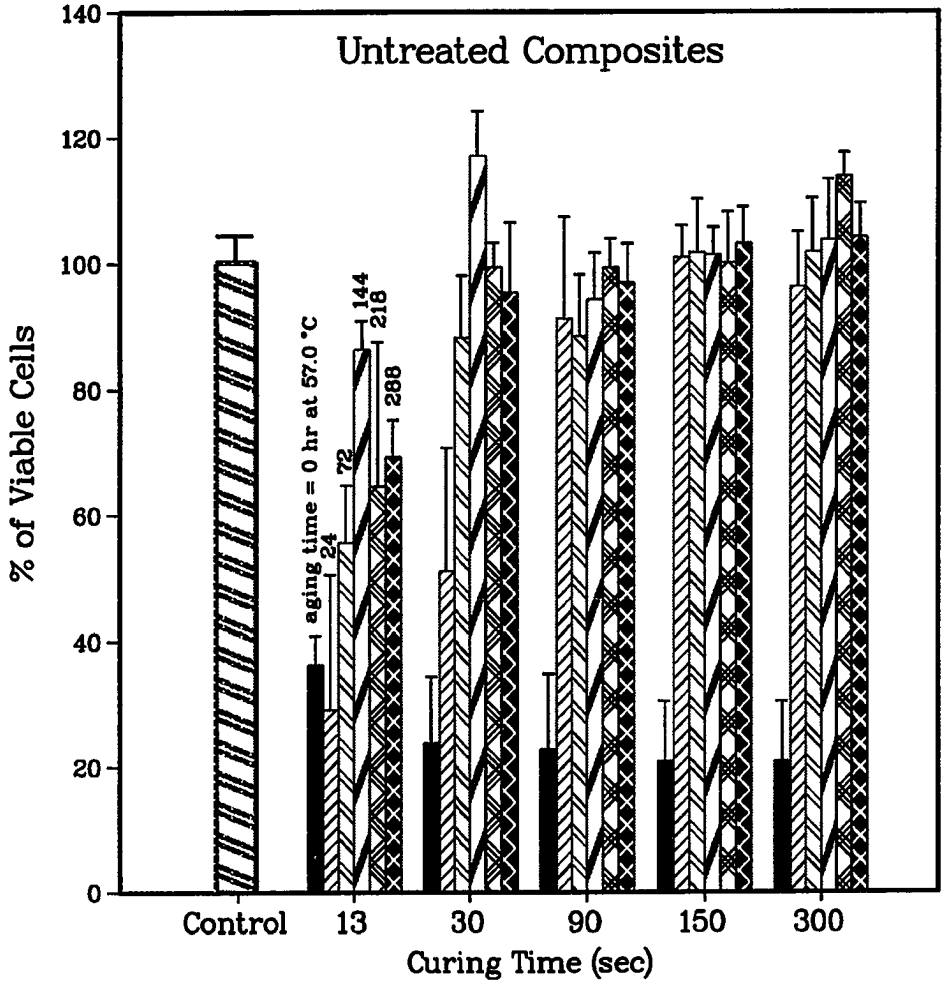

Figure 5.2: Percent of viable Balb/c 3T3 cells around aged UDMA-based composites as a function of different curing times.

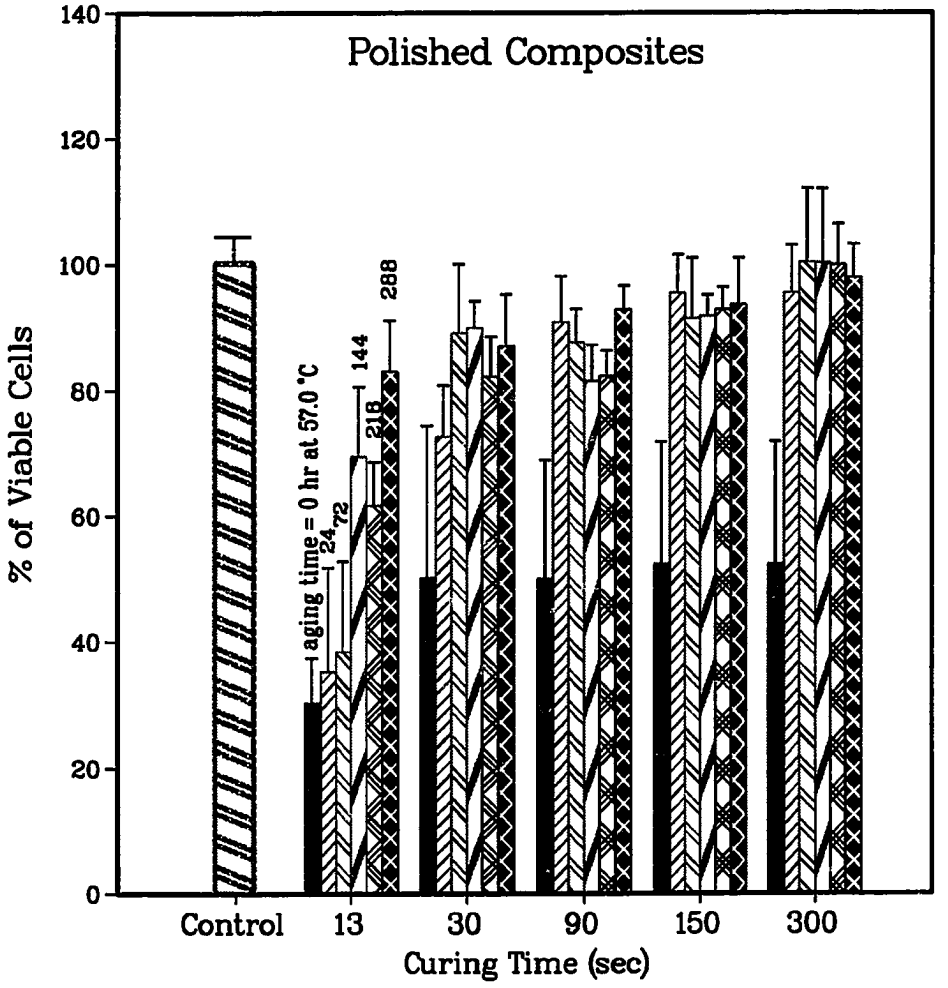

Figure 5.3: Percent of viable Balb/c 3T3 cells around aged polished UDMA-based composites as a function of different curing times.

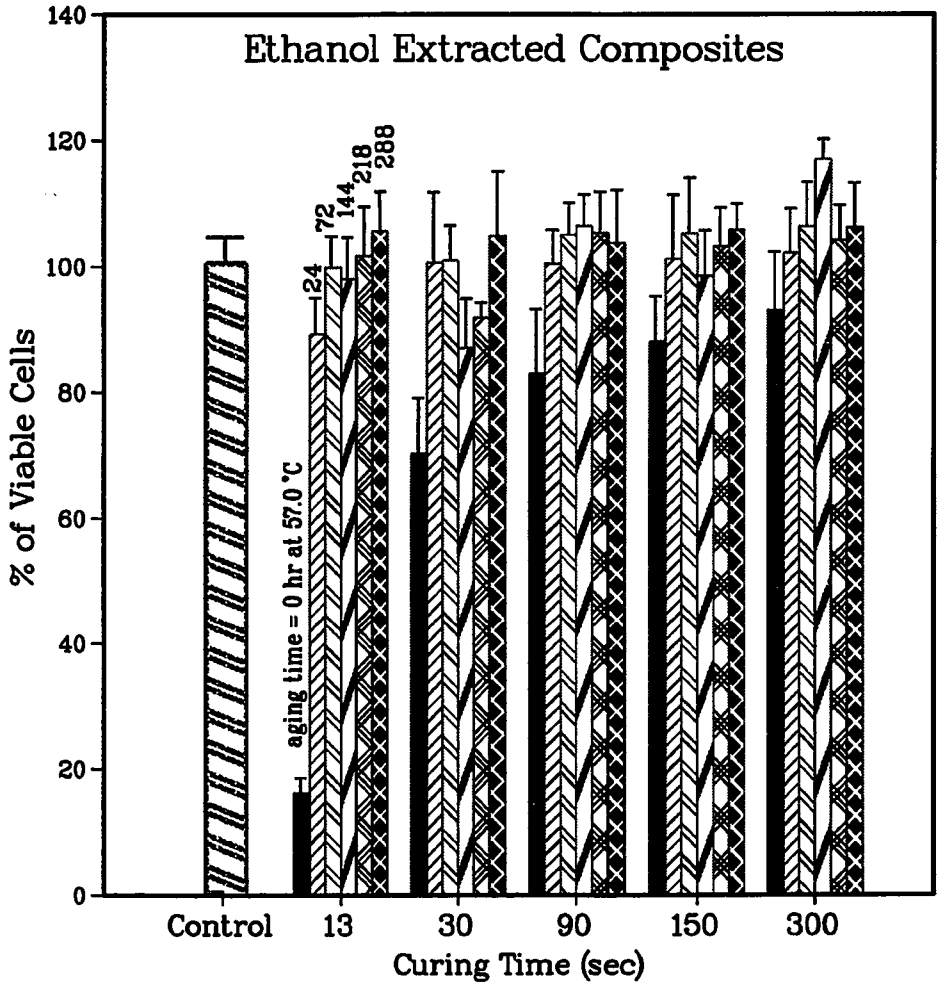

Figure 5.4: Percent of viable Balb/c 3T3 cells around aged ethanol extracted UDMA-based composites as a function of different curing times.

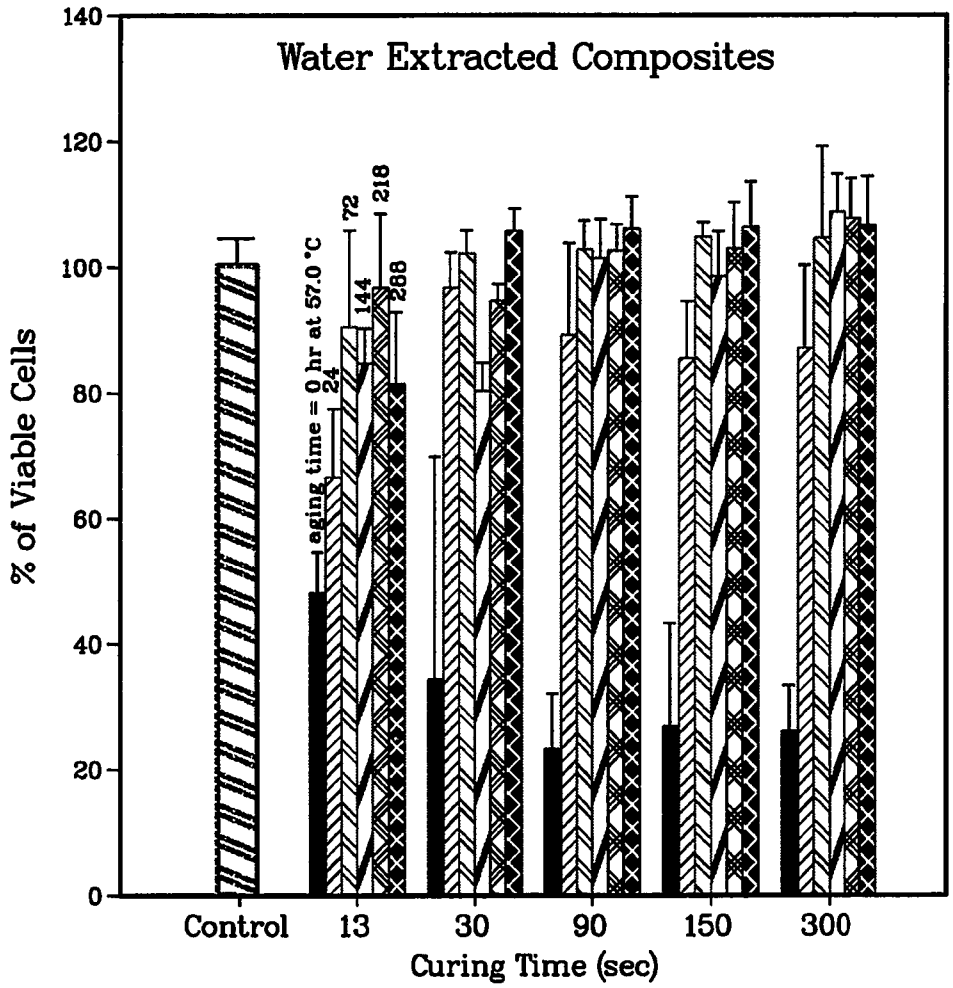

Figure 5.5: Percent of viable Balb/c 3T3 cells around aged water extracted UDMA-based composites as a function of different curing times.

the cell viability increased continuously with curing time until it reached constant values of 104.1 ±5.4, 97.9 ±5.2, 106.2 ±7.4 and 106.6 ±7.2 % of the Teflon control in the presence of untreated, polished, ethanol, and water extracted composites, respectively, when samples were aged for 288 hrs. However, the viability of the cells decreased with increasing curing time when exposed to untreated or water extracted samples but were not aged at 57 °C (i.e. aged for 0 hrs). For instance, the percent of cell viability decreased from 48.1 ± 6.3 to 26.0 ± 6.6 % in the presence of 0 hrs aged water extracted composites.

The effects of different aging times of composites at 57 °C on the percent of viable cell are shown in Figures 5.6 - 5.9 for untreated, polished, and extracted composites with ethanol and water, respectively. ANOVA showed that the effect on the cell viability among cells exposed to composites that were aged for different times at 57 °C was statistically significant different ($p = 0.05$). There was a substantial increase in the cell viability within the first 24 hrs of aging except with untreated composites. Composites cured from 30 - 300 sec reached a plateau after 72 hrs when the cells were exposed to ethanol/water extracted composites. This increase was more gradual when the composites were cured for 13 sec with visible light, and only occurred with ethanol/water extracted composites (Figure 5.8).

Percent of leachables against curing times for composites subsequently extracted with ethanol and water after aging for different times in an oven at 57 °C are shown in Figures 5.10(a) and 5.10(b), respectively. The percent of leachables determined from both ethanol and water extractions decreased with the increase in exposure time of composites to visible light during curing and reached limiting values at 90 sec. In general, the amount of leachables extracted by both solvents showed similar trends with increasing aging time. That is, the amount of leachables seemed to increase

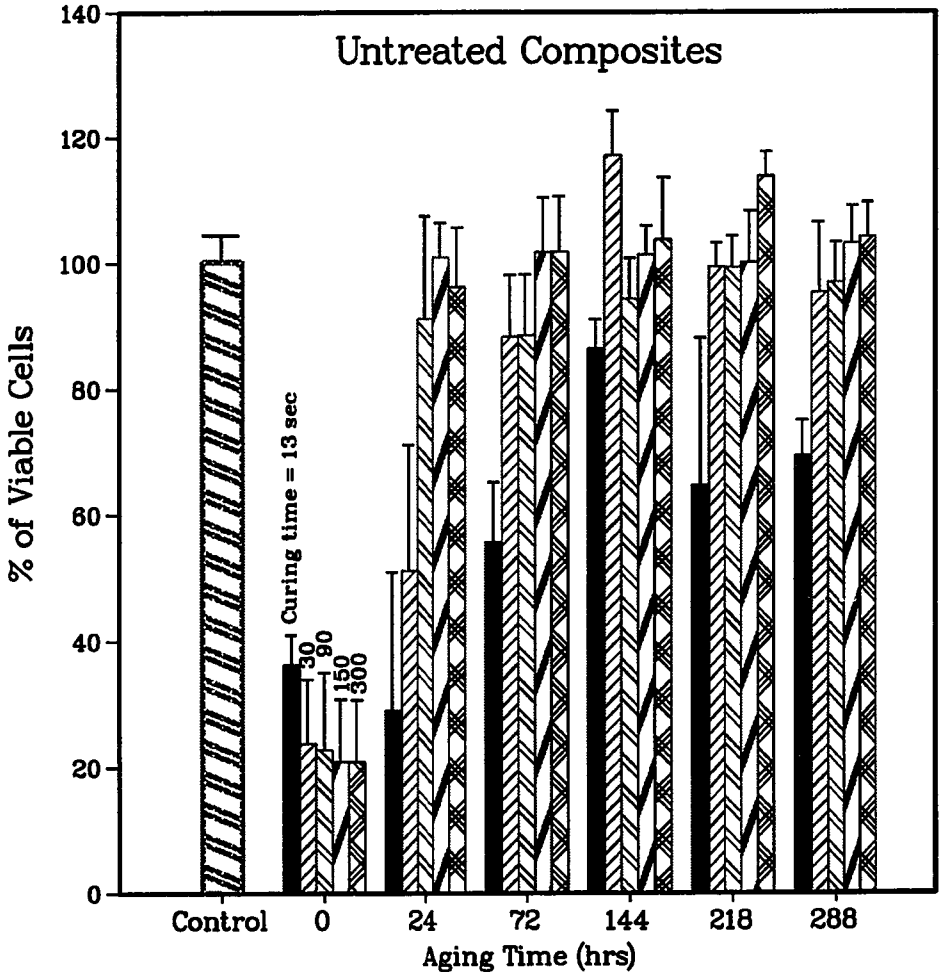

Figure 5.6: Percent of viable Balb/c 3T3 cells around cured UDMA-based composites as a function of different aging times.

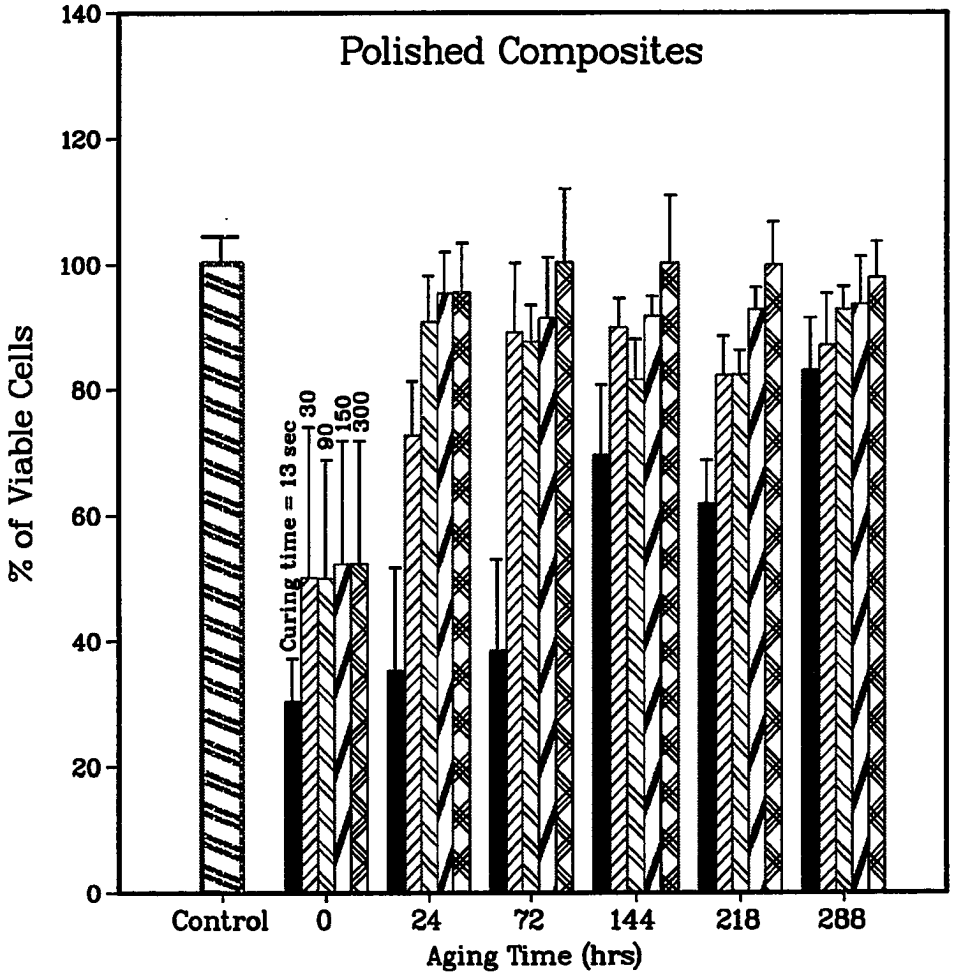

Figure 5.7: Percent of viable Balb/c 3T3 cells around cured polished UDMA-based composites as a function of different aging times.

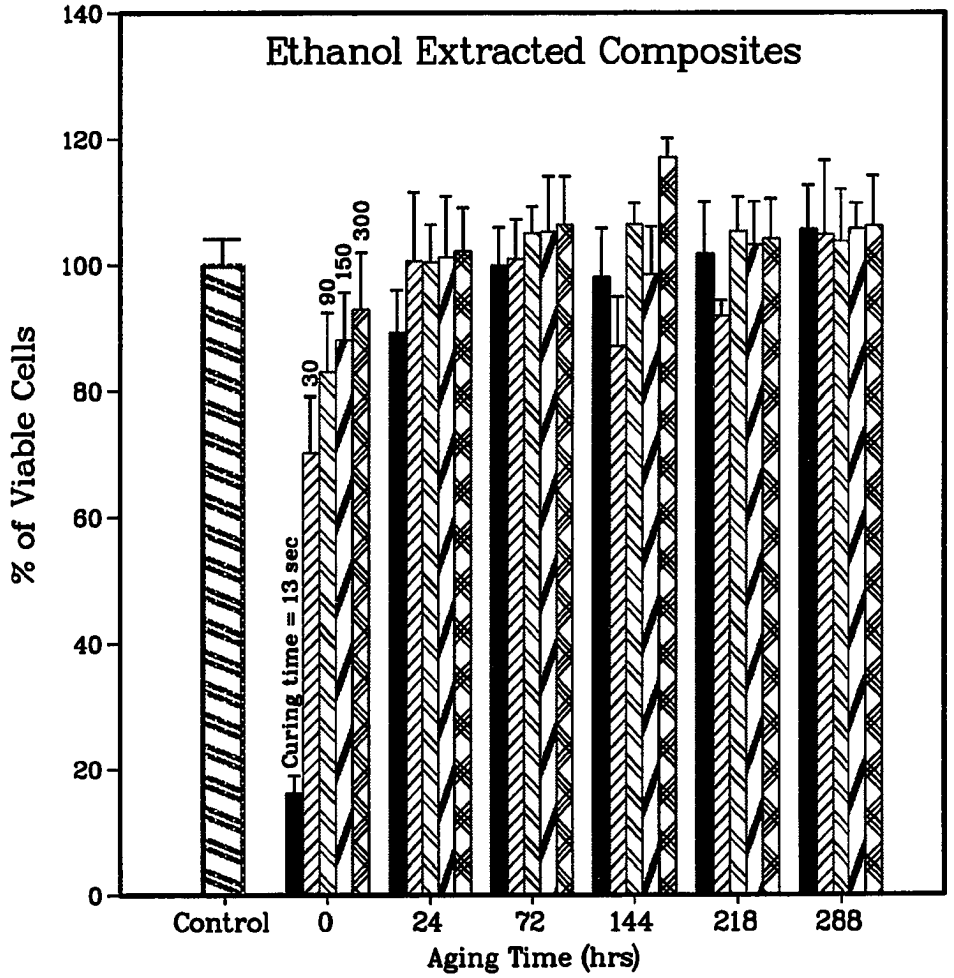

Figure 5.8: Percent of viable Balb/c 3T3 cells around cured ethanol extracted UDMA-based composites as a function of different aging times.

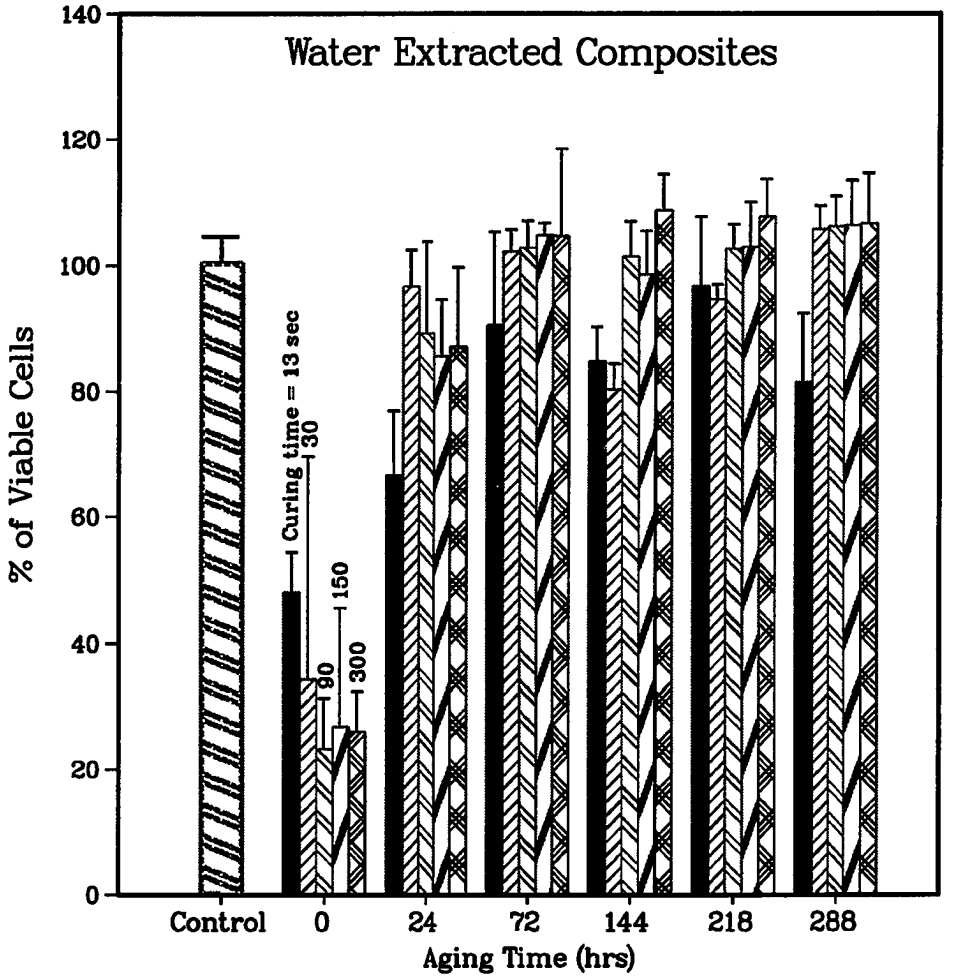

Figure 5.9: Percent of viable Balb/c 3T3 cells around cured water extracted UDMA-based composites as a function of different aging times.

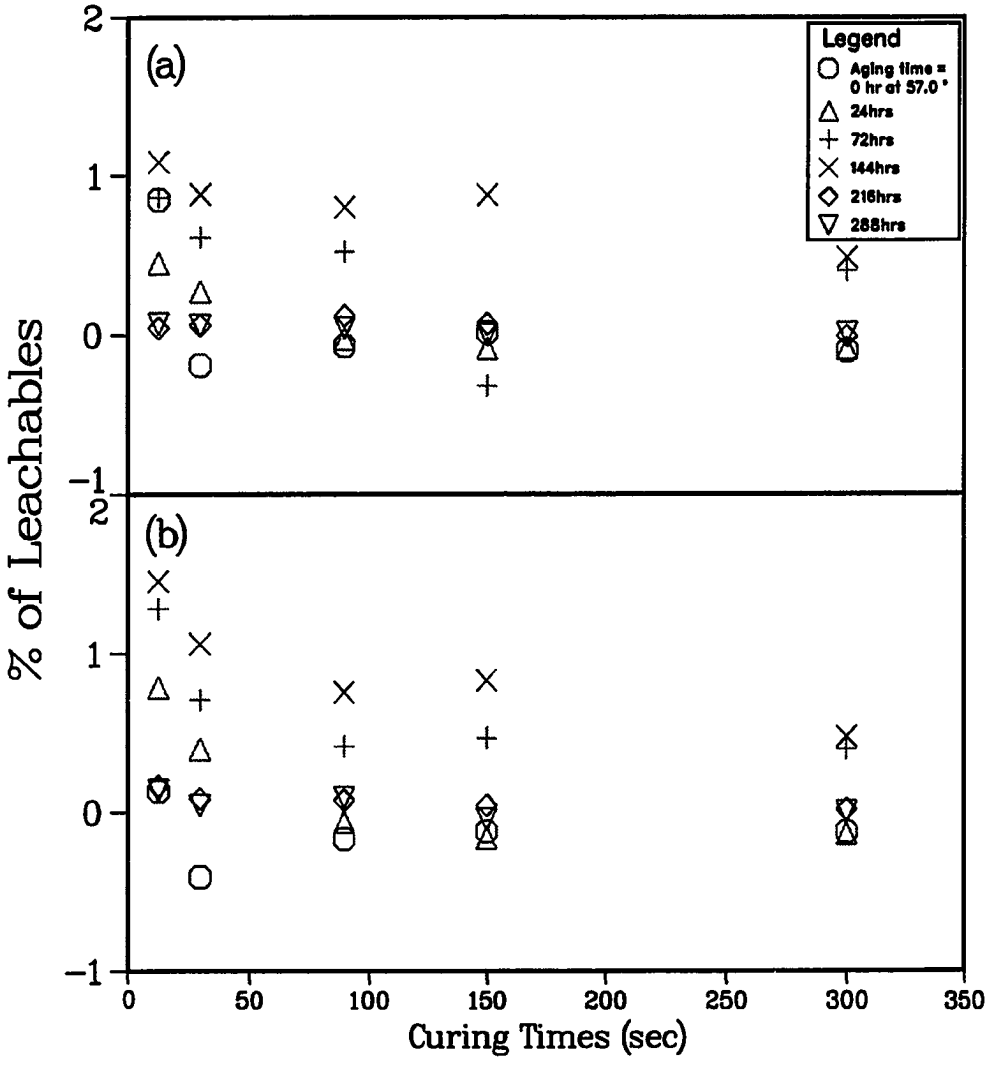

Figure 5.10: Percent of leachables as a function of curing time (sec) for aged composites extracted with (a) 75 (b) deionized water.

until the aging time of 144 hrs and then they decreased to near 0 % at 288 hrs. However, at short aging times (0 hrs), the percent of leachables were low and below 0 % when the composites were cured for 30 sec.

Finally, the effect of different treatments of composites as a function of aging time are shown in Figures 5.11(a) and 5.11(b) for composites exposed to visible light for 13 and 300 sec, respectively. By ANOVA, there was a statistically significant difference ($p = 0.05$) among the different treatments on the percent of cell viability. With the exception of composites cured and aged for 13 sec and 0 hrs of aging, ethanol extracted composites had the lowest toxic effects on the cells that were growing around them. Polishing had variable effects on short-cured (13 sec) composites, but had much better effects on composites cured for 300 sec. Aging of 300 sec cured composite resin for 24 hrs increased the cell viability to about 95 % and further aging improved viability. Water-extracted composites had lower toxic effects on the cells than the untreated composites when the composites were cured for 13 sec (Figure 5.11(a)), while their toxicity effect was comparable with the untreated composites when they were cured for 300 sec (Figure 5.11(b)).

5.3.2 Identification of Leachables

The fractions of UDMA monomer and uncured UDMA polymer mixtures as a function of retention time obtained from the HPLC analysis are shown in Figures 5.12(a) and 5.12(b), respectively. These figures show peaks of six major fractions (1 to 6, Figure 5.12(a)) that were collected for the UDMA monomer and two additional fraction (1′ and 2′, Figure 5.12(b)) for a total of eight were retained for the UDMA polymer mixture. The common retention time for the peaks were 3.5, 6.3, 10.3, 16.2, 21.5 and 24.0 min, while the additional peaks were eluted at 2.5 and

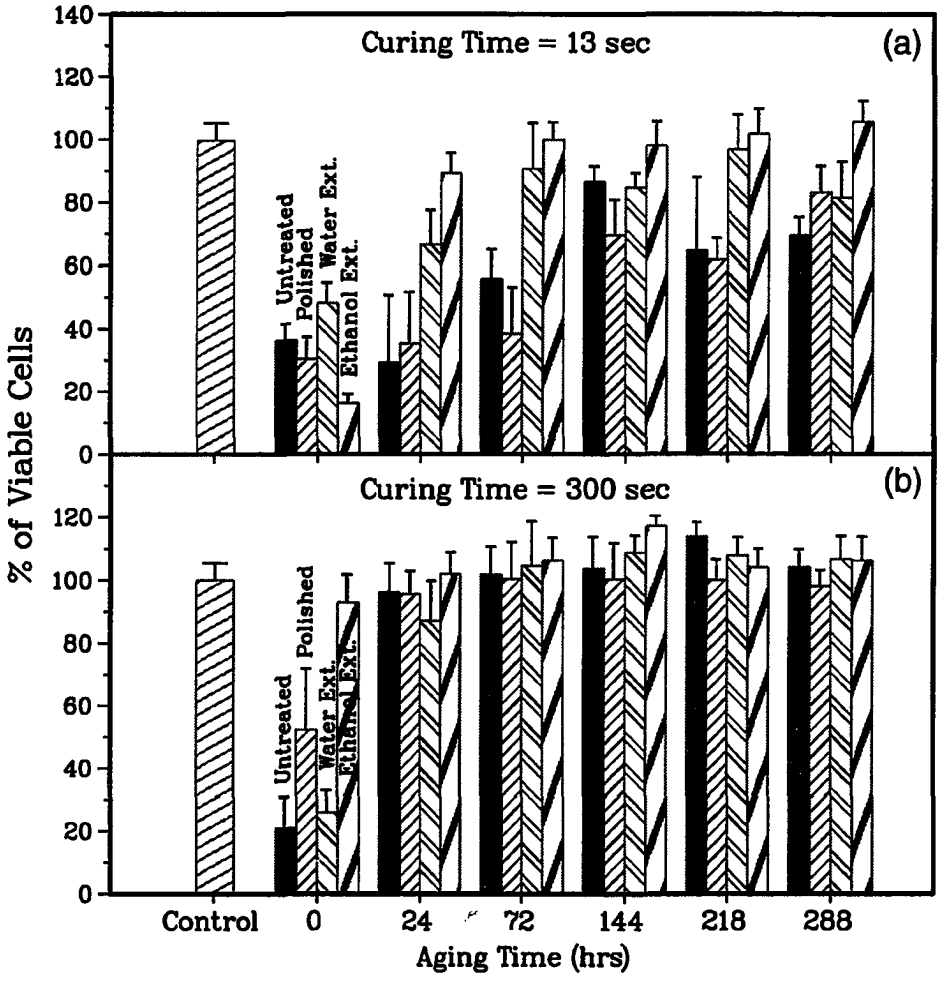

Figure 5.11: Percent of viable Balb/c 3T3 cells around untreated, polished ethanol and water extracted composites as a function of aging times for (a) 13 sec and (b) 300 sec curing time.

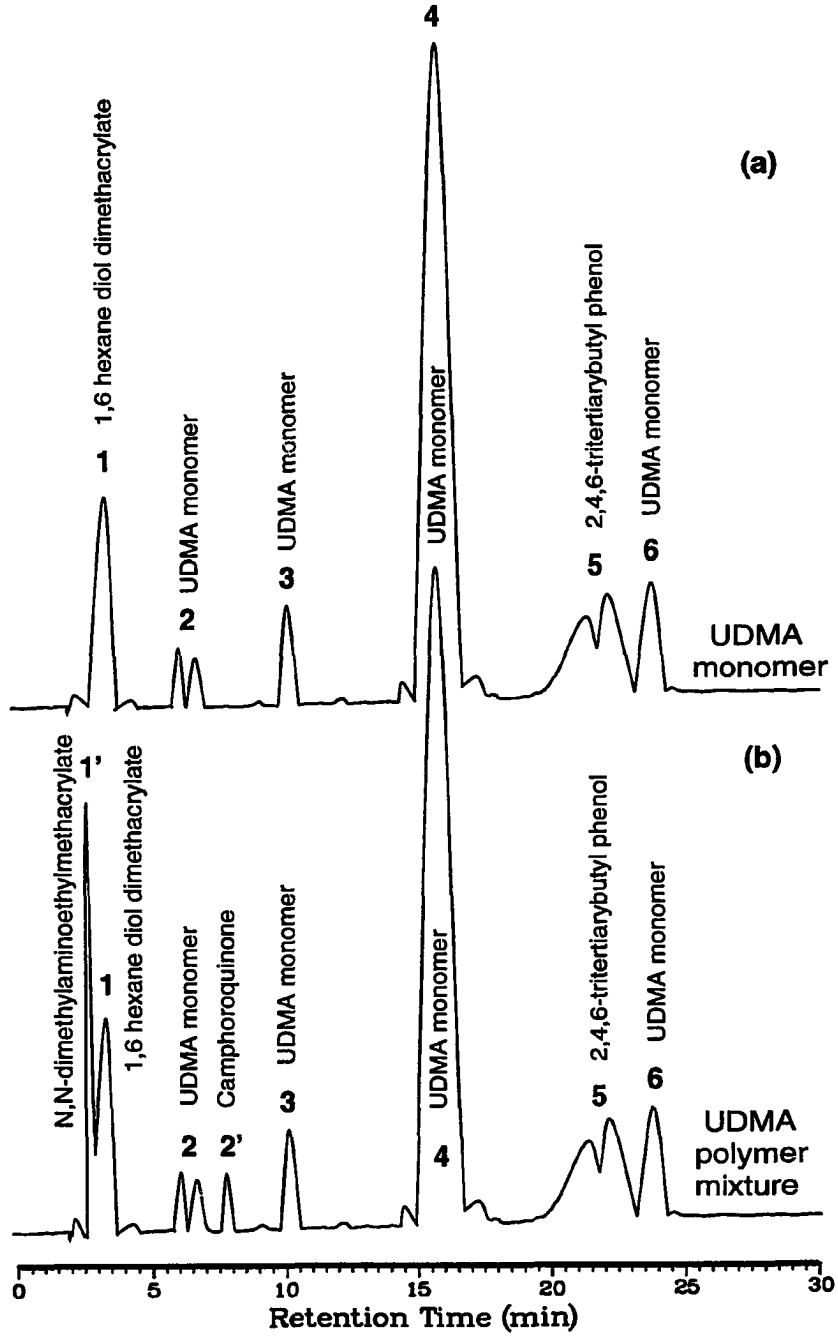

Figure 5.12: High performance liquid chromatographs of (a) UDMA monomer and (b) uncured UDMA polymer mixture.

7.7 min. These two additional peaks are characteristics of DMAEMA and CQ, respectively.

The amount of material extracted from the polymerized composite powder was 1.12 $\pm$ 0.1 % and retention times of its fractions determined from the HPLC analysis are shown in Figure 5.13(b). To show the details of this analysis, a magnification of the fraction peaks is shown in Figure 5.13(c). The extracted components showed three main features in these figures, namely, that (a) the major component was retained at 16.2 min (peak 4), (b) the peak retained at 2.5 min (peak 1′) in the unpolymerized UDMA mixture did not exist in the extract, and (c) the peak retained at 7.7 min (peak 2′) appeared minutely.

The mass spectrum of UDMA monomer is shown in Figure 5.14. The spectrum of the UDMA monomer showed a clear peak which corresponded to the molecular ion of UDMA that has a mass to charge ratio (m/e) of 471. The m/e, which gives the molecular weight of the original molecule, as 471 is close to the molecular weight of the monomer (470 gm/mole). The spectrum also showed fragmentation patterns of the monomer such as the presence of fragment ion peaks of propene or secondary amine (m/e = 41), primary amide or primary amine (m/e = 44), propene ketone, (m/e = 55), 2-methyl propene ketone (m/e = 69), 2-methyl propene ethyl ester (m/e = 113) and 1,3-methyl 5-hexene 2-amide (m/e = 154).

The mass spectra of the extract fractions 1, 2, 4 and 5 are shown in Figures 5.15 - 5.18, respectively. The m/e of fraction 1 of the extract (Figure 5.15) eluted at 3.5 min was 252 which corresponded to 1,6 hexane diol dimethacrylate molecular weight, while the highest m/e value of 764 gm/mole corresponded to the molecular ion of 1,6 hexane diol dimethacrylate oligomer. The m/e peaks showed fragmentation patterns that supported this identification, namely, the m/e peaks that occurred at 57, 71, 83

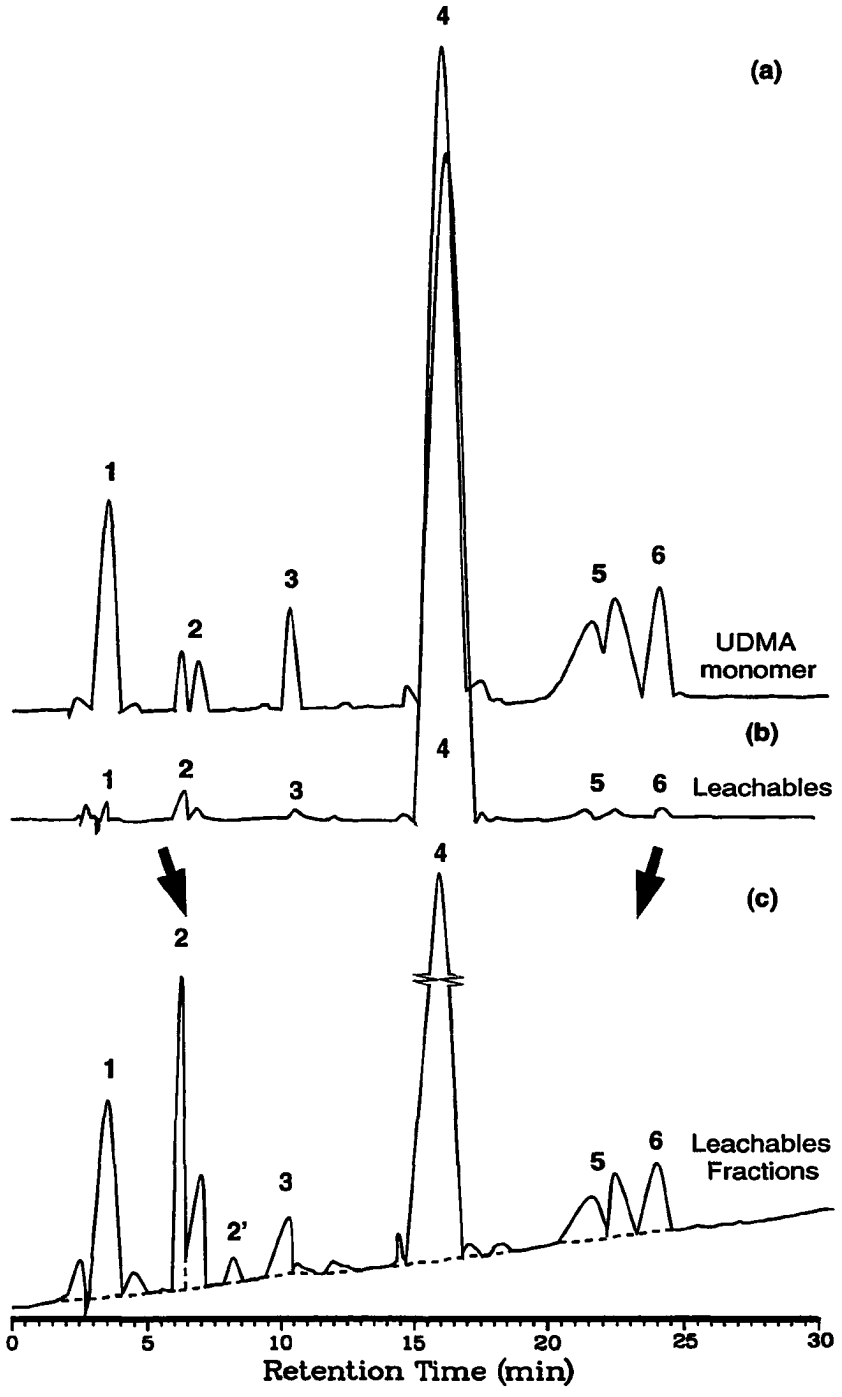

Figure 5.13: High performance liquid chromatographs of (a) UDMA monomer (b) leachables from UDMA-based composites extracted from ethanol and (c) a magnification of minor peaks of the leachables.

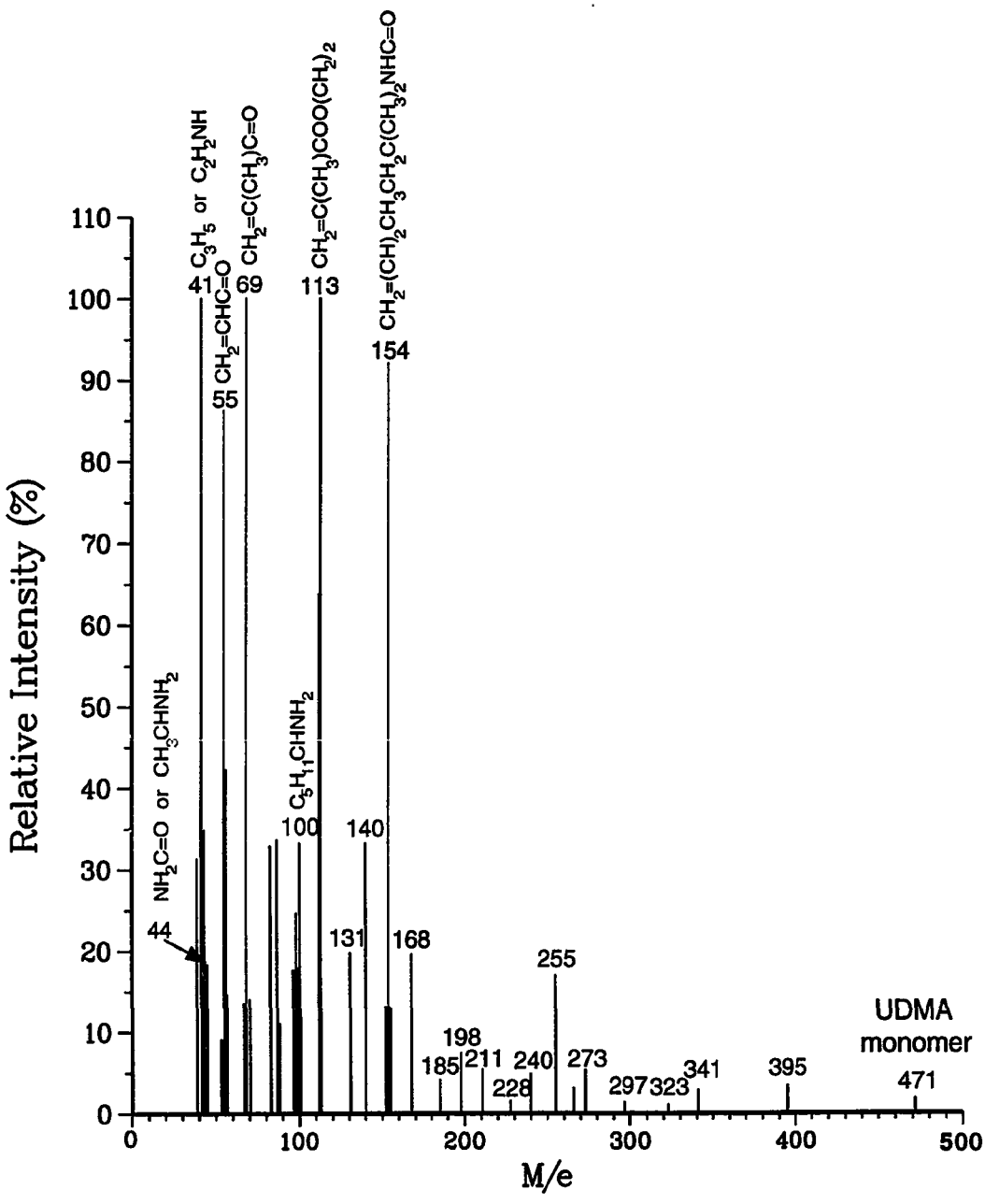

Figure 5.14: Mass spectrum of UDMA monomer diluted with 75 % ethanol.

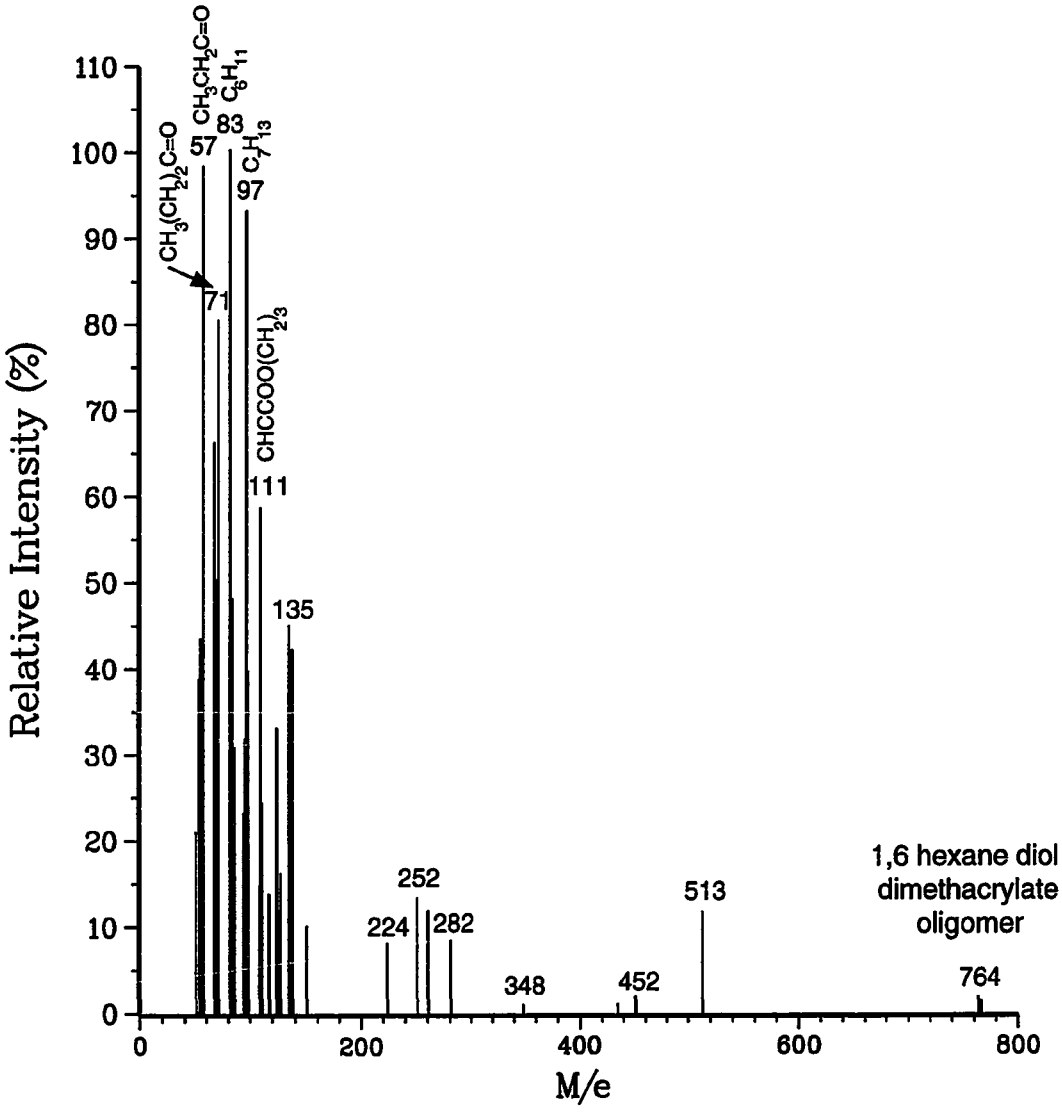

Figure 5.15: Mass spectrum of fraction #1 of leachables extracted by 75 % ethanol with retention time of 3.5 min.

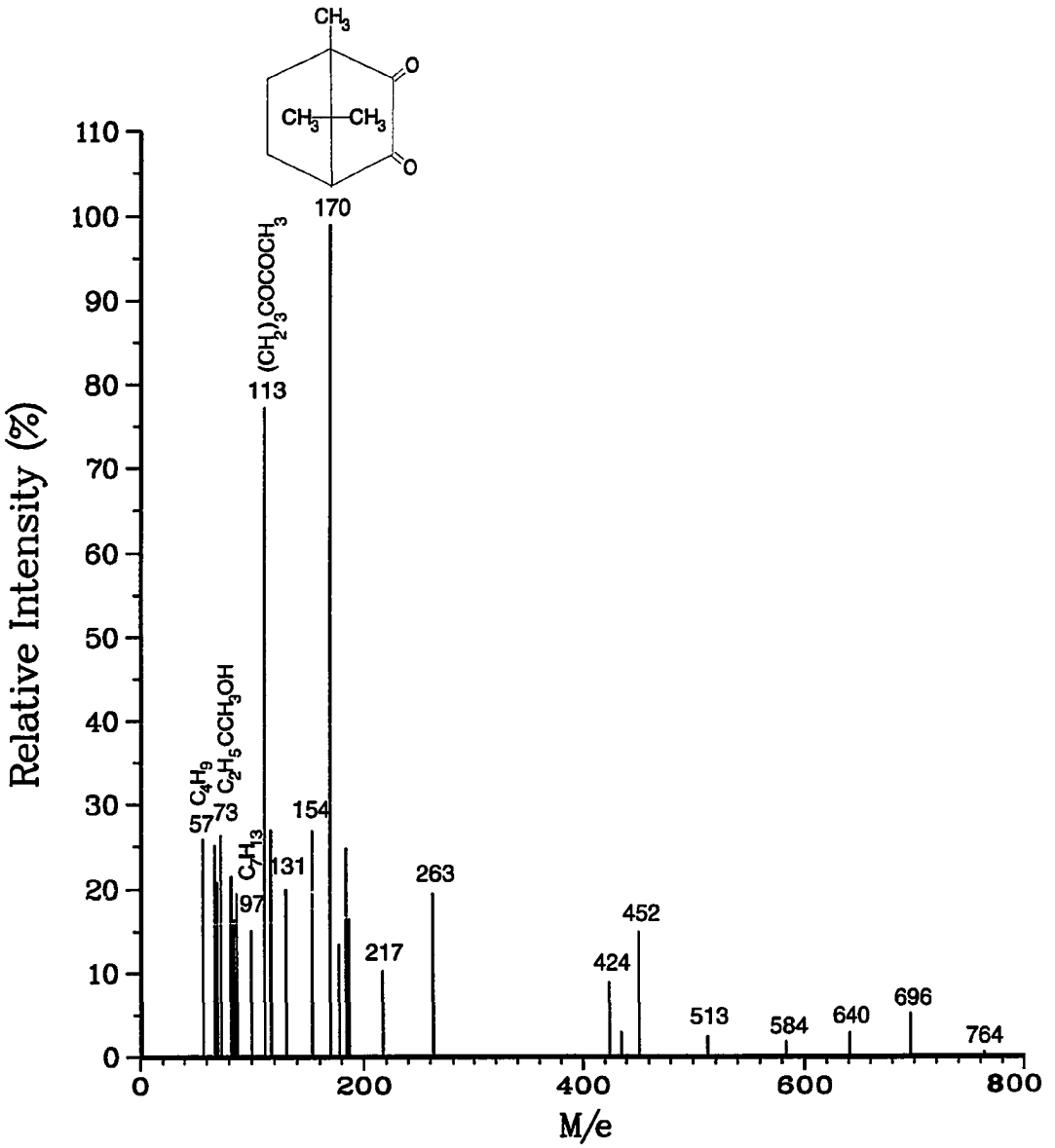

Figure 5.16: Mass spectrum of fraction #2 of leachables extracted by 75 % ethanol with retention time of 6.3 min.

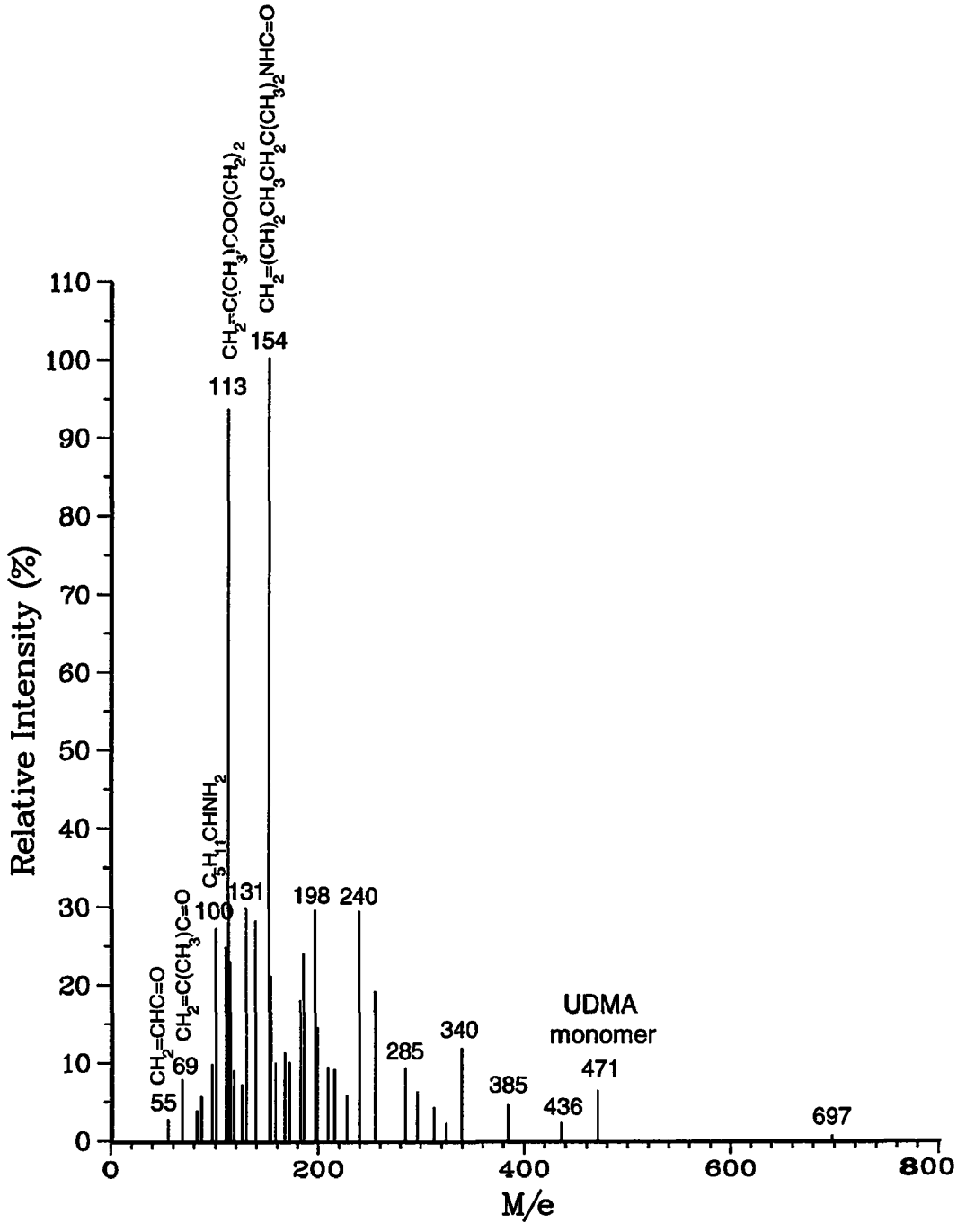

Figure 5.17: Mass spectrum of fraction #4 of leachables extracted by 75 % ethanol with retention time of 16.2 min.

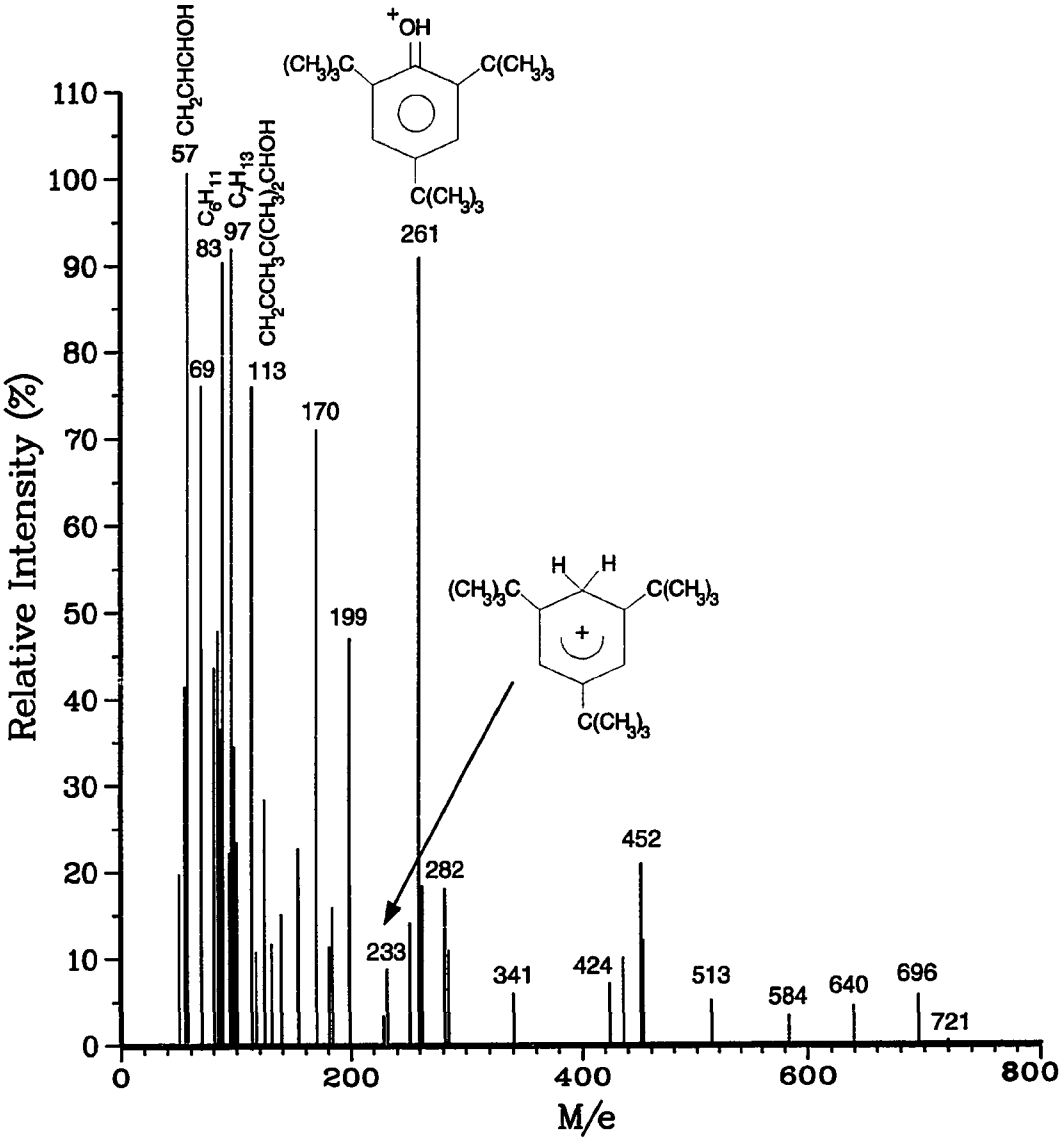

Figure 5.18: Mass spectrum of fraction #5 of leachables extracted by 75 % ethanol with retention time of 21.5 min.

and 111 which corresponded to 1-propanone, 1-butanone, 1-hexene and dipropyl ester, respectively, which are the constituent of 1,6 hexane diol dimethacrylate co-monomer. The mass spectrum of fraction 2 of the extract (Figure 5.16) showed a primary m/e peak of 170 which is equal to the molecular weight of CQ. The mass spectrum of the major component eluted at 16.2 min (fraction 4) showed m/e (Figure 5.17) peaks corresponded to the UDMA monomer and oligomer, where the characteristic m/e peaks occurred at 113, 154, 471 and 697. The main m/e peak in the mass spectum of fraction 5 (Figure 5.18) occurred at 261 which is the molecular ion of 2,4,6-tritertiarybutyl phenol.

5.4 Discussion

In this study, a profile of percent of cell viability in the presence of UDMA-based composite resins in *in vitro* cell culture was established in Figure 5.2. This profile correlates the biocompatibility between curing time of the composites by visible light and post-curing time (aging) with heat to ensure maximum polymerization. This profile suggests that curing the composite for a minimum of 150 sec and post-curing it for at least 24 hrs at 57 °C is required to give comparable biocompatibility of the restorative composite to the negative control.

The *in vitro* cell culture results indicate that curing the composites by visible light up to 300 sec but without postcuring did not decrease the cytotoxic effects of the composite nor make them biocompatible to the cells, if they were not extracted by either water or 75 % ethanol. This incompatibility may be related to the capability of the resin to release organic components that consists of residuals of uncured monomers and oligomers. The explanation is consistent with the observations of Rathburn *et al.* [83] who showed that extraction of composites with organic solvents

to remove the unreacted species reduced their cytotoxicity by only 90 %. The explanation is also supported by determining the LD_{50} values for the various components of the resins which exerted cytotoxic effects on the Balb/c 3T3 cells [44].

Since higher exposure time of the composite to light increases the depth of cure [21, 23] and thus increases the hardness of composites, which also correlates well with the degree of conversion [34, 84], one would assume higher biocompatibility with higher exposure time. However, it was surprising that composites cured with visible light for 300 sec without aging were comparable or worse in biocompatibility than those cured for 13 sec 5.2. This may be attributed to the presence of unreacted double bonds at the surface of the composites due to oxygen inhibited layer rendering it toxic even though it was exposed to light for longer period. This is supported by the increase in the biocompatibility when the samples were polished (Figure 5.3). Such explanation was also supported by Vankerckhoven *et al.* [105] who found that polishing composites resin caused an important decrease in the quantity of the double bonds due to its thermal effect.

Aging of the composite resins by heat increases the degree of polymerization [113], thus decreasing the percentage of residual double bonds and increasing the crosslinking of the polymer network. This aging decreases the diffusion of polymer molecules and limits the number of molecules available for leaching into solvents or into cell culture. Such a decrease in the diffusion of polymer molecules was reflected by marked improvement of the biocompatibility in the composites and the decrease in the percent of leachables at longer aging times.

The cytotoxicity evaluation showed that extraction of composites with 75 % ethanol/water mixture improved the biocompatibility more than extraction of the composites with water. This indicated that the ethanol/water mixture extracted

more unbound monomer and oligomer due to its ability to penetrate the polymerized resin network and swell it more effectively than water. However, the values for the percent leachables were lower for samples extracted with the ethanol mixture than those extracted by water when the composites was cured for short periods of time. For instance, the percent leachables were found to be 1.1 $\pm$ 0.13% and 1.5 $\pm$ 0.68% in 75 % ethanol/water and 100 % water extractants, respectively, when the composites were cured for 13 sec and post-cured for 144 hrs. Such a contradiction indicates that not all of the solvent sorbed by the resin had been eliminated by desiccation. This was apparent from the negative values of the percent leachables that resulted for composites cured and post-cured at 30 sec and 0 hrs, respectively. This effect was greater in the ethanol/water mixture, which suggests that the ethanol, being a better solvent for the UDMA composites, has a greater ability to bind to the polar groups in the resin than water. This resulted in greater gain of weight of the composites as compared to the gain of weight that took place in water, thus the net amount of leachables were less in the composites extracted by ethanol mixture. This observation was also noted by Ferracane and coworkers [35] who gave a similar explanation.

75 % Ethanol/water extraction of composites cured for 30 to 300 sec with visible light and with 0 hr aging time improved the biocompatibility from 47 to 74 %, respectively, while water extraction of the composites decreased the compatibility from 7 to 4 %. The polished composites, on the other hand, improved the biocompatibility from 33 to 38 % when the composites were cured for 30 to 300 sec, respectively. Thus, removing the oxygen-inhibited layer increased the biocompatibility by 33 %, while extracting the composites with ethanol/water improved the biocompatibility by additional 44 % assuming the first 33 % in bicompatibility improvement was due

to the extraction of the unpolymerized component at the surface. These results indicate that indeed the release of unpolymerized components from the surface as well as the bulk of composites are responsible for cellular responses. Furthermore, one can conclude that approximately 33 % of cellular response was due to the release of the unpolymerized components from the surface of the composites, while about 44 % of the response was due to the chemical release from the bulk.

In either case the resulting residues from the leachables were present in concentration of approximately 1.12 % by weight. HPLC and mass spectroscopy of these residues indicated that the major component released from the composites was identified to be the UDMA monomer and small quantities of fragments of this monomer such as acrylic esters moieties. Mass spectroscopy analysis of minor fractions of the extract revealed that 1,6 hexane diol methacrylate, camphoroquinone and 2,4,6-tritertiarybutyl phenol were identified as minor components. The methacrylate is used as a comonomer to reduce the viscosity of the monomer and to increase the crosslinking of the polymer matrix, while the camphoroquinone is used as a photochemical initiator. The phenol is included in the monomer system as an inhibitor to prevent premature polymerization.

5.5 Concluding Remarks

The results of *in vitro* study suggest that curing the light-activated composites for minimum of 150 sec and post-curing for 24 hrs is required to attain comparable biocompatibility with the negative control, Teflon. Removing the oxygen-inhibited layer from these composites improved the biocompatibility by 33 %, while extracting the composites with 75 % ethanol/water decreased the cytotoxicity by 77 %. Chemicals released from the surface accounted for approximately 33 % of cellular re-

sponse, while 44 % of the response was due to chemical components released from the bulk. The primary leachable material from the UDMA composites resin was UDMA monomer. Small quantities of 1,6 hexane diol methacrylate, camphoroquinone and 2,4,6-tritertiarybutyl phenol were also found.

CHAPTER VI

SUMMARY AND CONCLUSIONS

Of the vast variety of biomaterials, synthetic polymer-based composites are used in wide range of applications, such as orthopaedics and dental restorations. These composites consist of inorganic fillers entrapped in a three-dimensional highly cross-linked organic polymer matrix. The filler and the polymer are chemically attached by a coupling agent such as organofunctional silane. The combination of the two phases gives enhanced material properties for these particular applications than the individual phase. In these polymer-based composites, the properties of the organic matrix and the stability of the organic-inorganic interface strongly influence the behavior of the composite material. A particular class of these resin composites consists of an organic matrix composed of difunctional monomers which undergo polymerization by a free radical mechanism that is initiated by radiant energy (visible light).

Despite the advances that were made in these composite resins in the last 30 years, problems with light-cured composites still exist and remain under investigation. Some of these problems are incomplete conversion, continual resin curing, failure of the organic-inorganic bond and hydrolytic degradation of this bond in the biological environment. These problems lead to poor esthetics and loss of anatomic

form. Therefore, the goals of this research were:

1. To examine the continual curing of resin of a difunctional vinyl monomer and the effect of presence of an inorganic phase on this continual curing process using microcalorimetry.

2. To investigate the polymer-filler interaction in order to determine how a non-compatible inorganic phase modifies the molecular behavior of the composite resin as compared to the pure polymer using dielectric measurements, and to determine how a modification of this inorganic phase by silanation affects these molecular behaviors.

3. To determine the effect of moisture on the polymer and polymer-filler interface with and without a coupling agent using dielectric measurements.

4. To examine the effects of different curing- and post-curing times on the cytotoxicity of UDMA-based composites in *in vitro* cell culture before and after leaching and polishing the composites, and to identify the major components that might be responsible for cells reactions.

To achieve these goals, a urethane dimethacrylate- (UDMA) based composite, which is commonly used in restorative dentistry as an anterior restoration, was the choice for a biomaterial. The composite was formulated from UDMA monomer, zirconia-silica filler, and 3-methacryloxypropyltrimethoxysilane (MAPM) or 4-aminobutyltriethoxysilane (ABTE) silanated zirconia-silica filler, using *dl*-camphoroquinone as a catalyst and 2-dimethylaminoethylmethacrylate as an accelerator. The filler was silanated by depositing the silanes from aqueous solution of 75 % ethanol (190 % proof) to 25 % silane (weight ratio). The mixed composite paste was polymerized by visible light.

Continual Curing of Resin

Isothermal enthalpy measurements were determined using a Tian-Calvet microcalorimeter to follow the reaction rates of UDMA, ZS filled-UDMA and MAPM-silanated ZS filled-UDMA cured for different curing times. These rates were also measured at different annealing temperatures. The rates of enthalpy changes were measured and the changes of enthalpy as well as the conversion were calculated. From these results, several conclusions were drawn:

1. Annealing low cured UDMA polymer as well as UDMA-based composite did not increase the crosslink density with time to that of the highly cured resins, leaving more unreacted double bonds at the end of the curing and post-curing cycle that are unable to proceed in the polymerization due to reaching either the gel or the vitrification point.

2. Annealing low cured UDMA and UDMA-based composite at high temperature (65.5 °C) displayed an endothermic reaction that might be due to the reduction of the photoinitiators.

3. Low amount of filler incorporation (25 wt %) restricts the molecular motion of the surface layer of the polymer onto filler particles, and regards the composite as being densely crosslinked polymer.

4. Silanation of the filler displayed an endothermic reaction that might be due to the dynamic equilibrium that is developed at the interface between the organic and inorganic interface in the composite.

Effects of Different Additives

The dielectric loss tangent and capacitance were measured for ZS-filled UDMA composed of different filler to resin ratios and MAPM- as well as ABTE-silanated ZS-filled UDMA containing different silane concentrations. The real and imaginary dielectric permittivities and the real and imaginary electric moduli were calculated. From these results, several major conclusions were drawn:

1. UDMA shows three relaxations α, β, and γ. The α-relaxation is attributed to the segmental motion of the main chains, the β-relaxation to the motion of free amide groups, and the γ-relaxation to the local motion of $(CH_2)_n$.

2. Adding zirconia-silica to the UDMA shows pronounced effect on the behavior and on the thickness of the boundary layer at the interface. Increasing filler concentration restricts the mobility of the main chains and decreases the thickness of the surface layer, while allowing more movement to the local chains in the loosely packed layer. These changes near the interface are due to the reduction of the conformational numbers and the need of more conformational changes of the main chains for the transition of molecular segments from one position to another to occur during the relaxation.

3. MAPM was shown to be a compatible silane with the zirconia-silica and UDMA system. Such compatibility was observed through the effectiveness of the chemical linkage of the silane to the filler and the polymer without forming separate interphase. The effective chemical bonds formed between the coupling agent and the composite depends on the concentration of the silane. In the case of MAPM-silanated zirconia-silica-filled UDMA, the optimum silane concentration is about three times the minimum uniform coverage. Above this

concentration, high plasticization effects start to develop.

4. ABTE was shown to be an incompatible silane for zirconia-silica-filled UDMA system. The incompatibility was demonstrated by the occurrence of a new peak that characterizes an interphase. This interphase is made of low molecular unreactive cyclic amino structures that contain protonated amines. These amines cause charge separation upon the application of the electric field and were shown as a separate dispersion.

Effects of Moisture

The dielectric loss tangent and capacitance were measured for UDMA, ZS-filled UDMA and MAPM-silanated ZS-filled UDMA that were conditioned with different amount of moisture. The real and imaginary dielectric permittivities and the real and imaginary electric moduli were calculated. From these results, several major conclusions were drawn:

1. Water molecules can only be found as fragments that form nonfreezing clusters. These water clusters contain charges that are not stabilized by the hydrated amide groups.

2. Bulk water can exist at the interface between the filler and the polymer in composites that contain unsilanated filler. This type of water can form disordered structures of ice at low temperatures and can evaporate at high temperatures.

3. Moisture in composites containing silanated filler behaves more or less like the UDMA polymer at low temperatures, but the composite becomes more plasicized than the polymer at high temperatures.

4. Dielectric measurements are a good tool for detecting phase transitions in a system and investigating water-polymer interactions.

Biocompatibility

For cytotoxicity evaluation, the UDMA-based composites were cured for different curing times and aged at 57.0 °C for different times. For each curing and aging condition, the samples were either untreated, polished, or extracted with different solvents. Extraction of the samples was carried out by either distilled water or a mixture of 75 % ethanol/water (volume ratio). The samples were extracted for 48 hrs at ambient temperatures. Cytotoxicity evaluation was carried out for all testing condition using *in vitro* test culture. The cell line used was Balb/c 3T3 embryonic mouse fibroblasts. The cytotoxicity measurement was evaluated by measuring succinic dehydrogenase activity in the mitochondria of the cells using MTT-formazan production, which is a reflection of cell viability. The cell viability was determined as a percent of the negative control, (Teflon in this case).

For identification of leachables, the UDMA-based composites were cured for 30 sec with visible light, ground and extracted using the mixture of 75 % ethanol/water for a total of 72 hrs. The resultant extract was first quantified and was separated into fractions using high performance liquid chromatography (HPLC). The fractions were identified using mass spectroscopy (MS). From these results, one can conclude that:

1. Curing the light-activated composites for a minimum of 150 sec and post-curing for 24 hrs is required to attain comparable biocompatibility with the negative control.

2. The decrease in biocompatibility was mostly due to release of the chemicals from the bulk. Chemicals released from the surface accounted for approx-

imately 33 % of cellular response, while 44 % of the response was due to chemical components released from the bulk.

3. The primary leachable material from the UDMA composites resin was UDMA monomer. Small quantities of 1,6 hexane diol methacrylate, camphoroquinone and 2,4,6-tritertiarybutyl phenol were also found.

BIBLIOGRAPHY

BIBLIOGRAPHY

[1] Aldrich, P., McGee, R., Yalvac, S., BoneKamp, J., and Thurow, S., (1987). "Maxwell-Wagner-Sillars relaxations due to glass occlusions in a thermoset composite," *J. Appl. Phys.*, 62(11):4504-4509.

[2] Allen, K. W., Hansrani, A. K., and Wake, W. C., (1981). "The structure and properties of films of siloxane coupling agents," *J. Adhesion*, 12:199-219.

[3] Anderson, D. A. F., Ferracane, J. L., and Zimmermann, E. R., (1987). "Cytotoxicity of combinations of dental composites components," *J. Dent. Res.*, 66:133, Abst. No. 214.

[4] Anderson, D. A. F., Zimmermann, E. R., Ferracane, J. L., and Kaga, M., (1988). "Cytotoxicity of variably cured light-activated dental composites," *J. Dent. Res.*, 67:226, Abst. No. 905.

[5] Anderson, D. A. F., Ferracane, J. L., and Seale, N. S. (1989). "Pulpal response to variably cured and sealed dental composites," *J. Dent. Res.*, 68:346, Abst. No. 1319.

[6] Antonucci, J., and Toth, E., (1983). "Extent of polymerization of dental resins by differential scanning calorimetry," *J. Dent. Res.*, 62(2):121-125.

[7] Arkles, B., (1987). **Silane coupling agent chemistry**, *Petrarch Systems Catalogue*, Pennsylvania: Bristol, pp. 59.

[8] Asmussen, E., (1975). "NMR-analysis of monomers in restorative resins," *Acta Odont. Scand.*, 33:129-143.

[9] Baird, M. E., (1967). **Progress in polymer science**, edited by A. D. Jenkins (Pergamon Press, London,) 1:161-184.

[10] Bean, T. A. *et al.*, (1994). "Effect of esterase on methacrylates and methacrylate polymers in an enzyme simulation for biodurability and biocompatibility testing," *J. Biomed. Mat. Res.*, 28:59-63.

[11] Baker, W. O., and Yager, W. A., (1942). *J. Am. Chem. Soc.*, 64:2171.

[12] Billmeyer, F., (1984). **Textbook of polymer science**, John Wily & Sons, New York, pp. 49-56.

[13] Borisova, T. I., and Chirkov V. N., (1973). "The mechanism of the low temperature dielectric relaxation of polymers containing low molecular weight impurities," *Vysokomol. soyed.*, A15(10):2304-2309.

[14] Boyd, R. H., (1959). "Dielectric loss in 66 nylon (polyhexamethylene adipamide)," *J. Chem. Phys.*, 30(5):1276-1283.

[15] Brännström, M., and Nyborg, H., (1972). "Pulpal reaction to composite resin restorations," *J. Prosthet. Dent.*, 27:181-189.

[16] Brown, G. L., (1980). "Clustering of water in polymers," **Water in polymers**, edited by S. P. Rowland, ACS symposium series 127, (American Chemical Society, Washington, D. C.,) pp. 441-450.

[17] Burke, F., (1985). "Light-activated composites: the current status," *Dent. Update*, 12(3):184-186.

[18] Caughman, W. F., Caughman, G. B., Dominy, W. T., and Schuster, G. S., (1989). "Cellular responses to glass ionomer and composite resin cements," *J. Dent. Res.*, 68:346, Abst. No.1320.

[19] Chan, R. K., Pathmanathan, K., and Johari, G. P., (1986). "Dielectric relaxations in the liquid and glassy states of glucose and its water mixtures," *J. Phys. Chem.*, 90:6358-6362.

[20] Coelho, R., (1979). **Physics of dielectrics for the engineer**, Elsevier Scientific Publishing Company, Amsterdam.

[21] Cook, W. D., (1982). "Depth of cure in the UV photopolymerization of dimethacrylate-based dental filling materials," *J. Macromol. Sci-Chem.*, A17(1):99-111.

[22] Cook, W. D., and Standish, P. M., (1983). "Polymerization kinetics of resin-based restorative materials," *J. Biomed. Mater. Res.*, 17:275-282.

[23] Cook, W. D., and Standish, P. M., (1983). "Cure of resin based restorative materials. II. White light photopolymerization resins," *Aust. Dent. J.*, 28(5):307-311.

[24] Cox, C. F., Keall, C. L., Keall, H. J., Ostro, E., and Bergenholtz, G., (1987). "Biocompatibility Of surface-sealed dental materials against exposed pulps," *J. Prosthet. Dent.*, 57:1-8.

[25] Craig, R. G., (1981). "Chemistry, composition, and properties of composites resins. Symposium on composite resins in dentistry," **Dental Clinics of North America**, pp. 219-239.

[26] Craig, R. G., (1982). "Photopolymerization of dental composite systems," **Posterior composites proceedings of international symposium on posterior composite resin**, Chapel Hill, North Carolina, pp. 245-251.

[27] Craig, R. G., et al., (1989). **Restorative dental materials**, The C.V. Mosby Company, St. Louis, 8th Ed., pp. 142-144.

[28] Craig, R. G., and Mohsen, N. M., (1992). "Effect of silanation of filler on their wettability by oligomer," *J. Dent. Res. Spec. Iss.*, 71:240.

[29] Deodhar, S., (1980). "Measurement of bound (nonfreezing) water by differential scanning calorimetry," **Water in polymers**, edited by S. P. Rowland, ACS symposium series 127, (American Chemical Society, Washington, D. C.,) pp. 273-286.

[30] Dibenedetto, A., Gomez, J., Schilling, C., Osterholtz, F., and Haddad, G., (1990). "Thermochemical stability of interphases in glass reinforced composites," *Mat. Res. Soc. Symp. Proc.*, 170:297-302.

[31] Douglas W. H., Craig R. G., and Chen, C. C. (1979). "A new composite restorative based on a hydrophobic matrix," *J. Dent. Res.*, 58(10):1981-1985.

[32] Dutta, A., and Ryan, M. E., (1979). "Effect of fillers on kinetics of epoxy cure," *J. Appl. Polym. Sci.*, 24:635-649.

[33] Fabulyak F. Y., and Lipatov, Y. S. (1973). "Nuclear magnetic relaxation of different types of oligomers in the bulk and in the boundary," *Vysokomol.Soyed.*, A15(7):1513-1516.

[34] Ferracane, J. (1985). "Correlation between hardness and degree of conversion during the setting reaction of unfilled dental restorative resins," *Dent. Mater.*, 1:11-14.

[35] Ferracane, J., and Condon, J., (1990). "Rate of elution of leachable components from composite," *Dent. Mater.*, 6:282-287.

[36] Flory, P., (1969). **Principles of polymer chemistry**, Cornell University Press, New York.

[37] Freund, M. and Munksgand, E. C. (1990). "Enzymatic degredation of Bis-GMA/TEGDMA polymers causing decreased microhardness and greater wear *in vitro*," *Scand. J. Dent. Res.*, 98:351-355.

[38] Gordon J., Howard, G., and Shanks R. A. (1982). "The influence of filler particles on the mobility of polymer molecules," *J. Macromol. Sci-Chem.*, A17(2):287-295.

[39] Hanai, T., (1960). "Theory of the dielectric due to the interfacial polarization and its application to emulsions," *Kolloid-Zeitschrift*, Band 171:23-31.

[40] Hanai, T., (1961). "Dielectric properties of emulsions III. Dielectric behavior of W/O emulsions," *Kolloid-Zeitschrift*, Band 177:57-61.

[41] Hanai, T., Koizumi, N., and Gotoh, R., (1959). "Dielectric properties of emulsions I. Dielectric constants of O/W emulsions," *Kolloid-Zeitschrift*, Band 167:41-43.

[42] Hanks, C. T., Anderson, M., and Craig, R. G., (1981). "Cytotoxic effects of dental cements on two cell culture systems," *J. Oral. Pathol.*, 10:101-112.

[43] Hanks, C. T., Craig, R. G., Diehl, M. L. and Pashley, D. H., (1988). "Cytotoxicity of dental composites and other materials in a new in *in vitro* device," *J. Oral. Pathol.*, 17:396-403.

[44] Hanks, C., Strawn, J., Wataha, J., and Craig, R., (1991). "Cytotoxic effects of resin components on cultured mammalian fibroblasts," *J. Dent. Res.*, 70(11):1450-1455.

[45] Hanson, E., (1983). "After-polymerization of visible light activated resins: Surface hardness vs. light source," *Scand. J. Dent. Res.*, 91:406-410.

[46] Hasted, J., (1961). **Progress in dielectrics**, edited by J. Birks (Spottiswood, London,) 3:101-105.

[47] Hedvig, P. (1977). **Dielectric spectroscopy of polymers**, John Wily & Sons, New York.

[48] Inokoshi, S., Iwaku, M. and Fusayama, T. (1982). "Pulpal response to a new adhesive restorative resin," *J. Dent. Res.*, 61(8):1014-1019.

[49] Ishida, H. and Koenig, J. L. (1978). "The reinforcement mechanism of fiberglass reinforced plastics under wet conditions: A review," *Polym. Eng. & Sci.*, 18(2):128-145.

[50] Jain, S. K., and Johari G. P., (1988). "Dielectric studies of molecular motions in the glassy states of pure and aqueous poly(vinylpyrrolidone)," *J. Phys. Chem.*, 92:5851-5854.

[51] Jain, S. K., and Johari G. P., (1990). "Conductance and relaxations in the glassy and rubber states of aqueous poly(vinylpyrrolidone): A cryofixation medium," *J. Polym. Sci.: Part.B: Polym. Phys.*, 28:763-773.

[52] Johari G. P., (1984). "The electrostatic field and the molecular dipole moment in the polymorphs of ice," *J. Chem. Phys.*, 80(9):4413-4422.

[53] Johnson, G. E., Bair, H. E., Matsuoka, S., Anderson, E. W., and Scott, J. E., (1980). "Water sorption and its effect on a polymer's dielectric behavior," **Water in polymers**, edited by S. P. Rowland, ACS symposium series 127, (American Chemical Society, Washington, D. C.,) pp. 451-468.

[54] Johnson, W., Leung, R., and Fan, P., (1985). "A Mathematical model for post-irradiation hardening of photoactivated composite resin," *Dent. Mater.*, 1:191-194.

[55] Kolařik, J., and Janáček, J.,(1967). *J. Polym. Sci: Part C*, 16:444.

[56] Lacabanne, C., Lavergne, C., Michel, L., Dufresne, A., Martinez, J. Boye, J., and Cottu, J., (1992). "Viscoelastic properties of composites," **Composite material**, edited by A Di Benedetto, L. Nicholais and R. Watanabe, Elsevier Science Publishers, Amsterdam pp 115-125.

[57] Lamb, D., and Ellis, B., (1983). Letter to the editor, *J. Dent. Res.*, 62:160.

[58] Leung, R., Fan, P., and Johnson, W., (1983). "Post-Irradiation polymerization of visible light-activated composite resins," *J. Dent. Res.*, 62:363-365.

[59] Li, Y., Swartz, M., Phillips, R., Moore, B., and Roberts, T., (1985). "Effect of filler content and size on properties of composites," *J. Dent. Res.*, 64:1396-1401.

[60] Lee, A., and McKenna, G., (1988). "Effect of crosslink density on physical ageing of epoxy networks," *Polymer*, 29:812-1817.

[61] Lipatov, Y. S. (1977). "Relaxation and viscoelastic properties of heterogeneous polymeric composition," *Advances in Polymer Science*, 22:1-59. New York: Springler-Verlag.

[62] Lipatov, Y. S., and Fabulyak F. Y. (1972). "Relaxation processes in the surface layers of polymer at the interface," *J. Appl. Polym. Sci.*, 16:2131-2139.

[63] Lipatov, Y., and Sergeeva, L. (1974). **Adsorption of polymers**, John Wily & Sons, New York.

[64] Lipatov, Y. U., Rosovizky, V. F., and Shifrin, V. V., (1982). "Viscoelastic properties of the model system: Epoxy resin-glass beads-poly(buthylmethacrylate)," *J. Appl. Polym. Sci.*, 27:455-460.

[65] Lutz, F., et al., (1983). "Dental restorative resins: Types and characteristics," *Dent. Clin. N. Am.*, 27:697-712.

[66] Lutz, F., and Phillips, R., (1983). "A classification and evaluation of composite resin systems," *J. Proth. Dent.*, 50:480-488.

[67] Malladi, D., Colba, J., and Filisko, F., (1982). *J. Macromol. Sci.-Phys.*, B21:71.

[68] Mangion, M. B., and Johari, G. P. (1990). "Relaxation of thermosets. III. Sub-T_g dielelectric relaxation of bisphenol-A-based epoxide cured with different cross-linking agents," *J. Polym. Sci. Polym. Phys.*, 28:71-83.

[69] Matsumoto, H., et al., (1986). "Depth of cure of visible light-cured resin: clinical simulation," *J. Prosth. Dent.*, 55:574-578.

[70] McCrum, N., Buckley, C., and Bucknall, C., (1988). **Principles of polymer engineering**, Oxford University Press, New York, pp. 11-14.

[71] McCrum, N. G., Read, B. E., and William, G. (1967). **Anelastic and dielectric effects in polymeric solids**, John Wiley & Sons, London.

[72] Moynihan, C. T., Boesch L. P., and Laberge N. L. (1973). "Decay function for the electric field relaxation in vitreous ionic conductors," *Phys. Chem. Glasses*, 14(6):122-125.

[73] Pathmanathan, K. and Johari, G. P. (1991). "Dielectric and conductivity relaxations in poly(hema) and of water in its hydrogel," *J. Polym. Sci.: Part.B: Polym. Phys.*, 28:675-689.

[74] Pathmanathan, K., Johari, G. P., and Ripmeester, J. A., (1989). "Dielectric and calorimetric studies of β-cyclodextrin undecahydrate," *J. Phys. Chem.*, 93:7491-7494.

[75] Peyser, P. and Bascom W. D. (1977). "Effect of filler and cooling rate on the glass transition of polymers," *J. Macromol. Sci-Phys.*, B13(4):597-610.

[76] Plueddemann, E. P., (1970). "Adhesion through silane coupling agents," *Paper at 25th annual SPI RP/C Conference*, Section 13-D, pp. 1-10.

[77] Plueddemann, E. P., (1974). "Catalytic effect in bonding thermosetting resins to silane-treated fillers. In fillers and reinforcements for plastics," edited by Deanin R.D., and Schott N.R., Advances in Chemistry Series, Vol. 134, Washington DC, *Am. Chem. Soc.*.

[78] Plueddemann, E. P., and Stark, G. L., (1974). **Interface in polymer matrix composites**, E. P. Plueddemenn, ed., Academic Press, New York.

[79] Plueddemann, E., (1978). **Additives for plastics,** Vol. II, R. B. Seymour, ed., Academic Press, pp. 49.

[80] Plueddemann, E. P. (1982). **Silane coupling agent**, Plenum Press, New York.

[81] Puffer, R., and Šebenda, J. (1967). "On the structure and properties of polyamides. XXVII. The mechanism of water sorption in polyamides," *J. Polym. Sci: Part C*, 16:79-93.

[82] Pusatcioglu, S. Y., Fricke, A. L., and Hassler, J. C., (1979). "Heats of reaction and kinetics of a thermoset polyester," *J. Appl. Polym. Sci.*, 24:937-946.

[83] Rathbun, M. A., Craig, R. G., Hanks, C. T., and Filisko, F. E., (1991). "Cytotoxicity of bis-GMA dental composite before and after leaching in organic solvents," *J. Biomed. Mater. Res.*, 25:443-457.

[84] Rueggeberg, F., (1987). "Depth of cure parameters in light-cured composite," *Master Thesis,* The University of Michigan.

[85] Rupley, J. A., Yang, P. H., and Gordon, T., (1980). "Thermodynamic and related studies of water interacting with proteins," **Water in polymers**, edited by S. P. Rowland, ACS symposium series 127, (American Chemical Society, Washington, D. C.,) pp. 111-132.

[86] Ruyter, E., (1982). "Polymerization and conversion in composite resins," *Posterior Composites Proceedings of International Symposium on Posterior Composite Resin,* Chapel Hill, North Carolina, pp. 254-283.

[87] Ruyter, E., and Györösi, P., (1976). "An infrared spectroscopic study of sealants," *Scand. J. Dent. Res.*, 84:396-400.

[88] Ruyter, E., and Svendsen, S., (1978). "Remaining methacrylate groups in composite restorative materials," *Acta. Odont. Scand.*, 36:75-82.

[89] Ruyter, E., and Øysaed, H., (1987). *J. Biomed. Mat. Res.*, 21:11-23.

[90] Shu, C., (1992). "Isothermal enthalpy changes of PS/PP blends," *Ph.D. Thesis*, The University of Michigan.

[91] Smyth, C. (1955), **Dielectric behavior and structure**, McGraw-Hill Book Company Inc., New York.

[92] Soderhölm, K., (1981). "Degradation of glass filler in experimental composites," *J. Dent. Res.*, 60:1867-1875.

[93] Soderhölm, K., (1983)"Leaking of fillers in dental composites," *J. Dent. Res.*, 62:126-130.

[94] Soderhölm, K., and Calvert, P., (1983). "Effects of water on glass-filled methacrylate resins," *J. Mater. Sci.*, 18:2957-2962.

[95] Soderhölm, K., Zigan, M., Ragan, M., Fischlschweiger, W., and Bergman, M., (1984). "Hydrolytic degradation of dental composites," *J. Dent. Res.*, 63:1248-1254.

[96] Soderhölm, K., (1985). "Filler systems and resin interface," *International Symposium on Posterior Composite Resin Dental Restorative Materials*, pp. 139-160.

[97] Spangberg, L., Rodrigues, H. Langeland, L., and Langeland, K., (1973). "Biological effects of dental materials." *Oral. Surg.*, 36:713-724.

[98] Stanley, H. R., Bowen, R. L., and Folio, j., (1979). "Compatibility of various materials with oral tissues. II. responses to composite ingredients," *J. Dent. Res.*, 58:1507-1517.

[99] Starkweather, H. W., (1980). "Water in nylon," **Water in polymers**, edited by S. P. Rowland, ACS symposium series 127, (American Chemical Society, Washington, D. C.,) pp. 433-440.

[100] Struik, L. E., (1978). **Physical aging in amorphous polymers and other materials**, Elsevier, New York.

[101] Takashi, H., Masayoshi, F., Shuji, Y. and Tetsuo, K., (1982). "The effect of moisture on the dielectric relaxations in wood," *J. Appl. Polym. Sci.*, 27:439-453.

[102] Tant, M., and Wilkes, G. (1981). "An overview of the non-equilibrium behavior of polymer glasses," *Poly. Eng. Sci.*, 21(14):874-895.

[103] Tobias, M., Edmund, C., Shiere, F. R., and Clark, R. E., (1973). "Pulpal reaction to a resin-bonded quartz composite material," *J. Dent. Res.*, 52:1281-1286.

[104] VanBeek, L., (1967). **Progress in dielectrics**, edited by J. Birks (CRC, Ohio,) 7:88-93.

[105] Vankerchoven, H., et al., (1982). "Unreacted methacrylate groups on the surfaces of composites resins," *J. Dent. Res.*, 61:791-795.

[106] VonHippel, A., (1956). **Dielectrics and Waves**, Wiley, New York, pp. 228-236.

[107] Wadhwa, L. H., Walsh, W. K. (1982). "Morphology and mechanical properties of radiation-polymerized urethane-acrylates. I. Pure oligomers," *J. Appl. Polym. Sci.*, 27:591-600.

[108] Watts, D., McNaughton, V., and Grant, A., (1986). "The development of surface hardness in visible light-cured posterior composites," *J. Dent.*, 14:169-174.

[109] Whiting R. and Jacobsen P. H. (1980). "Dynamic mechanical properties of resin-based filling materials," *J. Dent. Res.*, 59(1):55-60.

[110] Woo, L., Ling, M., and Cheung, W. (1991). "Advanced testing methods for biomaterials," **High performance biomaterials**, edited by M. Szycher, Technomic Publishing Company Inc., Lancaster, pp 91-123.

[111] Woodward, Sauer, Deeley and Kline (1957). *J. Colloid Sci.*, 12:363.

[112] Wu, P., (1989). "Recovery of Pressure-Densified polystyrene," *Ph.D. Thesis*, The University of Michigan.

[113] Wu, W., (1983). "Degree of cure and wear resistance of dental composites," *J. Dent. Res*, 62:26 Abst No. 192.

[114] Young, R., (1987). **Introduction to polymers**, Chapman and Hall, London, pp. 31-54.

[115] Ziegel, K. D. and Romanov, A. (1973). "Modulus reinforcement in elastomer composites. I. Inorganic Fillers," *J. Appl. Polym. Sci.*, 17:1119-1131.